Jason Omedes Llorente

The potential of error-related potentials. Analysis and decoding for control, neuro-rehabilitation and motor substitution

Departamento

Instituto de Investigación en Ingeniería [I3A]

Director/es

MONTESANO DEL CAMPO, LUIS

Tesis Doctoral

THE POTENTIAL OF ERROR-RELATED POTENTIALS. ANALYSIS AND DECODING FOR CONTROL, NEURO-REHABILITATION AND MOTOR SUBSTITUTION

Autor

Jason Omedes Llorente

Director/es

MONTESANO DEL CAMPO, LUIS

UNIVERSIDAD DE ZARAGOZA

Instituto de Investigación en Ingeniería [I3A]

2019

The Potential of Error-Related Potentials

Analysis and decoding for control neuro-rehabilitation and motor substitution

Universidad Zaragoza

Jasón Omedes Llorente

Escuela de Ingeniería y Arquitectura

Departamento de Informática e Ingeniería de Sistemas

The potential of error-related potentials. Analysis and decoding for control, neuro-rehabilitation and motor substitution

Universidad Zaragoza

Instituto Universitario de Investigación
en Ingeniería de Aragón
Universidad Zaragoza

Jasón Omedes Llorente

Thesis submitted in fulfillment of the requirements for the degree of Doctor of Philosophy in Biomedical Engineering

Supervised by:

Luis Ángel Montesano del Campo

Universidad de Zaragoza

October, 2018

Resumen y conclusiones

Las interfaces cerebro-máquina (BMIs, por sus siglas en inglés) permiten la decodificación de patrones de activación neuronal del cerebro de los usuarios para proporcionar a personas con movilidad severamente limitada, ya sea debido a un accidente o a una enfermedad neurodegenerativa, una forma de establecer una conexión directa entre su cerebro y un dispositivo. En este sentido, las BMIs basadas en técnicas no invasivas, como el electroencefalograma (EEG) han ofrecido a estos usuarios nuevas oportunidades para recuperar el control sobre las actividades de su vida diaria que de otro modo no podrían realizar, especialmente en las áreas de comunicación y control de su entorno.

En los últimos años, la tecnología está avanzando a grandes pasos y con ella la complejidad de dispositivos ha incrementado significativamente, ampliando el número de posibilidades para controlar sofisticados dispositivos robóticos, prótesis con numerosos grados de libertad o incluso para la aplicación de complejos patrones de estimulación eléctrica en las propias extremidades paralizadas de un usuario, que le permitan ejecutar movimientos precisos. Sin embargo, la cantidad de información que se puede transmitir entre el cerebro y estos dispositivos sigue siendo muy limitada, tanto por el número como por la velocidad a la que se pueden decodificar los comandos neuronales. Por lo tanto, depender únicamente de las señales neuronales no garantiza un control óptimo y preciso.

Para poder sacar el máximo partido de estas tecnologías, el campo de las BMIs adoptó el conocido enfoque de "control-compartido". Esta estrategia de control pretende crear un sistema de cooperación entre el usuario y un dispositivo inteligente, liberando al usuario de las tareas más pesadas requeridas para ejecturar la tarea sin llegar a perder la sensación de estar en control. De esta manera, los usuarios solo necesitan centrar su atención en los comandos de alto nivel (por ejemplo, elegir un elemento específico que agarrar, o elegir el destino final donde moverse) mientras el agente inteligente resuelve problemas de bajo nivel (como planificación de trayectorias, esquivar obstáculos, etc.) que permitan realizar la tarea designada de la manera óptima.

En particular, esta tesis gira en torno a una señal neuronal cognitiva de alto nivel originada como la falta de coincidencia entre las expectativas del usuario y las acciones reales ejecutadas por los dispositivos inteligentes. Estas señales, denominadas potenciales de error (ErrPs), se consideran una forma natural de intercomunicar nuestro cerebro con máquinas y, por lo tanto, los usuarios solo requieren monitorizar las acciones de un dispositivo y evaluar mentalmente si este último se comporta correctamente o no. Esto puede verse como una forma de supervisar el comportamiento del dispositivo, en el que la decod-

ificación de estas evaluaciones mentales se utiliza para proporcionar a estos dispositivos retroalimentación directamente relacionada con la ejecución de una tarea determinada para que puedan aprender y adaptarse a las preferencias del usuario.

Dado que la respuesta neuronal de ErrP está asociada a un evento exógeno (dispositivo que comete una acción errónea), la mayoría de los trabajos desarrollados han intentado distinguir si una acción es correcta o errónea mediante la explotación de eventos discretos en escenarios bien controlados. Esta tesis presenta el primer intento de cambiar hacia configuraciones asíncronas que se centran en tareas relacionadas con el aumento de las capacidades motoras, con el objetivo de desarrollar interfaces para usuarios con movilidad limitada. En este tipo de configuraciones, dos desafíos importantes son que los eventos correctos o erróneos no están claramente definidos y los usuarios tienen que evaluar continuamente la tarea ejecutada, mientras que la clasificación de las señales EEG debe realizarse de forma asíncrona. Como resultado, los decodificadores tienen que lidiar constantemente con la actividad EEG de fondo, que típicamente conduce a una gran cantidad de errores de detección de firmas de error. Para superar estos desafíos, esta tesis aborda dos líneas principales de trabajo.

Primero, explora la neurofisiología de las señales neuronales evocadas asociadas con la percepción de errores durante el uso interactivo de un BMI en escenarios continuos y más realistas. Se realizaron dos estudios para encontrar características alternativas basadas en el dominio de la frecuencia como una forma de lidiar con la alta variabilidad de las señales del EEG. Resultados, revelaron que existe un patrón estable representado como oscilaciones theta que mejoran la generalización durante la clasificación. Además, se utilizaron técnicas de aprendizaje automático de última generación para aplicar el aprendizaje de transferencia para discriminar asincrónicamente los errores cuando se introdujeron de forma gradual y no se conoce presumiblemente el inicio que desencadena los ErrPs. Además, los análisis de neurofisiología arrojan algo de luz sobre los mecanismos cognitivos subyacentes que provocan ErrP durante las tareas continuas, lo que sugiere la existencia de modelos neuronales en nuestro cerebro que acumulan evidencia y solo toman una decisión al alcanzar un cierto umbral.

En segundo lugar, esta tesis evalúa la implementación de estos potenciales relacionados con errores en tres aplicaciones orientadas al usuario. Estos estudios no solo exploran cómo maximizar el rendimiento de descodificación de las firmas ErrP, sino que también investigan los mecanismos neuronales subyacentes y cómo los diferentes factores afectan las señales provocadas.

La primera aplicación de esta tesis presenta una nueva forma de guiar a un robot móvil que se mueve en un entorno continuo utilizando solo potenciales de error como retroalimentación que podrían usarse para el control directo de dispositivos de asistencia. Con este propósito, proponemos un algoritmo basado en el emparejamiento de políticas

para el aprendizaje de refuerzo inverso para inferir el objetivo del usuario a partir de señales cerebrales.

La segunda aplicación presentada en esta tesis contempla los primeros pasos hacia un BCI híbrido para ejecutar distintos tipos de agarre de objectos, con el objetivo de ayudar a las personas que han perdido la funcionalidad motora de su extremidad superior. Este BMI combina la decodificación del tipo de agarre a partir de señales de EEG obtenidas del espectro de baja frecuencia con los potenciales de error provocados como resultado de la monitorización de movimientos de agarre erróneos. Los resultados muestran que, en efecto los ErrP aparecen en combinaciones de señales motoras originadas a partir de movimientos de agarre consistentes en una única repetición. Además, la evalanción de los diferentes factores involucrados en el diseño de la interfaz híbrida (como la velocidad de los estímulos, el tipo de agarre o la tarea mental) muestra cómo dichos factores afectan la morfología del subsiguiente potencial de error evocado.

La tercera aplicación investiga los correlatos neuronales y los procesos cognitivos subyacentes asociados con desajustes somatosensortiales producidos por perturbaciones inesperadas durante la estimulación eléctrica neuromuscular en el brazo de un usuario. Este estudio simula los posibles errores que ocurren durante la terapia de neuro-rehabilitación, en la que la activación simultánea de la estimulación aferente mientras los sujetos se concentran en la realización de una tarea motora es crucial para una recuperación óptima. Los resultados muestran que los errores pueden aumentar la atención del sujeto en la tarea y desencadenar mecanismos de aprendizaje que al mismo tiempo podrían promover la neuroplasticidad motora.

En resumen, a lo largo de esta tesis, se han diseñado varios paradigmas experimentales para mejorar la comprensión de cómo se generan los potenciales relacionados con errores durante el uso interactivo de BMI en aplicaciones orientadas al usuario. Se han propuesto diferentes métodos para pasar de la configuración bloqueada en el tiempo a la asíncrona, tanto en términos de decodificación como de percepción de los eventos erróneos; y ha explorado tres aplicaciones relacionadas con el aumento de las capacidades motoras, en las cuales los ErrPs se pueden usar para el control de dispositivos, la sustitución de motores y la neuro-rehabilitación.

Abstract

Brain-machine interfaces (BMIs) allow the decoding of cortical activation patterns from the users brain to provide people with severely limited mobility, due to an accident or disease, a way to establish a direct connection between their brain and a device. In this sense, BMIs based in noninvasive recordings, such as the electroencephalogram (EEG) have offered these users new opportunities to regain control over activities of their daily life that they could not perform otherwise, especially in the areas of communication and control of their environment.

Over the past years and with the latest technological advancements, devices have significantly grown on complexity expanding the number of possibilities to control complex robotic devices, prosthesis with numerous degrees of freedom or even to apply compound patterns of electrical stimulation on the subjects own paralyzed extremities to execute precise movements. However, the band-with of communication between brain and devices is still very limited, both in terms of the number and the speed at which neural commands can be decoded, and thus solely relying on neural signals do not guarantee accurate control them.

In order to benefit of these technologies, the field of BMIs adopted the well-known approach of shared-control. This strategy intends to create a cooperation system between the user and an intelligent device, liberating the user from the burdensome parts of the task without losing the feeling of being in control. Here, users only need to focus their attention on high-level commands (e.g. choose the final destination to reach, or a specific item to grab) while the intelligent agent resolve low-level problems (e.g. trajectory planning, obstacle avoidance, etc) to perform the designated task in the optimal way.

In particular, this thesis revolves around a high-level cognitive neural signal originated as the mismatch between the expectations of the user and the actual actions executed by the intelligent devices. These signals, denoted as error-related potentials (ErrPs), are thought as a natural way to intercommunicate our brain with machines and thus users only require to monitor the actions of a device and mentally assess whether the latter is behaving correctly or not. This can be seen as a way to supervise the device's behavior, in which the decoding of these mental assessments is used to provide these devices with feedback directly related with the performance of a given task so they can learn and adapt to the user's preferences.

Since the ErrP's neural response is associated to an exogenous event (device committing an erroneous action), most of the developed works have attempted to distinguish

whether an action is correct or erroneous by exploiting discrete events under well-controlled scenarios. This thesis presents the first attempt to shift towards asynchronous settings that focus on tasks related with the augmentation of motor capabilities, with the objective of developing interfaces for users with limited mobility. In this type of setups, two important challenges are that correct or erroneous events are not clearly defined and users have to continuously evaluate the executed task, while classification of EEG signals has to be performed asynchronously. As a result, the decoders have to constantly deal with background EEG activity, which typically leads to a large number of missdetection of error signatures. To overcome these challenges, this thesis addresses two main lines of work.

First, it explores the neurophysiology of the evoked neural signatures associated with the perception of errors during the interactive use of a BMI in continuous and more realistic scenarios. Two studies were performed to find alternative features based on the frequency domain as a way of dealing with the high variability of EEG signals. Results, revealed that there exists a stable pattern represented as theta oscillations that enhance generalization during classification. Also, state-of-the-art machine learning techniques were used to apply transfer learning to asynchronously discriminate errors when they were introduced in a gradual fashion and the onset that triggers the ErrPs is not presumably known. Furthermore, neurophsysiology analyses shed some light about the underlying cognitive mechanisms that elicit ErrP during continuous tasks, suggesting the existence of neural models in our brain that accumulate evidence and only take a decision upon reaching a certain threshold.

Secondly, this thesis evaluates the implementation of these error-related potentials in three user-oriented applications. These studies not only explore how to maximize the decoding performance of ErrP signatures but also investigate the underlying neural mechanisms and how different factors affect the elicited signals.

The first application of this thesis presents a new way to guide a mobile robot moving in a continuous environment using only error potentials as feedback which could be used for the direct control of assistive devices. With this purpose, we propose an algorithm based on policy matching for inverse reinforcement learning to infer the user goal from brain signals.

The second application presented in this thesis contemplates the first steps towards a hybrid BMI for grasping oriented to assist people who have lost motor functionality of their upper-limb. This BMI combines the decoding of the type of grasp from low-frequency EEG signals with error-related potentials elicited as the result of monitoring an erroneous grasping. The results show that ErrPs are elicited in combination of motor signatures from the low-frequency spectrum originated from single repetition grasping tasks and evaluates how different design factors (such as the speed of the stimuli, type of grasp or mental task) impact the morphology of the subsequent evoked ErrP.

The third application investigates the neural correlates and the underlying cognitive processes associated with somatosensory mismatches produced by unexpected disturbances during neuromsucular electrical stimulation on a user's arm. This study simulates possible errors that occur during neurorehabilitation therapy, in which the simultaneous activation of afferent stimulation while the subjects are concentrated in performing a motor task is crucial for optimal recovery. The results showed that errors may increase subject's attention on the task and trigger learning mechanisms that at the same time could promote motor neuroplasticity.

In summary, throughout this thesis, several experimental paradigms have been designed to improve the understanding of how error-related potentials are generated during the interactive use of BMIs in user-oriented applications. Different methods have been proposed to shift from time-locked to asynchronous settings, both in terms of decoding and perception of the erroneous events; and it has explored three applications related with the augmentation of motor capabilities, in which ErrPs can be used for control of devices, motor substitution and neurorehabilitation.

Contents

List of abbreviations

ACC	Anterior cingulate cortex
ALS	Amyotrophic lateral sclerosis
ANOVA	Analysis of variance
BA	Brodmann area
BMI	Brain-machine interface
CAR	Common-average referencing
ConvNets	Convolutional neural networks
CSP	Common spatial patterns
CT	Computed tomography
ECG	Electrocardiography
ECoG	Electrocorticography
EEG	Electroencephalography
EOG	Electrooculography
EMG	Electromyography
ERD/ERS	Event-related (de)synchronization
ERN	Error-related negativity
ERP	Event-related potential
ErrP	Error-related potential
ERSP	Event-related power spectral perturbations
FDR	False discovery rate
FES	Functional electrical stimulation
fMRI	Functional magnetic resonance imaging
fNIRS	functional near-infrared spectroscopy
FMθ	Frontal midline theta

FRN	Feedback-related negativity
GA	Grand average
IC	Independent component
ICA	Independent component analysis
LDA	Linear discriminant analysis
LFP	Local field potentials
MEG	Magnetoencephalography
MMN	Mismatch negativity
MPA	Measure projection analysis
MRI	Magnetic resonance imaging
Ne	Error negativity
NN	Neural networks
NIRS	Near infrared spectroscopy
NMES	Nneuromuscular electrical stimulation
PCA	Principal component analysis
Pe	Error positivity
pMFC	Posterior medial frontal cortex
PSD	Power spectral density
RBF	Radial basis function
SCI	Spinal cord injury
SCP	Slow cortical potentials
SMA	Supplementary motor area
SSVEP	Steady-state visual evoked potentials
SVM	Support vector machine

List of Figures

List of Tables

1
Introduction

What makes human brains so special? How do they differ from hearts, livers, and other organs? All organ systems are enormously complicated structures, able to repair themselves and make detailed responses to external control by chemical or electrical input. Yet, only brains yield the amazing phenomenon of consciousness [Ingber & Nunez, 2011].

The brain immediately confronts us with its great complexity. The human brain weighs only one to two kilograms but contains about 100 billion neurons [Nunez, 2012]. Although that extraordinary number is of the same order of magnitude as the number of stars in the Milky Way, the latter cannot account for the complexity of the brain [Fischbach, 1992]. Modern neural science, as we now know it, began more than 100 years ago with the pioneering work of Santiago Ramón y Cajal (1854 - 1934) [Albright et al., 2000]. He provided the critical evidence for the neuron doctrine [Ramón y Cajal, 1995]. This doctrine profess the idea that neurons serve as the functional signaling units of the nervous system and that neurons connect to one another in precise ways processing and transmitting electrophysiological signals. This work, which was continued by numerous interdisciplinary specialists has provided a wealth of data creating the basis in the emergent field of brain research.

The first recording of neural activity was performed by Hans Berger in 1924, when ha placed the first scalp electrodes to observe alpha rhythms [Berger, 1929]. Since then, advances in technology have grown exponentially to develop different measuring techniques to record brain activity at a wide range of spatial and temporal scales (see Figure 1.1). Methods to measure brain activity are mainly classified according to their invasiveness. In the non-invasive side, we can find structural or static imaging measure changes on time scales that go from weeks to years and is accomplished with computed tomography (CT) [Miles, 2006] or magnetic resonance imaging (MRI) [Ogawa et al., 1990]. By contrast, intermediate time-scale methods like functional magnetic resonance imaging (fMRI) [Huettel et al., 2004], positron emission tomography (PET) [Bailey et al., 2005] and near infrared spectroscopy (NIRS) [Cope et al., 1988] track brain changes over seconds or min-
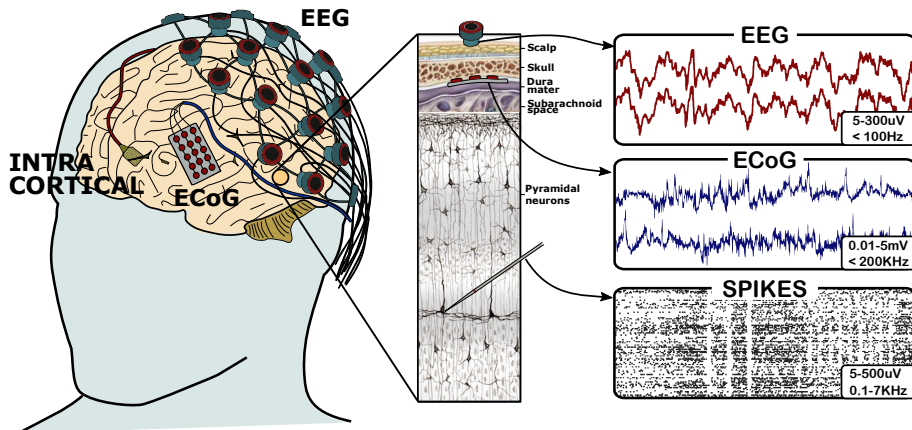
Figure 1.1: Main methods available for the study of the nervous system according to their invasiveness and spatio temporal resolution.

utes. More rapid dynamic measures are electroencephalography (EEG) [Niedermeyer & da Silva, 2005] and magnetoencephalography (MEG) [Hämäläinen et al., 1993], which operate with a resolution of milliseconds. On the other hand, invasive techniques require a neurosurgery procedure that involves opening the scalp and skull and penetrating the brain tissue. Sensors are very close to the source of neural activity and can be used to accurately measure trains of action potentials from single neurons [Li & Jasper, 1953] or large neuronal populations represented as local field potentials (LFPs) [Denker et al., 2011]. An intermediary approach that requires opening the skull but do not involve sensors penetrating the nervous tissue is known as electrocorticography (ECoG), in which a grid of electrodes is placed on the brains surface [Anderson et al., 2012]. The quality of the acquired signals usually increases with the invasiveness of the method since with invasive techniques the probe is closer to the source. However, intracranial electrodes implanted in living brains require surgical procedures and provide only very sparse spatial coverage, thereby failing to record the "big picture of brain functionality. Thus, despite their superior spatial and temporal resolution, in practice, intracranial data provide different information, not necessarily more information, than is obtained from the scalp [Nunez & Srinivasan, 2006].

In this thesis, we focus on non-invasive recordings, and more specifically in the ones that use electroencephalography. EEG measures the electrical activity of the brain recorded by means of electrodes placed on the scalp. The EEG arises from synchronized synaptic activity in populations of pyramidal neurons organized along cortical columns. In order to be measured with an electrode outside the head, the electrical signal has to travel from the brain, through the dura layers, the skull, and the scalp before finally reaching the EEG

sensors. Furthermore, the electrical activity of an individual neuron is too small to be measured as far away as the scalp, thus electrodes detect the sum of mixed activity from multiple neurons in their vicinity that produce a greater voltage than the firing of a single neuron [Kandel et al., 2000; Jackson & Bolger, 2014]. However, because the polarity of neurons can be both positive and negative, electrodes will only record measurable signal if neurons are arranged in a parallel fashion and fire synchronously. The combination of these factors provokes a smearing/attenuation effect on the measured signal leading to low signal-to-noise ratio and lack of fine spatial resolution. Nevertheless, EEG provides most of the existing data on neocortical dynamic behavior and its relation to cognitive events in humans. EEG posses numerous advantages, such as being a non-invasive technique with a very good temporal resolution, commercially available, easy to set-up and robust to possible external interferences. All of these elements made that, since its origins, EEG recording techniques were extendedly used in clinical environments to evaluate neurological disorders [Kuhlman, 1978; Sterman, 2000], and in laboratories to investigate brain function [Rockstroh, 1989] and therapeutic possibilities [Rice et al., 1993].

1.1 Brain-machine interfaces

In the early 1960s, a different application of EEG was born as a theoretical proposition on linking brains with machines, so that a person could interact with others or control devices only through mental commands without to activating the brain's natural output pathways of muscles or peripheral nerves [Vidal, 1973]. However, it has not been until the end of the 1990s, with the development of new technologies for sampling large-scale brain activity, when EEG based communication started to attract scientific attention, giving birth to brain-machine interfaces [Wolpaw et al., 2002].

A brain-machine interface (BMI) combines methods derived from neurophysiology, psychology, computer science, and engineering in an effort to establish real-time links between living brains and artificial actuators without the participation of peripheral nerves and muscles [Lebedev & Nicolelis, 2017]. They were primarily conceived as an alternative tool to joysticks, keyboards or eye-trackers, designed for people with severely limited mobility or cognitive impairment, being the most extreme case a person who has lost control of every part of his body including eye movements (i.e. locked-in syndrome [Kübler et al., 2001]). With this purpose, technologies based on computer displays, prosthetic devices and robotic systems were implemented and properly adapted to offer these users new opportunities to regain control over activities of their daily life that they could not perform otherwise, especially in the areas of communication and control of their environment.

In terms of communication, and depending on the motor and cognitive limitations of

the users, BMIs empower these patients with tools that range from emitting responses to open questions that can be answered with a "yes" or a "no" (i.e. "Are you hungry?") to controlling electronic devices similar to a keyboard (BMI-spellers) that allows them to compose words or even messages by focusing their attention in the characters they want to spell [Birbaumer et al., 1999; Donchin et al., 2000]. BMIs were also conceived for the control of devices, in which thoughts about different mental tasks can be decoded and translated into commands for a robotic device. For example, these BMIs could be used to enable a paralyzed patient to mentally drive his own BMI-adapted wheelchair [Millán et al., 2009] or manipulate a telepresence wireless robot from his own bed [Escolano et al., 2011].

Nowadays, these precursory BMI applications have gone through several improvements, and even though they are still under development, some of them have been successfully deployed at patients' homes. Interestingly, recent technological advancements did not only enhance the potential of these two aforementioned BMI applications but also expanded the scope of BMI usability. Particularly, the medical community has gained special interest in the concept of controlling assistive devices that can be deployed in clinical scenarios to help people in their recovery from motor injuries. Thus, in recent years, the focus of researches has been set on finding new ways of control directly linked to the usage of voluntary movement-related neural correlates to drive a BMI [de Jong et al., 2006]. In this sense, several studies Pfurtscheller et al. [2003]; López-Larraz et al. [2014]; Rupp et al. [2015] have demonstrated that is possible to decode the intention of performing a movement from users' brain signals to control orthosis or activate electrical stimulation of users' muscles. This has direct applications in the field of neurorehabilitation, which facilitates the recovery of patients who have reduced motor functionality by providing user-dependent therapies. Additionally, even if patients are unable to fully recover from their motor impairments, BMIs have proven to be also useful in the practice of motor substitution. Here, robotic prosthesis can be mentally controlled to replace the movements of the patients' own limbs, thus improving the quality of life of these users [Pfurtscheller et al., 2000; Müller-Putz et al., 2005]. Furthermore, EEG-based BMIs are also evolving towards non-therapeutic applications such as entertainment (gaming [Krepki et al., 2007; Krauledat et al., 2009], painting [Kübler et al., 2008], virtual reality [Bayliss, 2003; Leeb et al., 2007]).

Although BMI research will likely continue to focus on medical applications, as BMI progress continues, in a near future even healthy users could benefit from the use of this technology as if it was an extension of ourselves. Applications such as texting with our minds [Herff & Schultz, 2016], tunning the air conditioning at home just by thinking about the right temperature [Guger et al., 2008], or even driving a car [Zhang et al., 2015b] are
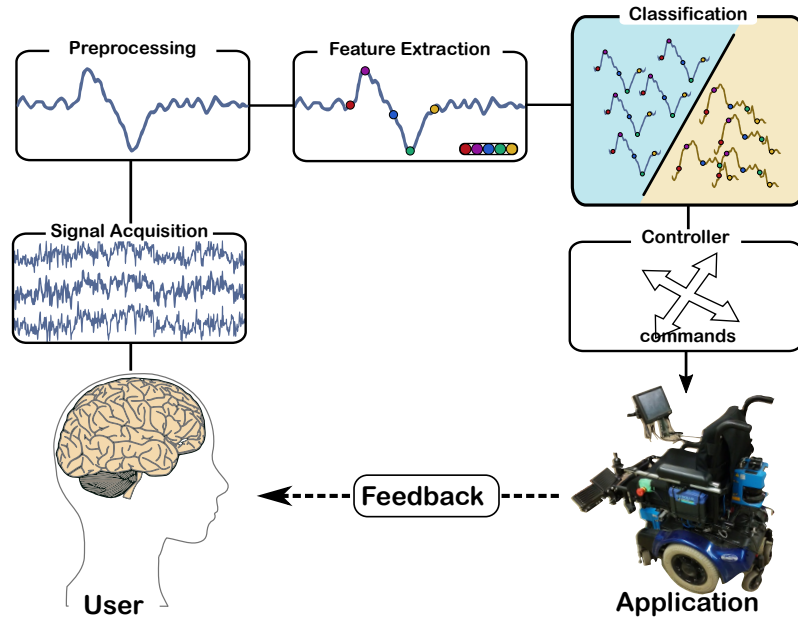
Figure 1.2: Diagram of a standard brain-machine interface. First, brain signals are extracted using one of the previously mentioned recording techniques (in the case of EEG, through electrodes placed on the scalp). Then these signals are processed and some features are extracted and sent to a classifier. The classification of such features results into commands for a device that will provide further feedback to the user.

just an example to the plausible future uses of these systems. In view of the limitless possibilities, many people that are not familiarized with the functionality of BMIs assume that these systems allow to listen into our brains and transmit the same information that other interfaces could otherwise provide in an easier and faster way [Allison et al., 2007]. Up to today, this perspective is not completely accurate. So how does a BMI really work?

In order to successfully communicate brain and machine, the BMI has to be able to distinguish specific features of brain activity patterns associated to a particular intention that will be identified by the system and translated into commands [Wolpaw et al., 2002]. Importantly, decoding these signals elicited during the interaction of human and machine must be done (with a few exceptions) in a single trial basis so they can be used to control a device in real time [Millán et al., 2010]. Figure 1.2 portrays this process. First, the electrical activity recorded from the scalp is processed and transformed in order to extract some relevant features that are then fed onto a classification algorithm. These features are coupled to a specific data-class and encode different information depending on the performed task. Ultimately, due to the large EEG sources of variability [Vidaurre et al., 2011b], for each subject and for each new task, it is necessary to execute a calibration phase in which the classifier learns how to map EEG activity onto the control space. As a result,

the class of future data can be automatically estimated and translated into commands that operates the device [Lotte et al., 2007]. Generally, BMIs can be categorized according to the experimental strategy that the user applies as input:

- Based on specific mental tasks, where users can learn to voluntarily modulate their brain activity performing mental orders such as word association, mathematical operations, auditory imagination, or the most commonly used, imagination of motor commands [Friedrich et al., 2013]. These systems based on sensorimotor rhythms or motor related cortical potentials use components in the frequency or time domain that are spontaneous in the sense that they are not dependent on specific cue-based events. Given their asynchronous essence, this is the preferred (but not the only) strategy for tasks of control [Pfurtscheller & Da Silva, 1999; Birbaumer et al., 2000; Wolpaw & McFarland, 2004].

- Based on focused attention on external stimuli. The EEG signals are obtained from the attention to endogenous synchronized events (visual, auditory, or tactile). These signals, also denoted as event-related potentials (ERPs), are generated by a population of neurons in response to a perceptual, cognitive or motor stimuli. In general, this strategy is easier to perform, since the BMI only requires that the user provides a goal or target for a predetermined task (by focusing on a specific stimuli) and the BMI can manage the rest of the real-time interaction to complete the job. Typically, the most commonly used ERPs are the P300, a positive deflection in parietal areas of the ongoing EEG about 300 ms after the occurrence of a particularly significant stimulus [Donchin et al., 2000]; or steady-state visual evoked potentials (SSVEP), EEG patterns generated in response to a rapid succession of visual stimuli that evoke a steady wave easily measured in the frequency spectrum [Müller-Putz & Pfurtscheller, 2008]. As most of these evoked potentials require a computer screen to be generated, this strategies are often found in applications for communication.

Whether the systems are based on specific mental tasks or on focused attention to external stimuli, in many of these approaches tasks tend to be artificially assigned with actions that are not intuitive for the users. Consequently, recent research has moved towards a third mental strategy based on natural control. This approach exploits brain patterns that are closely related to the user's intentions, thereby they constitute a natural and intuitive way of control, which is key to develop interfaces that users feel comfortable using in daily life activities. Especially, in contexts of rehabilitation and motor substitution there are naturally generated neural signatures that comes from motor related activity. Some examples are the readiness potential (originally Bereitschaftspotential), that reflects activity in the motor cortex during voluntary muscle movement preparation [Libet et al.,

1983]; oscillations in the low-frequency spectrum (14 Hz band), also denoted as slow cortical potentials (SCPs), used to decode distinctive information of movement kinematics, such as movement direction [Pistohl et al., 2008], hand position and velocity[Gu et al., 2009] or even grasping movements [Jochumsen et al., 2015]; and cognitive monitoring signals derived from mental states (fatigue, emotions, concentration, observed errors to name a few) [Zander & Kothe, 2011].

Notice that, as other conventional interfaces such as keyboards, joysticks or car steering wheels, BMIs take an input (in this case, one of the previously described mental strategies) and use translation algorithms to convert it into an output (words in case of communication, or commands for a device in the case of control). However, compared with the former conventional interfaces, BMIs transmit much lower information (they have a limited band-with) and they are less accurate (sometimes the decoding of brain signatures fails and they commit errors). For some applications this is not a hefty issue, for example BMI-spellers designed for people suffering from tetraplegia or amyotrophic lateral sclerosis (ALS) [Wolpaw et al., 2000]. These systems allow them to spell an average of 7 letters per minute, but when the patients do not possess any other way to communicate, slow communication is better than no communication. Per contra, these BMIs have been considered too slow for controlling rapid and complex sequences of movements, and with technological advancements also came the necessity of controlling devices with a higher number of degrees of freedom. In this sense, traditional BMIs may not be efficient to maintain high levels of control [Kronegg et al., 2005].

Shared-autonomy or shared-control was proposed as a way to surmount the bandwidth issue. Some investigation groups have already started to apply this concept in order to divide control tasks between two intelligent parties, the human user and the operated device [Galán et al., 2008]. Within this framework, an intelligent agent can be programmed to emulate control strategies by taking automatic decisions related with the requirements of the task to be performed while the user only require to provide high-level commands [Iturrate et al., 2009]. The implementation of shared-control strategies has supposed significant improvements in the way users can communicate with devices, since the user only needs to issue a high-level command and he can relax while the autonomous agent plans and executes the low-level commands necessary to accomplish the task. With that said, there still exist at least 2 drawbacks that remain unsolved.

- On one hand, shared-control do not face the aforementioned issue in which every BMI has a certain degree of misdetections. Consequently, chances are that the device manifests erratic behaviors that will not match with the user's expectations.

- On the other hand, systems that implement this strategy use to be based on rigid

paradigms that have been preprogrammed for a specific application. This is useful in terms of carrying out the designated task, but often it results in lack of adaptability to the user's requirements.

What do we humans do to adapt to our environment? And how could we transfer human adaptive behavior to improve BMI control? Neurophysiology studies have reported that humans present a common behavior for adaptation [Rabbitt, 1966]. This consists in continuously monitoring our daily activities, evaluating the adequacy in which we perform these tasks, so we can implement appropriate behavioral adjustments in case they are needed [Ullsperger et al., 2014b]. Let us look to an example. Since we are born, we learn how to perform the tasks that will form part of our daily life in a trial-and-error basis. Before we master the skills of walking, riding a bike, grabbing objects or even playing tennis we have to fail repeatedly. This iterative process works because immediately after we are aware that we have committed a mistake there are brain mechanisms that account for this error and adjust our future actions so we minimize the number of misdoings. In other words, we use our own errors as a reinforcement learning mechanism [Sutton & Barto, 1998] to correct and adapt our behavior. Then, the question is: Is it possible to capitalize on the errors that inherently appear during the control of a BMI and exploit them to enable the correction of actions executed by an intelligent device and/or to improve its adaptability? And more precisely, how can we use this information in control tasks such as controlling external devices, motor substitution or neurorehabilitation?

1.2 Error related signatures

To answer the preceding questions, in this thesis we focus on a specific cognitive signal directly related to the user's error processing mechanisms. Nowadays, it has already been demonstrated that brain signatures elicited from the perception of errors can be measured from the user's EEG, appearing as a special kind of event-related potential (ERP) that originates after the user commits or observes an error. Usually, these signals have a poor signal-to-noise ratio but since they are associated to an external stimulus, it is possible to extract time-locked averages of several repetitions to a common stimulus response, therefore eliminating most of the random noise while conserving the intrinsic essence of the ERP components.

Take as an example a virtual cursor performing discrete movements on a computer screen (represented by a blue square in Figure 1.3(left)). Let us say that an observer knows that the objective of this cursor is to reach a desired target position (green square), in this case by moving towards the left. However, if the virtual cursor does not know the location of this target, its movements will be random. Figure 1.3(right) depicts the aver-
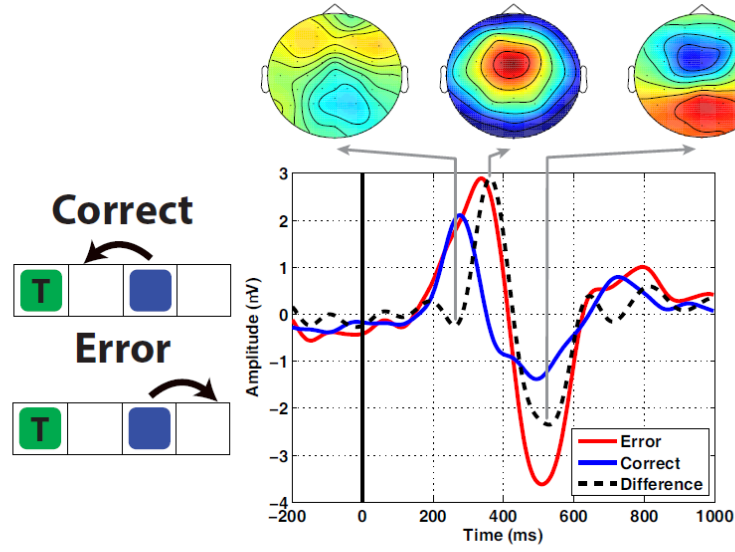
Figure 1.3: Left: Reaching task in which a virtual cursor (blue) has to reach a desired target location (green) moving in a 2D grid. Random movements through the grid evoke correct and erroneous neural responses in an external observer's brain. Right: Average of the EEG signals recorded during several repetitions of correct (blue) and erroneous (red) movements of the virtual cursor. Difference between error and correct responses (black-dashed line) corresponds to the mental process of error processing.

aged neural responses elicited in the observer's brain after monitoring several repetitions of correct (blue line) and erroneous (red line) actions executed by the virtual agent. Here, the difference between brain responses to correct and incorrect events (dashed-black line) represents the cognitive contribution of error processing mechanisms. Managing to successfully decode these potentials on-line, would enable a potential user to provide natural feedback for an intelligent controller so it could learn from its mistakes and through an iterative process adapt to the user's preferences (see Figure 1.4). This being said, our objective consists on using this type of signals in the context of motor-related applications such for the control of mobile devices, to accelerate the recovery in neurorehabilitation therapies or even to substitute the movements of a lost limb. However, as it will be shown shortly, sometimes this requires to better improve the understanding of how these errors are generated during the interactive use of a BMI and how to implement them in a natural way to obtain the optimal performance.

Keeping our objective in mind, in this section we present an overview of error-related neural correlates research. First, we introduce experimental findings both in neuroscience and in the field of BMIs where EEG signatures related to error processing have been observed. Secondly, we review the most recent theories about the underlying neural mech-
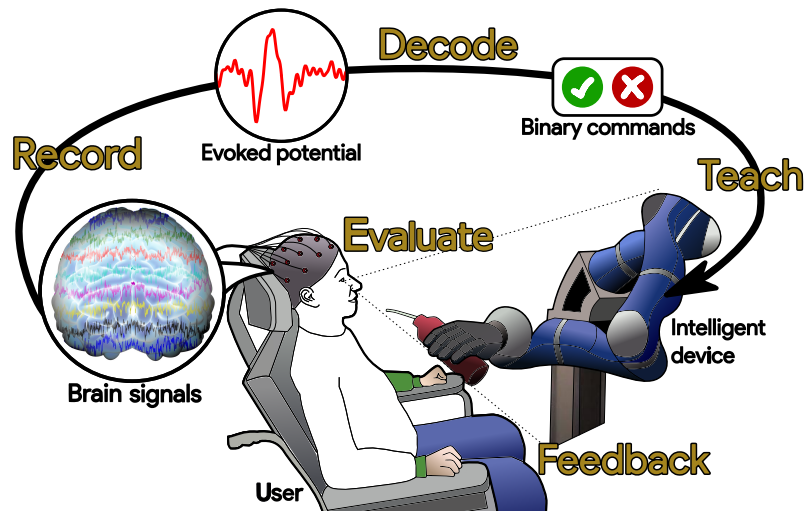
Figure 1.4: Brain-machine interface using shared-control and error-related potentials. In this type of BMI, EEG signals are recorded from the scalp and processed as in a standard BMI. However, instead of decoding brain patterns to directly control an external device, the latter has the ability to perform intelligent actions. Thus, the user only requires to mentally asses the correctness of the device's actions to teach it reach a mutual goal.

anism that give rise to these error potentials. Lastly, we describe the current framework of errors in the context of BMIs: applications, challenges and our proposed approach and contributions.

1.2.1 Errors in the literature. Tasks, names and morphology

In the literature, these EEG neural correlates related to error processing have been analyzed under different experimental conditions and have been assigned names depending on the tasks in which they have been observed and the variability of their spatio-temporal signatures. First evidence of these neural correlates was observed during an ERP study associated with error commission where subjects performed a fast choice reaction task. The most common example is the Eriksen Flanker task, where subjects have to rapidly identify whether a target stimulus has congruent/incongruent directional response according to the surrounding non-target stimuli [Eriksen, 1995]. The elicited potential is characterized by a negative deflection at midline fronto-central scalp locations 100 ms following error commission, and has been termed as "error negativity" (Ne, [Falkenstein et al., 1991]) or more commonly "error-related negativity" (ERN, [Gehring et al., 1993]). This negative deflection is followed by a centro-parietal positive component, denoted as "error positivity" (Pe) [Falkenstein et al., 2000] between 200 and 500 ms after the response, see representations

of Figure 1.5(top).

ERN is usually observed when the subject commits an error, but it has also been observed in the presence of negative feedback, often called feedback-ERN or feedback-related negativity (FRN) [Hajcak et al., 2006]. The FRN, peaks between 250 to 300 ms after the presentation of feedback stimulus (e.g. losses in gambling tasks [Miltner et al., 1997]). Commonly, FRN is followed by a parietal positivity referred to as P3b, a delayed subcomponent of the P300 [Nieuwenhuis et al., 2004], see Figure 1.5(middle). In this sense, FRN can be elicited by different feedback stimuli, including auditory [Tourville et al., 2008], visual [Goodale et al., 2004] and somatosensory [Miltner et al., 1997].

More recently, similar neural correlates have also been observed when the errors are committed by a different person or by a computer/device, which had a main impact in the BMI community and received the name of error-related potentials (ErrPs) [Ferrez & Millán, 2008a]. These error signatures are related to observation [Chavarriaga & Millán, 2010; Pavone et al., 2016] and interaction errors [Iturrate et al., 2014; Spüler & Niethammer, 2015]. They share very similar morphologies [Kim & Kirchner, 2016], a sharp negative fronto-central peak at 250 ms, followed by a centro-parietal positivity after 320 ms and a second broader fronto-central negative peak around 450 ms. Frequently, these peaks are denoted using their respective sign and latency (N2/P3/N4), see Figure 1.5(bottom). A representative paradigm to generate this kind of error potentials consists in a virtual cursor that spontaneously moves towards right or left direction. An ErrP will be elicited whenever the device moves in a direction contrary to the desired one [Iturrate et al., 2014]. For a detailed visual description of the most typical tasks investigated in neuroscience and their corresponding error correlates measured at the scalp, see Figure 1.5.

1.2.2 Theories on functional significance of error processing mechanisms

It is not entirely clear to what extent these signals share common underlying processes. However, regardless of their name and nature, neuroimaging and neuropsychological studies have consistently shown that the posterior medial frontal cortex (pMFC), and in particular the dorsal anterior cingulate cortex (ACC, see middle area of Figure 1.5), is activated during tasks that involve error processing mechanisms [Dehaene et al., 1994; Carter et al., 1998; Pizzagalli et al., 2001; Debener et al., 2005]. Nowadays there exist (at least four) different theories that attempt to explain the link between neural signatures recorded at the scalp (ERN/FRN/ErrP) and the ACC.

During the first years after the discovery of the ERN, the dominant view suggested a "comparator theory" [Coles et al., 2001]. A comparison process computes the difference between the internal representation of a correct response and the actually performed action. The mismatch between these two representations originates the error signal and
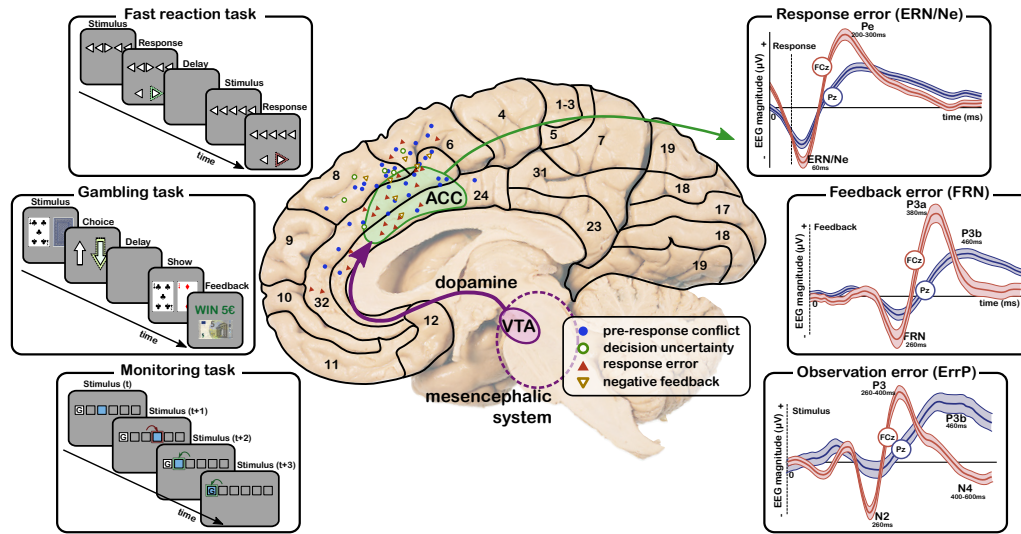
Figure 1.5: (Left) Most common tasks applied in the study of error processing described in the bibliography. (Right) Associated neural correlates to each one of these tasks. (Middle) Schematic interpretation of the reinforcement learning approach next to activation origin of errors reported in 38 fMRI studies published between 1997 and 2004 investigating brain activity associated with pre-response conflict, decision uncertainty, response errors, and negative feedback. The majority of activations cluster in the posterodorsal medial frontal cortex, in the region where areas 8, 6, 32, and 24 border each other. Parts of the figure have been adapted from Ullsperger et al. [2014a].

the amount of discrepancy is the main influence on its amplitude. In this model, the ERN could reflect the output of the comparison process, where the ACC acts like the comparator [Brooks, 1986].

An alternative point of view discussed that in order for the previous "comparator theory" to work, the brain would need to have access to the correct action. Thus, why is not the brain executing the correct response? [Botvinick et al., 2001; Yeung et al., 2004; Gehring et al., 2018]. Instead, it was postulated that the ACC is involved in a "conflict-monitoring" process [Carter et al., 1998; Botvinick et al., 2001; Yeung et al., 2004]. Response conflict occurs when a task concurrently activates more than one response tendency. In this way, response conflict can track performance accuracy without the brain knowing which response is correct. Thus, the addition of activations for erroneous and correct response tendencies at the time of the response is the main factor that modulates ERN amplitude.

Currently, the most accepted theory suggests that reward prediction error signals are conveyed to the ACC via phasic changes in the activity of the mesencephalic dopamine system. Thereafter, the ACC uses these signals to reinforce adaptive behaviors [Holroyd

& Coles, 2002]. The rational adopts a "reinforcement learning" approach and holds that the ERN is elicited when a neural system detects that the mismatch between the expected and actual outcomes of an action are worse than expected and use it to train the motor system to improve task performance. Furthermore, it proposes that the degree of success or failure of an action modulates the phasic dopamine signals, which can be measured at the scalp as changes in the magnitude of the ERN.

A recent extension to the reinforcement learning framework is the prediction of response outcome theory [Alexander & Brown, 2010]. This hypothesis suggests that the medial prefrontal cortex predicts the outcomes of an action based on past experiences, and it compares the predicted response outcomes to the one that actually occurs. Unlike in the previous approach, this model is not dependent on a dopaminergic signal and does not distinguish between correct or erroneous outcomes. Therefore, the main determinant of ERN amplitude on a given experimental trial is the perceived probability of the occurrence of an error in that trial [Brown & Braver, 2005]. Thus, if the most expected outcome to a given event is an undesired one, this will not generate an ERN, while it would be present for an unexpected correct outcome.

1.2.3   Application of errors in BMIs.

Despite there is still no consensus about the specific neurophysiological mechanism that underly the generation of brain signals related to the monitoring of errors, a large volume of studies reporting error-related neural correlates both in neuroscience (ERN and FRN) or in the BMI field (ErrPs) have consistently used EEG to measure these signatures in the scalp areas over the ACC. Most of these studies have designed experimental paradigms where responses to errors come triggered by a discrete and well-controlled feedback stimulus. Precise event onsets facilitate to exploit the time-locked nature of such neural correlates, which yields higher signal to-noise ratios, beneficial for both the characterization and the decoding of error-related potentials. Additionally, several studies have shown that error-related signatures are rather stable and do not vary significantly over time [Chavarriaga & Millán, 2010]. Yet, a recent study proved that different tasks of these BMIs induce a magnitude and phase change in the components of error potentials [Iturrate et al., 2012] which has also been reported in experiments that studied stimuli contrast [Luck, 2014], the dependence on error likelihood [Chavarriaga & Millán, 2010] or the need to keep subjects focused and engaged in the task [Hajcak et al., 2005].

In lights of this, the field of brain-machine interfaces generally concentrates its efforts in the design of experimental paradigms and classification algorithms to decode these neural correlates in a single trial basis, so they can be used to control devices [Millán et al., 2010]. These decoding techniques usually exploit the raw temporal signal of these potentials (i.e.

the amplitude and latency of the ErrP at several channels), which in principle encodes different information for correct and wrong events evaluated by the user. In fact, several studies have already demonstrated the feasibility of decoding error signals originated when a human observes a device committing an error with classification accuracies superior to 80% [Schalk et al., 2000]. Some of the most common usages of ErrP decoding in the field of BMI is to complement other neural correlates such as motor rhythms in applications for the on-line correction of the BMI's output or recalibrating the internal BMI classifier. In the former application, ErrPs are exploited to rectify the initial decision of a BMI in order to prevent an erroneous command from being fully executed [Blankertz et al., 2003; Ferrez & Millán, 2008b; Dal Seno et al., 2010]. In the latter, ErrPs that appear after the BMI have executed a mistake can be applied to recalibrate the system using this newly recorded information related to the error and reduce the possibility of errors reappearing in the future [Artusi et al., 2011; Llera et al., 2011, 2012]. A more complex application of ErrPs consists on utilizing them as a unique signal to control the BMI. Figure 1.6(left) depicts a possible application of ErrPs in this context. ErrP decoding is used for learning sequential policies that enables a device to execute optimal strategies to reach a designated goal [Chavarriaga & Millán, 2010; Iturrate et al., 2013a]. The working principle relies on a user that monitors the actions of a computer cursor performing step by step movements in a two-dimensional grid. According to the correctness in which the device take course of action, different (correct/error) potentials are elicited. Hence, these evoked potentials intrinsically linked to each movement are used as feedback so the intelligent agent can learn the optimal behavior to perform at each state and ultimately reach the desired position.

The previous studies have done an excellent work to show that in well-controlled laboratory conditions, single trial errors can be detected for a wide variety of control protocols. In this sense, as displayed in Figure 1.6(left), the tasks that have been designed to elicit error responses commonly exploit abstract stimuli as a means to capitalize on the favorable properties of the time-locked signatures, which leads to applications that may not have a clear relevance for the users.

In this thesis we go a step further and aim at exploiting error-related potentials generated in situations that are natural and meaningful for the target population which in this case are applications directly linked with the augmentation of motor capabilities such as the control of devices, restoring or substituting paralyzed limb functionality and to enhance recovery during neuro-rehabilitation therapy. But what happen when we attempt to transfer these experimental paradigms to more realistic and asynchronous scenarios? In most of our daily life routines, specially those related with motion, the executed actions appear as gradual changes rather than sudden sequential movements (e.g. BMI controlled wheelchairs [Galán et al., 2008; Iturrate et al., 2009] or robotic arms [Kreilinger et al.,

DISCRETE PROTOCOL   **CONTINUOUS PROTOCOL**

(a)   (b)
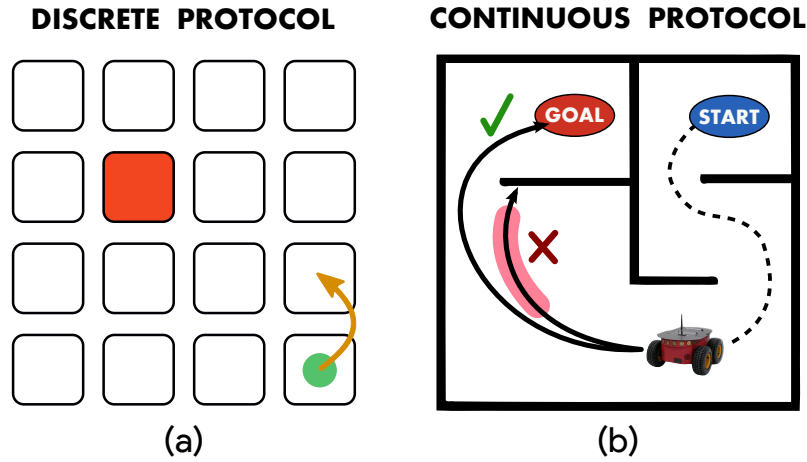
Figure 1.6: (Left) Discrete scenario, where a device performs discrete actions within a grid to reach a goal location (shadowed in red). (Right) Continuous scenario, where a mobile robot is navigating continuously through a maze. The error may be detected all along the shadowed part of the trajectory.

2012]). In these more realistic scenarios there may not exist a clear event that elicits the associated error potential. Figure 1.6(right) exemplifies this situation for a wheelchair navigation problem. The user is maneuvering his wheelchair through different rooms and at a given moment it slightly deviates from the correct path and collides with a wall. At this point, it is virtually impossible to precise when the device started to deviate and thus, when the error-related potential will be elicited. Indeed, the cognitive evaluation of detecting when the error occurs will depend on the subjective perception of each user, which introduces a considerable number of challenges to be solved before these ErrPs can be detected on-line.

- On one hand, in this type of setup, users continuously assess the controlled device behavior and, consequently, there is no such a thing as correct events. Instead, asynchronous detection has to deal with background EEG activity over longer periods of time.

- Secondly, since features based on the temporal domain are commonly exploit for the decoding of ErrPs, constantly dealing with background EEG may result in a large number of false positives, as EEG oscillations can easily resemble ErrP patterns.

- Last but not the least, the lack of fixed points in time to trigger the events makes it difficult to extract information to train our classification models to detect erroneous events during on-line control of a device.

In order to do overcome these challenges and develop natural and intuitive BMIs capable to adapt to the user specifications, this thesis addresses two main lines of work. With an eye on the discussed challenges, first we explore different factors that help us to improve the decoding of ErrPs in an asynchronous approach. In this sense, we seek to design new methods to train machine learning algorithms as well as to find alternative features that increase classification robustness, along with understanding the underlying cognitive mechanisms that triggers the generation of ErrPs during the performance of continuous tasks. Secondly, once the feasibility of asynchronously detecting neural responses associated to cognitive events has been demonstrated, we present three promising applications related with motion assistance. Namely, we have used ErrPs to: **i) Control devices** by teaching a mobile robot to navigate in a 2D continuous map and reach the desired destination. **ii) Motor substitution** tasks where errors can be combined with other natural neural correlates and assist to correct grasping movements to grab an object. **iii) Neuro-rehabilitation** therapies with muscular electrical stimulation, where the improper stimulation causes error-related signatures that can be further use to improve these therapies and promote motor learning.

1.3 Contributions

Following the aforementioned objectives of this thesis and focusing along the first line of work, we propose:

- **Usage of alternative features:** Exploring the usage of features in the frequency domain as a way of dealing with the signal variability induced by different tasks in the ErrP correlates observed in the temporal domain. In particular, we propose the usage of theta power ([4-8 Hz]), which have been linked to an associated event-related synchronization [Cohen, 2011], as a feature that enables a classifier to generalize better among different tasks. Our hypothesis relies on the less sensitive characteristics of frequency features to phase shifts variations, which in principle should lead to more stable patterns to train task-independent classifiers.

- **From time-locked to asynchronous error decoding:** We introduce a method to asynchronously detect error potentials in continuous scenarios. Unlike other asynchronous classification methods, we do not solely observe the evolution of a decoder's output around a known event, but we contemplate the continuous classification of the ongoing EEG, as we do not have prior knowledge of at what point the event is going to occur. The novel approach that we propose consists on using the neural correlates associated with clearly marked erroneous actions produced by a sudden change in direction to extract the features that characterize the occurrence of an error. Then, considering the good generalization properties of the spectral domain, time and frequency features can be combined using non-linear pattern recognition algorithms to train a classification model. Furthermore, state-of-the-art machine learning techniques, such as transfer learning, allow to apply the model trained on the sudden condition to asynchronously discriminate the hidden neural information related to error processing when the errors are introduced in a gradual fashion and thus, the onset that triggers the event is not presumably known.

Successful decoding of error-related signatures in continuous settings encourages us to open lines of investigation that aims to evaluate the application of these potentials in people with severe motor disabilities which is the principal target user group of BMIs today. Specially, this could have important benefits for the development of BMI applications in the context of restoration or motor substitution in which clinical population with limited ability to perform movements could still evaluate the correctness of actions performed by a device. In this second line of work, we transfer the tools and knowledge acquired from the two previous studies and show how to implement error-related signatures in applications of control of devices and the field of rehabilitation and motor substitution.

- **Control of devices: Teaching a mobile robot to navigate.** The first application-based study of this thesis aims to apply the previously developed tools to achieve the real-time control of a mobile robotic device. This thesis explores how to integrate the decoding of neural correlates associated to cognitive error signals for the control of intelligent devices. Specifically, we show how to exploit ErrPs as a stand-alone signal for the control of a real robot moving in a continuous space, in contrast with discrete action and state spaced presented in the literature Zander & Kothe [2011]. Here, we implement reinforcement learning techniques based on policy matching to infer the user's desired specifications from brain signals elicited during the continuous monitoring of this mobile device performing a reaching task.

- **Motor substitution: Hybrid BMIs for natural grasping.** Usually EEG-based systems lack of enough reliability, preventing them from being deployed at people's homes. One of the reasons is that BMIs tend to focus on the decoding of a single neural correlate to control device with numerous degrees of freedom, whereas we employ considerably larger sums of cognitive information to perform daily life activities. Then, why limit the inflow of information to one single biosignal channel? In this sense, hybrid BMI systems [Pfurtscheller et al., 2010; Müller-Putz et al., 2015] have been proposed as a special type of BMI that combine multiple sources of information to tackle new applications or to increase reliability, robustness and performance [Rohm et al., 2013; Rupp et al., 2015]. For our second application, we propose a hybrid BMI to perform a grasping task using brain processes that appear naturally during the task. Here, we use a 3D environment that recreated a real-life grasping scenario to validate our paradigm in which first, the type of desired grasp can be directly decoded from slow cortical potentials originated from single repetition of executed/imagined user's intended movement. And second, the action can be corrected based on ErrPs decoded while observing the execution of the decoded grasp. Furthermore, we analyze variations in morphology of the ErrP responses due to changes of different design factors that have to be carefully considered when designing a hybrid BMI, and how they affect the system performance.

- **Neurorehabilitation: Error signatures during neuromuscular stimulation.** The last application for patients that have suffered motor impairment conditions is focused in rehabilitation, so these people are able to relearn how to perform activities of their daily life through learning process. Whereas, traditional therapies have focused on passive facilitation of isolated movements or compensatory movements, innovative tendencies emphasize the importance of techniques that promote changes in the central nervous system. Among these novel techniques, neuromuscular elec-

trical stimulation (NMES) has been widely proposed as an effective treatment of recruiting non-damaged motor areas through afferent pathways to execute more effective movements [Cauraugh et al., 2000]. However, despite the large number of experiments on NMES, it has never been studied how mismatches in the afferent stimuli affect the neural correlates modulated in the brain. In this thesis, we hypothesize that unexpected disturbances during NMES will trigger brain mechanisms similar to those observed in error processing tasks. In this sense, we investigate the neural correlates elicited when different type of errors occur during the NMES on the superior limb.

In summary, this thesis: (*i*) propose spectral features to cope with generalization limitations of features in the time domain, (*ii*) presents a novel approach to decode error-related events in asynchronous scenarios where errors are introduced in a gradual fashion; and applies these tools to implement the usage of ErrPs in three BMI applications. (*iii*) Controlling a small mobile robotic device in a reaching task. (*iv*) The designing of a hybrid BMI for natural grasping of realistic objects. And finally, (*v*) investigation and characterization of the neural correlates originated from errors occurring during neuromuscular electrical stimulation for motor learning.

1.4 Scientific dissemination

The lines of work presented in this thesis have given rise to scientific advances divulged in international peer-reviewed journals and international conferences.

Publications in journals:

- J. Omedes, E. López-Larraz, A. Insausti, C. Bibian, L. Montesano, N. Birbaumer, A. Ramos-Murguialday . **Brain signatures of afference mismatch during neuromuscular electrical stimulation**. *(Under preparation)*, 2018.

- J. Omedes, A. Schwarz, GR. Müller-Putz, L. Montesano. **Factors that affect error potentials during a grasping task: toward a hybrid natural movement decoding BCI**. *Journal of neural engineering*, 2018.

- I. Iturrate, J. Grizou, J. Omedes, PY. Oudeyer, M. Lopes, L. Montesano. **Exploiting task constraints for self-calibrated brain-machine interface control using error-related potentials**. *PLoS one*, 10(7), 2015a.

- J. Omedes, I. Iturrate, J. Minguez, L. Montesano. **Analysis and asynchronous detection of gradually unfolding errors during monitoring tasks**. *Journal of neural engineering*, 12(5), 2015a.

Articles in conference proceedings:

- J. Omedes, A. Schwarz, GR. Müller-Putz, L. Montesano. **Hierarchical decoding of grasping commands from EEG**, in *39th Annual International Conference of the IEEE Engineering in Medicine and Biology Society (EMBC)*, Jeju, July 2017.

- J. Omedes, I. Iturrate, R.Chavarriaga, L. Montesano. **Asynchronous Decoding of Error Potentials During the Monitoring of a Reaching Task**, in *2015 IEEE International Conference on Systems, Man, and Cybernetics (SMC)*, Hong Kong, October 2015b.

- J. Omedes, I. Iturrate, L. Montesano. **Brain connectivity in continuous error tasks**, in *36th Annual International Conference of the IEEE Engineering in Medicine and Biology Society (EMBC)*, Chicago, August 2014b.

- J. Omedes, I. Iturrate, L. Montesano. **Asynchronous detection of error potentials**, in *6th Brain-Computer Interface Conference*, Graz, September 2014a.

- <u>J. Omedes</u>, I. Iturrate, L. Montesano. **Detection of event-less error related potentials**, in *2013 Workshop on Neuroscience and Robotics: Towards a robot-enabled, Neuroscience-guided healthy society on International Conference on Intelligent Robots and Systems (IROS)*, Tokyo, November 2013a.

- I. Iturrate <u>J. Omedes</u>, L. Montesano. **Shared control of a robot using EEG-based feedback signals**, in *2nd Workshop on Machine Learning for Interactive Systems: Bridging the Gap Between Perception, Action and Communication (MLIS)*, Beijing, August 2013a.

- <u>J. Omedes</u>, I. Iturrate, L. Montesano, J. Minguez. **Using frequency-domain features for the generalization of EEG error-related potentials among different tasks**, in *35th Annual International Conference of the IEEE Engineering in Medicine and Biology Society (EMBC)*, Osaka, July 2013b.

1.5   Thesis organization

The contents of this thesis are organized as follows.

Chapter 2 explores the usage of spectral features characterized as frontal midline theta modulations. Three experiments demanding increased cognitive load are used to demonstrate the superior generalization capabilities of these features to decode error-related potentials when the information used to train a classifier is interchanged among the different tasks.

Chapter 3 introduces a novel approach to decode error-related potentials in asynchronous settings where the occurrence of erroneous events is not presumably known a priori. Specifically, we exploit the combination of temporal and spectral features related to errors elicited from abrupt changes of direction to train a classification model, and apply transfer learning to asynchronously discriminate errors when they are introduced in a gradual fashion.

Chapter 4 presents a new way to communicate and teach a mobile robot to move in a continuous environment using only error potentials as feedback. With this purpose, we propose an algorithm based on policy matching for inverse reinforcement learning to infer the user goal from brain signals.

Chapter 5 considers factors that may affect the design of a hybrid brain-computer interface. Neural correlates of natural movements and interaction error-related potentials are combined to perform a 3D reaching task. In particular, this chapter focuses on the impact that three specific factors, derived from the hybrid BMI design, have on the evoked error signatures and classification.

Chapter 6 investigates the neural correlates and the underlying cognitive processes associated with somatosensory mismatches produced by unexpected disturbances during neuromsucular electrical stimulation of the upper-limb. We explore differences produced by activation/deactivation of the stimulation as well as the effect of the intensity level, and possible applications in the field of neurorehabilitation to promote motor learning.

Chapter 7, summarizes the general achievements of this thesis, discusses the significance of the results presented, and presents the future lines of work to continue the presented investigations.

2

Error-related potentials. From time to frequency

2.1 Introduction

This chapter constitutes the first steps of the current thesis towards the analysis and classification of error-related potentials (ErrPs) in the context of brain-machine interfaces (BMIs). In particular, the chapter acts as an introductory study to establish the foundations for the subsequent chapters that constitute this thesis. As we mentioned in Chapter 1, the on-line decoding of ErrPs using traditional classification methods relies on the fact that these signals are phase-locked to a trigger event [Luck, 2014; Cavanagh et al., 2009]. Consequently, successful single-trial detection has been carried out mainly in the temporal domain (using magnitude and latency of the ErrP components) [Chavarriaga & Millán, 2010; Iturrate et al., 2010]. Here, we introduce some of these tasks in which error responses are generated through the monitoring of virtual and real devices performing discrete movements in a 2D grid to reach a desired goal.

For all BMIs, included the ones that will be presented in this chapter, there is a requirement of recording a calibration phase to learn the mapping from EEG activity to the control space that operates the device (i.e. learn the brain patterns associated to correct and erroneous events). This calibration has to be carried out for each subject to deal with the large inter-user EEG variability [Millán et al., 2010]. In addition, a common procedure is also to recalibrate the BMI for each new task and even for the same task between sessions, to deal with the EEG variability [Vidaurre et al., 2011b,a]. In particular, BMIs that rely on external cues such as those using event-related potentials (ERPs; from which ErrPs are part of) [Luck, 2014], have a decent generalization among sessions. In this sense and since calibration phase tends to be a time-consuming operation, which is a major issue when deploying BMIs out of the lab, there has been an increased interest to

find techniques that remove or at least minimize the duration of this phase. Some studies have proposed to re-use information from previous experiments to train a classifier for a new experiment, thus reducing the calibration time. However, it has been shown that ERPs do not generalize well between different tasks [Iturrate et al., 2012]. This is because the amplitude and latency of their components are affected by factors such as spatial attention [Li et al., 2009]; stimuli contrast [Luck, 2014]; the probability of appearance of the expected stimulus [Luck, 2014]; the inter-stimulus interval [Sellers et al., 2006]; user-dependent factors such as age and cognitive capabilities [Polich, 1997]; and other cognitive aspects such as the stimulus evaluation time (i.e., the amount of time required to perceive and categorize a stimulus) [Kutas et al., 1977; Luck, 2014]. As a result, the use of temporal features significantly degrades ERP detection rate when the tasks in the calibration and execution phase are different.

A similar issue, where temporal features lose effectiveness, is present when transferring error-related potentials towards continuous scenarios, which is the ultimate purpose of the present thesis. In this second case, the removal of well-controlled and discrete onsets that trigger the erroneous responses is the source of latency shifts that in consequence reduces the reliability of temporal features. In this sense, identifying a solution to overcome the degradation of the detection rates for the transfer between tasks, may shed some light on how to circumvent the lack of precise onsets during asynchronous scenarios. In this chapter we explore the usage of frequency features, as these features are insensitive to phase shifts (and thus latency) variations. Furthermore, in principle no information from a new task is needed as long as the ERP amplitudes and frequency components remain similar. This chapter explores the usage of low frequency components of error potentials as a way of dealing with changes induced by different tasks in the temporal domain. The results show that although the detection accuracy within a single task is better in the temporal domain, there exists a stable pattern in the frequency domain that allows a classifier to generalize among tasks, and thus BMIs based on these features generalize better. In practice, the study also shows that it is possible to combine temporal and frequency features to obtain the best of both domains.

2.2 Methods

2.2.1 Participants and data recording

Six volunteer participants (five males and one female, mean age 27) participated in the study recorded in a laboratory of the École Polyechnique Fédérale de Lausane, Switzerland.

The EEG was recorded using a g.USBamp amplifier (g.tec medical engineering GmbH,
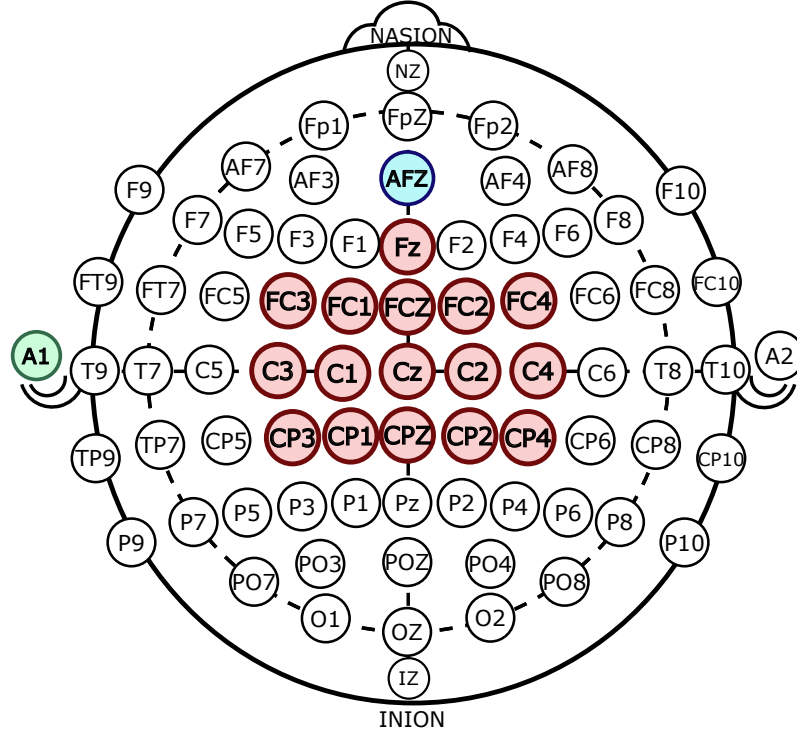
Figure 2.1: (Left) EEG set up according to the 10/20 international system. Electrodes used to record the EEG signal in these experiments are marked in red, ground electrode at AFz is depicted in blue and reference in the left earlobe in green.

Austria) with 16 active electrodes (Fz, FC3, FC1, FCz, FC2, FC4, C3, C1, Cz, C2, C4, CP3, CP1, CPz, CP2, and CP4 according to the 10/20 international system, with the reference and the ground placed at the left earlobe and AFz respectively (graphically displayed in Figure 2.1). The EEG was sampled at 256 Hz and power-line notch filtered at 50 Hz.

2.2.2 Experimental setup

Participants were instructed to observe movements performed by a device and evaluate them as correct when they were towards a target position and as incorrect otherwise, evoking non-error and error potentials. The participants were asked to restrict eye movements and blinks to specific resting periods. Three experimental conditions with progressively higher cognitive workload were designed (see Figure 2.2). In all the experiments, the device performed correct/incorrect movements until reaching a specific goal position. Time between actions was random and within the range [1.7, 4.0] s, with a 20% probability of performing an erroneous movement.
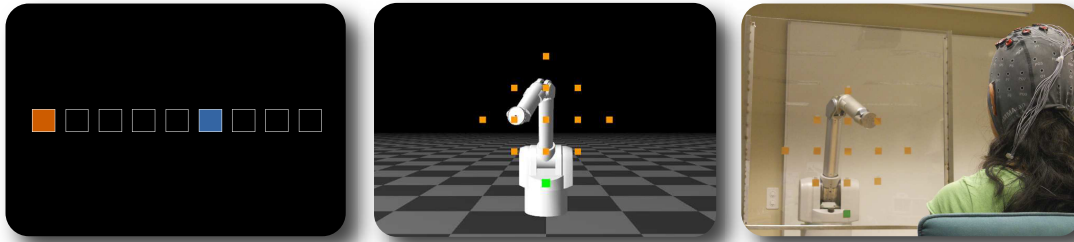
Figure 2.2: (Left) The first experiment consisted of a squared cursor (blue) that could execute two actions (move one position left or right) in a 1D grid with 9 different equally-distributed positions to reach a target (red). In experiments 2 (Middle) and 3 (Right) a virtual/real robot moves across 13 states (orange squares). At each state, the device can perform four actions (move left, right, up, or down) to reach the target (green square).

Experiment 1: Virtual Moving Square (Figure 2.2, Left).
Participants faced a computer screen showing a horizontal grid with nine different positions (states), including one blue moving square (device), and one red square (target position). The blue square could execute two actions: move one position to the left or to the right. When the device was at the boundaries (i.e., at the left- or right-most states), actions that moved the square out of the state space were not allowed. The time between two consecutive actions was random and within the range [1.7, 3.0] s. During the whole experiment, the target was either the left-most or right-most state.

Experiment 2: Simulated Robotic Arm (Figure 2.2, Middle).
Subjects faced a computer screen displaying a virtual robot (device). We simulated a Barrett whole arm manipulator (WAM) with 7 degrees of freedom using the RobotToolkit framework (http://lasa.epfl.ch/RobotToolKit). The robot could place its end-effector at 13 different positions represented by orange squares (states), with one position in green (target). It could perform four actions: moving one position to the left, right, up, or down. As before, when the device was at a boundary state, actions that moved the robot out of the state space were not allowed. In contrast to the first experiment, the robot's movements between two states were continuous, lasting ~ 500 ms. The time between two consecutive actions was random within the range [2.5, 4.0] s. For the training phase, the targets were the up and down most positions. For the reaching phase, the up, down, left, and right most positions were tested as targets.

Experiment 3: Real Robotic Arm (Figure 2.2, Bottom).
This experiment followed the same design as experiment 2 but involving a real robotic arm (Barret WAM). The robot was two meters away from the user and was pointing at states

in a Plexiglas transparent panel between the two. The distance between two neighbor states in the panel was 15 cm.

Each experiment lasted ~ 2.5 hours. They were always executed in the same order as presented above, with a time between sessions of 17.58 ± 10.09 days. For each subject and experiment, approximately 800 trials (around 160 and 640 error and non-error potentials) were acquired.

2.2.3 Electrophysiology analysis

For the time analysis, the time-locked averaged potentials were computed for the error, non-error and difference (error minus non-error averages) conditions at channel FCz. For the frequency analysis, the power spectral density (PSD) of each one-second trial was first computed using the Welch's method with a Hamming window and a window overlap of 50%. Then, the error, non-error and difference average PSDs were computed at channel FCz. The r^2 discriminability test [Wolpaw et al., 2002] between error and non-error conditions was computed for each channel and time instant (time analysis), and each channel and frequency component (frequency analysis).

2.2.4 Feature extraction

Two different sets of features were extracted. On one hand, the raw EEG was common-average referenced (CAR) and $[1, 10]$ Hz band-pass filtered. Temporal features were the EEG voltages of each trial of eight fronto-central channels (Fz, FC1, FCz, FC2, C1, Cz, C2, and CPz) [Iturrate et al., 2010] within a time window of $[200, 800]$ ms (being 0 the stimulus onset) subsampled at 64 Hz, leading to a vector of 312 features. Finally, the features were normalized within the range $[0, 1]$. Separately, the raw EEG was common-average referenced. For each of the channels used in the temporal features, the PSD was computed on one second of EEG after the stimulus onset as explained in subsection 2.2.3. The frequency features were the power values of each channel from the theta band ($[4, 8]$ Hz) $\pm$ 1 Hz (as previous studies suggested that the error potentials are generated within this band [Cavanagh et al., 2009]), which led to a vector of 200 features. Finally, the features were normalized within the range $[0, 1]$.

2.2.5 Methods for single trial classification

Previous studies showed that the usage of temporal features provoke a degradation of performance when training with one experiment and testing with another one (i.e. generalization) [Iturrate et al., 2012]. The objective of the present classification study was

to analyze whether the frequency features or the combination of both (temporal and frequency) are robust enough to generalize among different tasks (experiments).

Single-trial classification was carried out using a support vector machine (SVM) with a radial basis function (RBF) kernel, as this classifier presents high accuracies when classifying ERPs [Lotte et al., 2007] and error potentials in particular [Iturrate et al., 2010]. One important drawback of SVM is its sensitivity to imbalanced datasets. To avoid this drawback, the minority class (i.e. the error class) was oversampled by random replication to match the number of trials of the majority class (i.e. the non-error class) [Akbani et al., 2004].

To study the generalization capabilities of the different feature sets, each task data was divided into a training and a test set composed by 50% of the data each. The classifier was evaluated in two different conditions. First, the baseline accuracy was obtained by using the training and test sets of the same experiment E_j (denoted E_jE_j). Second, the classifier was trained using the train set of an experiment E_i and tested on the test set of another experiment E_j. The train-test combinations considered in the study were E_1E_2, E_1E_3, and E_2E_3, following the combinations studied in [Iturrate et al., 2014].

2.2.6 Statistical analysis

To analyze the statistical impact of the three type of features and the transfer between tasks on the classification performance, a factorial analyses of variance (ANOVA) with repeated measurements for the factors "feature domain" (time, frequency, time-frequency), "Experiment-train" (E1, E2 and E3) and "experiment-test" (E2 and E3) was computed. The analysis was carried out using the global accuracy performance for each case and subject. All the statistical analyses were processed using the commercial IBM SPSS software. Normal distribution of the data and homogeneity of variances were also tested before the analysis using the same platform. In the case that a main factor or interaction of the ANOVA reached significance (p<0.05), contrasts were tested by post-hoc two-tailed t-tests to further identify the source of differences, using Bonferroni's method for multiple comparisons.

2.3 Results

2.3.1 Results of the electrophysiology analysis

Figure 2.3 (first row) depicts the error, non-error and difference grand averages, for the three experiments. The three difference grand averages of the error potentials have an early negativity and two broader positive and negative components, in agreement with
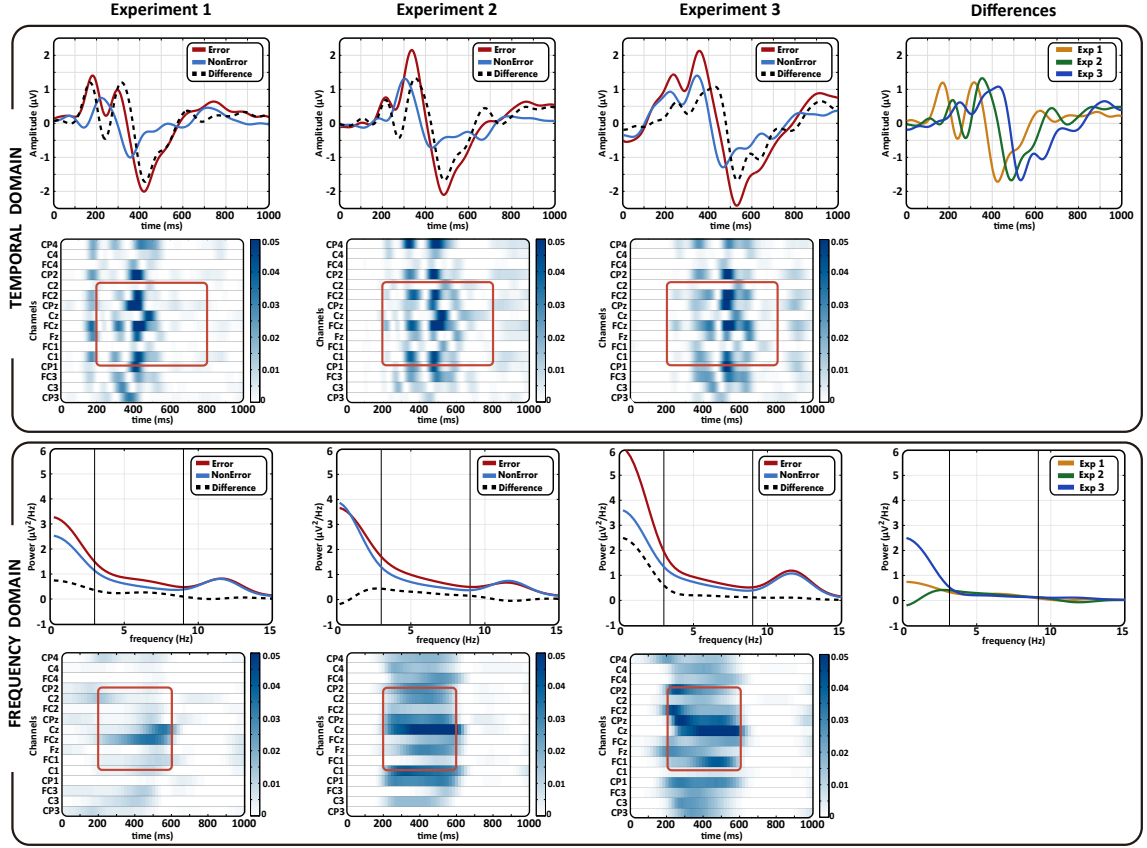
Figure 2.3: Electrophysiology results for experiments 1 to 3. First row shows the error, non-error and difference grand averages for channel FCz, and the last column the difference average compared for the three experiments. Second row shows the r^2 test of the temporal signals (x-axis: time, and y-axis: channels). Third and fourth row show the PSD averages (for channel FCz) and the r^2 test of the frequency signals. For each r^2 plot, the squared zone represents the window used for the extracted features.

other studies [Chavarriaga & Millán, 2010; Iturrate et al., 2010]. However, in line with previous works, the latencies of these peaks varied among the three experiments [Iturrate et al., 2014] (see figure 2.3, up-right-most plot). For instance, the latency of the broader negative peak was of 426, 492 and 535 ms for experiments 1 to 3. This variation in latency is also visible with the r^2 metric (Figure 2.3 second row). Notice how the r^2 patterns of fronto-central channels present a time shift among experiments.

Regarding the frequency analysis, Figure 2.3 third row depicts the error, non-error and difference PSD averages for the channel FCz for the three experiments. The difference averages were similar in the theta band for the three experiments (see Figure 2.3 third row, fourth column). This supports the fact that the main variation of the signals was due to latency differences, but not to amplitude differences (as described in [Iturrate et al.,
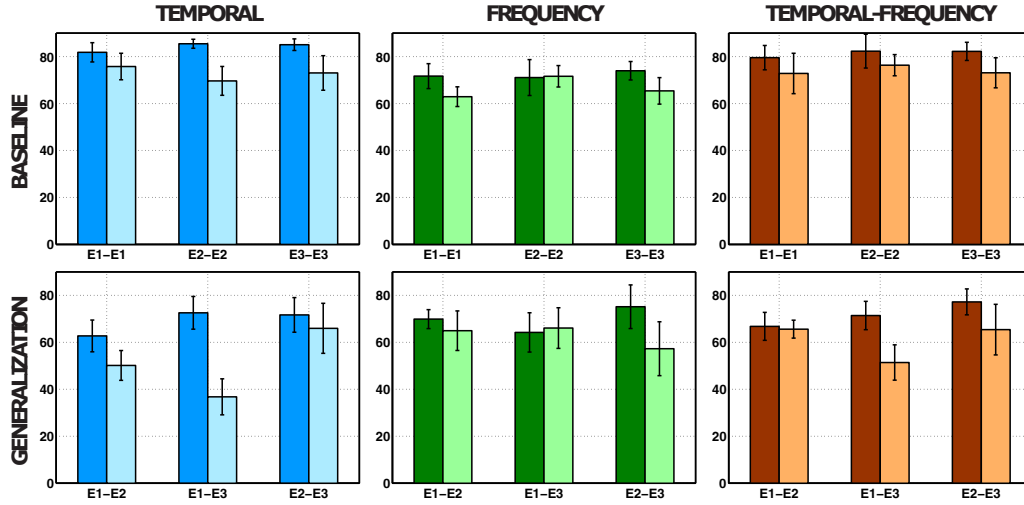
Figure 2.4: (Top) Baseline accuracies $\pm$ SEM (%) when training and testing with experiment j (denoted $E_j E_j$) (Bottom) Generalization accuracies $\pm$ SEM (%) when training with experiment i and testing with experiment j (denoted $E_i E_j$). Dark and light colors represent the non-error and error accuracies. Left, middle and right plots show the results when using the temporal, frequency, and combined set of features respectively. Notice that the baseline $E_j E_j$ should be compared to the generalization $E_i E_j$.

2014]). The r^2 discriminability patterns were in the theta band as suggested in [Cavanagh et al., 2009]. Notice that the r^2 values were progressively higher among experimental conditions. Despite there is not a clear reason of this increase in the r^2, it could be due to: a user habituation to the protocols (since the three experiments were always executed in the same order from 1 to 3); or a higher cognitive workload that generated stronger error components with greater r^2 values. This increase in separability could hinder the generalization from a more complex experiment to a simpler one ($E_i E_j$ with $i > j$), but not during the opposite generalization ($E_i E_j$ with $i < j$).

2.3.2 Classification results

Figure 2.4 depicts the baseline accuracies of $E_j E_j$, and the generalization accuracies of $E_i E_j$ for the temporal and frequency feature sets, and for the concatenation of both sets (c.f. subsection 2.2.4), averaged for all subjects.

Regarding the temporal features, the baseline of each experiment had high accuracies, being on average 78.78%, 77.54% and 79.04% for experiment 1 to 3. However, these features provoked an accuracy degradation when generalizing the classifier to another experiment, mainly due to the latency variations observed in the electrophysiology analysis. In fact, the mean accuracy dropped a 21.09%, 24.36% and 10.21% for the $E_1 E_2$, $E_1 E_3$ and $E_2 E_3$ cases. On the other hand, the use of frequency features resulted on lower base-
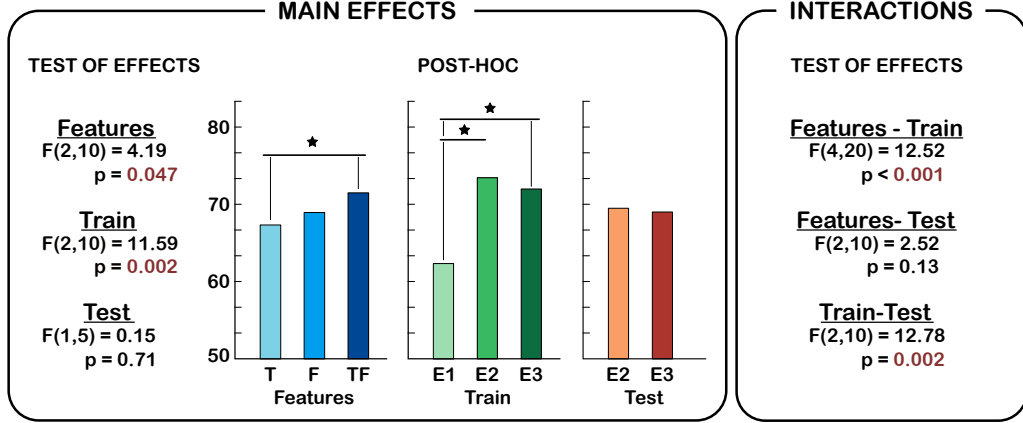
Figure 2.5: Estimated marginal measurements of classification performance based on the ANOVA analysis for the 3 studied factors. Left box depicts the effect of each factor in the classification results, and a post-hoc test to quantify which subfactors contributed the most to the achieved performance. Right box display the first order interaction among the different pairs of factors. The mark "*" denoted those factors which introduced statistical differences.

line accuracies than the temporal ones: 67.29%, 71.33% and 69.67% for experiments 1 to 3. However, the accuracy drop was substantially lower when generalizing the classifier: 3.91%, 4.52%, and 3.44% for E_1E_2, E_1E_3 and E_2E_3. For the baseline classifiers that use the temporal and frequency features, the accuracies presented very similar results to those obtained using the temporal features: 76.17%, 79.31%, and 77.64% for experiments 1 to 3. More interestingly, the generalization classifiers had accuracy drops of 13.11%, 16.23% and 6.35%; but the absolute accuracies were very similar to those obtained with the frequency features: 66.20%, 61.41%, and 71.32%, for E_1E_2, E_1E_3 and E_2E_3. Thus, the use of both set of features at the same time allowed to have the best of time and frequency domains.

These results confirmed that the temporal features had poor task-generalization capabilities due to the latency variations. However, the frequency features generalize better comparing the baseline and the generalization accuracies, suggesting that these features remained similar among experiments.

2.3.3 Classification results

Figure 2.5 displays the significant effects and interactions among factors as well as the estimated marginal measurements obtained from the execution of the 3*3*2 ANOVA.

The analysis reveals a significantly effect on the accuracy performance given by the type of feature used during the classification (F(2,10) = 4.19, p = 0.047). In particular, a post hoc test showed significant differences between using features from the temporal

domain and the combination of time and frequency features (p = 0.035). Regarding to the experiment used to train the classifier, the analysis shows that the models trained with the first experiment lead to a significant lower accuracy (61.86%) compared to those models trained with the second (72.40%, p = 0.039) and third experiments (71.01%, p = 0.048). Finally, the experiment used to test the model did not reveal any significant differences (F(1,5) = 0.15, p = 0.047), obtaining accuracies of 68.65% and 68.19% for experiment 2 and 3 respectively.

On the other hand, there was significant interactions between the type of features and the experiment used to train the classification model (F(4,20) = 12.52, p < 0.001). This interaction reinforces the effect that was shown in section 2.3.2, where depending on the experiment we use to train or model and the feature domain that we use we obtained different performances. This effect is also seen in the significant interaction between train and test experiments (F(2,10) = 12.78, p = 0.002). Given the higher performance obtained when the data used to train and test the model belongs to the same experiment.

2.4 Discussion

This initial chapter has introduced three different monitoring tasks where subjects mentally assessed the correctness of actions performed by virtual and real devices. These experiments followed the conventional paradigm in which device's actions are time-locked to well-defined and controlled events that appear in a step-by-step fashion. This paradigm allows to align the elicited responses generated from the perception of correct and erroneous stimulus and thus, apply the methods that have been described in section 6.2. In particular, the present chapter introduces an important challenge in current BMI technology, namely how to minimize the calibration time, as it is one of the major difficulties, especially when we are dealing with patients, who tends to get quickly tired. Some researches have proposed diverse techniques to tackle this issue such as pre-recording a pool of subjects to create a meta-model for classification [Kindermans et al., 2012] using adaptive classifier [Vidaurre et al., 2011b] or using data from similar tasks already performed by a specific subject [Iturrate et al., 2012]. However, in the case of BMIs based on event-related potentials, re-calibration is needed mainly due to differences in latency of the peaks that characterize the potential of interest. Specifically, a preceding study [Iturrate et al., 2012] revealed that these time shifts are discernible not only when comparing the elicited potentials among different subjects but they are also present when the same subject perform different tasks. This chapter builds on these results showing the presence of these latency changes, and how they affect the conventional classifiers based on temporal features during the generalization among different tasks, provoking large drops

in accuracy. In this regard, we proposed the usage of EEG features extracted from the theta frequency spectrum to train classification models that have better generalization properties when transferring information among different tasks (completely avoiding the re-calibration process) than those based on temporal features. Furthermore, the combination of features of both domains allows to obtain classifiers with performances similar to the temporal alone on one task, and similar to the frequency alone in generalization (i.e. the best properties of both domains).

2.4.1 Discussion of results

The EEG signatures related to error processing from each of the three presented tasks were analyzed using standard methods that have been extensively used in experimental protocols linked to observation errors [Chavarriaga & Millán, 2010; Iturrate et al., 2012]. The resulting signals followed the same morphology described in previous studies, composed by a sharp negative fronto-central peak at 250 ms, followed by a centro-parietal positivity after 320 ms and a second broader fronto-central negative peak around 450 ms. Observing the grand averages depicted in the top part of Figure 2.3, we can visually discern that the signal computed as the difference between error minus correct ErrP responses clearly matched the typical waveform reported in the bibliography [Kim & Kirchner, 2016]. Notice that as we have already mentioned, there existed a delay in the latency of the dominant components of the ErrP that increased from 50 ms between experiment 1 and 2, to 100 ms between experiment 1 and 3. We hypothesize that this time shift depends on the cognitive workload required to perform each task [Luck, 2014]. On the other hand, looking at the frequency spectrum displayed in the bottom side of 2.3, we found a significant power increase in the oscillations below 10 Hz for those brain responses elicited from erroneous events compared to correct events. Furthermore, the magnitude of this power within the theta band ([4 - 8] Hz) was consistent among the three different experiments. This indicates that despite the variations of stimuli produces shifts in the time domain, spectral theta dynamics are more robust to these changes.

From a classification point of view, previous works on ErrP detection have mainly focused on exploiting features from the time domain, namely magnitude and latency from electrodes located at fronto-central regions of the scalp, to calibrate linear models such as linear discriminant analysis (LDA) by recording several instances of the subjects EEG data correspondent to the targeted brain patterns. These implementations have been able to successfully detect ErrPs elicited after the occurrence of an erroneous event under a wide repertoire of experimental protocols reaching average accuracy performances of around 80% [Chavarriaga et al., 2014]. Following this approach, we obtained classification accuracies of 78.78%, 77.54% and 79.04% for experiments 1 to 3 respectively, which concurs

with the results reported in the literature. However in the attempt of removing the time consuming calibration phase by training our model using pre-recorded data from a different task, resulted in an average drop of performance around 20%. This make evident the significant impact produced by the time shifts of the ErrP peaks in the error detection rates. On the other hand, the usage of frequency domain features following a standard calibration procedure entails classification results around 10% lower than the ones obtained from temporal features. Nevertheless, their performance remained stable when the data used for training and testing the model belonged to different experiments. This revealed the superior generalization attributes of these features. Finally, we examined the effect of combining both sets of features. Since they belong to different domains, we decided to utilize a non-linear classifier (i.e. RBF-SVM) that could account for any existent non-linear relationship between them. Interestingly, the results showed that this combination get the best of temporal and frequency domains, achieving comparable or superior results for both types of calibration models.

Interestingly, an ANOVA statistical analysis validates the obtained results. Here, we found that indeed there are significant differences depending on the type of features that we use to train our model, especially between using only temporal features or combining them with those of the frequency domain. Furthermore, the task used for training the model had an important effect on the performance results. In the case of training with the most basic task (virtual device moving left or right), and using this data to detect errors in one of the two other tasks the obtained performance was the worst. On the other hand, the second and third experiment were more similar, and the performance seems to decay slightly when using a real device. Hypothesized due to the increased cognitive workload of evaluating the movement of a real device. Notice that for the design of the ANOVA model we only considered the experimental combinations of E1-E2, E1-E3, E2-E2, E2-E3, E3-E2 and E3-E3. We excluded the additional combination of testing our models in the first experimental protocol for several reasons: 1) Since we only had data from 6 subjects, including more combinations would create a more complex model, diminishing the relevance of the results. 2) The complexity of the whole model would have made more difficult to understand the interactions among factors. 3) From a practical point of view, it makes little sense to use a highly cognitive demanding task (i.e. experiment 3) to learn a model that let us discriminate brain patterns on a relatively simple task (i.e. experiment 1).

2.4.2 Future work and follow up

As future work, it would be interesting to explore alternative neural correlates of error-related potentials that provide extra information to boost or strengthen the decoders. For

instance, there has been a growing interest in studying not only what areas of the brain are active when performing a specific task, but also the functional interactions among different brain regions [Taylor et al., 2007]. One way of doing this is through the assessment of brain connectivity. This inspired us to design an additional study that has not been included in this thesis [Omedes et al., 2014b], where we aimed to characterize the brain connectivity during an experimental paradigm of error-related potentials using metrics based on the coherence and phase slope index of communication between different brain neural sources. Our results based suggested that in presence of an error potential the coherency within the theta band increases and propagates from central to parietal brain regions. Following up in these results, Zhang et al. estimated connectivity patterns using multivariate auto-regressive models that also showed increased ErrP modulations in theta and alpha bands between fronto-central and fronto-lateral areas [Zhang et al., 2015a]. Furthermore, they used the normalized direct transfer function metric to compute connectivity features and train a classification model, reporting a performance (in terms of area under the curve) of around 76% compared to 85% using temporal features, and up to 87% when combining them. This reveals that connectivity patterns carry discriminant information about the perception of correct and erroneous actions complementary to that obtained only from temporal features.

Finally, following the trajectory of the work presented in this chapter, there has been more groups that have started to combine time and frequency features in their classification models to obtain a more robust decoding performance. For example, in the next chapter we will present how we used these frequency features and transference of information to achieve the asynchronous detection of error-related potentials during the monitoring of a virtual device executing continuous trajectories [Omedes et al., 2015a]. Based on a recent ECoG study [Milekovic et al., 2012], Spüler & Niethammer recorded EEG data during the control of a video game and investigated the occurrence of two types of error, namely execution and outcome errors. They found that during the same task, the two types of error displayed different ErrP morphology and also exhibited variations in their spectral response. This allowed them, by utilizing error-related temporal and spectral responses, to discriminate these errors in an event-locked fashion [Spüler & Niethammer, 2015]. In [Mousavi et al., 2017], they also study the usage of different spectral bands to establish if they can be used not only to generalize among task but also among sessions to correct feedback perceived while executing a motor imagination task. Or Tessadori et al. that also combined time and frequency features to study whether tactile feedback can improve the detection of ErrPs and whether a mismatch between visual and tactile stimuli can also affect this performance [Tessadori et al., 2017]. Even though their results were not conclusive, this is a promising attempt for future applications based on error-

driven learning.

3

Asynchronous detection of gradually unfolding errors

3.1 Introduction

As we introduced in Chapter 1, most studies on cognitive control processes, such as those analyzing error-related responses, have been designed and used tasks involving sudden-onset stimuli [Ullsperger et al., 2014a; Luck, 2014; Chavarriaga et al., 2014], to analyze the recorded neural activity locked to the event onset. Similarly to neuroscience studies, time-locked analyses are also part of current developments of brain-machine interfaces (BMIs) [Millán et al., 2010]. For example, studies have used the brain potentials associated to the observation of errors (ErrPs) committed by a device not only to drive, but also to learn and adapt the BMI based on the user assessment of the operation [Chavarriaga et al., 2014]. As shown in Chapter 2, these BMIs have relied on precise onsets to decode measurable EEG patterns time-locked to the occurrence of the event [Chavarriaga et al., 2014], such as actions on a discrete grid [Blankertz et al., 2003; Chavarriaga & Millán, 2010; Iturrate et al., 2014] or sudden changes or interruptions during continuous movements of a device during reaching and tracking tasks [Diedrichsen et al., 2005; Krigolson & Holroyd, 2007; Milekovic et al., 2012].

However, human perceptual decisions comprise continuous internal processes, which do not necessarily imply immediate responses or time-locked brain activations to an onset. In this regard, there are many control paradigms where the events that require a cognitive evaluation might appear gradually rather than suddenly (e.g. BMI-controlled wheelchairs [Galán et al., 2008; Iturrate et al., 2009]). Several works have theorized about the existence of an internal evidence accumulation model for perception [Ploran et al., 2007; Hesselmann et al., 2010], leading to a decision only upon reaching a certain boundary [Kersten et al., 2004]. Interestingly, similar accumulation models have also been used to model human

performance monitoring [Steinhauser & Yeung, 2010], which in turn has been linked to evidence accumulation models in perception [Den Ouden et al., 2012]. Despite promising initial findings with EEG recordings have already corroborated the existence of evidence accumulation models under perceptual decisions [O'Connell et al., 2012; Twomey et al., 2015], it is still unknown whether these control cognitive processes also generate measurable EEG signatures in gradual evaluation tasks.

In the previous chapter, we learned about the effective generalization properties of features extracted from the theta frequency spectrum and how they can be used next to non-linear machine learning techniques as a means of improving robustness for ErrP detection. Coincidentally, this spectral signature in the theta band has been commonly reported in activities related with control processes involving unexpected novel information, conflicting stimuli, punishing/rewarding feedback or observation/self-realization of error execution. Following these lines of research, the present chapter aims to study the existence of EEG-measurable signatures - in the form of frontal midline theta activities (FMθ) [Cavanagh & Frank, 2014]- elicited by the observation of errors executed by an external device under a monitoring task to establish a framework for the analysis of ErrP under continuous scenarios. The asynchronous detection of gradual FMθ dynamics would allow BMIs to widen the scope of applications limited to the date to time-locked analyses. Moreover, regarding neuroscience studies, this tool could be used to further analyze the neural dynamics that underlie the cognitive activity of these gradually unfolding processes.

During our experiments, a virtual device executed continuous trajectories to reach a goal position, existing the probability to follow a wrong trajectory leading to an error or mismatch. Participants had to observe these trajectories and accumulate evidence before evaluating the task performance. The experiment design included two mismatch conditions: first, sudden changes in the executed trajectory; and second, gradually unfolding erroneous deviations from the correct trajectory. We studied the stimuli responses in the time domain as the bi-phasic modulation N2/P3 complex and in the spectral domain as FMθ dynamics. These brain responses were analyzed in both conditions at scalp and brain-source levels and the identified EEG signatures were used to asynchronously detect these occurrences of the mismatch events during the monitoring task. The results obtained with eight subjects show that: (*i*) brain-source analyses reveal the existence of brain activity linked to human cognitive mechanisms for the sudden condition, and for the gradual condition to a lesser extent; (*ii*) contrary to the sudden mismatch events, gradual mismatches did not show any discernible scalp EEG pattern, and thus it was not possible to build a model to detect these patterns; and (*iii*) it is nonetheless possible to use a model trained on the sudden condition to asynchronously detect patterns originated during gradual mismatch evaluation. Furthermore, a post-hoc scalp and brain-source analysis of the

asynchronously decoded gradual mismatches, evidences that there is in fact associated and discernible FMθ EEG activity, which is originated in brain areas related to cognitive control [Cavanagh & Frank, 2014].

3.2 Methods

3.2.1 Participants and data recording

Eight healthy right-handed male subjects (mean age 27 years) voluntarily participated in the study recorded in a laboratory of the University of Zaragoza. Participants were seated on a comfortable chair approximately one meter away from a computer screen where the visual protocol was displayed.

EEG activity was recorded using a commercial g.Tec g.USBamp system (Guger Technologies, Graz, Austria) with 32 active electrodes distributed according to the extended 10/20 international system (FP1, FP2, F7, F8, F3, F4, T7, T8, C3, C4, P7, P8, P3, P4, O1, O2, AF3, AF4, FC5, FC6, FC1, FC2, CP5, CP6, CP1, CP2, Fz, FCz, Cz, CPz, Pz and Oz), with the ground on FPz and the reference on the left earlobe; additionally, electrooculographic (EOG) activity was recorded using 6 monopolar electrodes (placed above and below each eye, and from the outer canthi of the left and right eyes [Croft & Barry, 2000]), with the ground on FPz and the reference on the left mastoid. EEG and EOG signals were digitized with a sampling frequency of 256 Hz and power-line notch filtered at 50 Hz. EEG data was spatially filtered using common-average-reference (CAR) and high-pass filtered at 0.5 Hz using a zero-phase Butterworth filter of 4th order. Additionally, using the 6 monopolar EOG electrodes, the horizontal, vertical and radial ocular activity was computed as in [Croft & Barry, 2000] to remove electro ocular contamination from the EEG signal using a regression algorithm [Schlögl et al., 2007]. The data acquisition was developed under a self-made visualization and EEG recording software.

3.2.2 Experimental design

The visual protocol consisted in a blue ball (device), which performed continuous trajectories towards one of three possible fixed targets placed at the top right, center and left sides of the screen. The possible targets were represented as squares of dashed lines, and the current target was filled in blue (see Figure 6.1). The device always started to move up towards the targets from the bottom-center of the screen. The trajectories executed by the device lasted on average 3.5 seconds, required around 30° of vertical eye-movement and belonged to one of three possible experimental conditions:
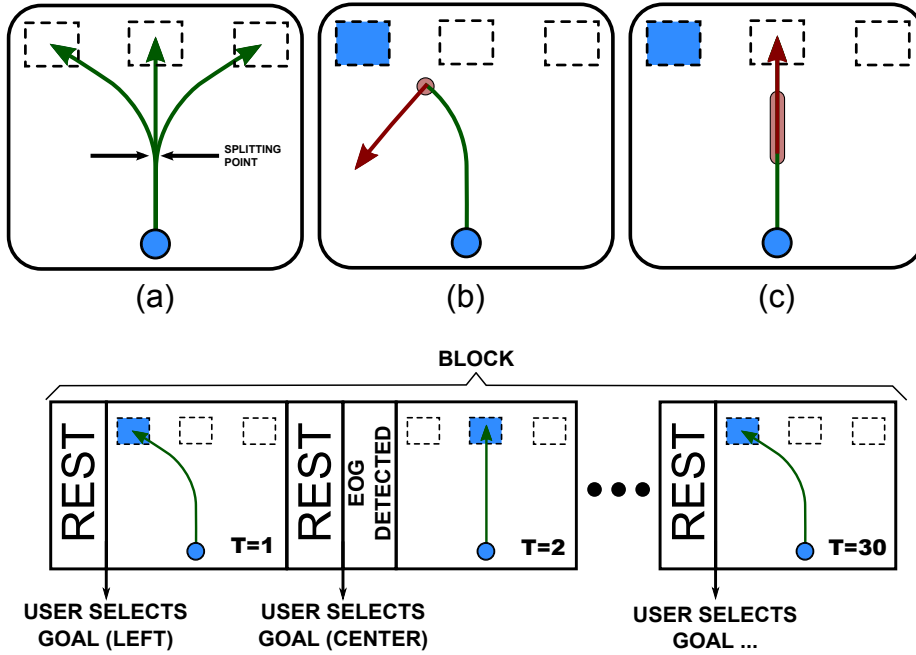
Figure 3.1: (Top) (a) Experimental protocol with the device (blue) and the three possible correct trajectories (green lines). (b) Example of a mismatch for the sudden condition. (c) Example of a mismatch trajectory for the gradual condition. Areas where the mismatch was expected to be elicited are shadowed in red. (Bottom) Block scheme composed of 30 trajectories. Each movement started immediately after pressing the corresponding key to choose a new goal, except if EOG activity was detected.

- **Correct condition**: The device moved straight to the top until reaching the splitting point situated at the center of the screen. Then, it continued to the top or shifted to the correct target. The device always followed the same path towards the target, as shown in Figure 6.1a.

- **Sudden mismatch condition**: The device firstly started as in the correct condition (Figure 6.1b). A short time after reaching the splitting point, the mismatch was induced as a random, sudden change of direction of at least 25 degrees. This condition resembled sudden-onset stimuli from previous studies [Chavarriaga & Millán, 2010; Iturrate et al., 2014].

- **Gradual mismatch condition**: The device underwent a gradual change of direction immediately after reaching the splitting point. More precisely, the device followed one of the trajectories of the correct condition, but leading to a different target from the selected one, Figure 6.1c.

Participants were asked to fixate their gaze and to avoid eye movements or blinks during the monitoring task. They were requested to use three buttons to freely choose one of the three possible targets to reach. Despite the frequency with which the subjects selected each goal was not controlled during the experiment, they were instructed to try to keep an equitable distribution of 1/3 for each selected target. Then, they had to monitor the trajectories performed by the device by continuously evaluating them as a mismatch or correct during the whole path. After each execution, subjects rested as much as they needed and selected the next target whenever they wanted. Once the user chose a target, the device immediately started a new movement when the magnitude of all EOG channels was below 40 μV. If EOG or muscular activity were detected during a trial, that trial was rejected.

Figure 6.1(bottom) shows the scheme of the experiment. Each session was organized in 16 blocks of 30 trials each with a break of few minutes between blocks. Each block could only contain either sudden or gradual mismatch events and they were presented alternating between both conditions. In this sense, blocks consisted of 70% correct and 30% of either sudden or gradual mismatch trials respectively. A total of 160 correct and 80 mismatch events per condition and participant were recorded with an average time per block of 4 minutes resulting in sessions of about 1.5 hours.

3.2.3 Scalp level analysis

The EEG data obtained in the sudden and gradual conditions were analyzed in time and time-frequency domains following previous cognitive studies were the mismatch event onset was known [Ferrez & Millán, 2008a; Chavarriaga & Millán, 2010; Cohen, 2011; Iturrate et al., 2013b]. In the experimental protocol, the event onset for the sudden mismatch condition was the time where the device performed the sudden change in direction. For the correct and gradual conditions, the onset was the time instant where the device reached the splitting point (i.e. the point where curve trajectories deviate from the straight line). Notice that, in the gradual mismatch condition, the time when the subject perceived the event was unknown.

For the temporal domain analysis, EEG was $[1, 10]$ Hz bandpass filtered and time-locked responses were averaged for all participants at channel FCz [Nieuwenhuis et al., 2004] for the mismatch, correct and difference (mismatch minus correct averages). Scalp topographies at the most relevant peaks of these potentials were also computed. An r^2 discriminability test between mismatch and correct conditions was computed for each channel and time instant.

For the time-frequency analysis, the data of the two mismatch conditions were epoched within the window -500 to 1000 ms around the onsets. The event-related synchronizations

(ERSs) were calculated using Morlet wavelets based on a convolution with a wavelet-width of 12 cycles. ERSs data within a time window of -500 to 0 ms before the onset was used as baseline. A statistical significance test based on bootstrapping was run over the ERSs following [Graimann & Pfurtscheller, 2006].

3.2.4 Brain-sources level analysis

sLoreta was used to estimate the origin of intra-cranial activity in the sudden and gradual conditions on the averaged potentials at the occurrence of the most prominent peaks [Pascual-Marqui, 2002]. In addition, measure projection analysis (MPA) [Bigdely-Shamlo et al., 2013] was used to compare the brain activity during the cognitive mismatch processing from 3D EEG sources across subjects and conditions. This algorithm decomposes the signal using independent component analysis (ICA), and estimates the dipolar brain source of each component separately. Then, it clusters the components of all subjects into the most representative brain domains according to a similarity metric based on the event-related power spectral perturbations (ERSP) at each dipole location involved in the processing of an event (i.e. related neural activity to the mismatch). In the experimental protocol, MPA was computed separately for the epoched trials of the three experimental conditions (correct, sudden mismatch and gradual mismatch) and the brain domains were reported together with their associated ERSPs [Makeig, 1993] for each condition. As a sanity check, we lastly performed both of these analysis on the correct trials, time-locked to the splitting point as with the events in the gradual mismatch condition.

3.2.5 Classification

3.2.5.1 Feature extraction.

Temporal and frequency features were extracted from the most relevant common spatial patterns (CSPs) [Dornhege, 2003] associated to mismatch event responses. First, EEG signal was $[1, 10]$ Hz butterworth bandpass filtered. Separated CSPs for each condition (sudden and gradual) were computed using a one-second window for mismatch and correct trials starting at their respective onsets (see subsection 3.2.3). The two first CSPs that maximized the variance of the mismatch events were retained and used to filter the EEG signals for feature extraction. Temporal features were the EEG voltages within a one-second window of the signal downsampled to 64 Hz, forming a vector of 128 features. In the frequency domain, the power spectral density (PSD) was computed from the same temporal window, by means of the Welch's method with a Hamming window and a window overlap of 250 ms. Frequency features were the power values of each component from the theta band ($[4, 8]$ Hz) ± 1 Hz following previous findings [Cohen, 2011], leading to a vector
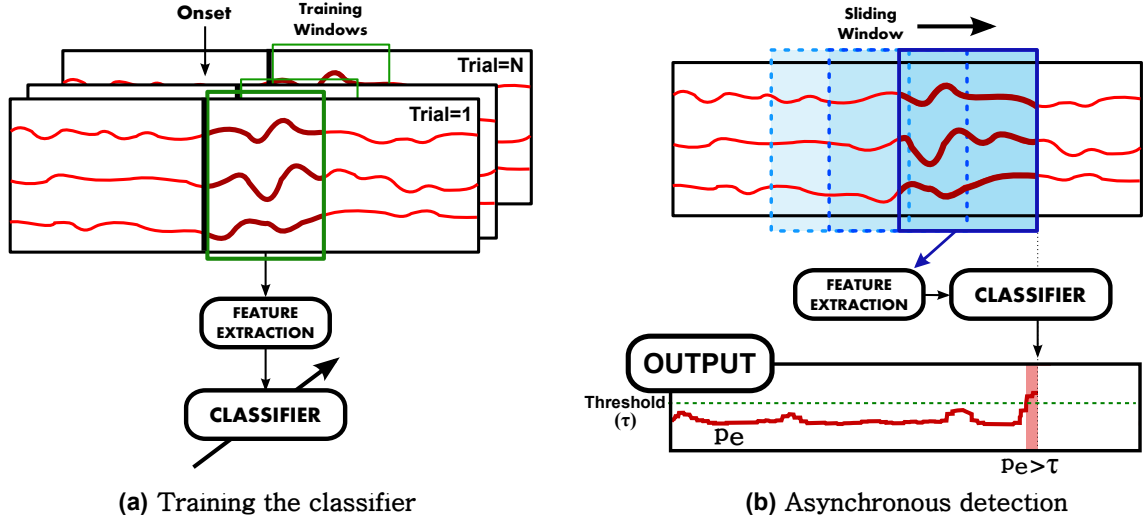
Figure 3.2: Classification process. a) *Training the classifier*: After CSPs has been applied to the EEG signal, feature are extracted from the training set using a one second window relative to the onset of mismatch and correct events in order to train the classifier. b) *Asynchronous detection*: A sliding window is applied over the CSP filtered EEG signal of the test set. The evaluation of the extracted features from the consecutive windows gives a probability estimate (p_e) between 0 and 1. A mismatch event will be detected when this probability is higher than a fixed threshold $(p_e > \tau)$. Notice that the outcome of the classifier is delayed the width of the window with respect the occurrence of the event.

of 14 features. Finally, both set of features were concatenated and normalized within the range $[0, 1]$.

3.2.5.2 Asynchronous classification of error-related activity.

As in Chapter 2, features were used to train a support vector machine (SVM) classifier with a radial basis function (RBF) kernel [Lotte et al., 2007] to asynchronously detect mismatch events from EEG during the motion of the device [Iturrate et al., 2010]. For the training set, features were obtained from a one-second long window starting at the defined onsets (see Figure 3.2a). All parameters (including EOG regression coefficients, CSPs and normalization values and SVM tuning) were computed using only training datasets to avoid overfitting [Ferrez & Millán, 2008a; Chavarriaga & Millán, 2010; Iturrate et al., 2013b]. The minority class of the training set (i.e. the mismatch class) was oversampled to match the number of trials of the majority class (i.e. the correct class) to avoid SVM sensitivity to imbalanced datasets [Akbani et al., 2004]. In the test set, features were extracted from a sliding window over the entire trial every 16 samples (62.50ms) and fed to the SVM classifier to obtain a continuous decoding of each trial (see Figure 3.2b).

Three train-test sets were built to evaluate the asynchronous classification performance.

The first two corresponded to training and testing with the same experimental condition (denoted *sudden-sudden*, and *gradual-gradual*) and were evaluated using 8-fold chronological cross-validation with each fold corresponding to a block of trials (see subsection 6.2.3). The third train-test set corresponded to training with the sudden mismatch condition, and testing with the data of the gradual mismatch condition (denoted *sudden-gradual*).

The evaluation metrics were the number of complete correctly classified trials and the percentage of false positive detections among trials. On one hand, the ouput of the SVM classifier was transformed into the probability of being a mismatch events p_e [Chang & Lin, 2011]. A correct trial was properly classified when no mismatch events were detected along the entire trial (i.e. probability of detecting a mismatch response p_e was below a given threshold τ for all the windows of the trial). A trial containing a mismatch (sudden or gradual) was considered correctly classified when no mismatch events were detected before the splitting point and at least one mismatch response was decoded (p_e was over the threshold τ) for the sliding window before 1200ms after the splitting point. Following this procedure, the percentage of mismatch and correct trials correctly detected were computed for each possible threshold $\tau \in [0, 1]$. Results were compared with the chance level of each pair of train-test sets, computed as the average classification performance obtained by shuffling 100 times the labels of the corresponding training data. On the other hand, to evaluate the rate of misdetections during asynchronous decodification, the false positive rate was computed as the number of windows containing false mismatch detections divided by the total number of classification steps.

3.2.6 Post-hoc analysis

The scalp and brain-source level analyses of the gradual condition were performed using the splitting point as onset of the mismatch events. However, gradually unfolding events have internal unknown onsets that may not be the best choice to align the signals (for instance, due to variable latencies). The ability to asynchronously detect mismatch responses allows to use the detection time as an alternative onset for time-locked analysis. Thus, we computed a post-hoc mismatch onset defined as the initial point of the one second length sliding window where the classifier detected a true positive during the sudden-gradual case. As a sanity check, the same analysis was done for the sudden-sudden one. Once these onsets were extracted, the scalp and brain-source level analyses were replicated (subsections 3.2.4 and 3.2.3).

SUDDEN CONDITION

GRADUAL CONDITION

(a) Temporal domain: (left) Grand Average , (right) r^2

(c) Temporal domain: (left) Grand Average , (right) r^2

(b) Time−Frequency domain

(d) Time−Frequency domain
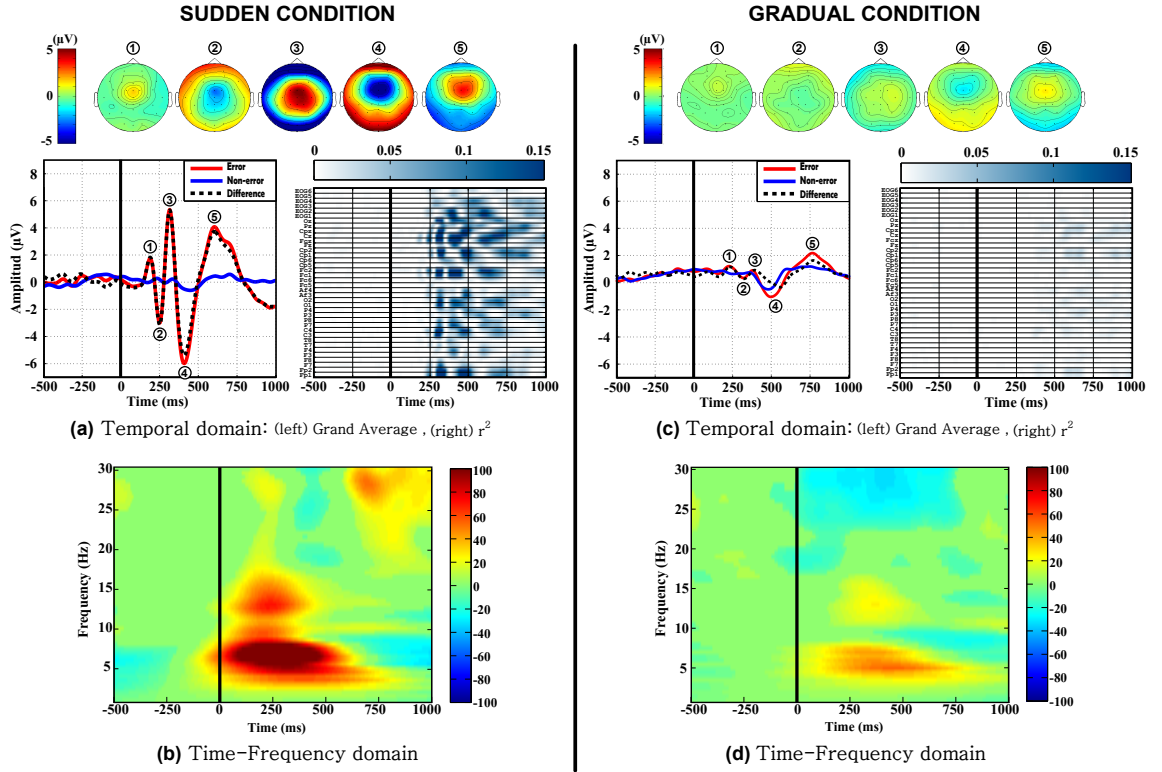
Figure 3.3: Scalp level analysis results for sudden (Left) and gradual (Right) mismatch conditions. (a and c, Left) Onset-locked signals on channel FCz averaged for all subjects, where responses to mismatch and correct events are represented in red and blue respectively, and difference average is shown in dashed black lines. Topographic interpolations of the most relevant peaks are also displayed. (a and c, Right) r^2 discriminability test between mismatch and correct potentials, where dark colors indicate larger differences between them. (b, d) Time-frequency plots, where red and blue represent significant event-related synchronizations/desynchronization on channel FCz, and green represent non-significant areas.

3.3 Results

3.3.1 Scalp level analysis

Figure 3.3 displays the results for the scalp level analysis for each of the two conditions (sudden and gradual in the left and right columns respectively).

Sudden mismatch condition (Figure 3.3, Left): Averaged ErrPs at channel FCz followed the same morphology found in previous time-locked studies with synchronous detectors [Chavarriaga & Millán, 2010; Iturrate et al., 2010], where the difference average was maximum at fronto-central areas, and was characterized by a positive peak at 150 ms, followed by a negative peak at 250 ms and a bi-phasic modulation at 310 and 400 ms (see Figure 3.3a, Left). An additional late positive peak was found at 600 ms, with maximum

magnitude in fronto-central sites. The r^2 test revealed that the main differences between mismatch and correct trials are in fronto-central channels close to the prominent positive and negative peaks (Figure 3.3a, Right). As expected from the experimental protocol design, there was no substantial discriminability in the EOG channels (top six rows of the r^2), which indicates that EOG activity was not correlated to the different conditions. The time-frequency analysis revealed statistically significant differences between mismatch and correct conditions in the theta band (Figure 3.3b). These results are in agreement with previous cognitive studies where the response of the subject's processing during the sudden stimuli has been characterized by an spectral increase in power in the theta band from sensors over the prefrontal cortex peaking around 300 milliseconds after the event onset [Cohen, 2011], also denoted as FMθ dynamics.

Gradual mismatch condition (Figure 3.3, Right): There were almost no differences between the mismatch and correct averaged signals, with a small negativity at 500 ms (Figure 3.3c), and the r^2 analysis revealed scarce discriminability between the two conditions. This indicated that there was no activation time-locked to the proposed onset (i.e. the splitting point). Time-frequency analysis showed a significant spectral power increase in theta band between 200 and 700 ms after the splitting point (Figure 3.3d). FMθ dynamics magnitude of this activation was around four times lower than the one obtained for the sudden mismatch condition.

3.3.2 Brain sources analysis

Figure 3.4 depicts the sLoreta source localization (first row) and the statistical MPA (bottom rows) for in sudden and gradual mismatch conditions (left and middle column respectively) as well as for the correct one (right column).

Sudden mismatch condition (Figure 3.4, Left): The sLoreta analysis was carried out in the most prominent negative peak of the grand averages (around 400 ms). The main activations were found in the pre-supplementary motor area (pre-SMA, Brodmann area 6) and the anterior cingulate cortex (ACC, Brodmann areas 24 and 32), in agreement with previous studies [Ferrez & Millán, 2008a; Iturrate et al., 2010].

Measure projection analysis computed two domains of brain source locations with a significant ERSP similarity among all subjects. For both domains, the ERSPs had a high activation of around 6.5 dB in the theta band between 200 and 500 ms after the onset of the event. MPA identified Brodmann areas 24 and 32 as the most representatives areas of activity for these domains (with a probability superior to the 70%), which agree with the brain sources obtained by sLoreta. The independent components of each domain contained at least 7 out of 8 subjects with similar ERSP contributing in the formation of such brain domains.

SUDDEN CONDITION **GRADUAL CONDITION** **CORRECT CONDITION**

(a) sLORETA Source Localization **(e)** sLORETA Source Localization **(i)** sLORETA Source Localization

(b) Measure Projection Domains **(f)** Measure Projection Domains **(j)** Measure Projection Domains

(c) ERSPs Measures **(g)** ERSPs Measures **(k)** ERSPs Measures

(d) Scalp maps (ICs) **(h)** Scalp maps (ICs) **(l)** Scalp maps (ICs)
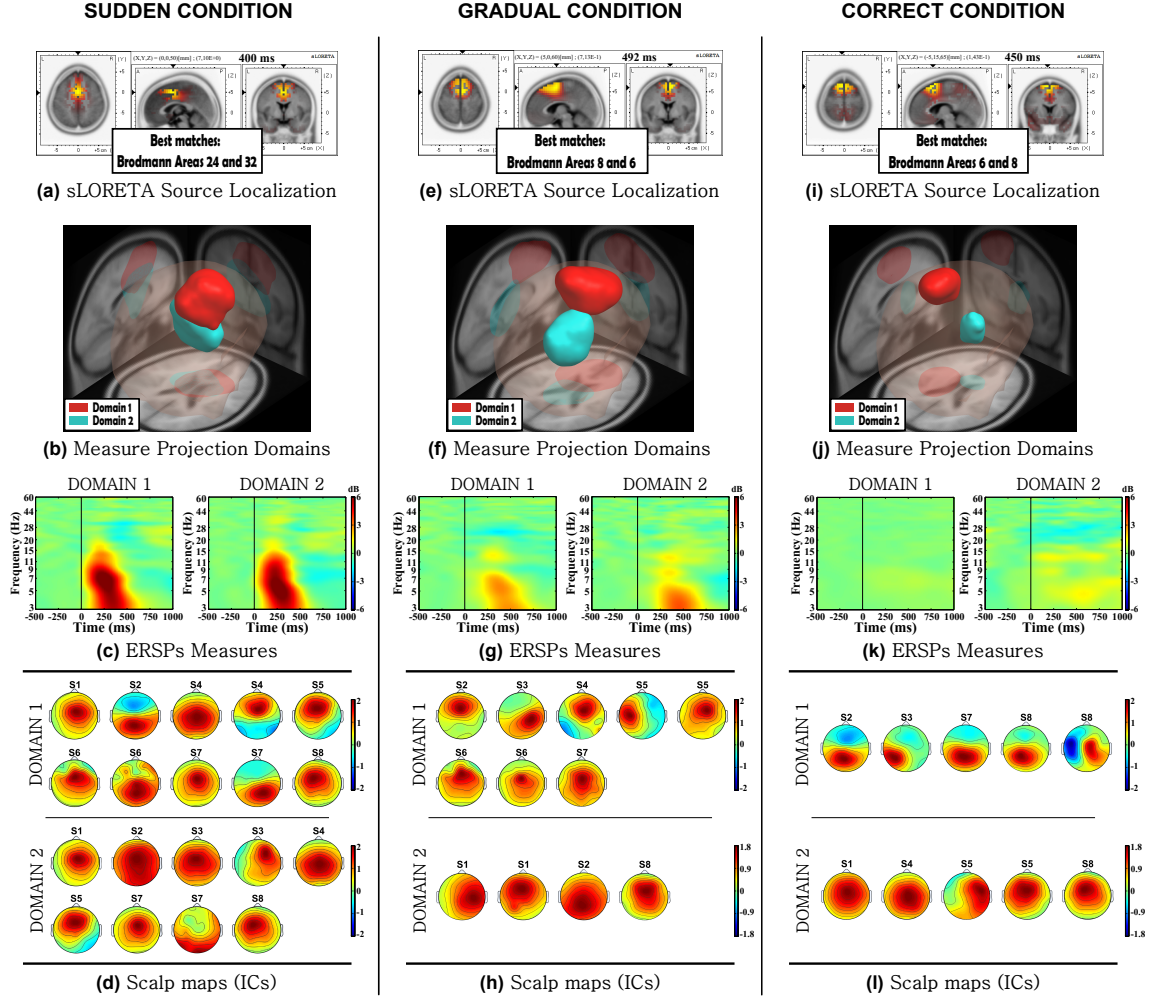
Figure 3.4: Brain-source level analysis results for sudden (Left) and gradual (Middle) mismatch conditions, as well as for correct events (Right). (a,e,i) sLoreta source localization of the grand average responses at the most prominent negative peak of each condition. Measure Projection Analysis results are shown in the lower part of the plot: (b,f,j) Brain domains with significant activations ($p < 0.01$) mapped from the corresponding ERSP measures (c,g,k), with red colors representing a larger synchronizations. (d,h,l) Independent components associated to the each subject's dipoles that formed each domain.

Gradual mismatch condition (Figure 3.4, Middle): sLoreta analysis was carried out on the negative deflection from the grad averages around 500 ms after the onset. The main activation areas were anterior and premotor cortex (Brodmann areas 8 and 6), which are believed to play an important role in planning complex movements in presence of uncertainty in a given task [Volz et al., 2005]. Nonetheless, it is worth noticing that the activation was one order of magnitude lower than the detected for the sudden condition.

MPA discriminated between two brain domains for this mismatch condition. Whereas
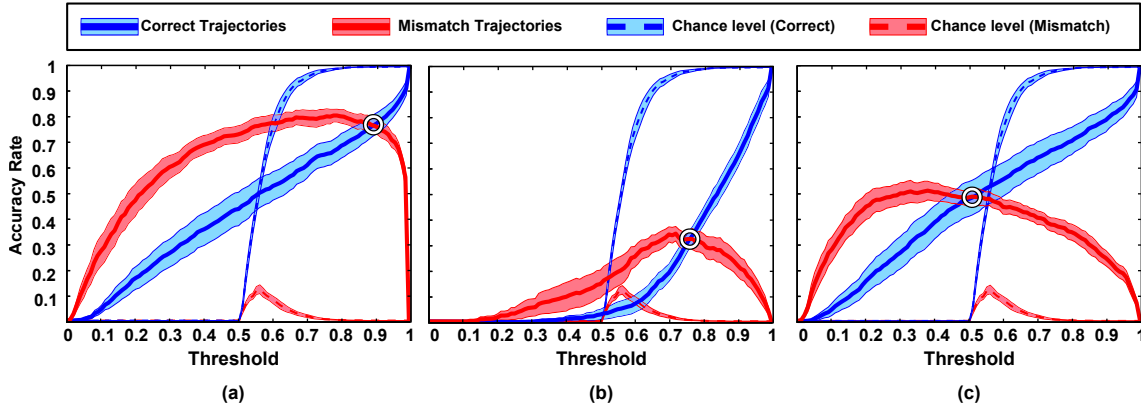
Figure 3.5: Percentage of trajectories with and without mismatch events properly decoded according to different threshold values ([0,1]) applied to the classifier output for each train-test pair. Red and blue solid lines represent, respectively, the percentage of correctly detected trajectories containing (or not) mismatch events, whereas dashed lines depicts the chance level (lines and shadows represent mean ± SEM). The optimal operation point (i.e. the threshold value where the performance was maximum) is marked with a circle.

the ERSP measure of the first domain resembles the activation obtained for the sudden condition, the one of the second domain is mainly centered on the low-theta band with a power activation of 2.9 dB in a time window between 250 and 750 ms after the splitting point. Furthermore, the first domain was most likely located near to left and right superior frontal gyrus (Brodmann areas 6, 8 and 32), while the second one was located in the surrounding of the brainstem, the cingulate gyrus and Brodmann areas 23 and 24. This may reveal that, despite there is an initial evidence of cognitive processing mechanism during gradual deviations, it shows weaker and broader brain activations compared to sudden stimuli.

Correct condition (Figure 3.4, Right): sLoreta analysis was carried out on the grand averages at the time instant with highest signal-to-noise ratio (a small negative deflection at around 450 ms). The results reveal broad activations centered around the premotor cortex (Brodmann areas 6 and 8); nevertheless, the magnitude of this activity is fifty times lower than for sudden events and five times lower than for gradual events.

Two brain domains were extracted using MPA. The ERSP for each domain had no activity stronger than 1 dB. Furthermore, these regions were composed by a smaller amount of ICs (only half of the subjects were voting for each cluster) than for the mismatch conditions, which suggests that for this correct condition there is no activity generated around the splitting point similar to the one found in the other conditions.

3.3.3 Single-trial asynchronous classification

Figure 3.5 displays the detection rates over the trials obtained for each of the train-test sets, for threshold values between 0 and 1. For all the train-test pairs (Figure 3.5), the percentage of trials with no mismatch events correctly classified increases with the threshold, while the number of trials containing mismatch events increases up to a maximum and then decreases. For the sudden-sudden set (Figure 3.5a), the performances of the classifier on both types of trials (with/without mismatch events) are optimal in terms of bias (i.e. same detection performance for both types of trials) for a threshold value of 0.88 (marked with a circle in the figure), with a detection performance of 77% of the trials for both classes. Furthermore, the classifier results were always better than the chance level (dashed lines in the Figure 3.5a).

Regarding the classifier performance on the gradual-gradual set (Figure 3.5b), the accuracies were much lower than the previous case, with a minimum bias for a threshold value of 0.74, with a detection performance of 32%. The detected accuracy of the mismatch event class tends towards the chance level, whereas the accuracy of correctly detecting trials free of mismatch events was almost always below the chance level. Thus, the trained classifier was not able to achieve high detection rates for the gradual-gradual condition set.

The results of the sudden-gradual set are shown in Figure 3.5c. The accuracies were higher in this case, with 51% for a threshold value of 0.5. This is an increase of 19% with respect to the gradual-gradual case, and a decrease of 26% with respect to the sudden-sudden classification. Nonetheless, the results were above the chance level, which shows how it is possible to use a classifier to transfer information between the sudden and gradual mismatch conditions.

For the sudden-gradual detector, the analysis of the detection time with respect to the splitting point shows a dependence on whether the stimuli condition implies a modification of the trajectory. Figure 3.6 shows, for all the subjects, the time instants where the classifier properly detected a mismatch event (red crosses). When the erroneous trajectory deviates from the straight line (i.e. turns right or left), the detection time was on average 647.86ms (std: 159.15ms) from the splitting point for turns to the left and 606.64ms (std: 177.64 ms) for turns to the right (see Figure 3.6, histograms). On the other hand, when the presented event implied following a straight line, the detection time was similar on average but had a larger variance, 691.03ms (std: 258.50ms) after the splitting point. Notice also that in all cases several events were detected just after the splitting point. Further analysis revealed that this early detection was mainly due to the contribution of frequency features, which discriminated the neural signal as a mismatch response at the

time of initial deviations from the background EEG before temporal signatures appeared (see Supplementary Figures S1 and S2). As a comparison, the previous analysis was carried out but with the time instant where the sudden mismatch events were detected (see histogram in Supplementary Figure S3), aligned to the original onset of the sudden mismatch condition. In this case, the events were detected on average 507.54 (std: 60.2042m)s after the sudden onset with a much lower variance.

Finally, we analyzed the percentage of false detected events during the asynchronous classification (Figure 3.7). Similarly to the previous results, in the sudden-sudden set there was a $3.04\% \pm 2.22\%$ of false positives during a trial. This means that a 3% of a mismatch-free trajectory was detected as containing neural activity associated to a mismatch response. On the other hand, in the gradual-gradual set there was a significantly larger number of false positives ($6.95\% \pm 2.24\%$, Bonferroni-corrected two-tailed paired t-test, $t_7 = -4.37$, $p = 0.01$). Finally, in the sudden-gradual set, there was significantly less false positives than in the gradual-gradual set ($4.70\% \pm 2.09\%$, $t_7 = 4.12$, $p = 0.013$), whereas no significant differences were found between the sudden-gradual and the sudden-sudden sets ($t_7 = -2.61$, $p = 0.1$) showing again the transfer of information between conditions.

3.3.4   Post-hoc analysis

Figure 3.8 depicts the results obtained from the scalp level analysis, for true positives detected on the sudden-sudden (493 trials) and sudden-gradual (327 trials) classification scenarios. Error potentials on the sudden mismatch condition (Figure 3.8a,b) closely resembled in time and spatial characteristics those obtained on the initial scalp analysis (see subsection 3.3.1), except for the broader latest positivity. Thus, the onsets extracted from the classifier did not distort the signals. On the other hand, time-locked averages for the sudden-gradual set revealed the existence of broader and of lower amplitude (compared to the sudden condition) bi-phasic modulation at 550 and 700 ms with similar scalp topographies to those observed for the sudden mismatch condition; and the absence of early components associated to visual sensory processing [Luck, 2014]. Thus, the classifier was able to detect information previously hindered by the initial onset alignments (compare with Figure 3.3c). With respect to the analysis in time-frequency domain from the sudden-gradual set (Figure 3.8d), significant synchronizations were found within the time instant when a mismatch event was detected by the classifier and the second afterwards. This synchronization was more spread in time than for the sudden condition, and its significance was 35% higher than the one obtained for the initial analysis on the gradually unfolding condition (compare with Figure 3.3d).

Regarding the brain-source level analysis for the sudden-gradual post-hoc condition,
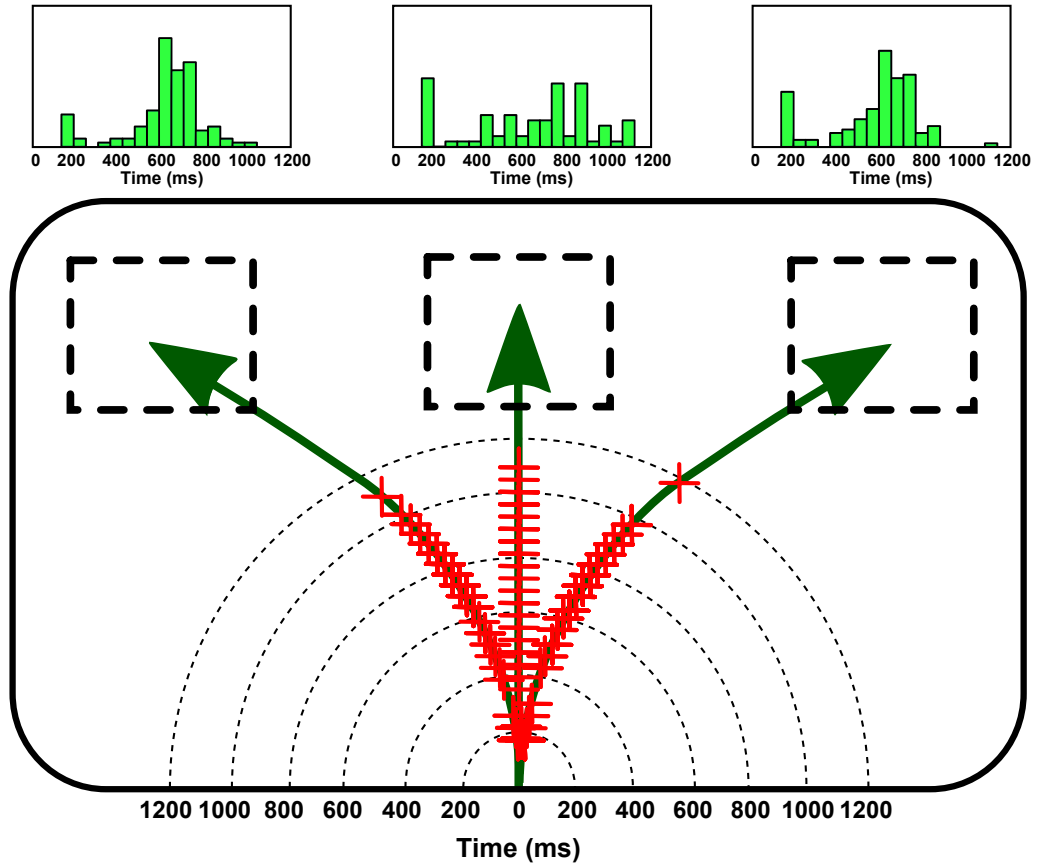
Figure 3.6: Time location of mismatch events properly classified (represented as red crosses) over their respective followed trajectories for all subjects. The elapsed time from the splitting point comes represented by the dotted arcs. The number of mismatch detections is depicted in the histograms shown over each target.
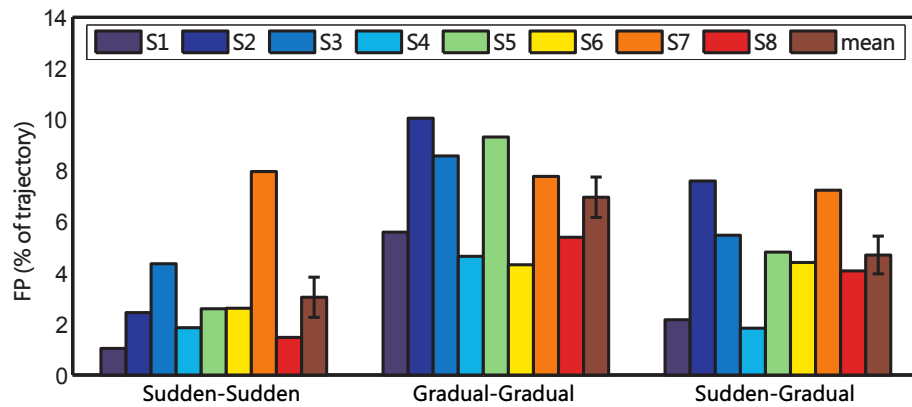
Figure 3.7: False positives for each train-test pair, calculated as the percentage of time each trial with no mismatch events was detected as a mismatch. The results are shown for each separate subject and averaged (mean $\pm$ SEM).

POST-HOC CONDITION SUDDEN-SUDDEN

(a) Temporal domain: Grand Average

POST-HOC CONDITION SUDDEN-GRADUAL

(c) Temporal domain: Grand Average

(b) Time−Frequency domain

(d) Time−Frequency domain
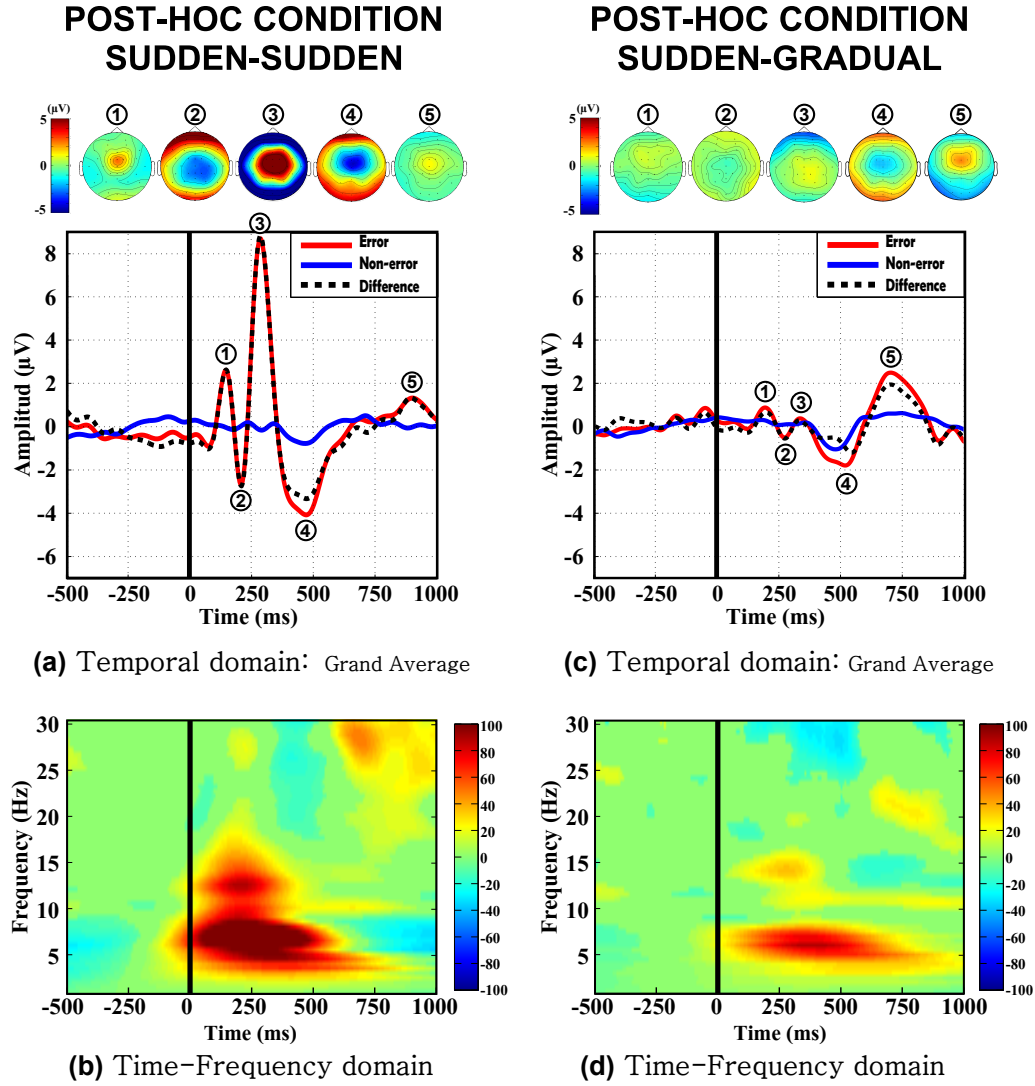
Figure 3.8: Scalp level analysis results for sudden-sudden (Left) and sudden-gradual (Right) post-hoc conditions. (a and c) Signals on channel FCz averaged for all subjects aligned to their time of detection, where mismatch and correct responses are represented in red and blue respectively, and difference average is shown in dashed black lines. Topographic interpolations of the most relevant peaks are also displayed. (b, d) Time-frequency plots, where red and blue represent significant event-related synchronizations/desynchronization on channel FCz, and green represent non-significant areas.

POST-HOC CONDITION

(a) sLORETA Source Localization

(b) Measure Projection Domains

(c) ERSPs Measures

(d) Scalp maps (ICs)
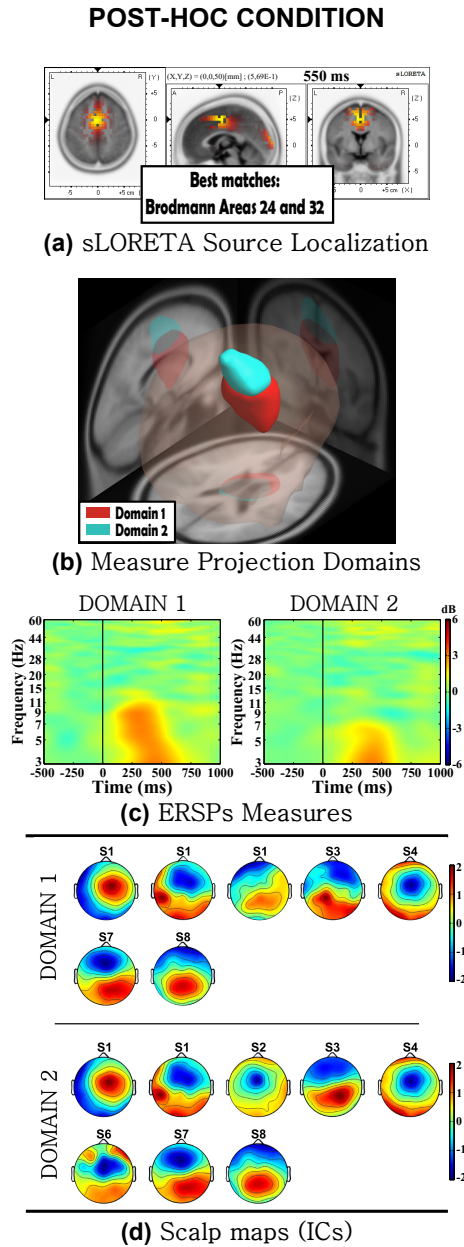
Figure 3.9: Brain-source level analysis results for sudden-gradual post-hoc condition. (a) sLoreta source localization of the mismatch response grand average at the most prominent negative peak. Measure Projection Analysis results are shown in the lower part of the plot: (b) Brain domains with significant activations ($p < 0.01$) mapped from the corresponding ERSP measures (c), with red colors representing a larger synchronizations. (d) Independent components associated to the each subject's dipoles that formed each domain

the source localization was carried out on the 550 ms negative deflection (see Figure 3.9a), obtaining similar results to those obtained on the initial sudden mismatch condition (compare with Figure 3.4a). Furthermore, main activations areas were originated at Brodmann areas 24 and 32 (anterior cingulate cortex). Agreeing with these results, MPA (Figure 3.9b,c,d) also provided similar brain sources to those obtained in the original sudden mismatch condition (compare with Figure 3.4b,c,d), where two significant domains were found and centered around Brodmann areas 23, 24 and 32. Nonetheless, the activation of these domains was again of lower power and of a narrower frequency contribution, especially for Domain 2.

3.4 Discussion

This chapter studied the generation of cognitive responses under a continuous monitoring task, and compared EEG neural representations for two types of mismatch conditions: a sudden change with respect to the expected behavior and a gradual deviation. The gradual mismatch condition has been designed in such a way that events always occur at the same instant to eliminate factors that could affect the latency of the cognitive response. Nevertheless, users were not able to consistently evaluate these gradual events at the same time instant. In pursuance of freeing BMI applications from the burden of onset-locked detections, and to expand future neuroscience studies to these gradually unfolding cognitive processes we proposed the use of machine learning models and transfer of knowledge to extract meaningful neural information from the gradual mismatch condition. In this work, such approach allowed us to perform a post-hoc analysis, where event onsets were extracted from mismatch responses asynchronously detected using a classifier. Interestingly, this analysis revealed the existence of discernible EEG activity during gradual mismatches, which agreed with the results at brain-sources level for sudden events. Also, as suggested by the results, the monitoring of gradually unfolding cognitive processes may require the accumulation of evidence before effectively delivering the evaluation the movement.

3.4.1 Scalp and source level analysis

EEG signals elicited during sudden changes can be analyzed using time-locked responses as in most cognitive studies of event-related potentials both in discrete tasks [Blankertz et al., 2003; Chavarriaga & Millán, 2010; Iturrate et al., 2012] or in continuous ones [Diedrichsen et al., 2005; Krigolson & Holroyd, 2007; Milekovic et al., 2012]. The scalp level analysis revealed the presence of a N2/P3 modulation at a neural level and spectral oscillations in the theta band located over the frontal cortex for the sudden mismatch condition, which were corroborated by the brain-source level analysis. On the other hand,

in the gradual condition, the scalp-level analysis of time-locked responses did not reveal significant differences between mismatch and correct responses at a neural level. However, frontal FMθ dynamics were found and similar brain sources to those obtained in the sudden condition were activated. This indicates that, despite the stimuli did not vary among trials (i.e. deviations were always the same and occurred at the same point), users were not able to consistently evaluate the cognitive events with similar reaction times.

The absence of a neural event-related response for gradual unfolding processes could be interpreted as: (i) there does not exist such event-related responses associated to a cognitive stimulus during these gradual deviations, (ii) the cognitive response exists but it cannot initially be measured with EEG, either due to its low signal to noise ratio, and/or the lack a proper onset to align the potentials (i.e. the users was conscious of the mismatch with a variable latency). Both situations impeded further analyses of the data and the training of asynchronous decoders.

To overcome this limitation, we trained a model with the time-locked responses of the sudden mismatch condition and use it to recover event onsets on the gradual mismatch condition. The rationale under this model-based approach is that, if cognitive processing activity between two conditions shares some common temporal or spectral patterns, such as frontal midline theta dynamics, it is possible to transfer this information between conditions. By aligning the responses with the recovered onsets, we showed that the scalp and brain-source level analyses resulted in slightly different but discriminant temporal patterns, and similar frequency oscillations and brain sources compared to the sudden mismatch condition.

We hypothesize that the results suggest the existence of an evidence accumulation process during the observation of the mismatch monitoring task, where the user's evaluation is triggered after reaching a specific boundary. Interestingly, research using invasive sensory technology has started to study this phenomenon, where preliminary results obtained with ECoG suggested the existence of cognitive signatures under gradual and continuous conditions [Wander et al., 2013]. On EEG studies, O'Connell et al. recently suggested the existence of an accumulation-to-bound model within the human brain, where the decision is taken when reaching a certain boundary [O'Connell et al., 2012]. Similarly to the results presented here, the authors compared P3 ERP components under sudden or gradual changes of visual stimuli, drawing similar conclusions to the present ones. Steinhauser et al. proposed that self-performance monitoring followed this accumulation model under a task involving imperfect evidence [Steinhauser & Yeung, 2010]. Furthermore, in both works, the temporal characterization of the signal obtained resembled the one obtained in the post-hoc analysis presented here, where early sensory-evoked ERP components are not present, and only those components associated to cognitive processing remained as

broader peaks with a lower amplitude. In our work, this temporal characterization was carried out thanks to the onset extracted using an asynchronous detector, which might be associated to the boundary reach following the evidence accumulation. Indeed, this might be an explanation for the larger variance detection time during erroneous trajectories that followed straight lines: users were not aware of the location of the splitting point, and thus the time they needed to evaluate the trial varied substantially between trials and subjects.

However, caution is necessary since our proposed post-hoc analysis biases the results towards those trials resembling the pattern trained from the sudden mismatch condition. In fact, there could be different brain activations associated to gradual deviations that cannot be properly identified and characterized using the proposed method, and further research should be performed to fully understand the underlying neural mechanisms during gradual unfolding processes. As a first sanity check, we computed the post-hoc analysis also under the cross-validation folds of the sudden mismatch condition. As the results showed, we obtained very similar spatio-temporal modulation compared to those with the original onsets (subsection 3.3.1). Nonetheless, and in pursuance of fully answering these questions, additional experimental protocols using gradual processes should be developed and analyzed. Moreover, the combined use of fMRI and EEG [Rosa et al., 2010] would provide insights on the main activation areas of the brain during the execution of these experiments and identify which brain areas are responsible for the observed brain activity.

3.4.2 Asynchronous detection and relevance for BMIs

EEG based detection of event-related potentials has exploited the differences between two time-locked responses (correct/incorrect) to an event [Blankertz et al., 2003; Chavarriaga & Millán, 2010; Iturrate et al., 2014]. However, during the operation of a device, users continuously assess its behavior and, consequently, there is no such a thing as a correct event. Instead, asynchronous detection has to deal with background EEG activity over longer periods of time. The combination of temporal and frequency features extracted from the most discriminable common spatial patterns results in mismatch event detection rates comparable to the best reported results obtained with time-locked responses [Chavarriaga & Millán, 2010; Iturrate et al., 2012] despite the added difficulty of continuous classification. Although this could be due to the absence of correct events typically appearing in discrete tasks [Luck, 2014], it would be interesting to check whether the proposed features could improve the single-trial detection of ERP in those types of discrete tasks as suggested by previous works combining temporal and frequency features [Zhang et al., 2012; Omedes et al., 2013b].

The asynchronous detection of neural responses associated to cognitive events was already demonstrated in a previous study using electrocorticographic recordings [Milekovic

et al., 2013] and posteriorly replicated using EEG [Spüler & Niethammer, 2015]. In the first work, Milekovic et al. studied the continuous decoding of errors during a motor task. In the experimental task, the users played a video game where the objective was to control a spaceship using a joystick in order to avoid collisions with incoming obstacles, where execution errors were elicited as movement mismatches (i.e. the spaceship moved in the opposite direction of the joystick); and outcome errors were introduced by obstacle collisions. The work reported sliding window performances with accuracies of around 72% of true positive rate and 44% false positive rates, similar to the 80% true positive and 18% false positive rates of our experiment in the sudden mismatch condition.

As expected from the EEG analysis of neural responses in the gradual unfolding condition, the lack of discriminant information between mismatch and correct events resulted in low detection rates grazing the chance level. However, the proposed methodology shows that it is possible to create models using time-locked responses and detect cognitive events in different conditions with different EEG imprints. These results, asynchronous detection and transfer of knowledge between conditions, broadens the applicability of cognitive control processes decoded using BMIs and open the door to their deployment in more realistic settings such as adaptive rehabilitation devices (e.g. prosthetics) [Ramos-Murguialday et al., 2013], learning systems that exploit cognitive information to adapt the behavior of the device [Chavarriaga & Millán, 2010; Iturrate et al., 2013a], and in general within the context of BMIs where the neural responses could be used to improve existent human-machine interactions [Zander & Kothe, 2011].

3.5 Supplementary Material
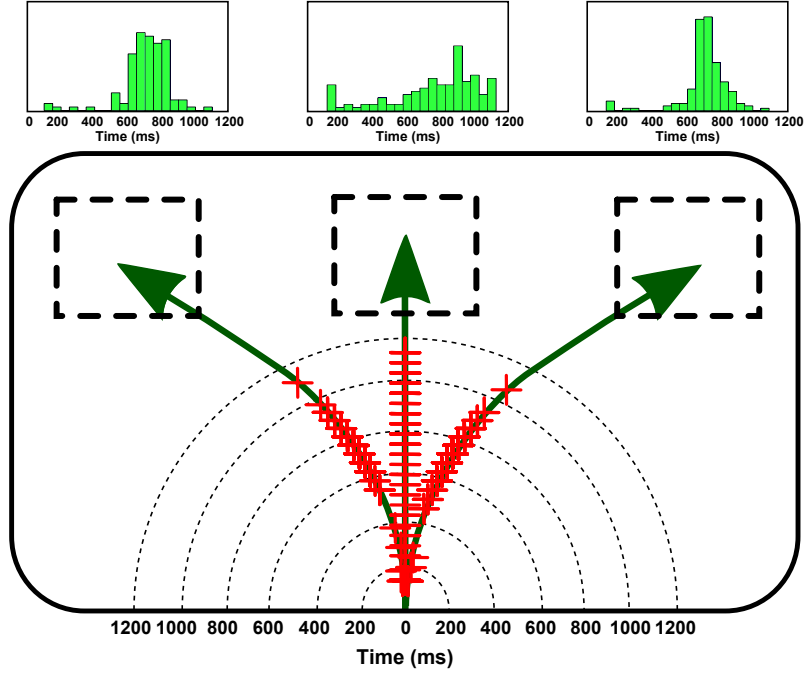
Supplementary Figure 3.10: Time location of mismatch events properly classified (only using temporal features) over their respective trajectories for all subjects. The elapsed time from the *splitting point* comes represented by the dotted arcs. The number of mismatch event detections is depicted in the histograms shown over each target.
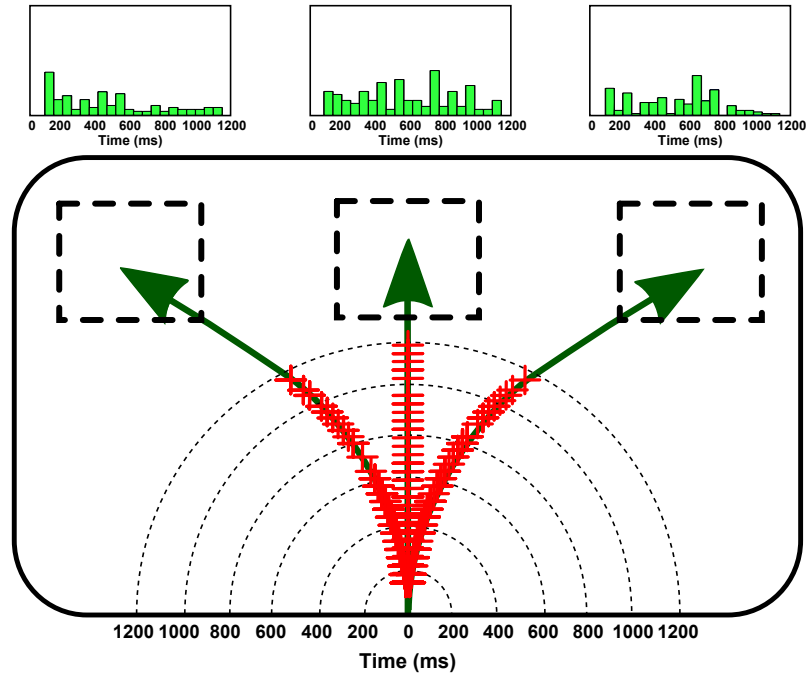
Supplementary Figure 3.11: Time location of mismatch events properly classified (only using frequency features) over their respective trajectories for all subjects. The elapsed time from the *splitting point* comes represented by the dotted arcs. The number of mismatch event detections is depicted in the histograms shown over each target.
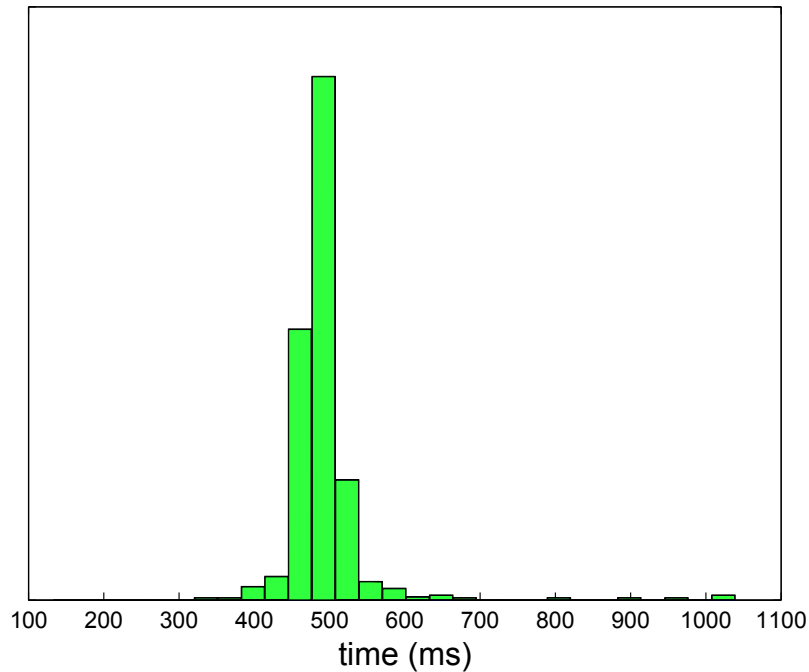
Supplementary Figure 3.12: Histogram representing the elapsed time from the event onset until the mismatch detection for the sudden condition.

4

Control of devices:
Teaching a robot to navigate using ErrPs

4.1 Introduction

Chapters 2 and 3 have demonstrated that error potentials appear during the continuous monitoring of trajectories executed by a device and the feasibility of decoding these potentials in single trial using frequency features and advanced machine learning algorithms. This opens the door towards out-of-the-lab scenarios, user-centered applications that can benefit from this type of error-based cognitive information such as the control of robotic devices or motor restoring therapies that may improve the daily life of real patients.

When learning complex tasks, robots are usually faced with vast action-state spaces which are difficult and expensive to explore without prior knowledge of the structure of the environment. Furthermore, there exist hazardous regions or configurations that should be avoided since they may be dangerous for the robot or people around the robot. Humans are naturally aware of the intrinsic structure and domain knowledge of a task and, consequently, they can provide feedback during robot operation for learning or control purposes. Indeed, this feedback is a very powerful way to provide supervision during robot learning for complex tasks [Knox & Stone, 2009]. This use of human feedback during robot operation and learning requires some kind of communication between the human and the robot, where the most common modalities include speech gestures and physical interaction [Austermann & Yamada, 2008].

Most work in this area has used a reinforcement learning framework to incorporate human feedback during the learning process [Isbell Jr et al., 2001]. Since feedback occurs through the interaction between human and robots, the human shapes the reward according to her own understanding of the task. Some authors have studied how to model binary feedback (e.g. approval or disapproval) and incorporate it to the learning process [Knox

& Stone, 2009, 2010, 2012]. Another important issue is that during interaction humans do not only provide feedback but also tend to provide guidance for future actions [Thomaz & Breazeal, 2006].

This chapter explores the usage of EEG-based BMIs as an alternative communication channel to provide feedback to robots using brain signals. As commented in the introduction of this thesis (Chapter 1), in most cases BMIs decouple the operation of the device from the mental task used to control the robot (e.g. motor imagery of body limbs to operate a virtual cursor) and there has been little effort in terms of using brain signals that directly encode cognitive information about the task itself and, in particular, feedback information about the behavior of the robot.

In this chapter, we propose the use of EEG error-related potentials as feedback for controlling a robot. We exemplify the main idea for a target reaching task in two different scenarios: a simple, virtual grid world; and a 2D real mobile robot navigation task. During the experiments, the role of the user was simply to evaluate the robot actions as correct or wrong, while the robot tried to learn and reach the intended user's goal. In order to cope with the limited information provided by ErrPs, we use a shared-control strategy based on the inverse reinforcement learning framework, where the robot maintains a belief over a set of possible targets updated using feedback signals extracted from brain activity during robot operation. For discrete worlds, the results show that the robot is able to reach the target using only ErrPs as feedback elicited from human observation. Finally, promising preliminary results for continuous domains and real robots are also reported using a mobile robot.

4.2 Shared-control of a reaching task

This section describes the proposed shared-control strategy that allows the robot to simultaneously infer the user's intended goal and reach it using ErrPs. The proposed shared control uses an inverse reinforcement learning algorithm to accumulate evidence about a set of predefined possible goals while executing a trajectory. This approach consists of two phases. The first one computes offline optimal trajectories (i.e. policies) for each potential target, while the second performs an online policy matching to rank them during robot operation based on error potentials elicited for wrong actions.

Here, we give a general view of the method, which is then particularized in the following sections 4.4.1.4 and 4.5.1.4. Let $\mathbf{s}$ and $\mathbf{a}$ denote the state of the world and a robot action. Given a set of possible targets, let $f_i(\mathbf{s}, \mathbf{a})$ be the value function [Sutton & Barto, 1998] that describes the value of executing action $\mathbf{a}$ in state $\mathbf{s}$ for a given target i. The optimal policies can be obtained from $f_i(\mathbf{s}, \mathbf{a})$ as:

$$\pi_i^*(\mathbf{s}) = \arg\max_{\mathbf{a}} f_i(\mathbf{s}, \mathbf{a}). \tag{4.1}$$

In the examples of the next sections these functions can be computed exactly, although in general it may be necessary to approximate them.

During the control phase, the value functions are used to estimate the probability of each target by measuring how well non-error actions match the policies of each target. At each time step t, the device performs an action $\mathbf{a}_t$ from state $\mathbf{s}_t$. Let $\mathbf{x}_t$ denote the EEG window corresponding to time t and $p(c_t = 1|\mathbf{x}_t)$ be the probability provided by the ErrP decoder described in future subsections 4.4.1.3 and 4.5.1.3. Let $p(\pi_i^* \mid (\mathbf{a}, \mathbf{s}, \mathbf{x})_{1...t})$ be the posterior probability of policy π_i^*, that is, of target i being the one selected by the user. This posterior is computed recursively for each new action executed by the robot

$$p(\pi_i^*|(\mathbf{a}, \mathbf{s}, \mathbf{x})_{1...t}) \propto p(\mathbf{a}_t|\pi_i^*, (\mathbf{s}, \mathbf{x})_t) \cdot p(\pi_i^*|(\mathbf{a}, \mathbf{s}, \mathbf{x})_{1...t-1}), \tag{4.2}$$

where the likelihood $p(\mathbf{a}_t|\pi_i^*, (\mathbf{s}, \mathbf{x})_t)$ measures the similarity between the executed action and the policy of target i when an error or non-error is detected from the EEG. The actual implementation depends on the protocol and is described in the next sections. The execution finishes when a probability $p(\pi_i^*)$ reaches a convergence criterion, p_c.

4.3 Data Recording

As in previous chapters, EEG and EOG activity were recorded using a g.tec system. For the EEG, 32 electrodes were recorded, distributed according to an extended 10/20 international system (FP1, FP2, F7, F8, F3, F4, T7, T8, C3, C4, P7, P8, P3, P4, O1, O2, AF3, AF4, FC5, FC6, FC1, FC2, CP5, CP6, CP1, CP2, Fz, FCz, Cz, CPz, Pz and Oz), with the ground on FPz and the reference on the left earlobe; for the EOG, 6 monopolar electrodes were recorded (placed above and below each eye, and from the outer canthi of the left and right eyes [Croft & Barry, 2000]), with the ground on FPz and the reference on the left mastoid. The EEG and EOG signals were digitized with a sampling frequency of 256 Hz, power-line notch filtered, and band-pass filtered at $[1, 10]$ Hz. The EEG was also space filtered using CAR. Also, horizontal, vertical, and radial EOG were computed to remove the ocular activity from the EEG using a regression algorithm [Schlögl et al., 2007].
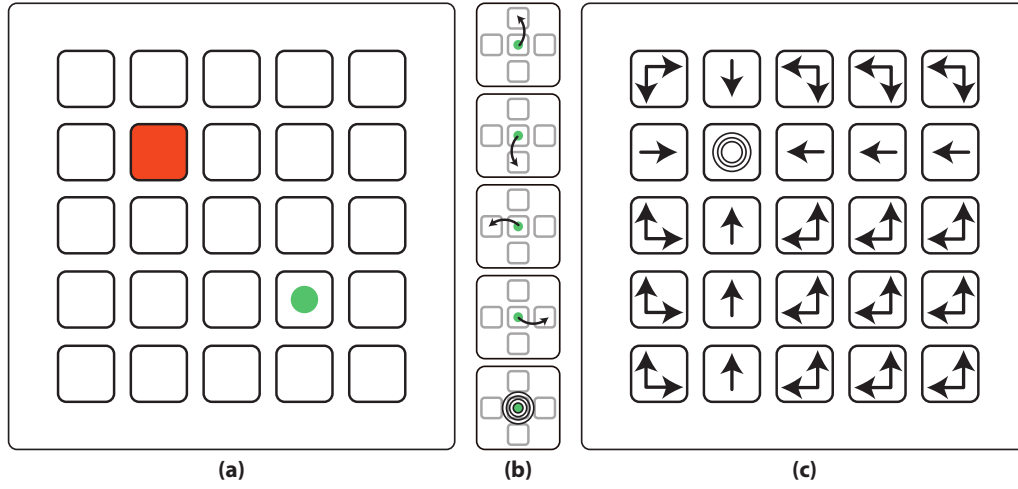
Figure 4.1: (a) Experimental protocol designed. The protocol showed a 5x5 grid with a virtual cursor (green circle) and a goal location (shadowed in red). (b) The cursor could perform five different actions (from top to bottom, move one position up, down, left or right, or performing a goal-reached action). (c) Optimal policy for the goal exemplified on (a).

4.4 Discrete reaching task

4.4.1 Methods

4.4.1.1 Experimental design

The visual protocol for the discrete scenario is shown in Figure 4.1. The protocol consisted of a virtual cursor (green circle) that could perform discrete actions within a 5x5 grid, and its goal was to reach the target location (shadowed in red). The cursor could perform five different instantaneous actions: move one position left, right, up or down; and a goal-reached action, represented as concentric blue circumferences (see Figure 4.1b). The time between two actions was random within the range $[3, 3.5]$ s. The users evaluated the actions as correct for (*i*) a movement towards the goal position, or (*ii*) a goal-reached action over the goal position; and as incorrect otherwise (see Figure 4.1c). Four subjects (mean age 26 ± 2 years) performed the experiments, seated one meter away of a computer screen displaying the protocol. Users were instructed not to move their eyes during the cursor actions, and to restrain blinks only to the resting periods.

During the calibration phase, the device performed random actions with 20% of probability of performing an incorrect one. This phase lasted for 30 minutes, acquiring around 80 correct and 320 erroneous examples. During the control phase, two different groups of goal locations were tested: (*i*) the first group (denoted fixed goals) was shared for all the subjects, and consisted of five goals and initial cursor positions (see Figure 4.4); (*ii*) for
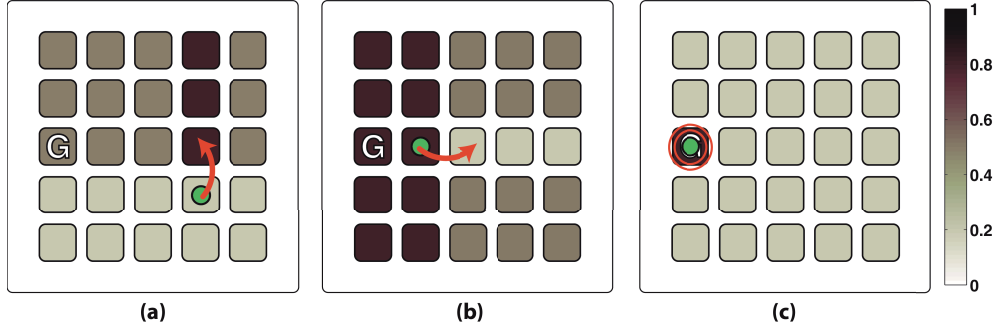
Figure 4.2: Likelihoods of each policy π_i after performing different actions: (a) correct movement with $p(c_t = 1|x_t) = 0.2$ (b) incorrect movement $p(c_t = 1|x_t) = 0.8$ (c) or a goal-reached action $p(c_t = 1|x_t) = 0.2$. The goal position is marked with a capital G.

the second group (denoted free goals), each user was asked to freely choose five different initial cursor positions and goals to reach.

4.4.1.2 Electrophysiology analysis

EEG data obtained from the calibration phase were time-locked to the movements of the virtual cursor and segmented using a time-window [-200, 1000]ms regarding to the onset of the events. Evoked responses for the error condition, correct condition and for their difference (error minus correct) were averaged for all participants at channel FCz [Nieuwenhuis et al., 2004]. The r^2 discriminability test [Wolpaw et al., 2002] between error and correct conditions was computed for each channel and time instant. Furthermore, scalp topographies as well as sLoreta source localization were computed to estimate the origin of intra-cranial activity at the occurrence of the most prominent peaks on the difference between the averaged error and correct potentials [Pascual-Marqui, 2002].

4.4.1.3 Calibration of error potentials

Features were extracted from eight fronto-central channels (Fz, FC1, FCz, FC2, C1, Cz, C2, and CPz) within a time window of $[200, 800]$ ms (being 0 ms the action onset) down-sampled to 64 Hz, forming a vector of 312 features. The features were then normalized, and its dimensionality reduced with principal components analysis (PCA) retaining 95% of the variance. A regularized linear discriminant (LDA) [Blankertz et al., 2011] was trained using the previous features. The classifier output has the form $y(\mathbf{x}) = \mathbf{w}'\mathbf{x} + b$, where $y(\mathbf{x}) < 0$ was classified as a correct assessment (class 0), and $y(\mathbf{x}) \geq 0$ as an error assessment (class 1). This output $y(\mathbf{x})$ was transformed into the probability that an example $\mathbf{x}$ was an error, $p(c = 1|\mathbf{x}) = \frac{1}{1+e^{-y(\mathbf{x})}}$ [Bishop, 2016].
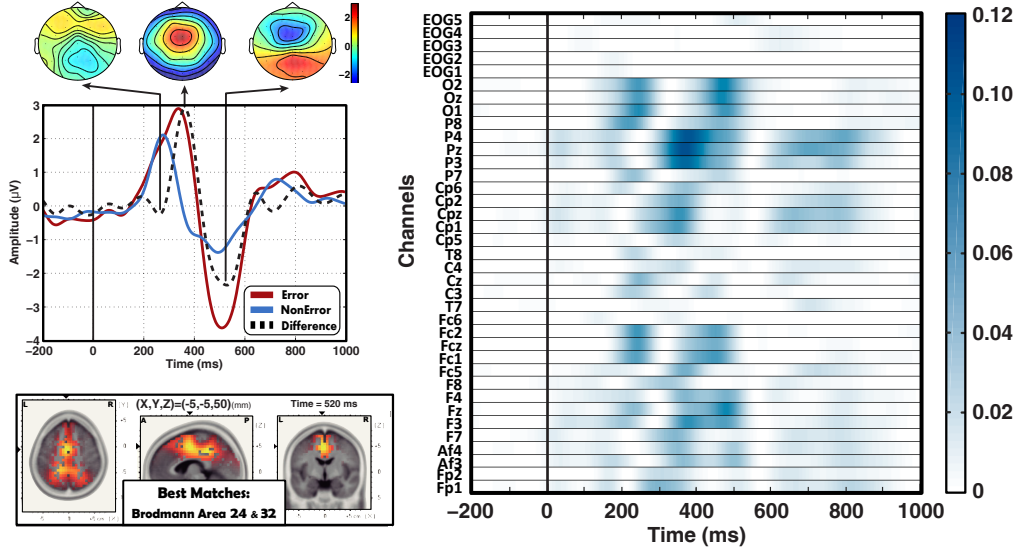
Figure 4.3: Action-locked averages from channel FCz (error, correct and difference in red, blue and black respectively), together with the color encoded topographic interpolation of the three most prominent peaks of the difference average. Time 0 ms indicates when the cursor executed an action.

4.4.1.4   Shared-control strategy

For this protocol, the value function $f_i(\mathbf{s}, \mathbf{a})$ was computed from the Q-values $Q_i^*(\mathbf{s}, \mathbf{a})$, which can be computed prior to the control phase using the Q-learning reinforcement learning algorithm [Sutton & Barto, 1998]. Once calculated, the Q-values were converted into probabilities, following a soft-max normalization:

$$f_i(\mathbf{s}, \mathbf{a}) = \hat{Q}_i^*(\mathbf{s}, \mathbf{a}) = \frac{e^{Q_i^*(\mathbf{s}, \mathbf{a})/\tau}}{\sum_{\mathbf{b}} e^{Q_i^*(\mathbf{s}, \mathbf{b})/\tau}}, \tag{4.3}$$

where τ is denoted the temperature (fixed to $\tau = 0.3$). This parameter served as a degree of reliability of the observed information (classifier output).

The likelihood function was computed as follows:

$$p(\mathbf{a}_t | \pi_i^*, (\mathbf{s}, \mathbf{x})_t) = p(c_t = 0 | \mathbf{x}_t) \cdot \hat{Q}_i^*(\mathbf{s}_t, \mathbf{a}_t) + p(c_t = 1 | \mathbf{x}_t) \cdot (1 - \hat{Q}_i^*(\mathbf{s}_t, \mathbf{a}_t)), \tag{4.4}$$

Notice that the first term of the likelihood represents how the policy π_i^* should be increased if the user's assessment was correct, while the second term penalized the policy π_i^* weighted by the probability of having and incorrect user's assessment. Figure 4.2 shows several examples of actions and likelihoods. For the performed experiments, a new action $\mathbf{a}_{t+1}$ was chosen following an ε-greedy strategy, and the run finished when reaching a convergence criterion of $p_c = 0.9$.
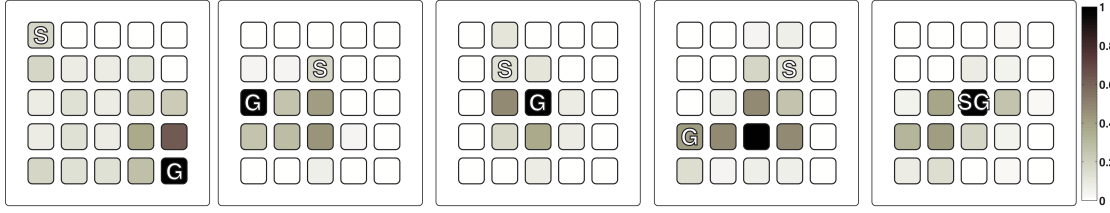
Figure 4.4: States visited by all the subjects, for each of the five runs executed with the fixed goals (from left to right, runs 1 to 5). Darker colors indicate more visited states. The range was normalized from 0 to 1 according to the most visited state for each run. The initial and goal positions are marked with an S and a G respectively.

4.4.2   Results

4.4.2.1   Electrophysiology analysis

Fig 4.3 shows the error, correct and difference grand averaged potentials (error minus correct averages) in channel FCz, averaged for all the four subjects. The difference grand average was characterized by three components: a negative deflection at around 250 ms, a positive deflection at around 400 ms, and a another negative component at around 500 ms. The r^2 discriminability patterns between error and correct events were larger around 200 and 450 ms for channels located in fronto-central areas, and around 375 ms in parietal sites. Comparatively, topographic interpolations of the two broader peaks of the difference average showed that the signals were generated mostly in fronto-central channels and the main source activations came from Brodmann areas 24 and 32. These results were in agreement with previous studies using error potentials [Ferrez & Millán, 2008a].

4.4.2.2   Control analysis

For each group of goals (fixed and freely-chosen), five metrics were evaluated: (*i*) Number of goals reached; (*ii*) number of actions needed to reach the goal, (*iii*) EEG seconds needed to reach the goal (net time); (*iv*) total time needed to reach the goal; and (*v*) classifier accuracy, measured as the percentage of detection of correct and erroneous signals. Note that the difference between the net and total times was the seconds belonging to inter-action intervals, which could be easily removed.

Table 4.1 shows the results for each subject and group of goals. The main result was that the device always reached the targets from any starting point, needing 25 ± 13 actions and 21 ± 8 actions (for the fixed and freely chosen goals) to reach the target. With inter-action intervals of around 3.25 s, the total time needed to reach the goals was of 80.76 ± 73.68 and 66.63 ± 26.85 seconds (fixed and free goals). Nonetheless, the net time (the seconds of EEG signal used for decoding) was of 19.88 ± 10.75 and 16.40 ± 6.61

seconds. The mean classifier accuracy was of 74.38 ± 4.66 and 77.67 ± 5.02. As expected, there was a significant negative correlation between the classifier mean accuracy and the time needed to reach the task ($r = -0.47, p = 0.038$ and $r = -0.79, p = 3 \cdot 10^{-5}$ for fixed and free goals).

Table 4.1: Results of the reaching task for the fixed and free goals

| | **S1** | | **S2** | | **S3** | | **S4** | | $\mu \pm \sigma$ | |
	Fixed	Free	Fixed	Free	Fixed	Free	Fixed	Free	Fixed	Free
♯ Targets reached (out of 5)	5	5	5	5	5	5	5	5	5 ± 0	5 ± 0
♯ Actions	16 ± 2	23 ± 9	43 ± 9	21 ± 7	23 ± 12	16 ± 6	17 ± 5	23 ± 11	25 ± 13	21 ± 8
Net time (s)	12.96 ± 1.91	18.08 ± 7.37	34.56 ± 7.10	16.48 ± 5.84	18.40 ± 9.73	12.96 ± 5.10	13.60 ± 4.38	18.08 ± 8.44	19.88 ± 10.75	16.40 ± 6.61
Total time (s)	52.65 ± 7.76	73.45 ± 29.93	140.40 ± 28.83	66.95 ± 23.73	74.75 ± 39.54	52.65 ± 20.73	55.25 ± 17.80	73.45 ± 34.29	80.76 ± 73.68	66.63 ± 26.85
Mean accuracy (%)	83.14 ± 15.15	78.75 ± 12.62	69.49 ± 4.13	82.48 ± 10.66	72.49 ± 3.74	88.18 ± 10.51	76.35 ± 8.89	78.66 ± 14.44	74.38 ± 4.66	77.67 ± 5.02

An interesting result is that it was not necessary to visit all the states before reaching the goal (see Figure 4.4). For instance, during run 3, mostly all the central states were visited, whereas the peripheral states were not. This could allow for a better scalability of the system (e.g. as the state space is increased, the percentage of visited states would decrease).

4.5 Continuous reaching task

4.5.1 Methods

4.5.1.1 Experimental design

The second experiment consisted in reaching a target location with a low cost mobile robot (ePuck, [Mondada et al., 2009]). The experimental protocol is shown in Figure 4.7a. The arena was a 200×200 cm^2 map, that was discretized into a 5×5 of possible goal positions. To ease the assessment of the robot actions by the user and for visualization purposes, each target was depicted as an icon of a different city. The robot moved in the following way. First, it executed a pure rotation motion to orientate the robot towards a desired direction (i.e. towards a goal). Then, it followed a straight line to the desired position. Despite the goal positions were discrete, the possible states and actions of the robot were continuous. In order to obtain a robust measure of the robot position, the robot was visually tracked in real time with a camera located on the ceiling.

The main difference with the previous protocol was that the robot moved continuously and the user constantly evaluated the robot actions. As long as the decoder did not detect an error, the robot continued its motion to the selected goal. The robot stopped for a second after reaching a goal or detecting an error. Then, it moved towards a new goal selected based on the probabilities of each target. The user was asked to look over the robot actions, evaluating them as correct when the robot advanced or turned towards the

goal, and when the robot stopped over the desired goal position. On the contrary, the user had to evaluate as incorrect those motions that were not oriented towards the goal, when the robot stopped on a wrong spot, or when the robot overpassed the desired position or orientation. Two subjects (mean age 27) performed this experiment. They were seated one meter away from the map (see Figure 4.7a), and were instructed to minimize eyes movements or blinks during the robot actions.

For continuous actions there is not a clear trigger that enables the performance of time-locked analyses or/and feature extraction. Thus, in this experiment the calibration phase required two steps, one to acquire error and another for non-error responses. In each step, the user had to evaluate the robot actions towards five predefined goals and he had to push a button when an error occurred (step one) or when the robot was executing a correct action (step two), always with separations of at least one second between two trigger events. These runs were repeated until acquiring around 70 examples of each class. The calibration phase lasted a total of 30 minutes. During the control phase, the user freely chose the initial and goal locations.

4.5.1.2 Electrophysiology analysis

Following the same procedure of the analysis performed in section 4.4.1.2, EEG data from the calibration phase were segmented using the time-window [-200, 1000]ms were the onset of correct and erroneous trials corresponded to the pressing of the two buttons previously described to asses the robot's behavior during calibration. Evoked responses for the error condition, correct condition and for their difference (error minus correct) were averaged for all participants at channel FCz. The r^2 discriminability test between error and correct conditions was computed for each channel and time instant. Additionally, scalp topographies and sLoreta source localization were also computed at the occurrence of the most prominent peaks on the difference between the averaged error and correct potentials.

4.5.1.3 Calibration of error potentials

As previously described, for the calibration phase two buttons were used to have a representative onset of erroneous and corrects events to enable feature extraction. During the control phase, this trigger is removed, and the classification is performed using a sliding window (fixed to steps of 62.50 ms for the experiments), as it was described in Chapter 3.

In addition, the absence of a proper cue difficult the ErrPs detection, making the temporal features described above insufficient to obtain low misdetection rates. As we learned in previous chapters, the proposed solution to mitigate this effect comes across
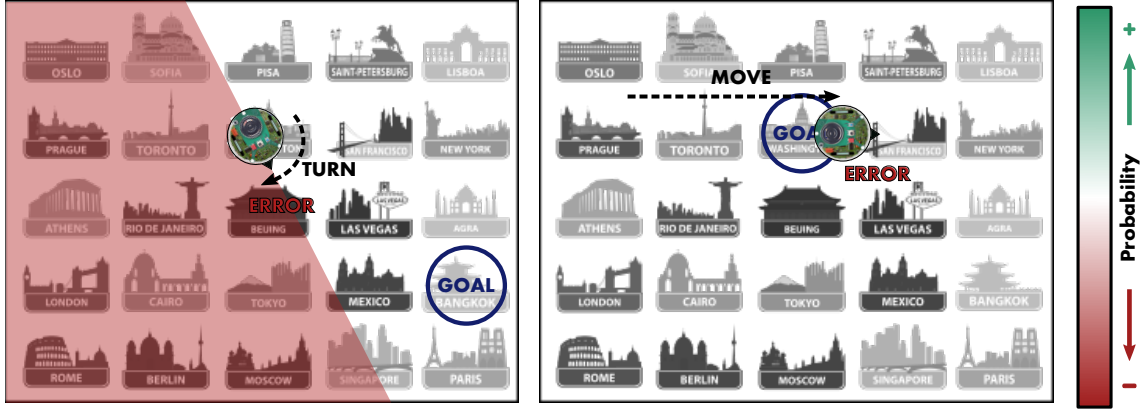
Figure 4.5: The mobile device executed 2 types of continuous actions on top of a map discretized in 25 different locations. First the device rotated its orientation towards the location with larger likelihood according to its current map of beliefs. If an error was detected during the rotation, the internal probability map was updated using the likelihood function graphically represented in the figure (left). If no error was detected, the device moved forward constantly updating the probability of those target locations in a determinate radius in front of it as it is depicted in the figure (right)

.

adding features from the frequency domain, namely the power spectral density (PSD), which are rather insensitive to time shifts. The PSD was calculated on 1000 ms of EEG for each of the eight fronto-central channels used before. The new features are the power values in the theta band ($[4, 8]$ Hz) $\pm$ 1 Hz for each channel (as previous studies suggest that the error potentials are generated within this band [Cavanagh et al., 2009]). Temporal and frequency features were concatenated conforming a total vector of 200 features. Single-trial classification was carried out using a support vector machine (SVM) with a radial basis function (RBF) kernel, whose output was the probability that an example $\mathbf{x}$ was an error, $p(c = 1|\mathbf{x})$.

4.5.1.4 Shared-control strategy

Let us encode each possible state as the position and orientation of the robot, $\mathbf{s} = (u, v, \theta)$, and each action as the combination of a turn and a linear movement $\mathbf{a} = (\theta_a, \rho)$ represented by the angle θ and distance ρ. In this case, we use a potential $U_i(u, v)$ to define the optimal policy for target i, ignoring the non-holonomic constraints of the robot. We used the symmetric 2D quadratic function:

$$U_i(u, v) = [u, v]' A_i[u, v] + b_i'[u, v] + c_i, \tag{4.5}$$

where A_i, b_i and c_i depend on the position of target i and the size of the map.

The likelihood function was computed differently depending on the action step (rotation or linear movement). While turning, the likelihood was computed as a piecewise function:

$$p(\mathbf{a}_t|\pi_i^*, (\mathbf{s}, \mathbf{x})_t) = \begin{cases} k_n & \text{if } (p(c_t = 1|\mathbf{x}_t) \geq T_e) \wedge (\theta_t - \theta_{t-1} > 0) \wedge (\theta_i - \theta_t \in (\ \ \ 0, \pi \ ]), \\ k_n & \text{if } (p(c_t = 1|\mathbf{x}_t) \geq T_e) \wedge (\theta_t - \theta_{t-1} < 0) \wedge (\theta_i - \theta_t \in (-\pi, \ 0 \ ]), \\ 1 & \text{otherwise} \end{cases}$$

(4.6)

$k_n < 1$ is a penalization constant, fixed to 0.2 for the performed experiments; and $(\theta_i - \theta_t)$ is the relative angle between goal i and the robot state $\mathbf{s}_t$. The three boolean conditions of the first two pieces of the likelihood describe: (i) the output of the classifier was considered an error based on a threshold $T_e \in [0, 1]$. Since we wanted to minimize the number of false positives (correct assessments detected as errors), we fixed this threshold to a high value, $T_e = 0.8$; (ii) the robot is turning clockwise or anti-clockwise; and (iii) the goal is located left or right relative to the current robot position and orientation. Intuitively, if an error was detected, this likelihood simply penalized those targets where the robot was turning to; on the contrary, no changes were made on the policies when the user's assessments were detected as correct.

For the linear movement step, the likelihood was computed as follows:

$$p(\mathbf{a}_t|\pi_i^*, (\mathbf{s}, \mathbf{x})_t) = \begin{cases} 1 + k_p \cdot \mathcal{N}(\theta_t - \theta_i \ ; \ 0, \sigma) & \text{if } (p(c_t = 1|\mathbf{x}_t) < T_e), \\ 1 - k_n \cdot \mathcal{N}(\theta_t - \theta_i \ ; \ 0, \sigma) & \text{if } (p(c_t = 1|\mathbf{x}_t) \geq T_e) \end{cases}$$

(4.7)

The first piece corresponds to a correct user's assessment and assigns a higher likelihood to goals in front of the robot ($k_p = 0.01$). The second one is applied when an error is detected and assigns a lower likelihood to targets in front of the robot ($k_n = 0.7$). We modeled the uncertainty in the user's perception of directions with a normal probability distribution with zero mean and standard deviation σ, fixed to have a field of view of $\pm$ 20 degrees. The difference between k_p and k_n reflects the fact that number of detected errors should be lower than the number of correct actions.

The next action was selected greedily as the optimal policy according to the potential function $U_i(u, v)$ of the target with the higher probability at that point in time. This basically rotated the robot to align it with the direction of the gradient of $U_i(u, v)$ and
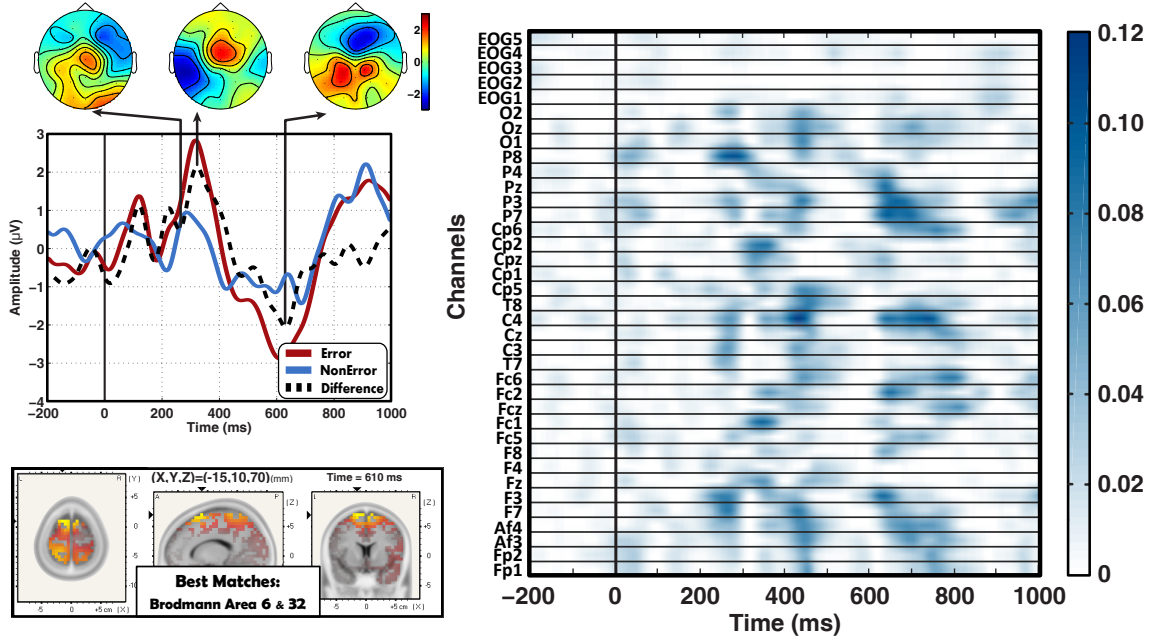
Figure 4.6: Action-locked averages from channel FCz (error, correct and difference in red, blue and black respectively), together with the color encoded topographic interpolation of the three most prominent peaks of the difference average. Time 0 ms indicates the time instant when users pressed the button.

then moved forward to the target. The run finished when reaching a convergence criterion of $p_c = 0.4$.

4.5.2 Results

4.5.2.1 Electrophysiology analysis

Figure 4.3 shows the error (red), correct (blue) and difference (dashed-black) grand averaged potentials in channel FCz. Observing the difference grand average between error and correct responses, we found a dominant positive peak at 360 ms and a broader negative deflection around 600 ms. Differences between error and correct responses according to the r^2 metric were more discriminable in fronto-central and centro-parietal areas for the positive peak at 360 ms, and more prominently in parietal channels for the negative deflection at 600 ms. Also, r^2 computed for EOG electrodes did not reveal any difference between conditions, which implies that eye movements were not used to control the robotic device. Source localization analysis suggested that the main activity for the dominant negative peak came from Brodmann areas 6 and 32, linked with the anterior cingulate cortex and pre-SMA, which has been also reported in previous ErrP studies Iturrate et al. [2012]; Chavarriaga & Millán [2010].
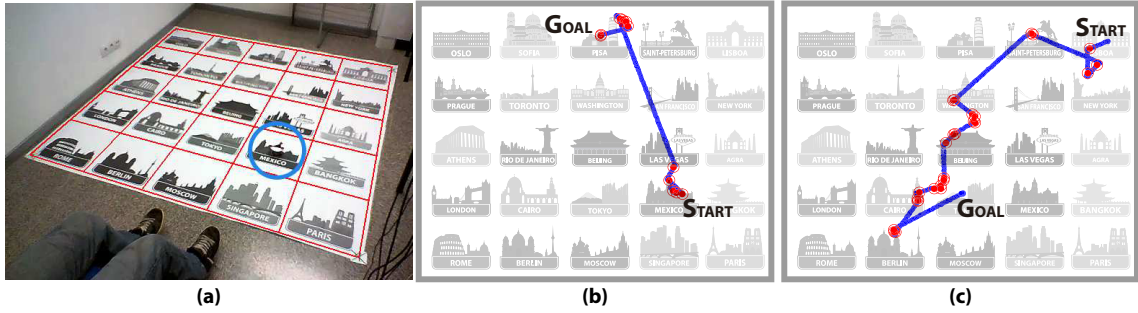
Figure 4.7: (a) Snapshot of the experiment performed, together with the grid superimposed to the image. The mobile robot location is marked with a circle. (b-c) Trajectories performed by the robot (marked in blue) during the two online runs. The initial and goal positions were from (b) Mexico to Pisa and (c) Lisbon to Tokyo. Each red mark indicates the moment when an error was detected from the EEG signal.

4.5.2.2 Control analysis

Figure 4.7(b-c) shows two representative trajectories resulting from controlling the mobile robot. The time elapsed from the start of the movement until goal reaching of each trajectory was 60 and 121 seconds respectively, counting up to 11 error events in the first run, and 26 in the second. The performed trajectories revealed some of the properties of the proposed protocol: (*i*) most of the errors were concentrated during turns. This allowed the robot to perform mostly long straight paths towards the believed goal location; (*ii*) as no errors are detected, the robot maintains a fixed trajectory, as can be seen on the subpath from Las Vegas to Pisa (see Figure 4.7b); and (*iii*) the system can recover from false positives. For instance, during the second run the robot chose to go from Beijing to Tokyo (see Figure 4.7c) but an error was detected. This made the robot deviate towards other goals (Cairo and Berlin), but in the end it reached the desired position.

4.6 Discussion

In this chapter, we have presented a way of controlling virtual and real devices using human feedback as the unique commanding tool. In order to cope with the limited transfer rates provided by the decoding of neural signals, we exploited a shared control strategy in which the user and the intelligent agent had the common objective of reaching a specific position. In this sense, the computer agent was programmed to maintain a belief over the different possible targets and execute its actions following a greedy policy towards the most likely position. At the same time, the user was monitoring the actions of this device and mentally evaluating the correctness of its decisions. Failing to execute the optimal movements towards the goal resulted in the generation of error-related potentials in the

user's brain, which were used to guide the robot using inverse reinforcement learning to update its internal map of beliefs. Therefore, user and device can be seen as a symbiotic relationship in which the user needs the device in order to explore the environment, and the device needs the user guidance in order to know where to move. The usage of this strategy allowed several users to reach their desired target position in a 5×5 grid world after 23 actions on average (less than one minute of EEG) in a virtual scenario. Furthermore, the preliminary results obtained for 2 subjects in real environments with a mobile robot were very promising, suggesting that it is possible to constantly determine the user's assessments while learning a task.

During the control of the virtual device, differences between error and non-error grand averaged signatures were characterized by a small centro-parietal negativity around 250 ms, followed by a fronto-central and sharp biphasic modulation in which the positive component peaked at 370 ms and the subsequent negative deflection had maximum magnitude around 500 ms. These error-related potential signatures describe a similar morphology to that observed in previous chapters of this thesis and in other studies that have reported the occurrence of ErrPs as the monitoring of discrete actions [Chavarriaga & Millán, 2010; Iturrate et al., 2012]. Analogously, the error-related brain signatures recorded during the control of the mobile robot resembled those of the previous task. Fronto-central sites of the scalp displayed maximum positive difference between error and non-error at 360 ms, whereas the larger negative peak was found more prominent in fronto-central channels at 600 ms. This supposed a slight delay in the appearance of these peaks compared to the virtual task. This phenomenon is in line with latency delays observed in Chapter 2, in which more difficult and cognitive demanding tasks manifested temporal shifts in the evoked potentials, specially those that appear later and are related with conscious processing [Schubert et al., 2006; Luck, 2014]. Nevertheless, despite the different latencies, main brain activation of this component was located in Brodmann areas 6, 24 and 32 for both tasks, which correspond to brain regions that have been reported to be involved in high-level functions, such as decision-making, performance monitoring and error processing [Liotti et al., 2000].

In the classification department, the ErrP accuracy detection rates for the discrete task ranged between 70% to 88% depending on the subjects and the the modality in which the goal was chosen (fixed or free). As we reported in the previous chapters, this performance is in line with other EEG studies that have successfully detected ErrPs elicited after the occurrence of discrete erroneous events [Iturrate et al., 2010; Chavarriaga et al., 2014]. On the other hand, during the control of the mobile epuck, the behavior of the robot and the assessment of the users are more subjective and thus estimating the ground truth of the decoded EEG signals to compute the classification performance is very intricate. In this

sense, we used two metrics that to some extent allowed to compare the results obtained among the two tasks. First, the number of required actions to reach the goal. The discrete control task took an average of 19 actions considering both correct and erroneous movements, whereas for the mobile device reaching the goal required an average of 18 errors. The second metric was computed as the necessary time to reach the desired target. Considering the inter-action interval (around 3.25 s) specified during the first task, the total time needed to reach the goals was of 80.76±73.68 seconds. Nonetheless, if we do not account for the inter-action intervals, which could be easily minimized, the net time was of 19.88±10.75 seconds. Notice that in this scenario the actions were instantaneous and this time represent the seconds of EEG signal used for decoding. In contrast, the epuck was continuously moving in a 200×200 cm^2 map taking between 60 to 121 seconds to reach the goal. This metrics do not only allow to compare the results among the two studied tasks but also can be used to contrast these performance results obtained from the control of devices using a BMI with other techniques that do not necessarily rely on brain signals such us EMG (i.e. muscular activity, eye trackers or even joysticks.

However, an important factor of our BMI-based protocols is that they are specially designed for people that may have lost their ability to move. In this sense, neither the user nor the device can reach the desired goal independently. The user is not able to reach the desired reward (e.g. in our paradigm a specific position) and the intelligent agent cannot updated its internal probability map without the neural assessments of the user. Both need to learn to cooperate and adapt to each other to solve the task.

One may consider that a clear limitation of the proposed experiments is that they only contemplate a restricted number of targets (i.e. a 5×5 grid). Even during the continuous control of the epuck, the actions and the map of states were continuous but the set of possible goals was discretized. This makes complete sense from an application-based point of view, in which a user could be interested in controlling his robotic wheelchair to reach a specific room at his house (e.g. the bedroom) or a specific location within a room (e.g. in front of his bed); or in a grasping task, be able to choose one item to grab (e.g. the glass of water) among a set of several objects. In this context, our encouraging results have shown that it is not necessary to explore the whole space of possible targets to reach the desired goal. For instance, during run 3 of the discrete task, mostly all the central states were visited, whereas the peripheral states were not; or for the trajectories displayed in 4.7 only a small percentage of the map was explored before reaching the goal. This is an interesting property of the proposed control scheme, since it allows for a better scalability of the system, due to the fact that each step of the trajectory provides information for multiple goals simultaneously. As a result, we could think that for application which required larger states spaces the percentage of visited states would actually decrease.

the exposition to continuously repeated stimulus produces that the response to it becomes less and less intense [Stein, 1966]. A major role of habituation is to limit the usage of attentional resources for stimuli that are no longer salient in terms of threat or reward [Groves & Thompson, 1970; Rolls, 2000].

Another key factor of our protocols consist in a control paradigm purely based on error detection, which alleviate the cognitive workload of the subject that only has to monitor the device actions and evaluate if they are right or wrong. However, this type of control could prompt an uncontrolled ratio of error vs correct assessments. In the literature, typically the percentage of erroneous events follow fixed ratios between 20% or 30% [Chavarriaga & Millán, 2010; Iturrate et al., 2013a]. Even though the use of ErrP in practical applications cannot assure a stationary percentage of errors, this ratio has empirically shown to generate more distinguishable EEG patterns and thus better accuracies [Chavarriaga & Millán, 2010]. Furthermore, the exposition to a large number of continuously repeated erroneous events may not only produce habituation generating less and less intense brain responses [Stein, 1966; Rolls, 2000] but also frustration for the users that lose the feeling of being in control [DiGiovanna et al., 2009]. As in our paradigm the agent behavior strongly rely on the previous user assessments and the inner probabilistic map, a fixed ratio of errors cannot be guaranteed. In this sense, we would expect that the quality of the signals generated by the users might be affected by the error rates, from random behaviors (80% of errors) to close to optimal behaviors (below 10%) [Iturrate et al., 2015a]. Nonetheless, in our experiments we did not find any substantial differences that prevented the successful control of the virtual agent or the epuck device.

Notice that these promising results require additional experimentation and need to be conducted with more subjects in order to validate them and establish more robust conclusions. Nevertheless, an avenue for future research could be the exploitation of more intelligent exploration strategies than the greedy one to infer the users' intended target. Also, we believe that this type of feedback will be very useful in combination with other neural correlates to maximize the information transfer rate [Ferrez & Millán, 2008b]. This could play an important role in application related to neurorehabilitation or neuroprosthetics, since the device can use this feedback to adapt its trajectories to the user preferences in a transparent way.

5

Motor substitution:
Hybrid BMIs for natural grasping

5.1 Introduction

As it was presented in Chapter 4, ErrPs can be effectively used to teach robotic devices how to explore and navigate an unknown scenario while successfully reaching the desired goal. Following the same principle, ErrPs can be thought as a way to improve the control of a prosthesis in motor rehabilitation and motor substitution applications for people with motor impairments after a stroke [Ramos-Murguialday et al., 2013] or a spinal cord injury [Müller-Putz et al., 2017a]. In this context, instead of relying on a completely exploratory behavior, it would be desirable to rely on a more manageable way to provide the desired patterns of action. Thus, EEG-based BMIs have tried to exploit natural motor correlates such as desynchronisation of motor rhythms or motor related potentials to decode motor intention [López-Larraz et al., 2014] or different types of motion [Müller-Putz et al., 2017b]. However, due to the non-stationary nature of EEG signals and its low signal to noise ratio, performance of this type of BMI is limited and hinders the development and deployment of this type of systems.

A possible way to overcome this limitation consists on correcting potential failures during the decoding of motor commands using ErrPs. In recent years, increasing efforts have been laid upon this concept of combining different mental tasks, commonly known as hybrid BMIs. Hybrid BMI systems [Pfurtscheller et al., 2010; Müller-Putz et al., 2015] have been proposed as a special type of BMI that combine multiple sources of information to tackle new applications or to increase reliability, robustness and performance [Rohm et al., 2013; Rupp et al., 2015]. Multimodal hybrid BMI incorporate other sources of information such as electrocardiography (ECG) [Scherer et al., 2007], electromyography (EMG) [Leeb et al., 2010], functional near-infrared spectroscopy (fNIRS) [Buccino et al.,

2016] or joysticks [Kreilinger et al., 2011]. Another approach exploits complementary neural tasks. For example, motor imagination can be used as a brain switch to enable the system to execute a secondary task [Müller-Putz et al., 2013] or combined with steady-state visual evoked potentials (SSEVP) as a selection tool [Allison et al., 2010].

This chapter presents the first steps towards a hybrid BMI for grasping, which combines the decoding of the type of grasp from EEG signals with error-related potentials (ErrPs) elicited as the result of monitoring an erroneous grasping. Such a BMI works in two steps. First, the type of intended grasp (in this particular case, pincer vs palmar) is decoded from slow cortical potentials (SCP), i.e. oscillations in the low-frequency spectrum (below 6 Hz) which have shown to have discriminative information for movement classification [Bradberry et al., 2009]. Previous studies have shown this can be used to distinguish grasps with ECoG [Pistohl et al., 2012] and EEG [Jochumsen et al., 2015; Schwarz et al., 2017], but with high misclassification rates. Second, the decoded action is executed and, when the decoding is not correct, the wrong grasping will elicit an ErrP that can be used to correct the action. As we have already seen in previous chapters, ErrPs have been used to correct the commands executed by a device [Schalk et al., 2000; Dal Seno et al., 2010], adapt classification algorithms [Artusi et al., 2011; Llera et al., 2011] or as learning for shared-control strategies [Chavarriaga & Millán, 2010; Iturrate et al., 2015a]. Additionally, in the context of hybrid BMIs, ErrPs have been combined with a right/left hand motor imagery task to enhance control of a virtual cursor moving through a grid [Ferrez & Millán, 2008a], with a P300 driven BMI-speller [Dal Seno et al., 2010] or with SSVEP to control a robotic arm [Kreilinger et al., 2012], but never with SCP.

Hybrid BMIs based on ErrPs usually exploit *interaction* and *observation* errors [Chavarriaga et al., 2014]. *Observation* ErrPs are elicited when unexpected disturbances occur while observing another person or artificial device committing an error [Chavarriaga & Millán, 2010; Kim & Kirchner, 2016], while *interaction* ErrPs occur when trying to control an interface and its actions differ from the initial user's intentions [Schalk et al., 2000; Ferrez & Millán, 2008a; Iturrate et al., 2014]. As it was emphasized in Chapter 2, several studies have shown that for a given experimental paradigm these ErrPs require subject dependent calibration. In this context, error-related signatures do not vary significantly over time [Chavarriaga & Millán, 2010] or across feedback modalities [López-Larraz et al., 2011]. However, there exist many factors that results on variations on the magnitude and latency of these waveforms such as user's age [Polich, 1997] and cognitive capabilities [Luck, 2014]; experimental related factors such as differences in the executed tasks [Iturrate et al., 2014]; stimuli contrast [Luck, 2014]; frequency of erroneous events [Chavarriaga & Millán, 2010]; or attention and engagement in the task [Hajcak et al., 2005]. Despite all the previous work on ErrP variations, ErrP-based hybrid BMIs have not considered how

the combination of two paradigms may modify the consequent ErrP and how this impact the reliability of the final system. Furthermore, ErrPs have not been previously studied in hybrid paradigms combined with SCP originated from single repetitions motor tasks like grasping. Thus, it is unclear whether the pairing of these tasks will result in measurable ErrP signals or whether the ErrP will be partially or completely masked by the preceding performed motor task.

In this chapter, we show that ErrPs are elicited in combination with SCPs originated from single repetition grasping tasks and we evaluate the impact that three design factors may have on the evoked ErrP. First, the speed of grasping may be constrained by the dynamics of the system (e.g. a prosthesis) and by safety issues. Different speeds may vary the user's perception of the feedback as shown in [Omedes et al., 2015a; Den Ouden et al., 2012]. Second, selecting the desired type of grasp requires different mental commands and the different feedback associated to each grasp may induce latency variations [Iturrate et al., 2014]. Third, to evaluate whether the usage of real versus imagined movements had an impact on the ErrP, the two most commonly reported mental strategies (motor execution and motor imagination [Müller-Putz et al., 2016]) were used to generate motor commands. We hypothesize that ErrPs can be decoded to identify wrong executed actions and that there will exist variations in the ErrP responses due to the different design factors that would affect performance. The experimental validation was based on a 3D environment that recreated a real-life grasping scenario. Thirteen healthy volunteers participated in this EEG experiment where they observed a virtual hand simulating their own limb, and attempted to control it using mental commands to grab one out of two familiar objects while assessing the correctness of the interface executed actions. We analyze the obtained ErrP to characterize the impact on the signals. Finally, we train state-of-the-art classifiers and evaluate how their performance is affected for the different conditions.

5.2 Methods

5.2.1 Participants and data recording

Thirteen self-reported right-handed healthy individuals (4 male, mean age 24 years) voluntarily participated in the study recorded in a laboratory of the Institute of Neural Engineering at Graz University of Technology. Participants gave their written informed consent and the study was conducted in accordance with the ethical standards of the 1964 Declaration of Helsinki.

EEG activity was recorded using three commercially available g.USBamp amplifiers (g.tec medical engineering GmbH, Austria) with 43 active electrodes distributed according

to the extended 10/20 international system (F7, F3, F1, Fz, F2, F4, F8, FC5, FC3, FC1, FCz, FC2, FC4, FC6, C5, C3, C1, Cz, C2, C4, C6, CP5, CP3, CP1, CPz, CP2, CP4, CP6, P7, P5, P3, P1, Pz, P2, P4, P6, P8, PO3, POz, PO4, O1, Oz and O2). The ground was placed on FPz and the reference on the right earlobe. Additionally, EOG activity was recorded using 3 active electrodes positioned above the nasion, and below the outer canthi of the eyes, forming a rectangular triangle and sharing the reference and ground [Schlögl et al., 2007]. EEG and EOG signals were recorded with a sampling frequency of 512 Hz and notch filtered at 50 Hz for power line noise removal. EEG data was spatially filtered using common-average-reference (CAR) and bandpass filtered using a zero-phase Butterworth filter of 8th order from 0.01 to 200 Hz. Electrode 3D positions were also recorded with a CMS 20 EP system (Zebris Medical GmbH, Isny, Germany). Additionally, ocular horizontal and vertical activity was computed using the 3 EOG electrodes to remove electro ocular contamination from the EEG signal using the regression algorithm presented in [Schlögl et al., 2007]. Data acquisition was carried out using an ad-hoc software based on the TOBI signal server and Simulink. The graphics of the virtual interface were programmed using Ruby language and data analysis was performed using self-created scripts using Matlab.

5.2.2 Experimental design

The objective of the experimental protocol was to analyze the variability of error potentials elicited due to varying different experimental factors while performing and evaluating a grasp decoding task. The interaction of the user with the system was through a 3D virtual environment that emulated the user's own limb (see Figure 6.1(top)). Using this interface, the experimental protocol consisted of trials where the subject performed two sequential tasks. First, the subject had to generate a motor command. Thereafter, the virtual hand executed a motion and the subject had to monitor and evaluate if this executed motion was the intended one.

Participants were seated on a comfortable armchair, approximately one meter away from a computer screen, with their right forearm resting on a table in horizontal position and the fist closed, where they monitored the visual protocol. They were asked to fix their gaze on the center of the screen at the position of the virtual hand, and restrict eye movements and blinks to the rest periods. Figure 6.1(top) shows the scheme and timeline of the experiment. Each trial started with a three seconds rest period during which the user can relax and move. The virtual hand was shown on a table in a similar position and orientation as the participant's one with the word "REST" displayed above it. Next, the word rest disappeared and a two second idle period, during which the user should not move, provided an artifact-free baseline signal. Next, one of two objects (a bottle or a
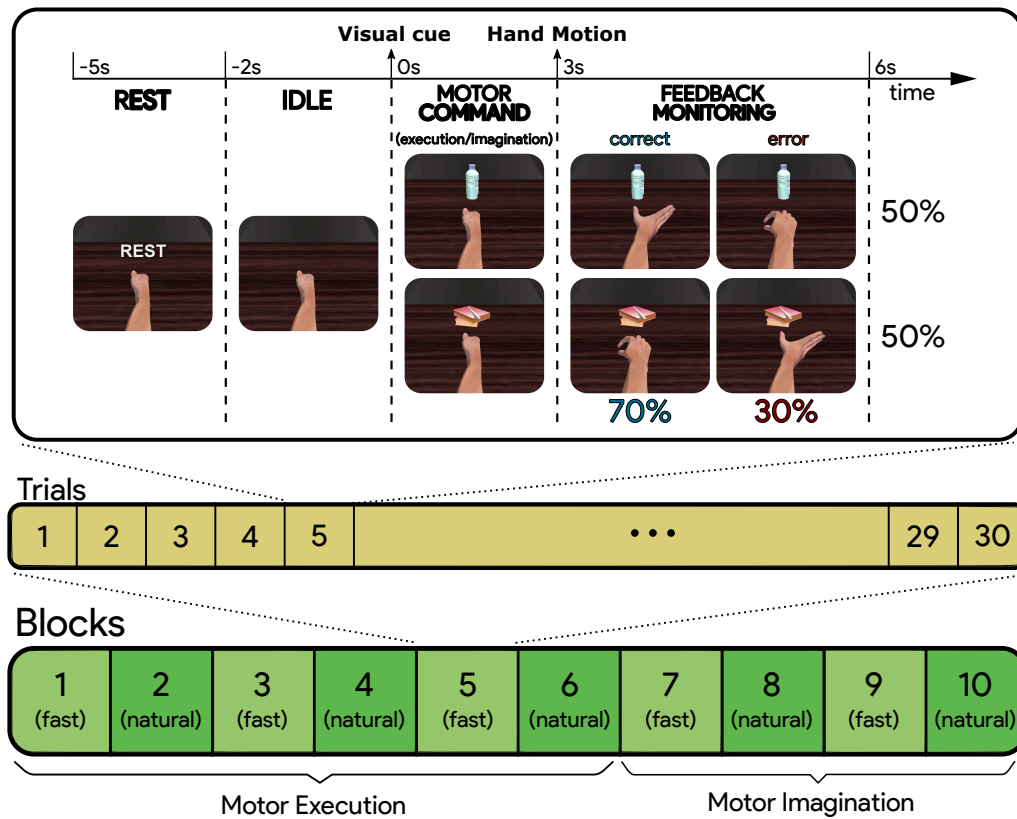
Figure 5.1: Scheme of the experimental protocol: trials (top), blocks (middle) and sequences of blocks (bottom). At top, timeline of the trial with the timing for the different phases, the frequency of each type of grasp and the frequency of error and correct actions. At bottom, distribution of blocks for slow and fast execution and for the mental strategy to be used to generate motor commands.

pen) appeared on the virtual table with equal probability. The object indicated the user the type of grasp and remained visible until the end of the trial. The bottle required a palmar grasp (opening and closing the hand), while the pen required a pincer grasp (thumb and index extension accompanied by a certain degree of arm pronation). Subjects were instructed to either execute or imagine once the grasping as soon as they saw the object appear on the monitor.

After three seconds, the virtual interface executed a predefined hand movement, palmar grasp or pincer grasp. Subjects were briefed that the BMI would try to "read their mental commands" to execute their intended grasp and that they should evaluate if the executed action was correct. A photodiode was used to synchronize the onset of the events to the beginning of the movements. Additionally, to keep a consistent error rate, the action was not decoded online and errors were generated with a probability of 30%. After three seconds, a new trial started.

The experiment consisted of ten blocks of 30 trials. Three different factors were modified. First, at the trial level the two types of grasps were equally likely. Second, blocks alternated between fast and slow grasping actions. In even blocks, grasping lasted 1.3 seconds whereas in odd blocks feedback was executed three times faster. Third, in the first 6 blocks of the experiment, participants were asked to execute the intended grasp, while in the last four they had to imagine the grasping. The sequence followed this order to make easier the habituation to the performed movements [Wriessnegger et al., 2014]. A total of 210 correct and 90 error events per participant were recorded with an average time per block of 6 minutes resulting in sessions of about 1.5 hours duration.

5.2.3 Electrophysiology analysis

This study focuses on the analysis the ErrP elicited during the evaluation task. EEG signal were analyzed in time and time-frequency domains following previous ErrP studies [Ferrez & Millán, 2008a; Cohen, 2011; Omedes et al., 2015a].

For the temporal domain analysis, EEG was bandpass filtered using a zero-phase Butterworth filter of 4th order from 1 to 10 Hz [Ferrez & Millán, 2008a] and time-locked to the onset of the visual feedback (i.e. the beginning of the grasp action at second 3 in Figure 6.1). Evoked responses in the time-window [2.5, 4.5]s were averaged for all participants at channel FCz [Nieuwenhuis et al., 2004] for the error condition, the correct one and for their difference (error minus correct averages). Scalp topographies at the most relevant peaks of these potentials were also computed. Statistically significant differences ($p < 0.05$) along time between error and correct conditions were assessed at each time instant using a two-tailed paired t-test corrected for multiple comparisons using the Benjamini & Hochberg procedure to control the false discovery rate (FDR) [Benjamini & Hochberg, 1995]. This method is preferred to Bonferroni for cases like ours where there is a large number of values to be screened compared to the amount of data available. Furthermore, sLoreta was used to estimate the origin of intra-cranial activity on the difference between the averaged error and correct potentials at the occurrence of the most prominent peaks [Pascual-Marqui, 2002]. For the time-frequency analysis, trials were segmented in the window [-1.5, 6]s where zero correspond to the appearance of the object; the interval [-1.1, -0.1]s is used as baseline, and the window [3, 6]s correspond to the EEG signal related to the evaluation of the executed action. Event-related (de)synchronizations (ERD/ERS) were calculated using Morlet wavelets based on frequency domain convolution with a wavelet-width of 8 cycles. T-percentile bootstrap analysis ($\alpha = 0.05$) was used to extract statistical significant components as in [Graimann & Pfurtscheller, 2006].

5.2.4 Statistical analysis

To analyze the impact of the three design factors, overall effects on the dynamics of the evoked brain responses to the monitored feedback were computed using a 4*2 factorial ANOVA with repeated measures for factors "feedback" (error, correct), "speed" (fast, slow), "movement" (palmar, pincer grasp) and "command" (execution, imagination). All the statistical analyses were computed using the commercial IBM SPSS software. Normal distribution of the data and homogeneity of variances were also tested before the analysis using the same platform. In the time domain, the analysis was carried out on the average magnitude and latency of the most representative peaks of the ErrP (P3 and N4) at the location with the highest expected activity, FCz [Cavanagh et al., 2009]. These magnitude and latency were computed for each of the 16 possible combinations of factors (e.g. one possible combination would be: error feedback + fast speed + palmar grasp + motor imagination command) by averaging for each subject all the trials of each combination and, then, extracting the P3 and N4 components. Similarly, in the time-frequency domain, another 4*2 factorial ANOVA with the same factors was computed for the spectral power at those time-frequency intervals and channels with larger significant ERS/ERD at group level. The average spectral power (in dB) was computed for each subject and combination using fixed group level intervals and channels. In the case that a main factor or interaction of the ANOVA reached significance, contrasts were tested by post-hoc two-tailed t-tests using Sirak's method for multiple comparisons.

5.2.5 Feature extraction and classification

A classifier was trained to discriminate between correct and error events, using a combination of temporal and frequency features. First, EEG signals were filtered between 1 to 10 Hz using a 4th order Butterworth bandpass filter. We epoched the signals using a one-second window aligned to the temporal onset of the virtual hand starting to move. To reduce the number of features maximizing the amount of information, examples for error and correct feedback trials were used to compute a set of spatial filters using the xDAWN method [Rivet et al., 2009]. The two best xDAWN filters that maximized the variance between error and correct events were retained and used to project the EEG signals into enhanced components for feature extraction. Temporal features were the EEG voltages within the one-second window of the signal resampled to 32 Hz, forming a vector of $32 \times 2 = 64$ temporal features. To include additional information from the frequency domain, we computed the power spectral density (PSD) using the same one-second temporal window after application of xDAWN spatial filters. The power was computed by means of the Burg's autoregressive power spectral density estimate of 16th order. Frequency

features were the power values of each of the two components from the *theta* band ([4, 8]Hz $\pm$ 1 Hz) leading to a vector of $7 \times 2 = 14$ features [Cohen, 2011]. Finally, both set of features were concatenated and normalized within the range [0, 1]. The previous features were used to train a support vector machine (SVM) classifier with a radial basis function (RBF) kernel [Lotte et al., 2007]. To avoid SVM sensitivity to imbalanced datasets [Akbani et al., 2004], the minority class of the training set (i.e. error class) was oversampled to match the number of trials of the majority class (i.e. the correct class).

This offline classifier was evaluated from two different points of view. First, the cross-validated average performance over subjects provides a measure of the single trial performance that can be achieved in error detection and it allows to measure the potential gain in a hybrid BMI. Second, specific classifiers were trained for each different factor to evaluate whether they had a practical impact on decoding. The procedure is as follows. For each subject, classification performance was evaluated using 4-fold cross validation, that is, data was randomly distributed in 4 blocks, each containing 25% of the data (75 trials). Three blocks (225 trials) were selected as the training set and were used to compute all the classification parameters (including xDAWN spatial filters, normalization values and SVM tuning). The remaining block was used to validate the model. Each of the four blocks was used as test to compute the averaged performance. To remove the effect of randomization, the reported performance is the average of ten repetitions with different blocks.

As mentioned above, the same process was repeated for each factor. Two classifiers, trained and tested only with trials belonging to a given value of a factor (e.g. only with trials corresponding to slow execution of grasping), were trained and evaluated using the same cross-validation approach. Results were compared with the chance level accuracy, computed as the average classification performance obtained by randomly shuffling 100 times the labels of the corresponding training data. From the distribution of values we computed the average and standard deviation. Being 56% accuracy the average chance level and 63% the threshold accuracy with a p-value of 0.05.

Also, significant differences between the pairs of subgroups were computed using a two-tailed paired t-test between the obtained results of each subject. The average performance was computed considering the ratio between error and correct events (30% to 70%).
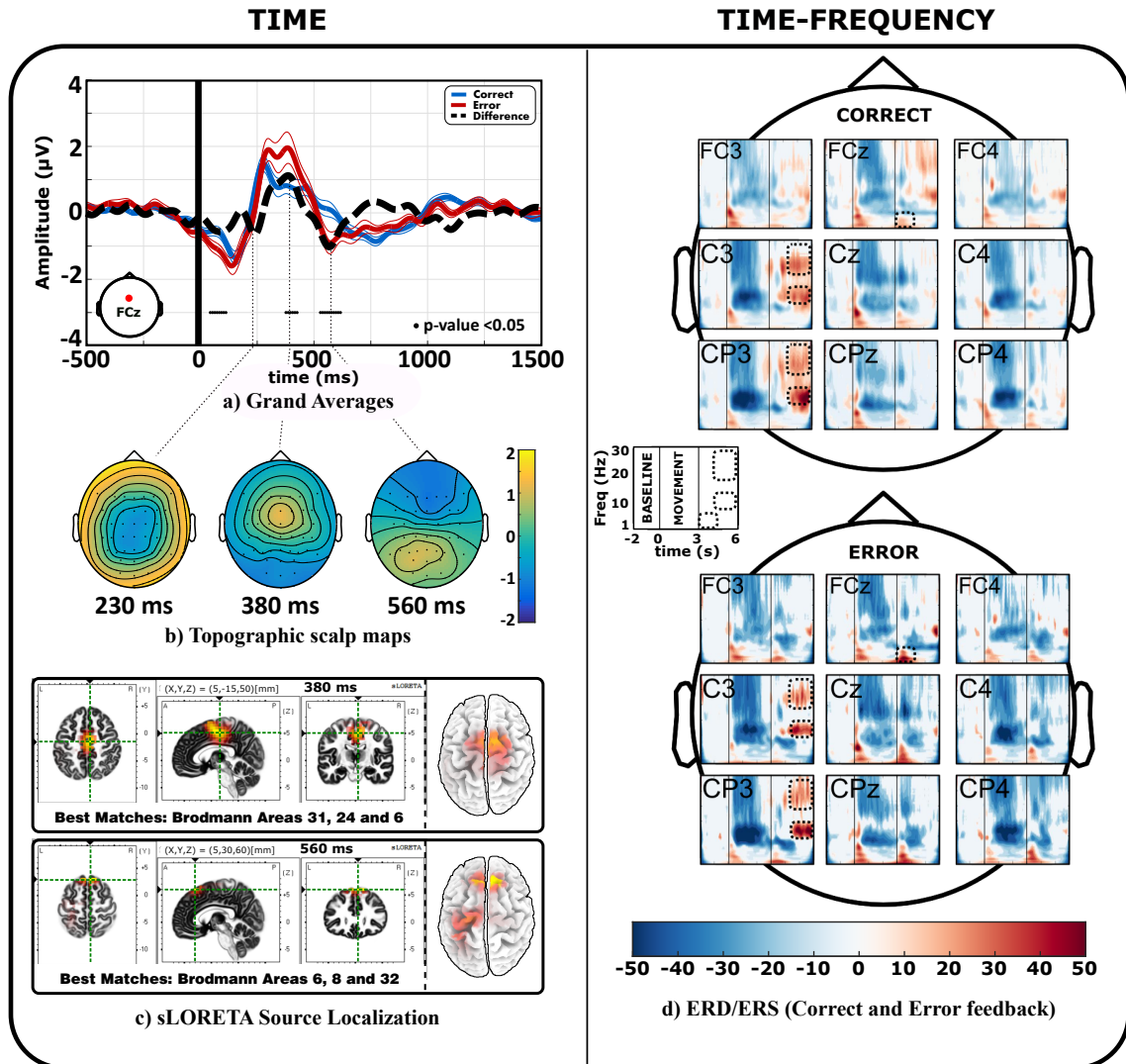
Figure 5.2: Electrophysiology analysis in time (Left) and time-frequency (Right) domains. (a) Onset-locked signals at channel FCz averaged for all subjects, where responses to error and correct feedback are represented in red and blue respectively, and difference average is shown in dashed black lines. Thin colored lines depict standard error of the mean (SEM) and small black dots indicate t-test significant differences between error and correct responses. (b) Topographic interpolations of the most relevant peaks. (c) sLoreta source localization of the difference average response at the most prominent positive and negative peak. (d) Time-frequency plots, where red and blue represent significant event-related (de)synchronizations respectively referred to the baseline [-1.1, 0.1]s. Most relevant time-frequency activity related to the feedback responses marked in dashed-black boxes indicate those time-frequency areas used later on in the ANOVA analisys.

5.3 Results

5.3.1 Electrophysiology analysis

Figure 5.2 displays the averaged feedback responses across trials and subjects at channel FCz, time-locked to the virtual hand movement onset for correct and erronous types of grasping. Here, morphological differences induced by the different factors were not considered, and thus averages were computed using all trials. The observed difference between the averaged correct and error responses shows the same morphology described in previous time-locked studies [Chavarriaga & Millán, 2010; Iturrate et al., 2014]. The maximum dissociations are found in fronto-central areas, characterized by a small bi-phasic modulation at 160 - 230 ms followed by a large positive peak (P3) centered at 350 ms and a negative deflection (N4) around 550 ms (see Figure 5.2(a)). Topographical maps at the peaks of the difference (error minus correct) show a fronto-central distribution around electrode FCz at 230 and 380 ms, whereas the topographical map at the peak at 560 ms shows a mixture of negative fronto-central and positive temporal-parietal activity (see Figure 5.2(b)). A sLoreta analysis was carried out on the most prominent positive and negative peak locations (P3 and N4) of the grand average difference response (see Figure 5.2(c)). For P3 (380 ms), main activations were found at the pre-supplementary motor area (pre-SMA, Brodmann area 6) and the anterior cingulate cortex (ACC, Brodmann areas 24 and 32), in agreement with previous studies [Ferrez & Millán, 2008a; Omedes et al., 2015a]. Regarding to the activations found at N4 (560 ms), the dominant activity was mostly located at Brodmann areas 6, 8 (regions of the frontal cortex involved in planning complex movements) and 32 (ACC).

Figure 5.2(d), shows significant event-related (de)synchornization for the error and correct trials. Note that in this case the whole trial is shown and the error response corresponds to the interval [3, 6]s. A strong desynchronization in *mu* and *beta* bands appears in the interval [3, 6]s related to the execution/imagination of the motor command. In the first second after the execution of the virtual grasp, a significant increase in power was observed in the upper *delta* and *theta* frequency bands [2, 8]Hz especially for fronto-central electrodes. The ERD was on average twice larger for the wrong grasps than for the correct ones. Furthermore, a significant *alpha* power decrease was found around 900 ms after the feedback stimulus (time interval [3.4, 4.4]s in Figure 5.2(d)), which was more dominant at the occipito-parietal channels and for erroneous feedback. By contrast, a later synchronization in upper *mu* and *beta* bands appeared in the interval from 1 to 3 seconds after the onset of the feedback (between 4 and 6 in Figure 5.2(d)) in the contralateral electrodes (C3 and CP3). In this case, the synchronization is more prominent for the correct feedback than for the erroneous one.

5.3.1.1   Statistical analysis

Independent 4*2 ANOVAs (feedback: error, correct; speed: fast, slow; movement: palmar, pincer grasp; command: execution, imagination) were run for the latency and magnitude of the P3 and N4 peaks and for the power of the *theta* synchronization, the *mu* rebound and the *beta* rebound found in the electrophysiology and source analyses of Section 6.3.1. For the ANOVAs in the time-frequency domain, the dependent variable was the average spectral power (in dBs) obtained from the channels and time-frequency intervals depicted in Figure 5.2(d) by dashed-black boxes. More specifically, the power in *theta* was obtained from FCz in a one second interval after the feedback onset, while *mu* and *beta* power was computed from channels C3 and CP3 between 1s to 3s after the feedback onset Figure 5.4 displays the estimated marginal measurements of those 4*2 ANOVAs with at least one significant effect and of the only significant interaction.

- **Feedback** (error/correct): As expected from the electrophysiology results, statistical analyses revealed that there was a significant effect of the type of feedback on the P3 magnitude ($F_{(1,12)} = 79.34; p < 0.0001$; $4.25 \pm .32\mu V$ for error compared to $2.63 \pm .22\mu V$ for correct feedback). In the same way, for the N4 peak, monitoring erroneous feedback elicited a more negative response ($-2.642 \pm .18\mu V$) compared to correct feedback ($-1.869 \pm .14\mu V$) at a significant level ($F_{(1,12)} = 48.65; p < 0.0001$). However, latency of these peaks did not seem to be affected by the nature of the stimuli ($F_{(1,12)} = 1.677; p = 0.22$ and $F_{(1,12)} = 0.858; p = 0.373$, for both P3 and N4 latencies). In the time-frequency domain the spectral power of higher *delta* and *theta* band was significantly larger ($F_{(1,12)} = 4.768; p = 0.05$) for erroneous monitored actions ($0.488 \pm .22dB$) than correct ones ($0.175 \pm .25dB$). The analysis also revealed a significant interaction, where the spectral power of *mu* and *beta* rebound synchronization was significantly more positive when the monitored feedback was a correct action compared to an erroneous one ($F_{(1,12)} = 9.29; p = 0.01$ for *mu* and $F_{(1,12)} = 9.524; p = 0.009$ for *beta* frequency band).

- **Speed** (fast/natural): The speed of the virtual grasp execution showed a significant effect at the P3 magnitude ($F_{(1,12)} = 9.68; p = 0.00899$): a higher magnitude ($3.74 \pm .29\mu V$) when the subject evaluated actions performed at a higher speed compared to slower movement speed ($3.15 \pm .26\mu V$). P3 and N4 latencies were also influenced by the speed of the stimuli. For faster actions these peaks appeared earlier ($324.65 \pm 12.06ms$ and $647.10 \pm 26.19ms$) compared to actions presented at a lower speed ($409.96 \pm 17.01ms$ and $734.63 \pm 18.64ms$), with p-values of ($F_{(1,12)} = 35.91; p < 0.0001$ and $F_{(1,12)} = 25.26; p < 0.0001$) for P3 and N4 respectively (see Figure 5.3(A)).
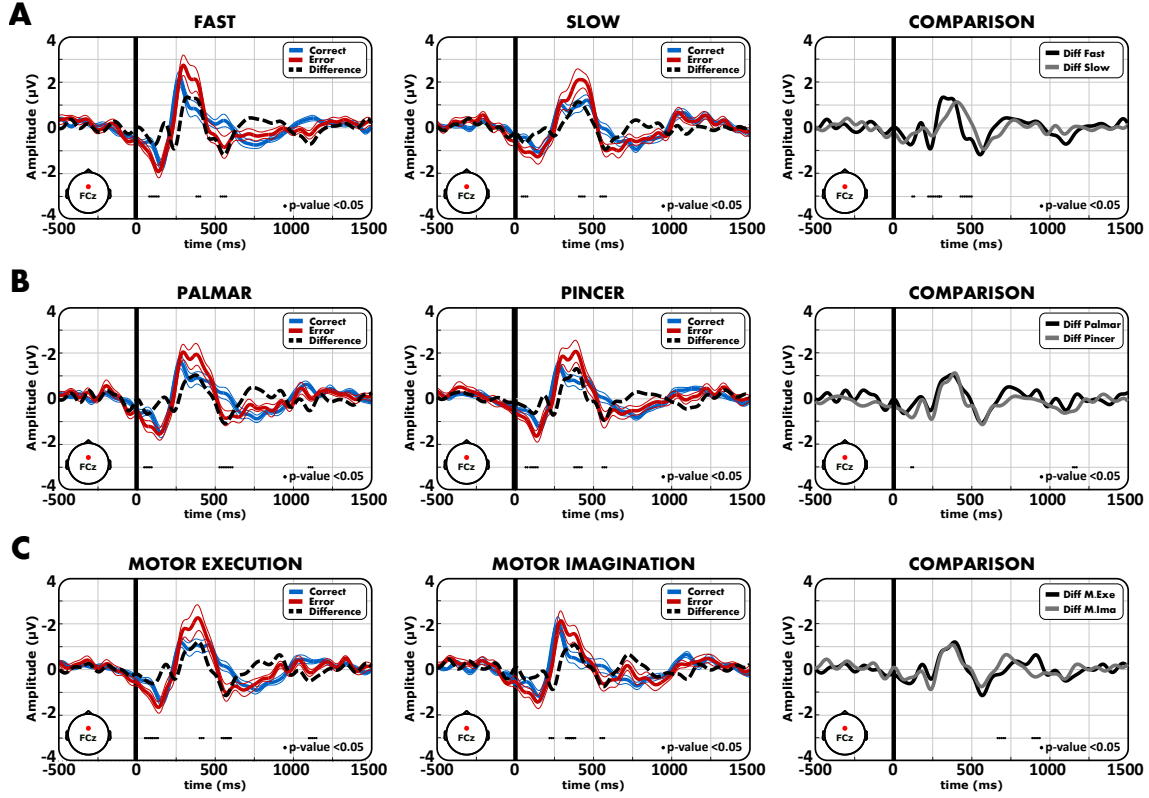
Figure 5.3: Electrophysiologal analysis comparing the grand averages at channel FCz for the different factors: (A) speed, (B) type of grasp and (C) mental strategy to produce a motor command. Responses to error and correct feedback are represented in red and blue respectively, and difference average is shown in dashed black lines. Thin colored lines depict standard error of the mean (SEM) and small black dots indicate t-test significant differences between error and correct responses.

Variations in grasping speed did not reveal significant differences in power of the time-frequency oscillations for *theta* ($F_{(1,12)} = 1.365; p = 0.265$), *mu* ($F_{(1,12)} = 0.237; p = 0.635$) or *beta* ($F_{(1,12)} = 0.054; p = 0.820$).

- **Movement** (palmar/pincer grasp): No statistical significant effects were found affecting the magnitude or latency of the ErrP modulations. As observed in Figure 5.4, the estimated marginal measurements for both type of movements evoked a P3 of the same magnitude ($F_{(1,12)} = 1.675; p = 0.220$) and latency ($F_{(1,12)} = 0.568; p = 0.465$). The magnitude of N4 peak ($F_{(1,12)} = 0.0085; p = 0.928$) did not change either and, even though there seems to be slightly differences in latency, they were not significant ($F_{(1,12)} = 2.31; p = 0.154$). Synchronization values of *theta*, *mu* and *beta* rebound were not found to be influenced by the type of grasp ($F_{(1,12)} = 0.244; p = 0.627$; $F_{(1,12)} = 0.021; p = 0.886$ and $F_{(1,12)} = 0.025; p = 0.877$ for *theta*, *mu* and *beta* band
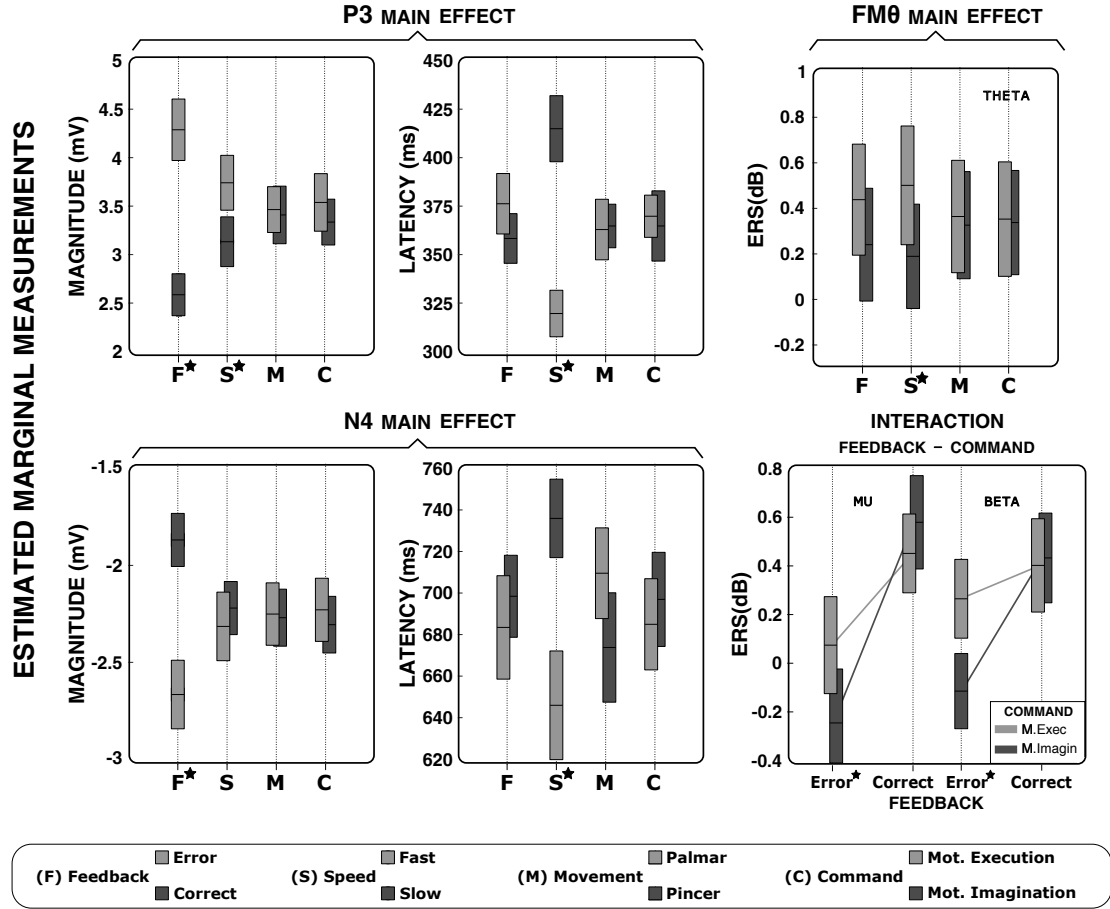
Figure 5.4: Estimated marginal measurements based on the ANOVA analysis for the 4 studied factors. From left to right, the first four graphs depicts the effect of each factor on the magnitude and latency of the ErrP peaks P3 and N4. The fifth graph represents the effect on *theta* synchronization. Last graph, shows the interaction between feedback and mental strategy to generate motor commands for the rebound found in *mu* and *beta* bands. The mark "*" denoted those factors which introduced statistical differences.

respectively). A more detailed comparison between the ErrP responses generated for both type of grasping movements can be observed in Figure 5.3(B). Two-tailed paired t-test, between the difference signals (error minus correct) computed for each time instant, revealed no statistical differences in the time interval [0.25, 1]s where the ErrP appears.

- **Command** (execution/imagination): No statistical significant effects were found affecting the magnitude or latency of the ErrP modulations. Estimated marginal measurements for motor execution and imagination did not evoke major variations of magnitude ($F_{(1,12)} = 0.183; p = 0.676$) or latency ($F_{(1,12)} = 0.083; p = 0.778$) of the peak P3 nor of the magnitude ($F_{(1,12)} = 0.926; p = 0.355$) or latency ($F_{(1,12)} =$

0.654; $p = 0.434$) of negative peak N4. However, a two-tailed paired t-test between the difference signals (error minus correct) computed for each time instant suggested difference between 700 and 900 ms (see Figure 5.3(C)). The ANOVA also did not reveal differences in the *theta*, *mu* or *beta* frequency bands ($F_{(1,12)} = 0.13; p = 0.912$, $F_{(1,12)} = 0.932; p = 0.353$ and $F_{(1,12)} = 4.545; p = 0.054$, respectively). A significant interaction between the mental strategy used to give a motor command and the nature of the feedback ($F_{(1,12)} = 6.628; p = 0.024$ for *mu* and $F_{(1,12)} = 17.758; p = 0.001$ for *beta*) was found. A post-hoc analysis suggested that when the subject monitored an erroneous feedback, the averaged spectral power (over the time-frequency band where the rebound is observed) had statistically smaller magnitude if she had previously performed motor imagery compared to motor execution. However, if the monitored feedback was a correct movement, the averaged spectral power has a higher magnitude, independently of the mental strategy used to give the previous motor command (see Figure 5.4).

5.3.2 Classification results

Table 5.1 depicts the accuracy of the correct vs error classifier for each subject and the overall average. In average, these results show values in the range between 60% and 80% accuracy, which is in line with previous ErrP studies [Omedes et al., 2015a; Spüler & Niethammer, 2015]. The estimated average performance resulted in 70.92% which takes into account that error and correct cases were not balanced. It is worth to mention the differences in performance across participants, where subjects 1, 4, 7 and 12 achieved rates of accuracy rounding 80% compared to subjects 9, 10 or 13 that barely reached 60%.

Figure 5.5 displays a pair-wise comparative of the average classification performance for the 13 subjects according to the different values of each experimental factors. A classifier evaluated only with trials with fast virtual grasps obtained an average of 75.65% accuracy compared to the 68.99% for slow movements. A two-tailed paired t-test comparing the performance of every subject yielded significant differences (p < 0.05) between these two speeds. Regarding to the classification according to the type of observed movement, palmar or pincer grasp, the difference was smaller and non-significant (72.78% and 70.94% for palmar and pincer respectively. Commands generated while executing the motion motor leaded to a higher overall accuracy of 71.38% compared to the 66.98% when using imagination. However these differences were no significant. All the evaluated results achieved performances significantly superior to chance level, 56%.

Table 5.1: ErrP individual classification for error/correct classes and their average performance. Values were obtained by averaging 10 repetitions of a 4-fold cross-validation.

	Error Acc(MEAN±SD)	Correct Acc(MEAN±SD)	Average ACC(MEAN±SD)
S1	71.25 ± 8.6	81.95 ± 5.6	79.10 ± 4.5
S2	61.37 ± 9.4	72.04 ± 7.7	69.20 ± 5.2
S3	66.87 ± 10.3	73.95 ± 8.3	72.06 ± 5.8
S4	74.87 ± 7.7	84.81 ± 4.7	82.16 ± 3.8
S5	68.00 ± 11.3	69.81 ± 10.5	69.33 ± 6.3
S6	62.12 ± 13.1	68.63 ± 8.4	66.90 ± 5.7
S7	73.37 ± 9.9	84.68 ± 4.6	81.66 ± 4.4
S8	60.00 ± 12.6	68.91 ± 11.7	66.53 ± 7.6
S9	57.12 ± 9.5	67.22 ± 7.9	64.53 ± 5.8
S10	50.62 ± 13.1	55.00 ± 11.7	53.83 ± 7.0
S11	63.75 ± 8.5	73.36 ± 6.4	70.80 ± 5.3
S12	68.62 ± 12.2	75.90 ± 8.2	73.96 ± 6.2
S13	56.25 ± 14.0	59.82 ± 10.1	58.86 ± 5.9
MEAN	**65.10 ± 11.0**	**73.03 ± 8.5**	**70.92 ± 5.8**
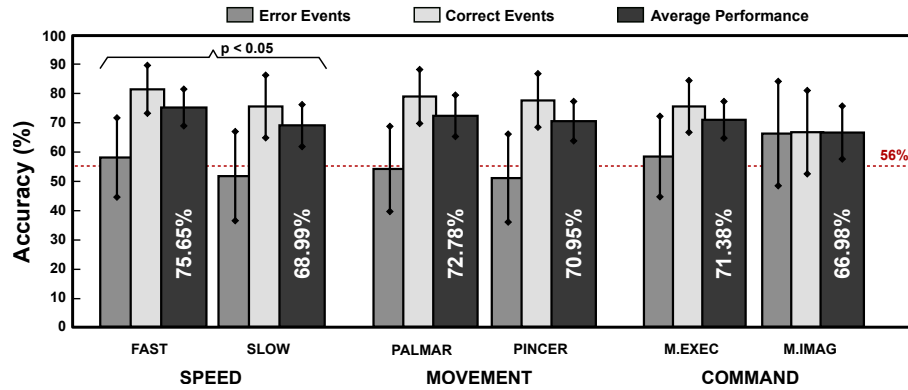
Figure 5.5: Comparative of ErrP classification according to the 3 different experimental factors (speed, type of grasping and mental strategy to elicit motor commands). The discontinuous red line represents the chance level computed as the average of 100 classifiers with randomly assigned correct and error labels. The discontinuous red line represents the chance level computed as the average of 100 classifiers with randomly assigned correct and error labels.

5.4 Discussion

In this chapter we have proposed a hybrid BMI to perform a grasping task using brain processes that appear naturally during the task. First, the type of grasp is directly decoded from the execution/imagination of the intended movement. Second, the action can be corrected based on ErrP decoded while observing the execution of the decoded grasp. The rationale under this approach is that natural and intuitive control is key to develop interfaces that can be used in rehabilitation or motor substitution. The experimental protocol, based on a simulated 3D virtual environment, showed that such a hybrid approach is feasible since ErrP can be decoded with accuracies over 70%. Furthermore, we have analyzed how practical design factors such as the speed of the prosthesis, usually neglected, can influence the performance of the hybrid system. An important result is that ErrP are rather stable when varying experimental factors such as the monitored movement, or the mental strategy participants use to generate the motor commands. However, latency and magnitude of the two most prominent peaks displayed in the *interaction* ErrP signatures were affected by the speed at which the virtual interface provided feedback to the users in terms of the represented grasping action. These insights should be taken into account when designing hybrid approaches in such a way that the system performance can be optimized and ultimately allow the deployment of these systems in real applications.

5.4.1 Error potential morphology

The EEG signatures related to error processing have been analyzed under different experimental conditions and have been assigned names depending on the tasks where they have been observed and the variability of their spatio-temporal signatures. In speed choice reaction tasks show a sharp negative deflection denoted error negativity (Ne) [Falkenstein et al., 1991] or error-related negativity (ERN) [Gehring et al., 1993] appears over fronto-central scalp areas around 100 ms after the pressing of a button. This negative deflection is followed by a centro-parietal positive component, denoted as error positivity (Pe) [Falkenstein et al., 2000] between 200 and 500 ms after the response. The feedback-related negativity (FRN) [Miltner et al., 1997; Cohen et al., 2007], on the other hand, peaks between 250 to 300 ms after the presentation of feedback stimulus (e.g. losses in gambling tasks). Commonly, FRN is followed by a parietal positivity referred to as P3b, a delayed subcomponent of the P300 [Nieuwenhuis et al., 2004]. The ErrP of the proposed experimental protocol are more related to *observation* [Omedes et al., 2015a; Chavarriaga & Millán, 2010; Pavone et al., 2016] and *interaction* errors [Ferrez & Millán, 2008a; Iturrate et al., 2014; Chavarriaga et al., 2014; Spüler & Niethammer, 2015]. They both share very similar morphologies [Kim & Kirchner, 2016], a sharp negative fronto-central peak at 250 ms,

followed by a centro-parietal positivity after 320 ms and a second broader fronto-central negative peak around 450 ms. Frequently, these peaks are denoted using their respective sign and latency (N2/P3/N4). The morphology of the ErrP presented in Figure 5.2 matches the typical waveform reported for *interaction* errors. The electrophysiology analysis of our ErrP showed that averaged differences between evoked responses to correct and error movements were characterized by the presence of the previously described negative and positive modulations peaking around 230, 350 and 550 ms respectively. These latencies are slightly larger that most of the ones reported in the literature. This is probably due to the fact that videos showed a gradual movement of the hand resulting in a delayed perception of the error (see [Omedes et al., 2015a; Den Ouden et al., 2012] for gradually unfolding event-related potentials). These neural patterns were especially pronounced at fronto-central sites for P3 and a mixture of fronto-central and temporal-parietal areas for N4. Please note that although the N4 has been mostly attributed to semantic mismatch [Kutas & Federmeier, 2011], several studies have shown that the N400 is also found in the context of observation of erroneous actions, when meaningful actions are involved [Balconi & Vitaloni, 2014]. The fact that the topographical distribution at 550 ms also display a positive temporal-parietal activity could indicate the presence of a P3b component, which has been hypothesized to be related to state estimation errors due to unexpected displacements/behaviors or the independent updating of brain internal models [Demchenko et al., 2016; Polich, 2007].

Time-frequency domain analyses comparing feedback responses to correct and error events revealed a significant increase of spectral oscillations in *theta* frequency band. These frontal midline theta ($FM\theta$) dynamics had a higher synchronization over the medial prefrontal cortex when the monitored feedback corresponded to an erroneous movement. This spectral signature in *theta* have been reported in previous cognitive studies, and it is believed to be involved in control processes [Cavanagh et al., 2009; Cavanagh & Frank, 2014]. Additionally, source localization analysis indicates that main activations originate at Brodmann areas 32, 24 and 6 which correspond to the anterior cingulate cortex and pre-supplementary motor area [Nieuwenhuis et al., 2004].

5.4.2 Impact of design factors

The main objective of hybrid BMI systems is to improve the overall functionality of the system by combining multiple sources of information. When combining ErrP with other neural mental task, it is necessary to make some choices in the way the hybrid BMI is designed which may affect the error responses and, consequently affect the performance [Abu-Alqumsan et al., 2017]. Some guidelines are already present in the literature such as the effect of stimuli contrast [Luck, 2014], the dependence on error likelihood [Chavarriaga

& Millán, 2010] or the need to keep subjects focused and engaged in the task [Hajcak et al., 2005]. A recent study [Abu-Alqumsan et al., 2017] on *interaction* ErrP intensively explored the invariance and variability of evoked ErrP signals among subjects, due to the mental processing required to perform a specific task and the timeline of the feedback. Main variations were assigned to different mental workloads, which agrees with research on *observation* ErrP [Iturrate et al., 2014]. Variations also occurred on grand average across subjects to a lesser extent. Finally, as already described by [Chavarriaga & Millán, 2010], ErrP signatures appeared to endure invariant for separate sessions (for a given subject and task). This study focused on other factors that have a direct impact on the hybrid BMI approach and that, to the best of our knowledge, have not received enough attention in the literature.

The first factor is the type of grasp, since it will require a different mental command from the user and a different visual feedback (i.e. the movement of the decoded motion will be different). Although one could expect some differences due to ongoing discussions on the effect of different visual features on the brain responses (color, orientation, luminosity or pattern [O'donnell et al., 1997; Li et al., 2014]), no differences were revealed due to the type of executed movement, palmar or pincer grasp. The study considers only two possible types of grasp and tried to limit the differences in their representation just to those related to movement. The results seem to indicate that neither the mental task associated to each grasp not the visual feedback affected the ErrP. However, more studies tackling this issue and considering a wider range of movements are necessary to validate this hypothesis and generalize it beyond grasping to more complex manipulation tasks (e.g. including reaching or different orientations [Iturrate et al., 2018]).

The second analyzed factor is the speed of grasping, which is highly relevant when controlling real devices with dynamic and safety constraints [Omedes et al., 2015a]. In this case, statistically significant differences were found in the responses to two different execution speeds (fast and slow) tested in the protocol. Qualitative and statistical comparisons of the magnitude and latency of the evoked ErrP revealed that a discriminable activity between correct and erroneous responses existed for both speeds. Faster actions resulted in lower latency (on average 80 ms earlier) and larger magnitude of the P3 and N4 peaks. Two possible causes may explain these differences. First, different speeds generate different responses. Second, for slower actions the time locking is less accurate and on average results have an increased latency and smaller amplitudes (see [Omedes et al., 2015a; Den Ouden et al., 2012]). The current protocol and instrumentation was not designed to provide reliable evidence for either of these possibilities, but several studies have theorized about the existence of an internal evidence accumulation model for perception [Ploran et al., 2007] and previous findings on EEG evoked potentials recordings have already cor-

roborated this theory [Twomey et al., 2015]. The speed of execution, which is not usually studied in virtual environments, becomes a relevant factor for rehabilitation and motor substitution applications where movements are usually slower than instantaneous virtual protocols and tend to gradually unfold over time (i.e. the difference between two movements may become apparent for the subject after an unknown and varying time depending on the speed of execution). In addition to a better understanding of the underlying mental process, speed is also an important factor in practice since it can be used in closed-loop control to either improve the brain response or to modify the feature extraction process before decoding (e.g. change the temporal windows according to the speed).

The same protocol was executed using the two most common strategies for motor based BMI: real movement and motor imagination. In contrast with the other two factors, this one was not randomized since it is common to include the attempt or execution of the real movement before testing the imagination of it [Müller-Putz et al., 2016]. Although this limits the significance of the analysis, it is still possible to compare the ErrP responses. Qualitative and statistical analyses carried out over the ErrP waveform did not reveal any appreciable difference between the two mental strategies. On the other hand, time-frequency domain analyses showed a post-movements late synchronization in *mu* and *beta* frequency bands, mainly in the contralateral channels, around 1500 ms after the start of the virtual hand action. Statistical analyses showed that when subjects executed or imagined performing a movement, and later on observed the same action being executed by the virtual interface, the power of this synchronization was higher than if the observed action did not match the user intentions. Furthermore, in the latter case where the virtual hand executed an erroneous action, the synchronization power was greater when the subject had previously executed the motor command than if it had only been imagined. This is also reflected in the source localization analysis of Figure 5.2. Where the latter components of the ErrP shows a simultaneous activation of the mismatch processing areas and of the contralateral motor cortex corresponding to Brodmann areas 1, 4 and 6. Despite this interaction during the monitoring of erroneous feedback, the observation of actions matching the subject's expectations did not show any significant interaction. After experiment completion, some subjects stated that they felt more integrated in the protocol and responsive to the feedback when they imagined the movements. Others mentioned that having to focus on imagining the movements and subsequently evaluating the feedback was cognitively demanding and sometimes they disconnected or were not attentive to the monitored feedback. Based on this interaction and the subjects' reports, we investigated whether they could be originated by a difference in workload between the two mental strategies used to produce motor commands. In such case, we could expect that the P3b component elicited in parietal channels of the scalp should exhibit a magnitude decrement

for the more cognitive demanding task [Causse et al., 2015]. Additional analyses revealed morphological P3b differences but these were not statistically significant. On the other hand, we also compared frontal midline theta and parietal alpha activations for motor execution against motor imagination. Results agreed with previous studies [Klimesch, 1999; Gevins & Smith, 2000] in which it has been reported greater theta and reduced alpha power for task with higher cognitive demand. Further research would be needed to validate these assumptions/interpretations/conjectures. Interestingly, the hypothesis of workload differences would support reported findings suggesting that patients may require additional cognitive resources to perform motor tasks that healthy subjects with unaffected motor skills [Hotz-Boendermaker et al., 2008].

5.4.3 Classification

In the classification context, hybrid-BMI interfaces using ErrP have been discussed in the literature in recent years as means of correcting the output of the BMI decoder [Millán et al., 2010]. Most implementations have focused on analyzing the potentials elicited by wrong actions after a command generated by different protocols such as P300 [Dal Seno et al., 2010] or classical paradigms of motor imagery [Ferrez & Millán, 2008b; Kreilinger et al., 2011]. In this chapter, we have shown that motor tasks relying in the imagination of natural movements can also be combined with the classification of *interaction* ErrP. In the context of natural movement decoding, the current state of the art is very recent and decoding performances have still not reached a plateau that allow robust control [Jochumsen et al., 2015; Schwarz et al., 2017]. Furthermore, as the number of movements increases, some of them can be easily misclassified due to similarity in brain patterns [Ofner et al., 2017]. On the other hand, ErrP classification accuracies are higher and relatively more stable and, as the findings of this work suggest, they seem to be robust to the type of movement executed by the monitored device, at least for the two examined palmar and pincer grasps. The combination would thus appear to be a natural means for disambiguating movements, especially in motor substitution tasks where timing does not play a crucial role. Our results indicate that for this particular interface, correct and error events were discriminated with an averaged accuracy of 70.92%. Four of the thirteen subjects showed proficiency in the task reaching accuracy values around 80% whereas 3 of them self reported that they did not feel in control and only reached performance values of 60% slightly over chance level, estimated at 56%. Additionally, dividing the trials according to the different pairs of factors revealed that feedback where the virtual hand performed a movement with a fast speed (i.e. resembling the traditional protocols where stimuli is presented instantaneously) achieved a significantly superior accuracy, 75.65%, compared to those hand movements performed at lower speed that obtained an average

accuracy of 68.99%.

5.4.4 Limitations and future work

The study aims to better understand how error potentials could be used to improve the BMI decoding of motor information during the control of a neuro-prosthesis. In particular, the combination of SCP and ErrP could contribute to important benefits for a clinical population with motor impairments due to neural disorders such as stroke or spinal cord injury. These end users with limited ability to perform movements could still evaluate the correctness of actions performed by a device. The current work presents the first steps for such hybrid BMI carried-out with able-bodied subjects. However, several subjects have consistently shown that motion decoding results with healthy subjects can be extrapolated to end users with spinal cord injury usually at the cost of some accuracy [Müller-Putz et al., 2017b]. Also, ErrP have been studied and decoded in people with amyotrophic lateral sclerosis [Spüler et al., 2012] and stroke [López et al., 2013]. These findings support the advantages of combining SCP and ErrP signals, yet studies in a clinical population with the injury located in the prefrontal cortex revealed that subjects can be aware of errors and yet not produce the characteristic ErrP correlates [Stemmer et al., 2004].

Second, we used a 3D virtual environment that simulated a realistic scene instead of a real neuro-prosthesis. In previous studies, it has been shown that the perception of a real life stimuli or a resembling virtual version of it generates very similar brain patterns [Iturrate et al., 2014]. In addition, virtual interfaces play an important role in the design of a BMI, since they can be used as safe and cost-effective prototypes for BMI applications before using them to control real-life devices [Lotte et al., 2012]. Furthermore, recent works showed the positive impact of virtual reality on the context of BMI training and performance, providing intuitive and engaging environments, in contrast to simplistic paradigms (circle moving on a computer screen, arrow pointing left or right or bars filling up [Müller-Putz et al., 2016]), that often appear to be boring and not intuitive for the user [Chavarriaga et al., 2017]. Along the same lines, in [Spinelli et al., 2018] a VR environment was used to investigate the appearance of errors in a reaching-to-grasp task depending on the magnitude of the trajectory deviation from the object to be grasped. And in [Pavone et al., 2016], they compared the brain activity originated due to the observation of erroneous grasping from a first-person or third-person perspective.

Third, the reported analysis was done simulating online conditions. Obtained results, achieved to discriminate between correct and erroneous events, with an average of 70.92% accuracy. Recent studies involving only a single task of error potential decoding [Omedes et al., 2015a; Spüler & Niethammer, 2015; Chavarriaga & Millán, 2010] indicate that classification performance could still be boosted. There are two reasons that could explain

this deficit of performance. First, none of the subjects had participated in a BMI experiment which combined the sequential execution of two paradigms, plus nine out 13 subjects were naïve to BMI experiments. After completion of the experiment, these participants reported that it was mentally demanding to keep focused on both tasks. Although most subjects obtained proficient results, it may be wiser in the future to first make them confident on each of the tasks before testing the combination. Second, the error rate was fixed to 30% to ensure an odd-ball paradigm. This percentage is in line with performance accuracies reported in previous studies that use SCP to classify grasping actions [Jochumsen et al., 2015; Schwarz et al., 2017; Müller-Putz et al., 2017a]. On the other hand, it is known that the number of errors has an influence on the brain signals and the decoding accuracy [Millán et al., 2010]. Future work should consider closed-loop operation together with training over a longer period of time to evaluate the system in real conditions. Furthermore, it should be possible to design procedures to maximize the final output of the system by different learning stages of the user.

Finally, one may wonder how a wider repertoire of movements could be integrated within this hybrid system for applications where more than two commands are required. It is expected that the increased complexity of the motor task would result in diminished accuracy ratios, as it has been reported in studies that tackled the decoding of several movements from the same limb [Müller-Putz et al., 2017b]. However, error potentials are binary signals, consistently and naturally generated during the evaluation of the observed stimuli. In this regard, this study showed that elicited ErrP are consistent disregarding the type of monitored movement. Thus, it is expected that detection accuracy of error potentials would remain constant, allowing to escalate into a high dimension of commands. Furthermore, larger studies will allow the analysis to go one step further and include more levels of interaction by increasing both the granularity of the factors (e.g. wider number of movements, diverse levels of speed during execution) or additional factors to consider (e.g. delay between visual cue and action executed by the device / observing a virtual or a real device). Also, it would be of interest for the future to analyze the ErrP signals that are originated when the interface shows a grasping feedback without the subjects performing any previous motor action (execution/imagination). This scenario would help to simulate the on-line control of a device where an asynchronous classifier fails to properly decode EEG signals, and attempts to execute a motor command without the active intention of the user. We hypothesize that this unexpected outcome would originate an error-related potential, the dynamics of which would vary significantly from the aforementioned obtained ErrP where the feedback is expected.

6

Neurorehabilitation:
Error signatures during neuromuscular
stimulation

6.1 Introduction

Previous chapters have demonstrated the usability of error-related potentials for different BMI applications. In Chapters 4 we used ErrPs to achieve the control of a robotic device by teaching a mobile robot how to navigate in a continuous map to finally reach the desired destination. And in Chapter 5, we developed a motor substitution application oriented for people that have completely lost mobility of their hand. Here, errors were combined with motor-related neural correlates, naturally generated when subjects attempt to mentally perform an action, to assist and correct grasping movements to finally grab an object. In the present chapter, we propose the usage of error-related potentials in the field of neurorehabilitation. In this field, BMIs have been proposed as a promising alternative to provide user-dependent therapies for stroke or incomplete spinal cord injury patients [Granat et al., 1993; Kwakkel et al., 2008], where error-related potentials could be implemented along with these techniques to promote motor learning.

Whereas, traditional rehabilitation therapies have focused on passive facilitation of isolated movements or compensatory movements using alternative muscles to accomplish the desired task, innovative tendencies in clinical environments emphasize the importance of techniques that promote changes in the central nervous system and not just repetition of movements [Daly & Wolpaw, 2008]. It has been demonstrated that giving personalized assistance according to the patients needs enhance recovery more than supplying full assistance all the time o no assistance at all [Reinkensmeyer, 2003]. In the same way, assistance loses effectiveness when sensory input is not directly coupled to motor output,

therefore active subject participation is required in order to provoke brain plasticity [Lotze et al., 2003]. These innovative findings have opened a wide number of possibilities for rehabilitation therapies based on intrinsic subject biosignals like those exploited by EMG [Cauraugh et al., 2000] or BMI [Cincotti et al., 2012] controlled systems that allow to regulate the provided assistance according to the muscular or brain biorhythms measured for each subject.

As we learned in Chapter 5, motor intention encoded in electrical brain oscillations can be decoded from the EEG using state-of-the-art machine learning techniques and translated into commands to operate virtual and real devices, which is especially useful for people that has completely lost motor functionality of their limbs. However, in the context of rehabilitation, depending on the degree of the injury, patients still retain some residual motor and sensory functions. In such case, it has been demonstrated that it is possible to stimulate afferent sensory nerves to induce functional recovery [Bunge et al., 1993]. Hence, instead of providing visual feedback through the monitoring of the movements of a robotic prosthesis or a device on computer screen, BMIs could be used to trigger a more natural somatosensory feedback associated to the neural activity of the subject's brain. Among the different techniques to apply proprioceptive feedback, neuromuscular electrical stimulation (NMES) has been widely proposed as an effective treatment of recruiting non-damaged motor areas through afferent pathways to execute more effective movements [Cauraugh et al., 2000]. Furthermore, the implications of using NMES are not limited to the electrically evoked contractions. It has been shown that the simultaneous activation of proprioceptive afferent pathways combined with task-related motor execution may have a bigger effect than applying both of them separately [Jarosiewicz et al., 2008; Grosse-Wentrup et al., 2011]. In this sense, the electrically evoked sensory volley travels through the spinal cord and ascends to the brain increasing activity in spinal and cortical circuits [Blickenstorfer et al., 2009]. This is believed to complete the sensorimotor cycle [Spiegel et al., 1999] which may induce the creation of new synaptic connexions promoting both short and long term neuroplasticity [Wolpaw & Tennissen, 2001; Kleim & Jones, 2008; Ramos-Murguialday et al., 2012].

Notwithstanding, compared to traditional rehabilitation therapies where assistance is delivered by a caretaker or by pre-recorded but consistent movements executed by a robotic arm, BMIs are not always accurate, which means that sometimes the decoding of brain signatures fails and they commit errors. In this regard, the BMI decoder could falsely interpret that the user is attempting to move and activate electrical stimulation when he is resting, or on the contrary it may deactivate the assistance when the user is still attempting to complete an action. On one hand, these unexpected patterns of stimulation result in the decoupling of mental engagement and sensory feedback, which in

principle dissipate the promising neuroplasticity benefits obtained from combining these two techniques. On the other hand, introducing unexpected disturbances may originate a cognitive mismatch between the subject's expectations and the perceived sensory events. Comparable experiments using vibrotactile and somatosensory stimuli, have reported a consistent negativity in response to deviants stimuli presented as infrequent changes (i.e. intensity, duration, frequency) of the stimulation in regard to a more frequent standard stimuli. These potentials originated from the perception of somatosensory oddball stimuli have been denoted as somatosensory mismatch negativity [Restuccia et al., 2009] and are associated with an increase of attention after high conflict trials [Van Veen & Carter, 2002].

In fact, recent research on the field of motor control has emphasized that errors are fundamental signals to drive motor adaptation, and their positive impact on the reorganization of the central nervous system [Emken et al., 2005]. In this sense, there has been a progression in the development of strategies that amplify movement errors or even introduce them as noise disturbances [Marchal-Crespo et al., 2014] which are also linked with an increase attention, higher muscular activation, and therefore better learning.

We hypothesize that unexpected disturbances during NMES will trigger brain mechanisms similar to those observed in error processing tasks. Therefore, in this chapter we focus in the neurophysiology analysis of the EEG correlates elicited as the results of random and unexpected disturbances along different time points of somatosensory stimulation. To isolate the impact of the sensory feedback on the elicited brain response from additional task-related neural correlates along with controlling the ratio of mismatches, NMES was synchronized to an external auditory cue instead of instructing the subjects to perform voluntary movement attempts. Furthermore, we investigated whether events associated to the activation vs deactivation of electrical stimulation triggered diverse cognitive processes and had an impact on the elicited responses. Also, different levels of intensity in the range from sensory threshold up to functional stimulation were tested. Up to our knowledge, this is the first time that unexpected disturbances in terms of the distribution of electrical stimulation has been explored. Our results suggest that the different components of the elicited waveform vary according to endogenous and exogenous factors. In particular, earlier components are more affected by intensity level whereas intermediate latency components solely depends on cognitive factors such as attention and expectancy of the perceived events.
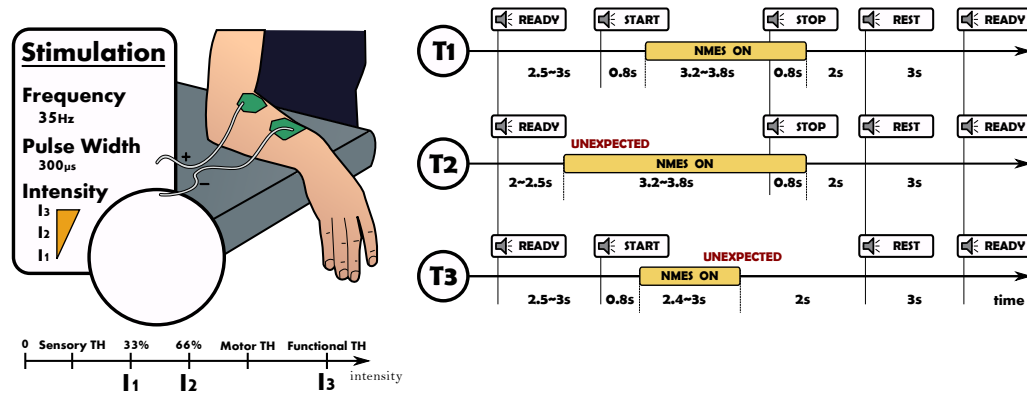
Figure 6.1: Experimental paradigm. Left: NMES parameters and squematic representation of the electrodes location. Right: Time-line of the 3 different types of trials found during the experiment. **T1)** No disturbances. **T2)** Electrical activation disturbances. **T3)** Electrical deactivation disturbances.

6.2 Methods

6.2.1 Participants and data recording

Ten self-reported right-handed healthy individuals (7 male, mean age 27 years) voluntarily participated in the study recorded in a laboratory of the Institute of Medical Psychology and Behavioral Neurobiology at the University of Tübingen. Participants gave their written informed consent and the study was conducted in accordance with the ethical standards of the 1964 Declaration of Helsinki.

Electroencephalographic activity was recorded using two commercially available BrainAmp amplifiers (Brainproducts GmbH, Germany) with an Acticap system composed by 32 active electrodes distributed according to the extended 10/20 international system (FP1, FP2, F7, F3, Fz, F4, F8, FC3, FC1, FCz, FC2, FC4, C5, C3, C1, Cz, C2, C4, C6, CP5, CP3, CP1, CPz, CP2, CP4, CP6, P7, P3, P4, P8, O1 and O2). The ground was placed on AFz and the reference at Pz. Additionally, two EMG bipolar electrodes (Myotronics-Noromed, USA) with a MR-compatible amplifier (BrainProducts GmbH, Germany) were attached at the side of the stimulator electrodes over the extensor muscles of the subject's forearm. This was done to obtain a precise cue onset for further time-locked analyses of the signal. EEG and EMG signals were recorded with a sampling frequency of 1000 Hz and notch filtered at 50 Hz for power line noise removal. The data acquisition was done with Brain Vision and the paradigm was designed using BCI2000 [Schalk et al., 2004].

6.2.2 Stimulation dose

To evoke optimal muscle contraction and avoid discomfort, typically three different parameters of stimulation can be adjusted [Bergquist et al., 2011]. Increasing the magnitude of NMES pulses produces a stronger depolarization, which penetrates deeper into the underlying muscular fibers generating larger contractions [Mesin et al., 2010]. Changing the duration of the pulses alters the relative recruitment of motor and sensory circuits. Short pulse durations (0.05 - 0.4 ms) preferentially activate motor axons, whereas longer pulses (0.5 - 1 ms) will recruit more sensory axons [Kiernan et al., 1996]. Finally, the frequency at which pulses are delivered lead to a temporal summation of muscle twitches. In general, NMES is delivered at frequencies high enough to produce fused contractions (20-40 Hz) [Baker et al., 2000], but not so high (<60 Hz) that the muscles fatigue rapidly [Kesar et al., 2008]. Often frequency and pulse width are set constant in the range of 20-50 Hz and 30-500 μs respectively, whereas pulse magnitude is varied ($\leq$ 120 mA) [Quandt & Hummel, 2014].

Previous to the execution of the experiment, subjects were seated on a comfortable chair with their right arm resting on a table and the hand relaxed. Neuromuscular electrical stimulation was delivered using two electrodes secured over the muscles extensor digitorum/extensor carpi ulnaris and connected to a neuromuscular stimulator (BoneSTIM, Tecnalia, Beocin, Serbia) as depicted in Figure 6.1. A process similar to [Smith et al., 2003] was followed to determine three levels of stimulation intensity. Here, a brief summary of the process is given for completeness. Starting from 5 mA, the stimulation intensity was slowly increased until the subjects indicated the beginning of stimulus perception, described as a slight tingling in the forearm. This intensity was defined as sensory threshold (STh). From this point, the intensity continued to grow until the stimulation caused a small twitching in the subject's fingers (motor threshold, MTh). Carefully, we gradually increased stimulation intensity until the full extension of the subject's fingers (functional threshold, FTh) was achieved. From this data, two sub-motor threshold intensity values were computed as $I_{low} = (MTh - STh) \times 0.33 + STh$, $I_{medium} = (MTh - STh) \times 0.66 + STh$. The third intensity value corresponded to the functional threshold $I_{high} = FTh$, see Figure6.1. Subjects verbally reported their level of discomfort, and during the experiment we ensure that stimulation intensity never reached pain threshold.

6.2.3 Experimental design

Subjects were seated on a comfortable chair with their right arm placed resting on a table and two electrodes for electrical stimulation fixed over the extensor muscles of the hand as exemplified in Figure 6.1. The experimental paradigm consisted in the succession of

auditory commands that guided the subjects through the protocol. Each trial began with the auditory command "READY", where subjects had to cease any type of movement, relax and focus their attention on the right arm. This idle period varied between 2.5 and 3 seconds and due to its neutral cognitive state, it was used as baseline activity for further analyses. Then, the auditory cue "START" indicated that the NMES device would proceed to the electrical stimulation of the arm. A delay of 800 ms amid the auditory cue and the beginning of the stimulation prevented possible overlap between the brain responses to the different category of stimuli. NMES was extended for a variable interval between 3.3 and 3.8 seconds until the "STOP" command announced the conclusion of the stimulation. Once again, a delay of 800 ms was used to prevent overlap among stimuli. Finally, trials ended with the auditory "REST" command. Subjects were free to blink or make small movements if necessary during this resting phase of 3 seconds, after which a new trial started.

During the sequence of trials three types of stimulation conditions were randomly alternated (see Figure 6.1): (T1) No disturbance, (T2) Electrical activation disturbance, (T3) Electrical deactivation disturbance, where the frequency of each condition was 60%, 20% and 20% respectively. In case of "No disturbances" the stimulation procedure followed the previously described sequence. In case of "Electrical activation disturbance", a violation of the subject's expectation was generated by activating the NMES during the variable interval between the commands "READY" and "START" without prior warning. Similarly, in the case "Electrical deactivation disturbance" NMES of the arm was automatically disconnected 500 ms before the auditory cue "STOP" that indicated the end of the stimulation. Notice that when the NMES was activated or disconnected before the auditory stimuli ("START" or "STOP", respectively) the latter was not played. The experiment was grouped in 9 blocks, where each block was composed by the continuous repetition of 30 trials. For each block of the experiment, one of the 3 stimulation intensity levels calculated in section 6.2.2 was applied in a randomly alternated order but with the same frequency (i.e. 1/3). During the duration of a block of trials the intensity remained constant. Resulting in a total of 270 trials and a duration of the experiment of 90 minutes.

6.2.4 Neurophysiology analysis

Trials were segmented and sorted into four different categories according to their stimulation pattern. (1) Epoches corresponding to the beginning of the stimulation with no disturbances, (2) epoches where the stimulation started in unexpected fashion, (3) epoches where the stimulation was suspended with no disturbances and (4) epoches where the stimulation concluded unexpectedly. Epoches corresponded to the time window from 500 ms before to 1000 ms after the electrical activation/deactivation onset of the NMES. This

onset was precisely determined using two EMG electrodes located next to the stimulation patches. Then, EEG signal were resampled from 1000 to 100 Hz band-pass filtered using a zero-phase Butterworth filter of 4th order from 1 to 10 Hz.

Resulting epoches were visually inspected and those segments with extreme values or channels corrupted by muscular or NMES noise were removed from further analyses. Additionally, independent component analysis (ICA) using the extended Infomax algorithm was performed to rectify the remaining muscular and possible EOG artifacts. Visual inspection was used to determine and remove the topographies of the independent components that corresponded to artifacts. Finally, cleaned epoches were reconstructed by inverse matrix multiplication.

To analyze the influence of each condition (intensity: low, medium, high; modality: activate, deactivate; and expectancy: expected, unexpected) in the evoked brain responses, we computed the grand averages of the EEG signals recorded from all the subjects. For each condition and subject, epoches were grouped according to its respective sub-levels (e.g. only epoches of high intensity stimuli, regardless of their modality or expectancy) and individual grand averages were computed. Then, the total grand averages were computed by combining the individual averages among subjects. Finally, the most prominent peaks of the averaged signals (i.e. N140, P300 and N400) were selected to estimate the origin of intra-cranial activity using the standardized source localization technique, sLORETA [Pascual-Marqui, 2002].

Furthermore, we analyzed the impact that stimulation mismatches (which is the factor of main interest in this study) had on the elicited potential morphology. For this purpose, we computed the difference between the mean waveforms evoked during correct and unexpected trials [Näätänen et al., 2007; Cohen, 2011; Omedes et al., 2015a]. To observe the somatosensory influence resulting from activating or deactivating the electrical current, brain responses were further divided according to the sensory modality of stimulation. Likewise, subgroups conformed by each intensity level ($I_{low}, I_{medium}, I_{high}$) were also created to isolate their effect on the averaged evoked responses. Statistically significant differences along time between unexpected and correct conditions were assessed at each time instant using a two-tailed paired t-test corrected for multiple comparisons using the Benjamini & Hochberg procedure to control the false discovery rate (FDR) [Benjamini & Hochberg, 1995]. Scalp topographies of the difference signal were also computed at the time-points where statistical differences were found.

6.2.5 Statistical analysis

Overall effects on the dynamics of the evoked brain responses were tested by a factorial analyses of variance (ANOVA) with repeated measurements for the factors "level of

intensity" ($I_{low}, I_{medium}, I_{high}$), "modality" (activation , deactivation of NMES) and "expectancy of stimulation" (expected, unexpected). The analysis was carried out using the magnitude of the most relevant peaks (N140, P300 and N400) extracted from the individual grand averages at the scalp location with the largest activity [Cavanagh et al., 2009], in which repeated measures accounts for the within subjects variability. These values were computed for each of the 12 possible combinations of factors; in which for each subject, all the trials of each combination were averaged, and then the values of N140, P300 and N400 components were extracted. Greenhouse-Geisser corrections were applied to compensate violations of sphericity, and in case that main factors or interactions reached significance (p<0.05), contrasts were tested by post-hoc two-tailed t-tests to further identify the source of differences.

6.3   Results

6.3.1   Neurophysiology and statistical analysis

The first objective of our study was to investigate the impact that each factor had on the evoked brain responses, quantify these contributions and locate their intra-cranial origin to obtain insights about the underlying mechanisms that generate these waveform differences.

First row of Figure 6.2 depicts the grand average waveform computed for each of the three analyzed conditions. Waveforms from fronto-central channels revealed a triphasic morphology composed by a prominent negative peak around 150 ms (N140), a wide positive component between 250 and 500 ms (P300) and a late negative deflection that extended from 500 to 750 ms (N400).

N140:

Figure 6.2 (2nd row, bottom side) shows several bars representing the estimated mean and standard error of the N140 component for each of the analyzed factors.

A factorial ANOVA determined that indeed there was statistically significant differences between conditions ($F(2,18) = 29.078$, $p < 0.001$ $\eta^2 = 0.764$). Subsequently, a post-hoc test revealed that the magnitude of the N140 component was statistically significantly lower for low (-1.525 μV SE: $0.29\mu V$, $p < 0.001$) and medium (-1.709 μV, SE: $0.20\mu V$, $p < 0.001$) intensity level of NMES compared to functional stimulation (-4.302, SE: $0.51 \mu V$). There was no statistically significant difference between the low and medium intensity levels groups ($p = 0.324$). Additionally, the analysis revealed that this magnitude was significantly larger ($F(1,9) = 31.601$, $p < 0.001$ $\eta^2 = 0.778$) for responses to
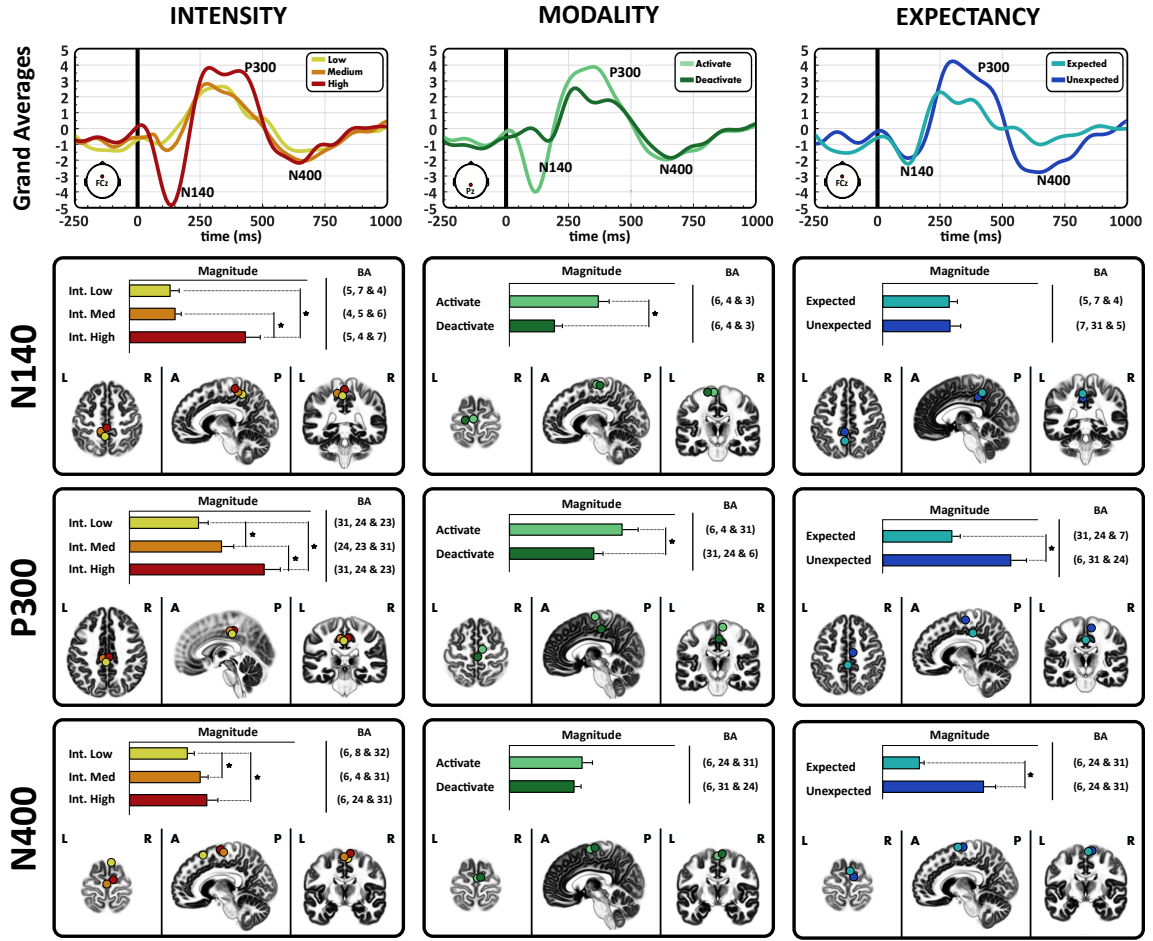
Figure 6.2: From left to right, each column represent each of the analyzed conditions (intensity, modality and expectancy). From top to bottom. First row: Grand averaged waveforms at the most representative electrode. Second, third and forth rows: Statistical analysis along with estimated peak magnitude, source localization activity and most relevant activated Brodmann areas for the N140, P300 and N400 peaks respectively. Color bars represent the estimated magnitude and standard error of each peak computed from the individual signal averages by SPSS. Statistical differences among the different pairs of analyzed levels are marked with a "*" symbol. Brain regions with the largest current density at the specific latency of the analyzed peaks were marked with their respective color. Brodmann areas were sorted by their proximity to the estimated sources of brain activity.

electrical activation (-3.33 μV, SE: 0.36 μV) compared to deactivating the stimulation (-1.694 μV, SE: 0.25μV). However, no significant differences were found regarding to the stimuli expectancy (F(1,9) = 0.011, p = 0.917η^2 = 0.001), obtaining an average magnitude of -2.527μV (SE: 0.35μV) and -2.49μV (SE: 0.26μV) for expected and unexpected stimulation respectively.

sLORETA was used to analyze the current source density of the grand average re-

sponses at the occurrence of the observed peaks. Cortical localization of the main activity along with the respective Brodamnn areas are depicted on Figure 6.2 (2th row, top side). For the three levels of intensity the main activated areas corresponded to Brodmann areas 4, 5, 6 and 7. Similarly, responses generated by the activation and deactivation of electrical stimulation had their origin in Brodmann areas 3, 4 and 6. Lastly, the N140 component of unexpected events had origin in Brodmann areas 5, 7 and 31 whereas brain responses from expected stimulation came from Brodmann areas 4, 5 and 7.

P300:

Analogously to the previous component, Figure 6.2 (3th row, bottom side) display the estimated mean and standard error of the P300 component. A significantly effect on P300 magnitude was observed with regard NMES intensity level (F(2,18) = 32.79, p = 0.001 η^2 = 0.697). A post hoc test showed a significantly progressive increment of magnitude from low ($2.59\mu V$, SE: $0.32\mu V$) to medium ($3.44\mu V$, SE: $0.41\mu V$, p = 0.001) and to functional ($5.03\mu V$, SE: $0.55\mu V$, p < 0.001) intensities of stimulation. Medium and high intensities also revealed significant differences (p = 0.009). The P300 was marginally larger (F(1,9) = 5.153, p = 0.049 η^2 = 0.364) for events corresponding to the beginning of stimulation ($4.21\mu V$, SE: $0.55\mu V$) compared to the end ($3.16\mu V$, SE: $0.29\mu V$). Finally, expectancy of stimulation events revealed to have a significant impact on the P300 magnitude (F(1,9) = 31.32, p < 0.001 η^2 = 0.777) where unexpected disturbances on the initialization or removal of the NMES resulted in an average peak value of $4.78\mu V$ (SE: $0.54\mu V$) compared to $2.59\mu V$ (SE: $0.26\mu V$) for expected events. In summary, the P300 increased with the level of NMES intensity and had a larger magnitude for unexpected disturbances of stimulation that for standard stimulation.

For the P300 component main activations were predominantly found at the pre-supplementary motor area and the posterior cingulate cortex, see Figure 6.2 (3th row, top side). Brodmann areas 24, 23 and 31 were identically activated for the three levels of intensity. Analogously, Brodmann areas 24 and 31, which has been suggested to play an important role in altering behavior in response to unexpected changes [Pearson et al., 2011] were involved in generating the P300 regardless the modality or expectancy of the events. However, this activity was slightly biased towards the pre-supplementary motor area (Brodmann area 6) for unexpected events and initialization of electrical stimulation.

N400:

Lastly, the estimated mean and standard error of the N400 component is shown in Figure 6.2 (4th row, bottom side). ANOVA accounting for the effect of stimulation intensity on

the N400 magnitude was Greenhouse-Geisser corrected to compensate sphericity violation. Results of the analysis reported statistical differences (F(1.65,14.851) = 5.01, p = 0.027 $\eta^2 = 0.358$) and the correspondent pot-hoc test revealed that the two highest intensities did not induce significant changes on the magnitude of this negative deflection (-2.65μV, SE: 0.25μV and -2.90μV, SE: 0.36μV for I2 and I3 respectively, p = 0.352). However, I1 (-2.17μV, SE: 0.21μV) produced a slightly smaller negativity than I2 (p = 0.021) and I3 (p = 0.022). The effect on the N400 magnitude due to electrical stimulation initialization (-2.73μV SE:0.34μV) or removal (-2.42μV SE:0.21μV) did not entail any significant differences (F(1,9) = 1.235, p = 0.295 $\eta^2 = 0.121$). On the other hand, evoked potentials resulting from unexpected events revealed to have a significant impact on the N400 magnitude (F(1.65,14.851) = 52.646, p < 0.001 $\eta^2 = 0.854$) reaching an average value of -3.77μV (SE: 4.04μV) compared to -1.38μV (SE: 0.13μV) for expected events.

Regarding to the activations found at N400, Figure 6.2 (4th row, top side), the dominant activity was originated at the posterior cingulate cortex (Brodmann area 31) and anterior cingulate cortex (ACC, Brodmann areas 24 and 32) alongside activations of regions of the frontal cortex (Brodmann areas 6 and 8) involved in the management of uncertainty [Volz et al., 2005].

6.3.1.1   Expectancy mismatch

Grand average waveform encoding expectancy mismatches time-locked to the activation/deactivation of electrical stimulation at electrode FCz are displayed in Figure 6.3. At the top (Figure 6.3A,D), the evoked potentials are grouped according to the level of stimulation intensity used. The morphology of the signal is characterized by three consecutive peaks. Initially a negative deflection around 140 ms (N140), usually present in somatosensory evoked potentials experiments [Desmedt & Tomberg, 1989], can be observed for both expected and unexpected events with relatively similar magnitude within each intensity level. Additionally, there seems to be a direct relationship between the level of intensity and magnitude of the aforementioned negative peak, as has already been described in previous studies [Nakajima & Imamura, 2000]. The second component is a positive peak between 200 and 400 ms. This component resemble the typical P300. As in the previous case, P300 magnitude seems to progressively increase in direct relationship to the intensity of stimulation. Furthermore, visual inspection of the signals revealed that this peak is larger for the responses originated by unexpected events. At later latencies, between 500 and 700 ms, a wide negativity was presented following the P300. This negative peak was smaller (i.e. less negative) for expected events that for unexpected disturbances at the beginning/end of the stimulation.

Grand average signal resulting from grouping the trials regardless to their intensity of
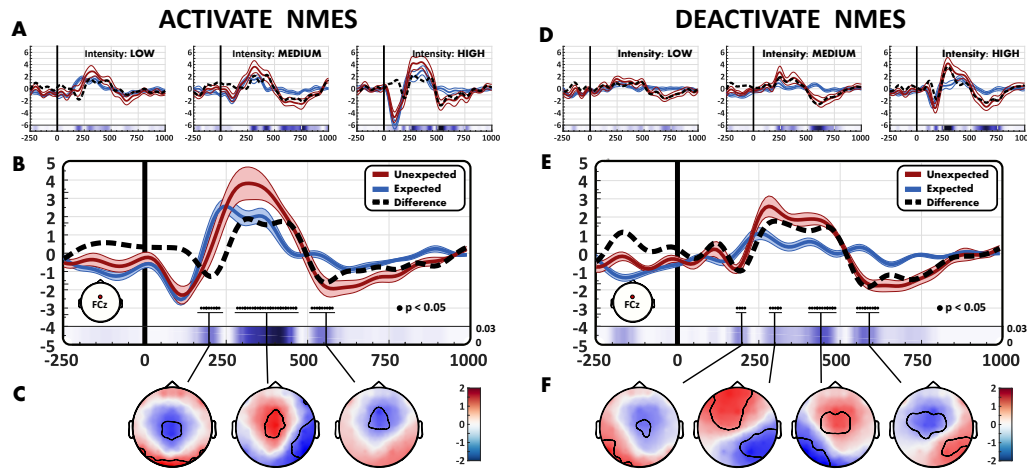
Figure 6.3: Grand averages waveforms at electrode FCz. Expected and unexpected events are depicted by blue and red lines respectively, and their differences is marked in dashed black line. Under the grand average signals, discriminant R2 metric is displayed in a white and blue scale, where darker colors represent higher level of disparity. Left side: Signals time-locked to the beginning of NMES. Right side: Signals time-locked to the removal of NMES. (A,D) Neural activity grouped according to the stimulation intensity level. (B,E) Grand averages regardless of stimulation intensity level. Black dots represent the time-intervals for which Bonferroni-corrected paired two-tailed t-test revealed statistical differences ($p < 0.05$) between unexpected and expected stimulation. (C,F) Topographic scalp representations of neural activity for the difference waveform at the intervals of statistical significance. Regions where significant differences were found are delimited with a black line.

stimulation are displayed in Figure 6.3B,E. These waveforms display qualitative similarities to the previously described potentials, characterized by an initial negativity around 120 ms, transitioning towards a P300-like component and a later negative deflection.

The difference wave between unexpected stimulation disturbances and expected stimulation at the beginning of a trial (Figure 6.3B), exhibits statistically significant differences ($p < 0.05$) for the negative peak conformed at 200 ms (N200), for a wide positivity from 300 to 470 ms and at the beginning of the later negative deflection around 600 ms. The scalp topography of the difference waveform at the discriminant time intervals previously reported are shown in Figure 6.3C where regions of statistically difference are delimited by a black line. These topographical representation revealed a central minima, followed by fronto-central positive and negative activity for the N200, P300 and N400 respectively. Additionally, P300 also revealed statistical activation at parietal electrodes of the ipsilateral area of the stimulated arm.

Correspondingly, the difference wave at the disconnection of the electrical stimulation (Figure 6.3E), reveals statistically significant differences at the negativity found around 200 ms (N200), at the initial and last points of the P300 like component (300 ms and

450 ms respectively) and at the beginning of the later negative deflection around 600 ms. The scalp topography of the difference waveform at the discriminant time intervals previously reported are shown in Figure 6.3F. Obtained topographical representation for NMES disconnection are in consonance with the results obtained for NMES initialization. Starting at the N200, activity was displayed as negativity located in central scalp areas, followed by the 2 components related to the P300 where the earlier representation displayed a frontal positivity combined with negative activity at the ipsilateral parietal side that transitioned into a single froto-central positive activation for later latencies (450ms). Lastly, topographical distribution of the N400 was intensified at fronto-central areas of the scalp.

6.4   Discussion

In the present chapter, we investigated neurophysiological correlates from subjects performing a sensory perception experiment in which electrical stimuli applied in their right forearm were randomly altered through unexpected disturbances in the stimulation. Alterations from the standard pattern of stimulation were introduced as early activation or deactivation of the electrical feedback. Up to our knowledge, the underlying neurophysiolgy mechanisms involved in processing the somatosensory mismatch between in this type of setting have not been previously explored. Additionally, to analyze the impact of stimulation intensity on the cognitive perception of the stimuli, three different levels of intensity going from sensory threshold to functional stimulation were chosen. Our results reveal that the somatosensory evoked potential from NMES in the forearm is modulated by exogenous (due to an external cause) and endogenous (generated from within) factors. First, early components were mainly affected by the level of intensity, where higher levels led to higher magnitude. Second, depending on the modality of the events (activating, deactivating the stimulation) the perceived potential was processed differently, having an impact in the N140 and P300. Third, unexpected disturbances displayed significant differences for late components, specially N400. Furthermore, source localization analyses revealed the activation of similar cortical areas involved in error processing, attention, performance monitoring and complex motor planning. This suggest that the perception of unexpected disturbances through afferent somatosensory pathways is proven to simultaneously activate learning and motor related cortical regions. If further studies prove this to be true, it could have important implications in the department of motor-control, facilitating learning and adaptive capabilities to minimize future errors and improve neuroplasticity.

6.4.1 Neurophysiolgy of somatosensory stimulation

Typically, event-related potentials evoked by somatosensory stimuli has been characterized by measuring their exogenous and endogenous components [Nakajima & Imamura, 2000]. For instance, those components with latency inferior to 100 ms (such as N20, P30 or P40) have been reported to be exogenous components because their amplitude only depends on stimulus intensity [Lesser et al., 1979] but it is independent of any performed cognitive tasks [Desmedt & Tomberg, 1989]. Those components elicited from 100 ms after stimulus presentation represent higher cortical information mechanisms involved in the processing of somatosensory feedback [Allison et al., 1992; Forss et al., 1996]. In this sense, two major components, namely the N140-P200 complex, have been consistently reported in a large variety of studies that investigated the correlation of these electrical modulation with pain, conscious perception and/or spatial attention [Desmedt & Tomberg, 1989; Dehaene & Naccache, 2001; Forster & Eimer, 2005]. However, in the literature, most of the research studies on somatosensory feedback, using vibrotactile or electrical stimulation, do not investigate phenomena that occur from 400 ms onwards.

In this study we were interested in investigating medium to late latency cognitive components originated from the perception of somatosensory mismatches introduced as electrical feedback distributed in the arm of the subjects. Here, we introduced three different factors that influence the internal processing of the somatosensory stimuli. We varied the intensity of electrical stimulation and we introduced unexpected perturbations that could appear as the random activation (at the beginning of a trial) or deactivation (at the end of a trial) of the electrical feedback. In our results, we observed the brain responses elicited for each of the varying conditions.

N140

For every analyzed condition, the averaged brain patterns revealed the existence of a sharp negative deflection around 150 ms with ±30 ms of latency variation depending on the studied condition, which can be linked to the previously described somatosensory N140. Variations on the N140 peak occurrence is an established phenomenon, where shortest latencies tends to be related to the absence of a cognitive task, and strong cognitive demands implies longer latencies [García-Larrea et al., 1995]. Indeed, our results (Figure 6.2 and 6.3) show that this potential appears earlier for stimuli related to activation of the electrical stimulation compared to its removal. Accordingly, our results also display slightly shorter latencies for expected events that for unexpected disturbances, which require more cognitive processing. A similar relationship can be observed for the magnitude of this peak, in which statistical differences were found for the different intensities and the modality,

but not regarding to the expectancy of these events. Some works have shown that the N140 is sensitive to exogenous factors (i.e. intensity of stimulation) [Allison et al., 1992; Forss et al., 1996] and in other studies it has also shown dependency with endogenous factors (i.e. cognitive perception of a masked event) [Schubert et al., 2006; Nakajima & Imamura, 2000]. Thus, it is not clear how much of these components is altered by endogenous or exogenous stimuli. Accordingly, the somatosensory N140 can be seen as a complex neural process that include both exogenous and endogenous components with different scalp topography, anatomical origin and functional significance [García-Larrea et al., 1995].

That explains the obtained significant differences where higher intensities of stimulation elicited a larger negative N140. Similarly, the unexpected activation of electrical stimulation had a superior impact on the magnitude of this peak, which leaded to an average of twice the amplitude than for the deactivation of the stimulation. The exogenous factor of the N140 is thus demonstrated by the large positive correlation between the amplitude of this component and the delivered stimulus intensity, which suggest that the primary generator mechanisms of the N140 may receive inputs from the somatosensory system.

In fact, source localization analysis for the different stimulation intensities consistently found the peak activity of the N140 in Brodmann areas (4, 5 and 7) which are involved in somatosensory processing, motor control, propioception and association [Libet et al., 1967; de Lafuente & Romo, 2005]. Even somatosensory stimuli using intensities near the sensory threshold trigger early S1 activations [Ray et al., 1999]. This is in line with the assumption that the N140 manifests cortico-cortical activation from the posterior parietal area 7b [Tomberg, 1999]. For the other two conditions (i.e. modality and expectancy of the stimuli), traces of brain activity were found in the primary somatosensory cortex and the posterior cingulate cortex which have been suggested to be implicated as a neural substrate for human awareness. Furthermore, all of these activations were found slightly sideways towards the contralateral area of the stimulated limb. Which agreed with studies that claim that suprathreshold stimulation triggers conscious perception, and is initially processed in contralateral S1 [Schubert et al., 2006]. In the present experiment, the N140 amplitude was also affected by the modality of the stimuli (i.e. (de)activation of electrical stimulation), whereas the expectancy of the events did not have a significant impact. It is not clear which are the underlying cognitive processes linked to these two conditions and thus how and why they affect differently the endogenous nature of the N140 component. It could be that these two processes are encoded by different neural populations and that the mismatch perception is not processed by the brain until later stages. Nevertheless, the observed variations of magnitude due to these two cognitive tasks, independently of the

stimulus intensity, suggests that endogenous influences may use alternative routes other than the somatosensory system to elicit the N140 potential [Nakajima & Imamura, 2000].

P300

The N140 was followed by a very broad positive peak with a maximum amplitude around 300 ms which rather slowly returned to the baseline level. Through careful observation of the grand averages of Figure 6.2, it is possible to differentiate a biphasic modulation. Inspection of the individual subject averages revealed the existence of two distinct positive peaks in the 200-450 ms time interval which varied in latency from subject to subject. This observation indicates that, due to the averaging process, the observed wide positive peak displayed at 300 ms in the total grand average response might actually be the result of two different psycho-physiological processes. One for the somatosensory elicited peak at 200 ms (P200) and another positive peak that in the literature is usually measured between 300 and 500 ms range, commonly known as P300. These two overlapping components are linked to the endogenous cognitive processes of stimuli perception [Hillyard & W, 1979]. And, even though the superimposition of P200 and P300 have been reported in past research [Miltner et al., 1989], most of psycho-physiology studies have extensively focus on the understanding of the P300 in a wide range of experimental condition including visual, auditive and somatosensory studies. In our results, the amplitude of the P300 recorded at fronto-central and parietal sites displayed a significant progressive increment regarding to the stimulus intensity. Even weak somatosensory stimuli could elicit a P300 [Barrett et al., 1979; Desmedt & Debecker, 1979], that grew from an average of 2.6μV at near sensory threshold stimulation to 5μV for functional stimulation. Notice that these values do not correspond with those of Figure 6.2 (top row), since they were computed from the most positive peak displayed by each subject, and not for a specific and fixed latency. Barrett et al. already described this effect using somatosensory stimuli of different intensities and suggested that the P300 may be determined by a combination of intensity and psychological effects.

Additionally, we also observed significant differences between the activation and de-activation of the somatosensory electrical stimulation, and especially between expected and unexpected events. Where unexpected disturbances elicited P300 responses of nearly double amplitude with respect their expected counterpart. Conventionally, novel stimuli of high saliency have been used to trigger the P300 potential. Then, it makes sense that unexpected disturbances which were presented less frequently than standard stimulation exhibit higher saliency and thus elicit larger responses. Along the same lines, it could be argued that activation of the somatosensory stimuli can be interpreted as a surprising transient event in contrast to the absence of electrical feedback of the resting state,

even when the upcoming stimulation was previously announced with the corresponding auditory cue. Consequently, our findings support that, as it happened with the N140 component, the amplitude of the P300 can be divided into an exogenous component defined as that part whose amplitude increases as a function of stimulus intensity, and an endogenous component defined as that part whose amplitude increases as a function of cognitive factors [Chica et al., 2013].

Although the P300 has been widely studied, the possible superposition of different endogenous potentials in that specific time interval has hindered the development of a confident model that explains the anatomical origins of this component. Intra-cortical recordings and functional imaging techniques in combination with EEG measurements have suggested that P300 mechanisms are originated around the Sylvian fissure, including the supramarginal, inferior and middle frontal gyrus and midline areas (anterior and posterior cingulate and SMA) [Linden, 2005]. However, differences in the specific executed task such as target probability, distractors, level of attention or modality of stimulation may introduce slight variations in the activated areas [Tarkka et al., 1996]. Our data suggested that, for most of the studied conditions, main activity came from the anterior cignulate gyrus and the dorsal posterior cingulate area. However, P300 responses elicited by unexpected disturbances and following initialization of the electrical stimulation reflected a more dominant activity towards the SMA and primary motor cortex

N400

The end of the P300 peak is followed by a wide negativity between 500 and 800 ms after the presentation of the somatosensory stimuli. In the literature, this broad negative-going activation measured at midline central or parietal areas of the scalp has been labeled N400, as its maximum negative peak uses to be found around 400 ms [Kutas & Federmeier, 2011]. This component was first reported in linguistic-related tasks that presented semantic anomalies but also for other lexical and contextual factors [Kutas & Hillyard, 1980; Duncan et al., 2009]. Nowadays, the N400 is not linked to any presumed psychological functionality of a particular mental operation. Instead, it is used to describe a characteristic morphology recorded in the time interval between 200 to 600 ms in response to a stimulus [Kutas & Federmeier, 2011]. In fact, N400-like potentials have also been reported in nonlinguistic paradigms, usually in tasks where subjects are presented with improbable or unexpected stimuli [Sitnikova et al., 2008]. Sometimes they have also received the name N450, specially for studies implicated in cognitive control or conflict monitoring during infrequent incongruent trials [Liotti et al., 2000]. These N400-like responses displayed similar morphology and timing that the semantic N400, but they were measured in more frontal sites of the scalp.

Accordingly, our results displayed a N400-like component of long duration with maximum peak magnitude around 600 ms. In comparison to other studies, our results elicited slower responses, probably due to the additional requirement of sensory awareness in comparison to automatic processes such as the perception of instantaneous oddball events [Giglio et al., 2013]. Nevertheless, the enhancement of this late component was found to depend mainly on the expectancy of the perceived event. In line with previous research, the N400 waveform for incongruent trials displayed an enhanced magnitude [West & Alain, 2000]. Those stimuli that were preceded by an auditory cue to inform the subjects of the incoming electrical stimulation revealed an almost flat N400-like response. However, if the stimulation started or stopped unexpectedly, the magnitude of the evoked response significantly increased, reaching its maximum magnitude at fronto-central site FCz. Both intensity level and modality of stimulation (activation/deactivation of the electrical current) had little to non effect on the averaged magnitude of this component. However, statistical analyses within individual subjects suggested that intensities well over sensory threshold produced a more prominent potential.

Cerebral generators of the N400 component have been mostly investigated using verbal-related tasks. Evidence of these studies indicate that neural contributions for the processing of semantic violations are located within the temporal lobe [Van Petten & Luka, 2006]. This was not the case in our results, which predominantly located the centers of cortical activity in Brodmann areas 6, 24, 31 and 32. These areas belong to the primary motor cortex, anterior cingulate cortex and dorsal posterior cingulate cortex, linked with attention and rational thought processes including performance monitoring, error processing and complex motor planning. This support recent hypothesis [Proverbio & Riva, 2009; Sitnikova et al., 2008] in which violations of semantic processing can be seen as a special case of perceiving an unexpected actions in a given situation. Thus, the N400 might not only reflect the incongruence of an action but also convey information about expectation processing as well as context understanding [Giglio et al., 2013].

6.4.2 Neurophysiolgy of unexpected disturbances

Previous studies have used electrical [Kida et al., 2012] or vibratory [Spackman et al., 2007] stimuli to investigate the brain patterns generated by somatosensory oddball events. Typically, these paradigms introduce a reduced amount of deviant stimuli among a sequence of repeated standard stimuli [Näätänen et al., 2007] in terms of modifying the duration [Akatsuka et al., 2005], frequency [Spackman et al., 2007], intensity [Duncan et al., 2009] or spatial location of the stimulus [Naeije et al., 2016]. It is important to notice that in our paradigm, oddball events are not deviants from a predefined stimulus but they occur as an unexpected disturbance of the time at which the subjects are expecting the

electrical stimulation to be activated/deactivated. Up to our knowledge, the underlying neurophysiolgy processes involved in processing the somatosensory mismatch between the subjects' expectations and the actual outcome during electrical stimulation in their arm have not been explored.

Let us represent the neural response to stimulation mismatches as the subtraction of the averaged potential elicited by electrical stimulation that had been announced ahead, from the averaged neural response originated from the unexpected activation/deactivation of electrical stimulation. Our results (see Figure 6.3) show that regardless of intensity level, the exogenous N140 component gets canceled out, and instead the difference between unexpected and expected events reveal a clear fronto-central negativity peaking at 200 ms. Furthermore, as we discussed in the preceding subsection, P300 and N400-like components exhibit a larger magnitude for rare and unexpected events. Thus, the difference signals representing the expectancy mismatch is also represented by these two midline components.

Concerning the global morphology of the triphasic response described above, it resembles the electrical waveform reported in visual EEG experiments of error monitoring where subjects mentally evaluate the correctness of actions performed by a computer or robotic device [Ferrez & Millán, 2008a; Chavarriaga & Millán, 2010; Iturrate et al., 2015b]. In the literature, neural mechanisms liable for detecting salient changes in the sensory environment have been largely studied. Many studies have found a fronto-central negative deflection peaking between 200 and 350 ms when conflict is enhanced during infrequent incongruent trials [Nieuwenhuis et al., 2004]. This mismatch detector potential has been denoted as N200, and changes of its amplitude has been associated with shifts of attention after high conflict trials [Van Veen & Carter, 2002]. It also has been liked to cognitive control, a concept that covers strategic monitoring and control of motor responses [Folstein & Van Petten, 2008]. However, recent research have argued that depending on their scalp distribution and specific latency N2 should be divided into different subcomponents that explain cognitive control, mismatch detection and attentional adjustment separately [Folstein & Van Petten, 2008]. Sometimes these components are hard to be precisely identified. For instance, the mismatch negativity (MMN), an early negative electrical potential recorded in fronto-central sites and around 150-250ms, has been consistently reported for deviants stimuli in the auditory sensory modality [Näätänen et al., 1978]. Analogously, Restuccia et al. showed that it is possible to record a somatosensory mismatch negativity (sMMN) in response to an infrequent change of vibration/electrical stimulus, mimicking the auditory MMN [Spackman et al., 2007]. It is not completely evident if the MMN is in fact a subcomponent of the more general N200 or a separate overlapping potential [Garrido et al., 2009]. Since they share topographical distribution and time interval, given our

experimental protocol and recording instrumentation, we do not posses enough evidence to make a clear distinction.

As for the mismatch negativity, P300 have also been observed across various sensory modalities (visual, auditory, tactile). However, the P300 tends to be more sensitive to the salience and significance of rare stimuli, and as such reflects a higher level of sensory processing [Friedman et al., 2001; Light et al., 2007; Polich, 2007]. Although it has been reported that deviant stimuli may elicit both MMN and P300 components [Hermens et al., 2010], several studies have found that variations of their respective magnitudes are often dissociated [Rinne et al., 2006], presumably due to their opposite nature (exogenous/endogenous) . The P300 reflects an orienting response to the violation of expected patterns of sensory stimulation and is associated with an involuntary switch of attention toward the deviant stimulus influenced by the activity of frontal-parietal attention networks [Polich, 2007; Lugo et al., 2014]

Finally, the phasic negative deflection around 400 ms appeared for the condition of high conflict, i.e. when the change of stimulation was not expected. This indicates an increased demand in cognitive control during this type of events, which is in line with the assumption that N400 is linked to cognitive control and conflict detection processes of the brain [Bartholow et al., 2005; Vanderhasselt & De Raedt, 2009]. Source localization techniques have located the neural generators of the N400 in the ACC [Liotti et al., 2000], which is involved in high-level functions, such as attention allocation, decision-making, performance monitoring and error detection.

Our results are consistent with findings from other sensory event-related potential and neuroimaging studies [Nee et al., 2011; Shenhav et al., 2013; Danielmeier et al., 2011] Given our paradigm constraints, we hypothesize that the components observed in our registered EEG waveform are the response towards an expected conflict of mismatch during stimulation. First, low-level cortical regions are activated to process sensory changes of stimulation. The detection of these changes recruits higher-level cortical networks that subsequently activate conflict monitoring mechanisms that raise sensory awareness. Then, through interactions between the anterior cingulate cortex and other frontal cortical structures [Gehring & Knight, 2000], attentional resources are set in motor control-related areas for optimal task performance in the attempt to minimize future errors [Johnson Jr et al., 2004; Vanderhasselt & De Raedt, 2009].

6.4.3 Limitations and Future work

Our results on healthy subjects should be further validated in a target population (i.e. stroke patients) and on an online paradigm where electrical stimulation is synchronized with the actual subject's intention of movement instead of using an external auditory cue.

A common characteristic in recording with patients is the lower signal-to-noise ratio compared with healthy controls. First, it is necessary to examine the impact that their brain lesion may have on the elicited electrical signals, which use to result in lower amplitudes. On top of that, frequently for these subjects is more difficult to control eye movements and other artifacts related with residual muscular movements. Thus, it would be advisable to record more trials to guarantee enough artifact-free responses that do not compromise the quality of signal analyses. Furthermore, future recordings should incorporate the tracking of behavioral motor-control measurements that proportionate additional information to quantify the increment in learning induced by unexpected stimulation disturbances compared to non-disturbances as it has been suggested in previous works [Wei et al., 2005; Marchal-Crespo et al., 2017].

From a different point of view, there exist the issue of exactly identifying the components of the recorded event-related responses. Let us consider a specific ERP component as the contribution to a recorded brain pattern of a particular neural mechanism in response to a specific stimulus [Näätänen et al., 1978]. The data used to perform neurophysiology analyses is typically inferred from the averaged responses of different trials and subjects, which implies that at a given time point this data may be affected by different processes specific to each subject. Thus, precisely identifying the particular latency and contribution of a determinate component is very complex. In our results, a clear example is given by the biphasic positive modulation found between 200 and 450 ms, where P200 and P300 components overlap.

Another methodological issue concerns the impact of functional electrical stimulation (i.e. highest level of stimulation used in this study) in the received afferent feedback. Our results have displayed significantly larger magnitude in the early ERP components associated with higher level of intensity. In agreement with previous studies we have hypothesized that this is due to the increased somatosensory afferent stimulus [Nakajima & Imamura, 2000].

However, functional stimulation recruited motor neurons of the arm resulting in the complete extension of the hand. Despite subjects were instructed to restrain ocular movements during the recording, the involuntary extension of the fingers captured their attention and thus they focus their eyes upon the electrically stimulated hand. Consequently, during high level intensity stimulation subjects were receiving both somatosensory and visual feedback, which may trigger the engagement of additional sensory mechanisms that contribute to the averaged waveform. Furthermore, gazing at the moving hand might introduce undesired ocular artifacts that contaminate the signal. On the bright side, our analyses did not reveal any statistical significant EEG activity coming from pre-frontal electrodes that could explain differences among neural responses for different intensities.

Nevertheless, for future implementations the subject's arm could be occluded using a blocking screen, or even use the screen to project additional visual feedback [Wei et al., 2005]; and use additional electro-oculographic electrodes to remove ocular activity from the EEG [Croft & Barry, 2000; Berg & Scherg, 1994]. Other alternative consists on recording two different groups of subjects, where only one group receives additional visual feedback, to analyze the possible impact of the join modality.

7

Discussion and future work

This thesis aims to exploit a cognitive neural signal extracted from human EEG after the perception of an error, namely error-related potentials. These signals are thought as a natural way to intercommunicate our brain with machines, providing them with feedback directly related with the performance of a given task so they can learn and adapt. Specifically, with the goal of developing interfaces that target those users with severely limited or reduced mobility, we have focused on tasks related with movement. Within this context, first we need to understand how the neural signatures associated with the perception of errors work during the interactive use of a BMI (i.e. how they are elicited in the brain and how we can implement algorithms to detect them). And second, how to integrate them in a natural way for a wide range of user-oriented applications that goes from the direct control of assistive devices to apply errors in therapy for neurorehabilitation or even to support other techniques in the replacement of the motor functionality originated by a lost limb. In order to do so, we have studied how to detect ErrPs in fully asynchronous settings, both in terms of decoding and perception of the erroneous events; and then we have explored three user-oriented applications in which ErrPs can be used for control of devices, motor substitution and neurorehabilitation. Here, we have not only focus on the decoding of error-related potentials to maximize the performance of the BMI, but we have also investigated the underlying neural mechanisms and how different factors affected the neurophysiology of the elicited signals when we considered it was relevant. Before diving into further discussions, let us prompt a brief summary of the contributions presented in each chapter of this thesis.

7.1   Summary

- Chapter 2 explored the usage of features in the frequency domain as a way of dealing with the signal variability induced by different tasks in the ErrP correlates observed

in the temporal domain. In particular, an increase in power at the theta band ([4-8 Hz]) after monitoring error actions allowed to teach a classification model how to generalize among different tasks.

- Considering the good generalization properties of the spectral domain, in Chapter 3, we combine time and frequency features with the usage of non-linear classifier and transfer learning techniques to asynchronously detect errors during the continuous trajectories of a device. This revealed the presence of perceptual mechanisms related to the processing of errors even when their associated EEG signatures are not measurable by means of grand averages and suggested the existence of evidence accumulation models in our brain that will only take a decision upon reaching a certain boundary.

- In Chapter 4, we showed how to use policy matching algorithms and probabilistic models to teach a robotic device how to explore and navigate through an unknown scenario. Here, mental assessments of whether the device was going in the right or wrong direction were translated into commands for the device, that ultimately reached the desired destination. The most important property of the presented control scheme is the scalability of the system, since each movement provides global information and as a result the percentage of the map that the robot needs to explore decreases for larger spaces.

- In Chapter 5, we demonstrated the feasibility of combining two neural correlates elicited naturally from the execution of a reaching and grasping task. We showed how specific factors originated by the combination of mental tasks of the hybrid system affected the ErrP modulations and how to tune these parameters to obtain the best performance during the grasping task. This have special impact when designing hybrid approaches in such a way that the system performance can be optimized and ultimately allow the deployment of these systems in applications oriented to help people restore lost mobility of their limbs.

- For those patients that still have residual mobility of their upper limb, a common rehabilitation technique consists in applying functional electrical stimulation directly on the muscles. In Chapter 6, we analyzed the brain patterns related to the mismatch originated when the users expectations of electrical stimulation were violated. We distinguished between the accidental electrical impulses delivered when the users were in a resting state, and the interruption of the stimulation while subjects were executing the task, and thus expecting the electrical current to keep flowing. We showed that in both cases the elicited brain activations resembled those observed for

interaction ErrPs described in previous chapters. Recruitment of conflict monitoring mechanisms in combination with the stimulation of afferent pathways that activate cortical areas related to motor-control may trigger reinforcement learning process to enhance adaptability and optimal performance. This suggests that perception of unexpected disturbances resulting from somatosensory feedback could provoke neuroplasticity, strengthening synaptic connexions to enhance task performance.

7.2 Discussion

As we mentioned previously, throughout this thesis, we have designed several experimental paradigms to improve the understanding of how error-related potentials are generated during the interactive use of BMIs in user-oriented applications. To do so, in addition to the experimental studies presented in Chapters 2 and 3, we have implemented and analyzed a total of 5 additional experiments [Omedes et al., 2013a,b, 2014a,b, 2015b]. These studies that have been published elsewhere helped us to establish the foundations to understand how to develop procedures that allowed us analyze and decode ErrPs during continuous realistic movements executed by virtual and real devices.

Additionally, many researchers have done an excellent work in the attempt to find applications where ErrPs can be used to correct the output of a BMI [Blankertz et al., 2003], as information to recalibrate the BMI classifier [Artusi et al., 2011] or to directly control robotic devices [Iturrate et al., 2013a]. However, too often, these proposals (including our first protocols) were designed as a proof of concept with experiments that are run on a computer screen using simplistic paradigms such as circles moving on a computer screen, bars filling up or restrictive grids [Müller-Putz et al., 2016], that often appear to be boring and not intuitive for the user [Chavarriaga et al., 2017]. In this sense, we have striven to approach these protocols to a more user-oriented scenario closer to the ultimate application. Throughout the thesis we have introduced the first steps to implement error-related signatures in a natural way for applications where errors can be used as a stand-alone signals for the complete control of robotic devices or be combined in multi-modal systems to support movement recovery in field of rehabilitation or to replace lost motor functionality. This process was done either by using real devices or designing virtual reality environments, which has been shown to produce resembling brain patterns that their real-life counterpart [Iturrate et al., 2014] and also suppose a positive improvement in terms of engagement from the user compared with more conventional paradigms [Chavarriaga et al., 2017].

Reckoning all our designed paradigms, a total of over 100 volunteers, distributed among 11 studies developed throughout the duration of this thesis, participated in our experi-

ments. The characterization of the recorded error-related EEG patterns was carried out mainly through two different stages: electrophysiology analyses and single-trial error decoding.

On one hand, following conventional procedures that have been commonly used in the literature, we used time-locked analyses based on the averaging of several repetitions of brain signals elicited by a common erroneous/correct stimulus (i.e. grand averages), convolutional wavelets to observe the time-frequency behavior of the brain dynamics and source localization techniques (sLORETA) that aim to locate the areas of the brain with largest activations at a given instant of time. Considering the additional complexity of using virtual reality and real devices, it is remarkable that in all our experiments we have been able to measure error potential correlates to a great extent. Interestingly, despite the existent differences among the presented tasks (i.e. monitoring a virtual ball moving on a screen, controlling the movements of a mobile robot, correcting the grasping actions of a simulated hand or being attentive to electrical stimulation received in the subject's own arm) where subjects were briefed to engage in different manners, errors were elicited by diverse stimulation processes and even the timing of the events varied among experiments, the majority of our subjects (about 80%) displayed similar brain patterns to those reported in previous ErrP studies [Blankertz et al., 2003; Chavarriaga & Millán, 2010; Iturrate et al., 2012]. The waveform of the ErrPs, up to some variations in latency and magnitude, exhibited three dominant modulations, commonly denoted as N2/P3/N4 (regarding to their valence and latency). In all the cases, measurements of these peaks resulted in largest magnitudes at the electrodes located over the fronto-central cortex, the same as a significant power increase for spectral oscillations in the theta band. Additionally, source localization analysis indicated that main activations originated at Brodmann areas 32, 24 and 6 which correspond to the anterior cingulate cortex and pre-supplementary motor area [Nieuwenhuis et al., 2004].

On the other hand, from the perspective of ErrP classification, a key aspect of this thesis was to identify the algorithms that yielded the highest performance at discriminating between error and correct actions in paradigms where the events were introduced as sudden stimuli, and discriminate errors from background EEG in the case of continuous scenarios. For the first case, several studies agree that temporal features contain the most relevant information at the time of discriminating between error and correct events [Blankertz et al., 2003; Ferrez & Millán, 2008a; Chavarriaga & Millán, 2010]. Commonly a spatial filter as CAR (common-average referencing) is used to posteriorly retain the electrodes located in the fronto-central areas of the brain (FCz and surrounding channels) and the magnitude at various time points of the signal between 0 and 1 seconds from the stimulus onset are selected as features. These features are fed into a classifier. In the literature there

exist numerous options that go from selecting a threshold to separate the two classes, to use more sophisticated techniques as linear discriminant analysis (LDA) or support vector machine (SVM), up to the growing interest on using complex neural networks (NNs) [Bashashati et al., 2007; Lotte et al., 2007; Blankertz et al., 2011]. In practice, most of these algorithms produce similar results, and for most cases LDA has become the default choice due to its simplicity and low computational cost. However, as it was previously mentioned, numerous studies (including ours) have suggested that time domain features are very sensitive to latency variations. Thus, combining them with frequency features results in better accuracy ratios and less false positive detections for the asynchronous decoding of ErrPs. In this context, our experiments revealed that without increasing computational complexity, using non-linear models such as SVM leads to slightly better results (between 5% and 8%) than linear methods like LDA.

Furthermore, another important aspect in the context of classification is the necessity of calibrating the model. In Chapter 2, we emphasized the importance of training a specific model for each subject and task in order to cope with the high variability of the EGG signals, and how there have been many researchers trying to overcome this limitation. In addition to the studies presented in this thesis, we also participated in the recording of an experimental paradigm based in a calibration-free approach for the control of a virtual device using ErrPs [Iturrate et al., 2015a]. This experiment had a similar design to the discrete paradigm presented in Chapter 4. However, for this study did not exist a calibration phase to train the system. Here, we tested a non supervised classification model that exploited constraints intrinsic to the executed task. By doing that, our model was able to simultaneously learn how to recognize ErrPs while the user was in control of the device as soon as the EEG recording system was set up. This concept may become of paramount importance for the deployment of user-focused applications where usability is the prime priority.

Among the different tasks presented in this thesis, most of the volunteer participants achieved accuracy ratios between 70% and 90%, which enabled the successful control of virtual and real devices. Thus, we believe that there is still even more room for improvement to explore novel ways that allow us to get closer to a final application. Nevertheless, for a small percentage of the volunteers, we did not manage to measure discernible EEG activity or these signals did not contain enough information to discriminate correct from erroneous events. This effect is not unusual and has been already described predominantly in experiments based on sensorymotor rhythms, where the term BMI illiteracy has been used to describe those subjects that do not achieve to voluntary modulate discriminable EEG patterns [Kübler & Müller, 2007]. Even though these interfaces were thought to work for any user, non-respondent subjects have been observed in other experimental

paradigms. Illiteracy appears to not depend so much on the algorithm used but on a property inherent in the subject, although it is still unknown if this originates from the effect of a poor signal-to-noise ratio, or because the cortical organization of their brain (which varies from one person to another) involved in the process is tangential to the scalp [Nijholt et al., 2008]. However, at the current date, and despite the extensive efforts that have been made to overcome this issue, for unexplained reason some people remain unable to use any particular BMI.

To conclude this discussion, it should be noted that all the experiments presented during the previous chapters have attempted to expand the usability of error-related signatures to bring them closer towards the deployment of applications centered around end-users such as it could be the grasp of various quotidian objects. Given the technical specificities of the different applications (e.g. start/stop of electrical stimulation) some of our experiments have been conceptually designed to make use of discrete events. Nonetheless, for others it has been necessary to develop procedures that enables the asynchronous decoding of errors during the continuous movements of the virtual device in Chapter 3 or the mobile robot of Chapter 4. For the latter cases, standard time-locked techniques cannot be exploited. In fact, when we attempted to compute the grand averages of the signals, the non-negligible latency variations among the different trials canceled each other resulting in a virtually flat average response. Throughout the thesis we introduced a possible way to develop a classification approach for the asynchronous detection of errors elicited during continuous movements of a device. Our model was not only able to asynchronously decode the appearance of mismatches, but also the time instants in which the subject perceived them, which allowed to perform post-hoc standard time-locked analyses (i.e. grand averages, source localization, among others) from the retrieved onsets. Even though the analyses revealed similar patterns to those observed for sudden events, it is necessary to account for the possible bias of our classifier given that the data used for training was obtained from an experimental condition using sudden stimuli.

7.3 Future work

We have hypothesized that our results support the existence of an evidence accumulation model during the evaluation of gradually unfolding tasks with errors [Hesselmann et al., 2010]. Similarly to our results, other authors have drawn analogous conclusions from P300 studies under gradual changes of visual stimuli [O'Connell et al., 2012]. Indeed, the existence of this model might be a plausible explanation for the larger variance in the detection of ErrPs during erroneous trajectories compared to spontaneous events. However, caution is necessary since our proposed methodology (i.e. asynchronous classification

followed by a post-hoc analysis) may have biased the outcome of the classifier towards the detection of those patterns resembling the signals from the discrete condition used to train the model. In fact, there could be different brain activations associated to gradual deviations that cannot be properly identified and characterized using our proposed method [Omedes et al., 2015a]. Thus, further research should be performed to fully understand the underlying neural mechanisms that generate error-related signatures during gradual unfolding processes.

Interesting options include the design of other asynchronous paradigms or/and to combine different recording techniques such as simultaneous recordings of EEG and fMRI, or even invasive methods [Rosa et al., 2010]. The current thesis has only focus on the investigation of error-related neural correlates from an EEG perspective. However, there exist evidence that these cognitive signals can also be measured using other recording technologies [Mahmoudi & Sanchez, 2011; Völker et al., 2018]. For instance, a recent work using ECoG reported the feasibility of asynchronously decoding neural responses associated to erroneous events. In this study [Milekovic et al., 2012], users played a video game where they controlled a spaceship using a joystick in order to avoid collisions with incoming obstacles. Different types of errors were elicited as mismatches in the direction of movement and obstacle collisions. The work reported asynchronous classification using a sliding window, although the erroneous events were linked to specific discrete stimulus. Additionally, several studies using invasive approaches have measured single-neuron firing activity associated to error processing under conventional paradigms [DiGiovanna et al., 2009]. Even though invasive BMIs face substantial technical difficulties and involve clinical risks, [Even-Chen et al., 2018] showed that intra-cortical electrodes implanted in the motor cortex to perform a typing task, could also be used to detect error-related signatures in terms of local field potentials and spikes signals. In this context, ErrPs can be detected faster than using non-invasive BMIs, between 200 and 400 ms after occurrence of the error. This enables higher information transfer rates, which in their study was translated into being able to correct spelling mistakes in real time. However, the accuracy of error detection was comparable to other protocols using non-invasive recordings. Thus, to justify the surgical procedure, these invasive BMIs should provide much more reliable levels of control that introduced a significant improvement in the patients quality of life [Nicolelis, 2003].

In fact, achieving the speed, accuracy, and reliability necessary for real-world applications remains one of the major challenges for BMI researchers working on invasive and non-invasive systems in order to compete with other assisstive technologies [McFarland & Wolpaw, 2008]. In practice, specific protocols have been able to improve the quality of life of severely paralyzed patients regardless of the current BMI limitations in performance.

For instance, BMI spellers have enabled users who might be unable even to breathe or move their eyes, to communicate with their families and caregivers [Dal Seno et al., 2010]; or BMIs used for rehabilitation have been successfully implemented to improve brain plasticity during therapy [Grosse-Wentrup et al., 2011]. On the other hand, especially for BMIs designed with the objective of restoring or substituting motor functionality, the reliability of the system is of paramount importance. Let us use as an example the control of a robotic wheelchair or a prosthetic arm. What user would be willing to rely on this technology if they knew that there was the sightliest chance, by which his wheelchair may collide against a wall or his prosthetic arm may drop a grabbed item if something goes wrong? In this sense, despite the numerous examples of impressive progress in the field of non-invasive BMI, there are important aspect in regard the extraction of information from the EEG that can be improved. For this reason, many researchers are putting a large effort on improving the accuracy at which brain patterns are decoded and their usability for on-line applications.

Following this line of research, in this thesis we have introduced the usage of spectral features and advanced machine learning techniques as means of increasing generalization and thus rise the performance in ErrP decoding during continuous trajectories. However, there exist the possibility that other alternative features also provide additional information to boost and strengthen BMI decoders. For instance, connectivity patterns could provide information about the functional interaction among different brain regions [Taylor et al., 2007]. In one of our here non-presented contributions [Omedes et al., 2014b], we studied and characterized these connectivity patterns originated during an experimental paradigm of error-related potentials using metrics based on the coherence and phase slope index. The obtained results suggested that in presence of an error potential the coherency within the theta band increases and propagates from central to parietal brain regions. Similarly, Zhang et al. estimated connectivity patterns using multivariate auto-regressive models that also showed increased ErrP modulations in theta and alpha bands between fronto-central and fronto-lateral areas, and combined temporal and connectivity features to increase around a 5% the performance at which erroneous events were detected [Zhang et al., 2015a].

In an complementary way, many researchers are focusing in the development of new computationally efficient machine learning algorithms that increase the precision with which neuronal activity is translated in commands for a device. Even though a vast amount of linear and non-linear algorithms have been suggested [Kim et al., 2003; Garrett et al., 2003], most of these methods frequently yield comparable results, and simple linear models tend to be sufficiently efficient in many practical BMI designs [Lebedev & Nicolelis, 2006]. However, in the recent years there has been an increasing interest in the field of

neural networks, and researchers have started to investigate the way in which they could be applied to BMIs to enhance the decoding of brain patterns [Ren & Wu, 2014]. Neural networks were created as a way to emulate the behavior of our brain in the attempt to unravel complex machine learning problems that other methods could not solve. In this sense, different architectural designs have been proposed, but in particular state-of-the-art convolutional neural networks (ConvNets) have revolutionized several technological fields such as computer vision or speech recognition [LeCun et al., 2015; Schmidhuber, 2015]. Deep ConvNets have the capability of learning local and global patterns from raw data without any a priori feature selection, which makes them very attractive for their use in brain signal processing. Consequently, the BMI community have started to investigate the potential of ConvNets for EEG brain signal decoding [Cecotti & Graser, 2011], but so far the results have failed to significantly outperform the ones obtained with simpler methods [Schirrmeister et al., 2017]. To all appearances, the poor signal-to-noise ratio and non-stationarity characteristics of EEG makes learning features a more complicated problem than for images or speech. On top of that, the datasets used for the experiments might still not be large enough to reveal the full potential of deep ConvNets, or the structure of EEG features may not display hierarchical patterns that ConvNets can exploit. Nevertheless, new technological advances are giving rise to the constant proposal of more robust and advanced algorithms, where hyperparameter optimization, dropout, batch normalization and even non-ConvNet architectures may translate to even better EEG decoding accuracies [Heilmeyer et al., 2018]. Furthermore, these networks can be applied not only to decode information from the EEG but to visualize and interpret what the network has learned from the EEG [Bashivan et al., 2015]. Thus, some day deep learning could become a powerful ally for neuroscientists not only to develop applications controlled by our minds, but also to visualize and clarify the different neural mechanisms behind the generation of EEG signatures and the information they convey.

Understanding the intrinsic nature of the measurable error-related signatures is fundamental not only to comprehend its influence over human behavior but also to correctly design applications that exploit these signals. In the field of psychophysiology and neuroscience, there is still an ongoing debate about whether these measured neural signals encode reward prediction errors (which is a signed quantity), or per contra, the degree at which actual outcomes are surprising (regardless of their valence) [Ullsperger et al., 2014a]. Apparently, this has not supposed a big issue in preliminary error-based BMI applications that solely contemplate the possibility of characterizing a movement as correct or erroneous linked to a spontaneous stimulus. In this scenario, if subjects are attentive to the tasks, they should be able to mentally asses to which of the two categories the observed action belongs. However, it may have undesired implications when dealing with

continuous movements, where the evoked signatures linked to the occurrence of an error have to be discriminated from the noisy EEG background activity, and otherwise it is assumed that the rest of the time the device is performing the correct behavior. To clarify the importance of differentiating this two concepts (erroneous vs surprising events) for the development of realistic BMI applications, let us use an example of a person mentally controlling the continuous movements of a robotic arm. At a given time, this user notices an error in the desired trajectory of the arm. Conceivably, this will elicit an error-related potential that the BMI will detect and elaborate a corrective action. Even though the undertaken corrections put the arm back on the right path, it is probable that this process involves unexpected changes in the trajectory of the movement that may generate a surprise-related response in the user's brain. If we are unable to discriminate whether the measurable EEG signatures, of what in the literature and during this thesis have been denoted as error-related potentials, convey information about saliency, valence or a mix of both; the corrective-surprising response of the previous example might be interpreted as an erroneous outcome. Thus, it is of paramount importance to investigate the existence of differences in the neural correlates elicited for both cases or to implement additional constraints during the design of these applications that allow to successfully discriminate them to avoid undesired responses. In the attempt to shed some light about this issue, the authors proposed a preliminary paradigm where a virtual device sporadically executed abrupt changes in its trajectory [Omedes et al., 2015b]. These movements were both from correct towards erroneous directions or as corrective actions from a previously initiated erroneous trajectory. The analyses to determine if there where differences in the elicited responses have not been completed and thus, they have not been included in the present dissertation.

Nevertheless, this effect is equally important for the on-line control of the other three practical applications proposed in this thesis. During the continuous control of a mobile robot (Chapter 4), despite we cannot be certain of whether the measured events were encoding surprise or erroneous movements, the device achieved to successfully follow the subjects' instructions to reach the specified goals. The other two studies were designed as proof of concept to investigate the applicability of ErrPs in motor substitution (Chapter 5) and neurorehabilitation (Chapter 6) scenarios. In this sense, a clear limitation of these two studies is that they were recorded off-line and the analyzed events resembled those of discrete paradigms. Currently, we are working on an extended closed-loop version of Chapter 6, where (de)activation of neuromuscular electrical stimulation depends both on additional neural correlates related to motor intention and the detection of error-related signatures. This would resemble the control paradigm of hybrid BMI presented in Chapter 5. Regarding to the latter, an with views of a future application, a trivial improvement

would consists in replacing the virtual interface by a real prostheses. In this situation, the dynamics and safety constraints of the prosthesis will require slower speeds to execute the actions. Thus, asynchronous classification methods introduced in Chapter 3 should be adapted to asynchronously detect errors during grasping movements. Furthermore, in order to expand the number of grasps that the BMI is able to decode, iterative strategies or probabilistic models similar to those of Chapter 4 could be adapted to maximize the likelihood of performing the desired action.

Despite the promising results obtained with healthy subjects, the ultimate goal of these experiments is to provide value for patients. To ensure adequacy and correct functionality, these experiments undergo different stages in which results are predominantly validated in able-bodied population [Cincotti et al., 2008]. However, when working with patients there exist at least two factors to consider. On one hand, if patients have a cognitive disorder or cerebral lesion, specifically around the ACC brain regions, it might result in distorted or inexistent EEG signatures in response to errors. Some studies on ALS and stroke patients have achieved to decode ErrP signatures [Spüler et al., 2012; López et al., 2013] not without difficulties. While all people's brain have the same cortical processing systems, there are individual variations in structure, especially in the case of patients and thus, each patient should be considered as a particular case and the employed methodology should be adapted accordingly. On the other hand, it is well established that in terms of classification, even when signal are detectable, accuracy performance tends to decrease slightly in comparison to healthy subject performances. This is particularly relevant when working with errors, since a poorer accuracy may lead to the occurrence of more errors. Even though there are studies reporting that even with a high error ratio it is still possible to decode ErrPs effectively Ferrez & Millán [2008a], there also exist the risk that users get habituated to the presence of errors.

Habituation refers to the process by which, the exposition to continuously repeated stimulus produces that the response to it becomes less and less intense [Stein, 1966]. A major role of habituation is to limit the usage of attentional resources for stimuli that are no longer salient in terms of threat or reward [Groves & Thompson, 1970; Rolls, 2000]. Even though some studies have suggested that ErrP responses are stable over time [Chavarriaga & Millán, 2010], these investigations did not extend the experimental recordings for more than a few weeks. In this sense, it is still unclear how habituation may impact the ErrP responses on end-users that are permanently in contact with this technology. On one hand, a plausible hypothesis insinuates that users may become accustomed to the appearance of determinate erroneous events, and as the expectancy of these errors grow, the associated brain responses decreases, resulting in a non-sustainable model for long-term usage [Sellers et al., 2010]. This theory is supported by neuroimaging experiments, that using emotional

event-related potentials have found that the amygdala, hippocampus and prefrontal cortex are essential for evaluating stimuli relevance [Rolls, 2000]. However, if repeated stimulus occur without associated consequences, these neural organisms rapidly habituate and the elicited activity diminishes over time [Tan & Nijholt, 2010]. In contrast, an additional study showed that when the stimuli convey positive and negative valence it was not possible to find significant habituation in the hippocampus or ventral temporal cortex [Wright et al., 2001], which may ensure the stability of error-related signatures over time. A more optimistic hypothesis compares long-term exposure to BMIs as "training", or a way to acquire experience and improve; same as when we learn to play a sport or a musical instrument. Several studies have demonstrated that training promotes neuroplasticity and learning mechanisms which strengthen the properties of synaptic junctions, thereby increasing their efficiency [Hebb, 1949; Tyler et al., 2002]. Longitudinal studies in subjects with spinal cord injury (SCI) or stroke and in a healthy control population revealed that in fact motor imagery training improves motor performance. These experiments with a variable extension (from a few weeks [Cramer et al., 2007] up to 8 years [Enzinger et al., 2008]) demonstrated that patients with partial or complete paralysis due to stroke or SCI can learn to effectively generate EEG bursts of μ and β oscillations through the imagination of their immobilized limbs [Buch et al., 2008]. It is questionable that the same principles can be extrapolated to naturally elicited brain signatures such as error-related potentials. However, a user could find strategies to become proficient at performing a given task. For instance, he could auto-induce a surprising response in presence of erroneous events and stay in a relaxed state during correct movements to maximize the differences among them. If that was the case, adequate co-adaptation techniques, where brain and machine simultaneously learn from each other, could be implemented to boost the performance of these systems [DiGiovanna et al., 2009].

As of today, control of devices exclusively through mental commands does not fulfill the necessary requirements for the public distribution of this technology. There is still a lot of work to do until these systems reach the necessary requirements for a satisfactory experience throughout their use, while ensuring safety for the users in specific cases (think about previous example of driving a wheelchair). Even though BMIs have been proven to be an exceptional solution for people with severe motor disabilities, there exist numerous assistive technologies that have been perfected and nowadays outperform BMIs when users are still capable of performing residual movements. Notwithstanding, at the vertiginous pace at which technology progresses, and the growing formation of start-ups and powerful companies devoted to the multidisciplinary field of brain science, it is expected that in the upcoming future we start to see applications where brain patterns are actively used as an essential component of commercial products. In fact, it is highly likely that some of these

futuristic gadgets may use error-related signatures as a fundamental unit to interpret the user's preferences and generate specific behavioral patterns adapted to each person.

Bibliography

[Abu-Alqumsan et al., 2017] Abu-Alqumsan, M., Kapeller, C., Hintermüller, C., Guger, C., & Peer, A. 2017. Invariance and variability in interaction error-related potentials and their consequences for classification. *Journal of neural engineering*, **14**(6), 066015.

[Akatsuka et al., 2005] Akatsuka, K., Wasaka, T., Nakata, H., Inui, K., Hoshiyama, M., & Kakigi, R. 2005. Mismatch responses related to temporal discrimination of somatosensory stimulation. *Clinical Neurophysiology*, **116**(8), 1930–1937.

[Akbani et al., 2004] Akbani, R., Kwek, S., & Japkowicz, N. 2004. Applying support vector machines to imbalanced datasets. *Pages 39–50 of: Proceedings of the 15th European Conference on Machine Learning (ECML)*.

[Albright et al., 2000] Albright, T. D., Jessell, T. M., Kandel, E. R., & Posner, M. I. 2000. Neural science: a century of progress and the mysteries that remain. *Cell*, **100**, 1–55.

[Alexander & Brown, 2010] Alexander, W. H., & Brown, J. W. 2010. Computational models of performance monitoring and cognitive control. *Topics in cognitive science*, **2**(4), 658–677.

[Allison et al., 2007] Allison, B., Graimann, B., & Gräser, A. 2007. Why use a BCI if you are healthy. *Pages 7–11 of: ACE Workshop-Brain-Computer Interfaces and Games*.

[Allison et al., 2010] Allison, B., Brunner, C., Kaiser, V., Müller-Putz, G. R., Neuper, C., & Pfurtscheller, G. 2010. Toward a hybrid brain–computer interface based on imagined movement and visual attention. *Journal of neural engineering*, **7**(2), 026007.

[Allison et al., 1992] Allison, T., McCarthy, G., & Wood, C. C. 1992. The relationship between human long-latency somatosensory evoked potentials recorded from the cortical surface and from the scalp. *Electroencephalography and Clinical Neurophysiology/Evoked Potentials Section*, **84**(4), 301–314.

[Anderson et al., 2012] Anderson, N. R., Blakely, T., Schalk, G., Leuthardt, E. C., & Moran, D. W. 2012. Electrocorticographic (ECoG) correlates of human arm movements. *Experimental brain research*, **223**(1), 1–10.

[**Artusi et al., 2011**] Artusi, X., Niazi, I. K., Lucas, M.-F., & Farina, D. 2011. Performance of a simulated adaptive BCI based on experimental classification of movement-related and error potentials. *IEEE Journal on Emerging and Selected Topics in Circuits and Systems*, **1**(4), 480–488.

[**Austermann & Yamada, 2008**] Austermann, A., & Yamada, S. 2008. Learning to understand multimodal rewards for human-robot-interaction using hidden markov models and classical conditioning. *Pages 4096–4103 of: Evolutionary Computation, 2008. CEC 2008.(IEEE World Congress on Computational Intelligence). IEEE Congress on.* IEEE.

[**Bailey et al., 2005**] Bailey, D. L., Townsend, D. W., Valk, P. E., & Maisey, M. N. 2005. *Positron emission tomography.* Springer.

[**Baker et al., 2000**] Baker, L. L., Wederich, C., McNeal, D. R., Newsam, C. J., & Waters, R. L. 2000. *Neuro muscular electrical stimulation: a practical guide.* Los Amigos Research & Education Institute.

[**Balconi & Vitaloni, 2014**] Balconi, M., & Vitaloni, S. 2014. Dorsolateral pFC and the representation of the incorrect use of an object: the transcranial direct current stimulation effect on N400 for visual and linguistic stimuli. *Journal of cognitive neuroscience*, **26**(2), 305–318.

[**Barrett et al., 1979**] Barrett, G., Halliday, A., Halliday, E., Rudolf, N. d. M., et al. 1979. The later components of the somatosensory evoked potential and the P300 in a threshold detection task. *Pages 140–150 of: Cognitive Components in Cerebral Event-Related Potentials and Selective Attention.* Karger, Basel.

[**Bartholow et al., 2005**] Bartholow, B. D., Pearson, M. A., Dickter, C. L., Sher, K. J., Fabiani, M., & Gratton, G. 2005. Strategic control and medial frontal negativity: Beyond errors and response conflict. *Psychophysiology*, **42**(1), 33–42.

[**Bashashati et al., 2007**] Bashashati, A., Fatourechi, M., Ward, R. K., & Birch, G. E. 2007. A survey of signal processing algorithms in brain–computer interfaces based on electrical brain signals. *Journal of Neural engineering*, **4**(2), R32.

[**Bashivan et al., 2015**] Bashivan, P., Rish, I., Yeasin, M., & Codella, N. 2015. Learning representations from EEG with deep recurrent-convolutional neural networks. *arXiv preprint arXiv:1511.06448.*

[Bayliss, 2003] Bayliss, J. D. 2003. Use of the evoked potential P3 component for control in a virtual apartment. *IEEE transactions on neural systems and rehabilitation engineering*, **11**(2), 113–116.

[Benjamini & Hochberg, 1995] Benjamini, Y., & Hochberg, Y. 1995. Controlling the false discovery rate: a practical and powerful approach to multiple testing. *Journal of the royal statistical society. Series B (Methodological)*, 289–300.

[Berg & Scherg, 1994] Berg, P., & Scherg, M. 1994. A multiple source approach to the correction of eye artifacts. *Electroencephalography and clinical neurophysiology*, **90**(3), 229–241.

[Berger, 1929] Berger, H. 1929. Über das elektrenkephalogramm des menschen. *Archiv für psychiatrie und nervenkrankheiten*, **87**(1), 527–570.

[Bergquist et al., 2011] Bergquist, A. J., Clair, J. M., Lagerquist, O., Mang, C. S., Okuma, Y., & Collins, D. F. 2011. Neuromuscular electrical stimulation: implications of the electrically evoked sensory volley. *European journal of applied physiology*, **111**(10), 2409.

[Bigdely-Shamlo et al., 2013] Bigdely-Shamlo, N., Mullen, T., Kreutz-Delgado, K., & Makeig, S. 2013. Measure projection analysis: a probabilistic approach to EEG source comparison and multi-subject inference. *Neuroimage*, **72**, 287–303.

[Birbaumer et al., 1999] Birbaumer, N., Ghanayim, N., Hinterberger, T., Iversen, I., Kotchoubey, B., Kübler, A., Perelmouter, J., Taub, E., & Flor, H. 1999. A spelling device for the paralysed. *Nature*, **398**(6725), 297.

[Birbaumer et al., 2000] Birbaumer, N., Kubler, A., Ghanayim, N., Hinterberger, T., Perelmouter, J., Kaiser, J., Iversen, I., Kotchoubey, B., Neumann, N., & Flor, H. 2000. The thought translation device (TTD) for completely paralyzed patients. *IEEE Transactions on rehabilitation Engineering*, **8**(2), 190–193.

[Bishop, 2016] Bishop, C. M. 2016. *Pattern recognition and machine learning*. Springer-Verlag New York.

[Blankertz et al., 2003] Blankertz, B., Dornhege, G., Schafer, C., Krepki, R., Kohlmorgen, J., Muller, K.-R., Kunzmann, V., Losch, F., & Curio, G. 2003. Boosting bit rates and error detection for the classification of fast-paced motor commands based on single-trial EEG analysis. *IEEE Transactions on Neural Systems and Rehabilitation Engineering*, **11**(2), 127–131.

[Blankertz et al., 2011] Blankertz, B., Lemm, S., Treder, M., Haufe, S., & Müller, K.-R. 2011. Single-trial analysis and classification of ERP componentsa tutorial. *NeuroImage*, **56**(2), 814–825.

[Blickenstorfer et al., 2009] Blickenstorfer, A., Kleiser, R., Keller, T., Keisker, B., Meyer, M., Riener, R., & Kollias, S. 2009. Cortical and subcortical correlates of functional electrical stimulation of wrist extensor and flexor muscles revealed by fMRI. *Human brain mapping*, **30**(3), 963–975.

[Botvinick et al., 2001] Botvinick, M. M., Braver, T. S., Barch, D. M., Carter, C. S., & Cohen, J. D. 2001. Conflict monitoring and cognitive control. *Psychological review*, **108**(3), 624.

[Bradberry et al., 2009] Bradberry, T. J., Rong, F., & Contreras-Vidal, J. L. 2009. Decoding center-out hand velocity from MEG signals during visuomotor adaptation. *Neuroimage*, **47**(4), 1691–1700.

[Brooks, 1986] Brooks, V. B. 1986. How does the limbic system assist motor learning? A limbic comparator hypothesis (Part 1 of 2). *Brain, Behavior and Evolution*, **29**(1-2), 29–41.

[Brown & Braver, 2005] Brown, J. W., & Braver, T. S. 2005. Learned predictions of error likelihood in the anterior cingulate cortex. *Science*, **307**(5712), 1118–1121.

[Buccino et al., 2016] Buccino, A. P., Keles, H. O., & Omurtag, A. 2016. Hybrid EEG-fNIRS asynchronous brain-computer interface for multiple motor tasks. *PloS one*, **11**(1), e0146610.

[Buch et al., 2008] Buch, E., Weber, C., Cohen, L. G., Braun, C., Dimyan, M. A., Ard, T., Mellinger, J., Caria, A., Soekadar, S., Fourkas, A., et al. 2008. Think to move: a neuromagnetic brain-computer interface (BCI) system for chronic stroke. *stroke*, **39**(3), 910–917.

[Bunge et al., 1993] Bunge, R. P., Puckett, W., Becerra, J., Marcillo, A., & Quencer, R. 1993. Observations on the pathology of human spinal cord injury. A review and classification of 22 new cases with details from a case of chronic cord compression with extensive focal demyelination. *Advances in neurology*, **59**, 75.

[Carter et al., 1998] Carter, C. S., Braver, T. S., Barch, D. M., Botvinick, M. M., Noll, D., & Cohen, J. D. 1998. Anterior cingulate cortex, error detection, and the online monitoring of performance. *Science*, **280**(5364), 747–749.

[Cauraugh et al., 2000] Cauraugh, J., Light, K., Kim, S., Thigpen, M., & Behrman, A. 2000. Chronic motor dysfunction after stroke: recovering wrist and finger extension by electromyography-triggered neuromuscular stimulation. *Stroke*, **31**(6), 1360–1364.

[Causse et al., 2015] Causse, M., Fabre, E., Giraudet, L., Gonzalez, M., & Peysakhovich, V. 2015. EEG/ERP as a measure of mental workload in a simple piloting task. *Procedia Manufacturing*, **3**, 5230–5236.

[Cavanagh & Frank, 2014] Cavanagh, J. F., & Frank, M. J. 2014. Frontal theta as a mechanism for cognitive control. *Trends in cognitive sciences*, **18**(8), 414–421.

[Cavanagh et al., 2009] Cavanagh, J. F., Cohen, M. X., & Allen, J. J. B. 2009. Prelude to and resolution of an error: EEG phase synchrony reveals cognitive control dynamics during action monitoring. *Journal of Neuroscience*, **29**(1), 98–105.

[Cecotti & Graser, 2011] Cecotti, H., & Graser, A. 2011. Convolutional neural networks for P300 detection with application to brain-computer interfaces. *IEEE transactions on pattern analysis and machine intelligence*, **33**(3), 433–445.

[Chang & Lin, 2011] Chang, C.-C., & Lin, C.-J. 2011. LIBSVM: a library for support vector machines. *ACM Transactions on Intelligent Systems and Technology (TIST)*, **2**(3), 27.

[Chavarriaga & Millán, 2010] Chavarriaga, R., & Millán, J. d. R. 2010. Learning from EEG error-related potentials in noninvasive brain-computer interfaces. *IEEE transactions on neural systems and rehabilitation engineering*, **18**(4), 381–388.

[Chavarriaga et al., 2014] Chavarriaga, R., Sobolewski, A., & Millán, J. d. R. 2014. Errare machinale est: the use of error-related potentials in brain-machine interfaces. *Frontiers in neuroscience*, **8**, 208.

[Chavarriaga et al., 2017] Chavarriaga, R., Fried-Oken, M., Kleih, S., Lotte, F., & Scherer, R. 2017. Heading for new shores! Overcoming pitfalls in BCI design. *Brain-Computer Interfaces*, **4**(1-2), 60–73.

[Chica et al., 2013] Chica, A. B., Bartolomeo, P., & Lupiáñez, J. 2013. Two cognitive and neural systems for endogenous and exogenous spatial attention. *Behavioural brain research*, **237**, 107–123.

[Cincotti et al., 2008] Cincotti, F., Mattia, D., Aloise, F., Bufalari, S., Schalk, G., Oriolo, G., Cherubini, A., Marciani, M. G., & Babiloni, F. 2008. Non-invasive brain–computer interface system: towards its application as assistive technology. *Brain research bulletin*, **75**(6), 796–803.

[**Cincotti et al., 2012**] Cincotti, F., Pichiorri, F., Aricò, P., Aloise, F., Leotta, F., de Vico Fallani, F., Millán, J. d. R., Molinari, M., & Mattia, D. 2012. EEG-based Brain-Computer Interface to support post-stroke motor rehabilitation of the upper limb. *Pages 4112–4115 of: 2012 Annual International Conference of the IEEE Engineering in Medicine and Biology Society.* IEEE.

[**Cohen, 2011**] Cohen, M. X. 2011. Error-related medial frontal theta activity predicts cingulate-related structural connectivity. *NeuroImage*, **55**(3), 1373–1383.

[**Cohen et al., 2007**] Cohen, M. X., Elger, C. E., & Ranganath, C. 2007. Reward expectation modulates feedback-related negativity and EEG spectra. *Neuroimage*, **35**(2), 968–978.

[**Coles et al., 2001**] Coles, M. G. H., Scheffers, M. K., & Holroyd, C. B. 2001. Why is there an ERN/Ne on correct trials? Response representations, stimulus-related components, and the theory of error-processing. *Biological psychology*, **56**(3), 173–189.

[**Cope et al., 1988**] Cope, M., Delpy, D. T., Reynolds, E. O. R., Wray, S., Wyatt, J., & Van der Zee, P. 1988. Methods of quantitating cerebral near infrared spectroscopy data. *Pages 183–189 of: Oxygen Transport to Tissue X.* Springer.

[**Cramer et al., 2007**] Cramer, S. C., Orr, E. L., Cohen, M. J., & Lacourse, M. G. 2007. Effects of motor imagery training after chronic, complete spinal cord injury. *Experimental brain research*, **177**(2), 233–242.

[**Croft & Barry, 2000**] Croft, R. J., & Barry, R. J. 2000. EOG correction of blinks with saccade coefficients: a test and revision of the aligned-artefact average solution. *Clinical neurophysiology*, **111**(3), 444–51.

[**Dal Seno et al., 2010**] Dal Seno, B., Matteucci, M., & Mainardi, L. 2010. Online detection of P300 and error potentials in a BCI speller. *Computational intelligence and neuroscience*, **2010**, 11.

[**Daly & Wolpaw, 2008**] Daly, J. J., & Wolpaw, J. R. 2008. Brain–computer interfaces in neurological rehabilitation. *The Lancet Neurology*, **7**(11), 1032–1043.

[**Danielmeier et al., 2011**] Danielmeier, C., Eichele, T., Forstmann, B. U., Tittgemeyer, M., & Ullsperger, M. 2011. Posterior medial frontal cortex activity predicts post-error adaptations in task-related visual and motor areas. *Journal of Neuroscience*, **31**(5), 1780–1789.

[**de Jong et al., 2006**] de Jong, R., Gladwin, T. E., & M't Hart, B. 2006. Movement-related EEG indices of preparation in task switching and motor control. *Brain research*, **1105**(1), 73–82.

[**de Lafuente & Romo, 2005**] de Lafuente, V., & Romo, R. 2005. Neuronal correlates of subjective sensory experience. *Nature neuroscience*, **8**(12), 1698.

[**Debener et al., 2005**] Debener, S., Ullsperger, M., Siegel, M., Fiehler, K., Von Cramon, D. Y., & Engel, A. K. 2005. Trial-by-trial coupling of concurrent electroencephalogram and functional magnetic resonance imaging identifies the dynamics of performance monitoring. *Journal of Neuroscience*, **25**(50), 11730–11737.

[**Dehaene & Naccache, 2001**] Dehaene, S., & Naccache, L. 2001. Towards a cognitive neuroscience of consciousness: basic evidence and a workspace framework. *Cognition*, **79**(1-2), 1–37.

[**Dehaene et al., 1994**] Dehaene, S., Posner, M. I., & Tucker, D. M. 1994. Localization of a neural system for error detection and compensation. *Psychological Science*, **5**(5), 303–305.

[**Demchenko et al., 2016**] Demchenko, I., Katz, R., Pratt, H., & Zacksenhouse, M. 2016. Distinct electroencephalographic responses to disturbances and distractors during continuous reaching movements. *Brain research*, **1652**, 178–187.

[**Den Ouden et al., 2012**] Den Ouden, H. E., Kok, P., & De Lange, F. P. 2012. How prediction errors shape perception, attention, and motivation. *Frontiers in psychology*, **3**.

[**Denker et al., 2011**] Denker, M., Roux, S., Lindén, H., Diesmann, M., Riehle, A., & Grün, S. 2011. The local field potential reflects surplus spike synchrony. *Cerebral Cortex*, **21**(12), 2681–2695.

[**Desmedt & Debecker, 1979**] Desmedt, J. E., & Debecker, J. 1979. Wave form and neural mechanism of the decision P350 elicited without pre-stimulus CNV or readiness potential in random sequences of near-threshold auditory clicks and finger stimuli. *Electroencephalography and Clinical Neurophysiology*, **47**(6), 648–670.

[**Desmedt & Tomberg, 1989**] Desmedt, J. E., & Tomberg, C. 1989. Mapping early somatosensory evoked potentials in selective attention: critical evaluation of control conditions used for titrating by difference the cognitive P30, P40, P100 and N140. *Electroencephalography and Clinical Neurophysiology/Evoked Potentials Section*, **74**(5), 321–346.

[Diedrichsen et al., 2005] Diedrichsen, J., Hashambhoy, Y., Rane, T., & Shadmehr, R. 2005. Neural correlates of reach errors. *The Journal of neuroscience*, **25**(43), 9919–9931.

[DiGiovanna et al., 2009] DiGiovanna, J., Mahmoudi, B., Fortes, J., Principe, J. C., & Sanchez, J. C. 2009. Coadaptive brain–machine interface via reinforcement learning. *IEEE transactions on biomedical engineering*, **56**(1), 54–64.

[Donchin et al., 2000] Donchin, E., Spencer, K. M., & Wijesinghe, R. 2000. The mental prosthesis: assessing the speed of a P300-based brain-computer interface. *IEEE transactions on rehabilitation engineering*, **8**(2), 174–179.

[Dornhege, 2003] Dornhege, G. 2003. Speeding up classification of multi-channel brain-computer interfaces: Common spatial patterns for slow cortical potentials. *IEEE EMBS Conference on Neural Engineering*, 595–598.

[Duncan et al., 2009] Duncan, C. C., Barry, R. J., Connolly, J. F., Fischer, C., Michie, P. T., Näätänen, R., Polich, J., Reinvang, I., & Van Petten, C. 2009. Event-related potentials in clinical research: guidelines for eliciting, recording, and quantifying mismatch negativity, P300, and N400. *Clinical Neurophysiology*, **120**(11), 1883–1908.

[Emken et al., 2005] Emken, J. L., Bobrow, J. E., & Reinkensmeyer, D. J. 2005. Robotic movement training as an optimization problem: designing a controller that assists only as needed. *Pages 307–312 of: Rehabilitation Robotics, 2005. ICORR 2005. 9th International Conference on.* Citeseer.

[Enzinger et al., 2008] Enzinger, C., Ropele, S., Fazekas, F., Loitfelder, M., Gorani, F., Seifert, T., Reiter, G., Neuper, C., Pfurtscheller, G., & Müller-Putz, G. 2008. Brain motor system function in a patient with complete spinal cord injury following extensive brain–computer interface training. *Experimental brain research*, **190**(2), 215–223.

[Eriksen, 1995] Eriksen, C. W. 1995. The flankers task and response competition: A useful tool for investigating a variety of cognitive problems. *Visual Cognition*, **2**(2-3), 101–118.

[Escolano et al., 2011] Escolano, C., Antelis, J., & Minguez, J. 2011. A telepresence mobile robot controlled with a noninvasive brain-computer interface. *IEEE Transactions on Systems, Man and Cybernetics (accepted).*

[Even-Chen et al., 2018] Even-Chen, N., Stavisky, S. D., Pandarinath, C., Nuyujukian, P., Blabe, C. H., Hochberg, L. R., Henderson, J. M., & Shenoy, K. V. 2018. Feasibility of automatic error detect-and-undo system in human intracortical brain–computer interfaces. *IEEE Transactions on Biomedical Engineering*, **65**(8).

[**Falkenstein et al., 1991**] Falkenstein, M., Hohnsbein, J., Hoormann, J., & Blanke, L. 1991. Effects of crossmodal divided attention on late ERP components. II. Error processing in choice reaction tasks. *Electroencephalography and clinical neurophysiology*, **78**(6), 447–455.

[**Falkenstein et al., 2000**] Falkenstein, M., Hoormann, J., Christ, S., & Hohnsbein, J. 2000. ERP components on reaction errors and their functional significance: a tutorial. *Biological psychology*, **51**(2-3), 87–107.

[**Ferrez & Millán, 2008a**] Ferrez, P. W., & Millán, J. d. R. 2008a. Error-related EEG potentials generated during simulated brain–computer interaction. *IEEE transactions on biomedical engineering*, **55**(3), 923–929.

[**Ferrez & Millán, 2008b**] Ferrez, P. W., & Millán, J. d. R. 2008b. Simultaneous real-time detection of motor imagery and error-related potentials for improved BCI accuracy. *Pages 197–202 of: Proceedings of the 4th international brain-computer interface workshop and training course*.

[**Fischbach, 1992**] Fischbach, G. D. 1992. Mind and brain. *Scientific American*, **267**(3), 48–59.

[**Folstein & Van Petten, 2008**] Folstein, J. R., & Van Petten, C. 2008. Influence of cognitive control and mismatch on the N2 component of the ERP: a review. *Psychophysiology*, **45**(1), 152–170.

[**Forss et al., 1996**] Forss, N., Merlet, I., Vanni, S., Ha, M., Hari, R., et al. 1996. Activation of human mesial cortex during somatosensory target detection task. *Brain research*, **734**(1-2), 229–235.

[**Forster & Eimer, 2005**] Forster, B., & Eimer, M. 2005. Covert attention in touch: Behavioral and ERP evidence for costs and benefits. *Psychophysiology*, **42**(2), 171–179.

[**Friedman et al., 2001**] Friedman, D., Cycowicz, Y. M., & Gaeta, H. 2001. The novelty P3: an event-related brain potential (ERP) sign of the brain's evaluation of novelty. *Neuroscience & Biobehavioral Reviews*, **25**(4), 355–373.

[**Friedrich et al., 2013**] Friedrich, E. V., Scherer, R., & Neuper, C. 2013. Stability of event-related (de-) synchronization during brain–computer interface-relevant mental tasks. *Clinical Neurophysiology*, **124**(1), 61–69.

[**Galán et al., 2008**] Galán, F., Nuttin, M., Lew, E., Ferrez, P. W., Vanacker, G., Philips, J., & Millán, J. d. R. 2008. A brain-actuated wheelchair: asynchronous and non-invasive

brain–computer interfaces for continuous control of robots. *Clinical neurophysiology*, **119**(9), 2159–2169.

[**García-Larrea et al., 1995**] García-Larrea, L., Lukaszewicz, A. C., & Mauguière, F. 1995. Somatosensory responses during selective spatial attention: The N120-to-N140 trasition. *Psychophysiology*, **32**(6), 526–537.

[**Garrett et al., 2003**] Garrett, D., Peterson, D. A., Anderson, C. W., & Thaut, M. H. 2003. Comparison of linear, nonlinear, and feature selection methods for EEG signal classification. *IEEE Transactions on neural systems and rehabilitation engineering*, **11**(2), 141–144.

[**Garrido et al., 2009**] Garrido, M. I., Kilner, J. M., Stephan, K. E., & Friston, K. J. 2009. The mismatch negativity: a review of underlying mechanisms. *Clinical neurophysiology*, **120**(3), 453–463.

[**Gehring & Knight, 2000**] Gehring, W. J., & Knight, R. T. 2000. Prefrontal–cingulate interactions in action monitoring. *Nature neuroscience*, **3**(5), 516.

[**Gehring et al., 1993**] Gehring, W. J., Goss, B., Coles, M. G. H., Meyer, D. E., & Donchin, E. 1993. A neural system for error detection and compensation. *Psychological science*, **4**(6), 385–390.

[**Gehring et al., 2018**] Gehring, W. J., Goss, B., Coles, M. G. H., Meyer, D. E., & Donchin, E. 2018. The error-related negativity. *Perspectives on Psychological Science*, **13**(2), 200–204.

[**Gevins & Smith, 2000**] Gevins, A., & Smith, M. E. 2000. Neurophysiological measures of working memory and individual differences in cognitive ability and cognitive style. *Cerebral cortex*, **10**(9), 829–839.

[**Giglio et al., 2013**] Giglio, A. C. A., Minati, L., & Boggio, P. S. 2013. Throwing the banana away and keeping the peel: neuroelectric responses to unexpected but physically feasible action endings. *Brain research*, **1532**, 56–62.

[**Goodale et al., 2004**] Goodale, M. A., Westwood, D. A., & Milner, A. D. 2004. Two distinct modes of control for object-directed action. *Progress in brain research*, **144**, 131–144.

[**Graimann & Pfurtscheller, 2006**] Graimann, B., & Pfurtscheller, G. 2006. Quantification and visualization of event-related changes in oscillatory brain activity in the time–frequency domain. *Progress in brain research*, **159**, 79–97.

[**Granat et al., 1993**] Granat, M. H., Ferguson, A. C. B., Andrews, B. J., & Delargy, M. 1993. The role of functional electrical stimulation in the rehabilitation of patients with incomplete spinal cord injury-observed benefits during gait studies. *Spinal Cord*, **31**(4), 207.

[**Grosse-Wentrup et al., 2011**] Grosse-Wentrup, M., Mattia, D., & Oweiss, K. 2011. Using brain–computer interfaces to induce neural plasticity and restore function. *Journal of neural engineering*, **8**(2), 025004.

[**Groves & Thompson, 1970**] Groves, P. M., & Thompson, R. F. 1970. Habituation: a dual-process theory. *Psychological review*, **77**(5), 419.

[**Gu et al., 2009**] Gu, Y., Dremstrup, K., & Farina, D. 2009. Single-trial discrimination of type and speed of wrist movements from EEG recordings. *Clinical Neurophysiology*, **120**(8), 1596–1600.

[**Guger et al., 2008**] Guger, C., Holzner, C., Grönegress, C., Edlinger, G., & Slater, M. 2008. Control of a smart home with a brain-computer interface. *Pages 339–342 of: Proceedings of the 4th international brain-computer interface workshop and training course.*

[**Hajcak et al., 2005**] Hajcak, G., Moser, J. S., Yeung, N., & Simons, R. F. 2005. On the ERN and the significance of errors. *Psychophysiology*, **42**(2), 151–160.

[**Hajcak et al., 2006**] Hajcak, G., Moser, J. S., Holroyd, C. B., & Simons, R. F. 2006. The feedback-related negativity reflects the binary evaluation of good versus bad outcomes. *Biological psychology*, **71**(2), 148–154.

[**Hämäläinen et al., 1993**] Hämäläinen, M., Hari, R., Ilmoniemi, R. J., Knuutila, J., & Lounasmaa, O. V. 1993. Magnetoencephalographytheory, instrumentation, and applications to noninvasive studies of the working human brain. *Reviews of modern Physics*, **65**(2), 413.

[**Hebb, 1949**] Hebb, D. O. 1949. *The organization of behavior: A neurophysiological approach.*

[**Heilmeyer et al., 2018**] Heilmeyer, F. A., Schirrmeister, R. T., Fiederer, L. D., Völker, M., Behncke, J., & Ball, T. 2018. A large-scale evaluation framework for EEG deep learning architectures. *arXiv preprint arXiv:1806.07741.*

[**Herff & Schultz, 2016**] Herff, C., & Schultz, T. 2016. Automatic speech recognition from neural signals: a focused review. *Frontiers in neuroscience*, **10**, 429.

[**Hermens et al., 2010**] Hermens, D. F., Ward, P. B., Hodge, M. A. R., Kaur, M., Naismith, S. L., & Hickie, I. B. 2010. Impaired MMN/P3a complex in first-episode psychosis: cognitive and psychosocial associations. *Progress in Neuro-Psychopharmacology and Biological Psychiatry*, **34**(6), 822–829.

[**Hesselmann et al., 2010**] Hesselmann, G., Sadaghiani, S., Friston, K. J., & Kleinschmidt, A. 2010. Predictive coding or evidence accumulation? False inference and neuronal fluctuations. *PLoS One*, **5**(3), e9926.

[**Hillyard & W, 1979**] Hillyard, S. A., & W, P. T. 1979. Event-related brain potentials and selective information processing in man. *Progress in clinical neurophysiology*, **6**, 1–52.

[**Holroyd & Coles, 2002**] Holroyd, C. B., & Coles, M. G. 2002. The neural basis of human error processing: reinforcement learning, dopamine, and the error-related negativity. *Psychological review*, **109**(4), 679.

[**Hotz-Boendermaker et al., 2008**] Hotz-Boendermaker, S., Funk, M., Summers, P., Brugger, P., Hepp-Reymond, M.-C., Curt, A., & Kollias, S. S. 2008. Preservation of motor programs in paraplegics as demonstrated by attempted and imagined foot movements. *Neuroimage*, **39**(1), 383–394.

[**Huettel et al., 2004**] Huettel, S. A., Song, A. W., McCarthy, G., et al. 2004. *Functional magnetic resonance imaging*. Vol. 1. Sinauer Associates Sunderland.

[**Ingber & Nunez, 2011**] Ingber, L., & Nunez, P. L. 2011. Neocortical dynamics at multiple scales: EEG standing waves, statistical mechanics, and physical analogs. *Mathematical Biosciences*, **229**(2), 160–173.

[**Isbell Jr et al., 2001**] Isbell Jr, C. L., Shelton, C. R., Kearns, M., Singh, S., & Stone, P. 2001. Cobot: A social reinforcement learning agent. *Pages 1393–1400 of: Proceedings of the 14th International Conference on Neural Information Processing Systems: Natural and Synthetic*. MIT Press.

[**Iturrate et al., 2009**] Iturrate, I., Antelis, J. M., Kubler, A., & Minguez, J. 2009. A noninvasive brain-actuated wheelchair based on a P300 neurophysiological protocol and automated navigation. *IEEE Transactions on Robotics*, **25**(3), 614–627.

[**Iturrate et al., 2010**] Iturrate, I., Montesano, L., & Minguez, J. 2010. Single trial recognition of error-related potentials during observation of robot operation. *In: Proc of the Annual Int Conf of the IEEE Engineering in Medicine and Biology Society (EMBC)*.

[**Iturrate et al., 2012**] Iturrate, I., Chavarriaga, R., Montesano, L., Minguez, J., & Millán, J. d. R. 2012. Latency correction of error potentials between different experiments reduces calibration time for single-trial classification. *In: Proc of the Annual Int Conf of the IEEE Engineering in Medicine and Biology Society (EMBC).*

[**Iturrate et al., 2013a**] Iturrate, I., Omedes, J., & Montesano, L. 2013a. Shared control of a robot using EEG-based feedback signals. *Pages 45–50 of: Proceedings of the 2nd Workshop on Machine Learning for Interactive Systems: Bridging the Gap Between Perception, Action and Communication.* ACM.

[**Iturrate et al., 2013b**] Iturrate, I., Montesano, L., & Minguez, J. 2013b. Task-dependent signal variations in EEG error-related potentials for brain-computer interfaces. *Journal of Neural Engineering*, **10**(2), 026024.

[**Iturrate et al., 2014**] Iturrate, I., Chavarriaga, R., Montesano, L., Minguez, J., & Millán, J. d. R. 2014. Latency correction of event-related potentials between different experimental protocols. *Journal of neural engineering*, **11**(3), 036005.

[**Iturrate et al., 2015a**] Iturrate, I., Grizou, J., Omedes, J., Oudeyer, P.-Y., Lopes, M., & Montesano, L. 2015a. Exploiting task constraints for self-calibrated brain-machine interface control using error-related potentials. *PloS one*, **10**(7), e0131491.

[**Iturrate et al., 2015b**] Iturrate, I., Chavarriaga, R., Montesano, L., Minguez, J., & Millán, J. d. R. 2015b. Teaching brain-machine interfaces as an alternative paradigm to neuroprosthetics control. *Scientific reports*, **5**, 13893.

[**Iturrate et al., 2018**] Iturrate, I., Chavarriaga, R., Pereira, M., Zhang, H., Corbet, T., Leeb, R., & Millán, J. d. R. 2018. Human EEG reveals distinct neural correlates of power and precision grasping types. *NeuroImage*, **181**, 635–644.

[**Jackson & Bolger, 2014**] Jackson, A. F., & Bolger, D. J. 2014. The neurophysiological bases of EEG and EEG measurement: A review for the rest of us. *Psychophysiology*, **51**(11), 1061–1071.

[**Jarosiewicz et al., 2008**] Jarosiewicz, B., Chase, S. M., Fraser, G. W., Velliste, M., Kass, R. E., & Schwartz, A. B. 2008. Functional network reorganization during learning in a brain-computer interface paradigm. *Proceedings of the National Academy of Sciences*, pnas–0808113105.

[**Jochumsen et al., 2015**] Jochumsen, M., Niazi, I. K., Taylor, D., Farina, D., & Dremstrup, K. 2015. Detecting and classifying movement-related cortical potentials

associated with hand movements in healthy subjects and stroke patients from single-electrode, single-trial EEG. *Journal of neural engineering*, **12**(5), 056013.

[**Johnson Jr et al., 2004**] Johnson Jr, R., Barnhardt, J., & Zhu, J. 2004. The contribution of executive processes to deceptive responding. *Neuropsychologia*, **42**(7), 878–901.

[**Kandel et al., 2000**] Kandel, E. R., Schwartz, J. H., Jessell, T. M., Siegelbaum, S. A., Hudspeth, A. J., et al. 2000. *Principles of neural science.* Vol. 4. McGraw-hill New York.

[**Kersten et al., 2004**] Kersten, D., Mamassian, P., & Yuille, A. 2004. Object perception as Bayesian inference. *Annu. Rev. Psychol.*, **55**, 271–304.

[**Kesar et al., 2008**] Kesar, T., Chou, L.-W., & Binder-Macleod, S. A. 2008. Effects of stimulation frequency versus pulse duration modulation on muscle fatigue. *Journal of Electromyography and Kinesiology*, **18**(4), 662–671.

[**Kida et al., 2012**] Kida, T., Kaneda, T., & Nishihira, Y. 2012. Modulation of somatosensory processing in dual tasks: an event-related brain potential study. *Experimental brain research*, **216**(4), 575–584.

[**Kiernan et al., 1996**] Kiernan, M. C., Mogyoros, I., & Burke, D. 1996. Differences in the recovery of excitability in sensory and motor axons of human median nerve. *Brain*, **119**(4), 1099–1105.

[**Kim & Kirchner, 2016**] Kim, S. K., & Kirchner, E. A. 2016. Handling few training data: classifier transfer between different types of error-related potentials. *IEEE Transactions on Neural Systems and Rehabilitation Engineering*, **24**(3), 320–332.

[**Kim et al., 2003**] Kim, S.-P., Sanchez, J. C., Erdogmus, D., Rao, Y. N., Wessberg, J., Principe, J. C., & Nicolelis, M. 2003. Divide-and-conquer approach for brain machine interfaces: nonlinear mixture of competitive linear models. *Neural Networks*, **16**(5-6), 865–871.

[**Kindermans et al., 2012**] Kindermans, P.-J., Verschore, H., Verstraeten, D., & Schrauwen, B. 2012. A P300 BCI for the masses: Prior information enables instant unsupervised spelling. *Pages 710–718 of: Advances in Neural Information Processing Systems.*

[**Kleim & Jones, 2008**] Kleim, J. A., & Jones, T. A. 2008. Principles of experience-dependent neural plasticity: implications for rehabilitation after brain damage. *Journal of speech, language, and hearing research*, **51**(1), S225–S239.

[**Klimesch, 1999**] Klimesch, W. 1999. EEG alpha and theta oscillations reflect cognitive and memory performance: a review and analysis. *Brain research reviews*, **29**(2-3), 169–195.

[**Knox & Stone, 2009**] Knox, W. B., & Stone, P. 2009. Interactively shaping agents via human reinforcement: The TAMER framework. *Pages 9–16 of: Proceedings of the fifth international conference on Knowledge capture.* ACM.

[**Knox & Stone, 2010**] Knox, W. B., & Stone, P. 2010. Combining manual feedback with subsequent MDP reward signals for reinforcement learning. *Pages 5–12 of: Proceedings of the 9th International Conference on Autonomous Agents and Multiagent Systems: volume 1-Volume 1.* International Foundation for Autonomous Agents and Multiagent Systems.

[**Knox & Stone, 2012**] Knox, W. B., & Stone, P. 2012. Reinforcement learning from simultaneous human and MDP reward. *Pages 475–482 of: Proceedings of the 11th International Conference on Autonomous Agents and Multiagent Systems-Volume 1.* International Foundation for Autonomous Agents and Multiagent Systems.

[**Krauledat et al., 2009**] Krauledat, M., Grzeska, K., Sagebaum, M., Blankertz, B., Vidaurre, C., Müller, K.-R., & Schröder, M. 2009. Playing pinball with non-invasive BCI. *Pages 1641–1648 of: Advances in neural information processing systems.*

[**Kreilinger et al., 2011**] Kreilinger, A., Kaiser, V., Breitwieser, C., Williamson, J., Neuper, C., & Müller-Putz, G. R. 2011. Switching between manual control and brain-computer interface using long term and short term quality measures. *Frontiers in neuroscience*, **5**.

[**Kreilinger et al., 2012**] Kreilinger, A., Neuper, C., & Müller-Putz, G. R. 2012. Error potential detection during continuous movement of an artificial arm controlled by brain–computer interface. *Medical & biological engineering & computing*, **50**(3), 223–230.

[**Krepki et al., 2007**] Krepki, R., Blankertz, B., Curio, G., & Müller, K.-R. 2007. The Berlin Brain-Computer Interface (BBCI)–towards a new communication channel for online control in gaming applications. *Multimedia Tools and Applications*, **33**(1), 73–90.

[**Krigolson & Holroyd, 2007**] Krigolson, O. E., & Holroyd, C. B. 2007. Hierarchical error processing: different errors, different systems. *Brain research*, **1155**, 70–80.

[**Kronegg et al., 2005**] Kronegg, J., Voloshynovskyy, S., & Pun, T. 2005. Analysis of bit-rate definitions for brain-computer interfaces. *Pages 1–7 of: International Conference in Human-Computer Interaction (HCI05).*

[**Kübler et al., 2008**] Kübler, A., Halder, S., Furdea, A., & Hösle, A. 2008. Brain painting–BCI meets art. *Pages 361–366 of: Proceedings of the 4th International Brain-Computer Interface Workshop and Training Course.*

[**Kübler & Müller, 2007**] Kübler, A., & Müller, K.-R. 2007. An introduction to brain-computer interfacing. *Toward brain-computer interfacing*, 1–25.

[**Kübler et al., 2001**] Kübler, A., Kotchoubey, B., Kaiser, J., Wolpaw, J. R., & Birbaumer, N. 2001. Brain–computer communication: Unlocking the locked in. *Psychological bulletin*, **127**(3), 358.

[**Kuhlman, 1978**] Kuhlman, W. N. 1978. EEG feedback training of epileptic patients: clinical and electroencephalographic analysis. *Electroencephalography and Clinical Neurophysiology*, **45**(6), 699–710.

[**Kutas & Federmeier, 2011**] Kutas, M., & Federmeier, K. D. 2011. Thirty years and counting: finding meaning in the N400 component of the event-related brain potential (ERP). *Annual review of psychology*, **62**, 621–647.

[**Kutas & Hillyard, 1980**] Kutas, M., & Hillyard, S. A. 1980. Reading senseless sentences: Brain potentials reflect semantic incongruity. *Science*, **207**(4427), 203–205.

[**Kutas et al., 1977**] Kutas, M., McCarthy, G., & Donchin, E. 1977. Augmenting mental chronometry: The P300 as a measure of stimulus evaluation time. *Science*, **197**(4305), 792.

[**Kwakkel et al., 2008**] Kwakkel, G., Kollen, B. J., & Krebs, H. I. 2008. Effects of robot-assisted therapy on upper limb recovery after stroke: a systematic review. *Neurorehabilitation and neural repair*, **22**(2), 111–121.

[**Lebedev & Nicolelis, 2006**] Lebedev, M. A., & Nicolelis, M. A. 2006. Brain–machine interfaces: past, present and future. *TRENDS in Neurosciences*, **29**(9), 536–546.

[**Lebedev & Nicolelis, 2017**] Lebedev, M. A., & Nicolelis, M. A. 2017. Brain-machine interfaces: From basic science to neuroprostheses and neurorehabilitation. *Physiological reviews*, **97**(2), 767–837.

[**LeCun et al., 2015**] LeCun, Y., Bengio, Y., & Hinton, G. 2015. Deep learning. *nature*, **521**(7553), 436.

[**Leeb et al., 2007**] Leeb, R., Friedman, D., Müller-Putz, G. R., Scherer, R., Slater, M., & Pfurtscheller, G. 2007. Self-paced (asynchronous) BCI control of a wheelchair in virtual environments: a case study with a tetraplegic. *Computational intelligence and neuroscience*, **2007**, 7.

[**Leeb et al., 2010**] Leeb, R., Sagha, H., Chavarriaga, R., et al. 2010. Multimodal fusion of muscle and brain signals for a hybrid-BCI. *Pages 4343–4346 of: Engineering in Medicine and Biology Society (EMBC), 2010 Annual International Conference of the IEEE*. IEEE.

[**Lesser et al., 1979**] Lesser, R. P., Koehle, R., & Lueders, H. 1979. Effect of stimulus intensity on short latency somatosensory evoked potentials. *Electroencephalography and clinical neurophysiology*, **47**(3), 377–382.

[**Li & Jasper, 1953**] Li, C.-L., & Jasper, H. 1953. Microelectrode studies of the electrical activity of the cerebral cortex in the cat. *The Journal of physiology*, **121**(1), 117–140.

[**Li et al., 2009**] Li, L., Yao, D., & Yin, G. 2009. Spatio-temporal dynamics of visual selective attention identified by a common spatial pattern decomposition method. *Brain Res*, **1282**, 84–94.

[**Li et al., 2014**] Li, Y., Bahn, S., Nam, C. S., & Lee, J. 2014. Effects of luminosity contrast and stimulus duration on user performance and preference in a P300-based brain–computer interface. *International Journal of Human-Computer Interaction*, **30**(2), 151–163.

[**Libet et al., 1967**] Libet, B., Alberts, W., Wright, E., & Feinstein, B. 1967. Responses of human somatosensory cortex to stimuli below threshold for conscious sensation. *Science*, **158**(3808), 1597–1600.

[**Libet et al., 1983**] Libet, B., Gleason, C. A., Wright, E. W., & Pearl, D. K. 1983. Time of conscious intention to act in relation to onset of cerebral activity (readiness-potential) the unconscious initiation of a freely voluntary act. *Brain*, **106**(3), 623–642.

[**Light et al., 2007**] Light, G. A., Swerdlow, N. R., & Braff, D. L. 2007. Preattentive sensory processing as indexed by the MMN and P3a brain responses is associated with cognitive and psychosocial functioning in healthy adults. *Journal of cognitive neuroscience*, **19**(10), 1624–1632.

[**Linden, 2005**] Linden, D. E. 2005. The P300: where in the brain is it produced and what does it tell us? *The Neuroscientist*, **11**(6), 563–576.

[**Liotti et al., 2000**] Liotti, M., Woldorff, M. G., Perez III, R., & Mayberg, H. S. 2000. An ERP study of the temporal course of the Stroop color-word interference effect. *Neuropsychologia*, **38**(5), 701–711.

[**Llera et al., 2012**] Llera, A., Gómez, V., & Kappen, H. J. 2012. Adaptive classification on brain-computer interfaces using reinforcement signals. *Neural Computation*, **24**(11), 2900–2923.

[**Llera et al., 2011**] Llera, A., van Gerven, M. A., Gómez, V., Jensen, O., & Kappen, H. J. 2011. On the use of interaction error potentials for adaptive brain computer interfaces. *Neural Networks*, **24**(10), 1120–1127.

[**López et al., 2013**] López, J., Úbeda, A., Iáñez, E., Climent, J. M., & Azorín, J. M. 2013. Error Potential Detection to Assist Movement Intention Decoding in Stroke Patients. *Pages 489–493 of: Converging Clinical and Engineering Research on Neurorehabilitation*. Springer.

[**López-Larraz et al., 2011**] López-Larraz, E., Creatura, M., Iturrate, I., Montesano, L., & Minguez, J. 2011. EEG single-trial classification of visual, auditive and vibratory feedback potentials in Brain-Computer Interfaces. *Pages 4231–4234 of: Engineering in Medicine and Biology Society, EMBC, 2011 Annual International Conference of the IEEE*. IEEE.

[**López-Larraz et al., 2014**] López-Larraz, E., Montesano, L., Gil-Agudo, Á., & Minguez, J. 2014. Continuous decoding of movement intention of upper limb self-initiated analytic movements from pre-movement EEG correlates. *Journal of neuroengineering and rehabilitation*, **11**(1), 153.

[**Lotte et al., 2007**] Lotte, F., Congedo, M., Lécuyer, A., Lamarche, F., & Arnaldi, B. 2007. A review of classification algorithms for EEG-based brain–computer interfaces. *Journal of neural engineering*, **4**(2), R1.

[**Lotte et al., 2012**] Lotte, F., Faller, J., Guger, C., Renard, Y., Pfurtscheller, G., Lécuyer, A., & Leeb, R. 2012. Combining BCI with virtual reality: towards new applications and improved BCI. *Pages 197–220 of: Towards Practical Brain-Computer Interfaces*. Springer.

[**Lotze et al., 2003**] Lotze, M., Braun, C., Birbaumer, N., Anders, S., & Cohen, L. G. 2003. Motor learning elicited by voluntary drive. *Brain*, **126**(4), 866–872.

[**Luck, 2014**] Luck, S. J. 2014. *An introduction to the event-related potential technique*. MIT press.

[**Lugo et al., 2014**] Lugo, Z. R., Rodriguez, J., Lechner, A., Ortner, R., Gantner, I. S., Laureys, S., Noirhomme, Q., & Guger, C. 2014. A vibrotactile P300-based brain–computer interface for consciousness detection and communication. *Clinical EEG and neuroscience*, **45**(1), 14–21.

[**Mahmoudi & Sanchez, 2011**] Mahmoudi, B., & Sanchez, J. C. 2011. A symbiotic brain-machine interface through value-based decision making. *PloS one*, **6**(3), e14760.

[**Makeig, 1993**] Makeig, S. 1993. Auditory event-related dynamics of the EEG spectrum and effects of exposure to tones. *Electroencephalography and clinical neurophysiology*, **86**(4), 283–293.

[**Marchal-Crespo et al., 2014**] Marchal-Crespo, L., Schneider, J., Jaeger, L., & Riener, R. 2014. Learning a locomotor task: with or without errors? *Journal of neuroengineering and rehabilitation*, **11**(1), 25.

[**Marchal-Crespo et al., 2017**] Marchal-Crespo, L., Michels, L., Jaeger, L., López-Olóriz, J., & Riener, R. 2017. Effect of error augmentation on brain activation and motor learning of a complex locomotor task. *Frontiers in neuroscience*, **11**, 526.

[**McFarland & Wolpaw, 2008**] McFarland, D. J., & Wolpaw, J. R. 2008. Brain-computer interface operation of robotic and prosthetic devices. *Computer*, **41**(10).

[**Mesin et al., 2010**] Mesin, L., Merlo, E., Merletti, R., & Orizio, C. 2010. Investigation of motor unit recruitment during stimulated contractions of tibialis anterior muscle. *Journal of Electromyography and Kinesiology*, **20**(4), 580–589.

[**Milekovic et al., 2012**] Milekovic, T., Ball, T., Schulze-Bonhage, A., Aertsen, A., & Mehring, C. 2012. Error-related electrocorticographic activity in humans during continuous movements. *Journal of neural engineering*, **9**(2), 026007.

[**Milekovic et al., 2013**] Milekovic, T., Ball, T., Schulze-Bonhage, A., Aertsen, A., & Mehring, C. 2013. Detection of Error Related Neuronal Responses Recorded by Electrocorticography in Humans during Continuous Movements. *PloS one*, **8**(2), e55235.

[**Miles, 2006**] Miles, K. A. 2006. Perfusion imaging with computed tomography: brain and beyond. *European Radiology Supplements*, **16**(7), M37–M43.

[**Millán et al., 2009**] Millán, J. d. R., Galán, F., Vanhooydonck, D., Lew, E., Philips, J., & Nuttin, M. 2009. Asynchronous non-invasive brain-actuated control of an intelligent wheelchair. *Pages 3361–3364 of: Engineering in Medicine and Biology Society, 2009. EMBC 2009. Annual International Conference of the IEEE*. IEEE.

[**Millán et al., 2010**] Millán, J. d. R., Rupp, R., Mueller-Putz, G., Murray-Smith, R., Giugliemma, C., Tangermann, M., Vidaurre, C., Cincotti, F., Kubler, A., Leeb, R., et al. 2010. Combining brain–computer interfaces and assistive technologies: state-of-the-art and challenges. *Frontiers in neuroscience*, **4**, 161.

[**Miltner et al., 1989**] Miltner, W., Johnson Jr, R., Braun, C., & Larbig, W. 1989. Somatosensory event-related potentials to painful and non-painful stimuli: effects of attention. *Pain*, **38**(3), 303–312.

[**Miltner et al., 1997**] Miltner, W. H., Braun, C. H., & Coles, M. G. 1997. Event-related brain potentials following incorrect feedback in a time-estimation task: evidence for a generic neural system for error detection. *Journal of cognitive neuroscience*, **9**(6), 788–798.

[**Mondada et al., 2009**] Mondada, F., Bonani, M., Raemy, X., Pugh, J., Cianci, C., Klaptocz, A., Magnenat, S., Zufferey, J.-C., Floreano, D., & Martinoli, A. 2009. The e-puck, a robot designed for education in engineering. *Pages 59–65 of: Proceedings of the 9th conference on autonomous robot systems and competitions*, vol. 1.

[**Mousavi et al., 2017**] Mousavi, M., Koerner, A. S., Zhang, Q., Noh, E., & de Sa, V. R. 2017. Improving motor imagery BCI with user response to feedback. *Brain-Computer Interfaces*, **4**(1-2), 74–86.

[**Müller-Putz & Pfurtscheller, 2008**] Müller-Putz, G. R., & Pfurtscheller, G. 2008. Control of an electrical prosthesis with an SSVEP-based BCI. *IEEE Transactions on Biomedical Engineering*, **55**(1), 361–364.

[**Müller-Putz et al., 2005**] Müller-Putz, G. R., Scherer, R., Pfurtscheller, G., & Rupp, R. 2005. EEG-based neuroprosthesis control: a step towards clinical practice. *Neuroscience letters*, **382**(1-2), 169–174.

[**Müller-Putz et al., 2013**] Müller-Putz, G. R., Pokorny, C., Klobassa, D. S., & Horki, P. 2013. A single-switch BCI based on passive and imagined movements: toward restoring communication in minimally conscious patients. *International journal of neural systems*, **23**(02), 1250037.

[**Müller-Putz et al., 2015**] Müller-Putz, G. R., Leeb, R., Tangermann, M., Höhne, J., Kübler, A., Cincotti, F., Mattia, D., Rupp, R., Müller, K.-R., & Millán, J. d. R. 2015. Towards noninvasive hybrid brain–computer interfaces: framework, practice, clinical application, and beyond. *Proceedings of the IEEE*, **103**(6), 926–943.

[**Müller-Putz et al., 2016**] Müller-Putz, G. R., Schwarz, A., Pereira, J., & Ofner, P. 2016. From classic motor imagery to complex movement intention decoding: The noninvasive Graz-BCI approach. *Pages 39–70 of: Progress in brain research*, vol. 228. Elsevier.

[**Müller-Putz et al., 2017a**] Müller-Putz, G. R., Ofner, P., Schwarz, A., Pereira, J., Luzhnica, G., di Sciascio, C., Veas, E., Stein, S., Williamson, J., Murray-Smith, R., et al. 2017a. MoreGrasp: restoration of upper limb function in individuals with high spinal cord injury by multimodal neuroprostheses for interaction in daily activities. *Proceedings of the 7th Brain-Computer Interface Conference 2017*, 338–343.

[**Müller-Putz et al., 2017b**] Müller-Putz, G. R., Ofner, P., Schwarz, A., Pereira, J., Pinegger, A., Dias, C. L., Hehenberger, L., Kobler, R., & Sburlea, A. I. 2017b. Towards non-invasive EEG-based arm/hand-control in users with spinal cord injury. *Pages 63–65 of: Brain-Computer Interface (BCI), 2017 5th International Winter Conference on.* IEEE.

[**Näätänen et al., 1978**] Näätänen, R., Gaillard, A. W., & Mäntysalo, S. 1978. Early selective-attention effect on evoked potential reinterpreted. *Acta psychologica*, **42**(4), 313–329.

[**Näätänen et al., 2007**] Näätänen, R., Paavilainen, P., Rinne, T., & Alho, K. 2007. The mismatch negativity (MMN) in basic research of central auditory processing: a review. *Clinical neurophysiology*, **118**(12), 2544–2590.

[**Naeije et al., 2016**] Naeije, G., Vaulet, T., Wens, V., Marty, B., Goldman, S., & De Tiège, X. 2016. Multilevel cortical processing of somatosensory novelty: a magnetoencephalography study. *Frontiers in human neuroscience*, **10**, 259.

[**Nakajima & Imamura, 2000**] Nakajima, Y., & Imamura, N. 2000. Relationships between attention effects and intensity effects on the cognitive N140 and P300 components of somatosensory ERPs. *Clinical Neurophysiology*, **111**(10), 1711–1718.

[**Nee et al., 2011**] Nee, D. E., Kastner, S., & Brown, J. W. 2011. Functional heterogeneity of conflict, error, task-switching, and unexpectedness effects within medial prefrontal cortex. *Neuroimage*, **54**(1), 528–540.

[**Nicolelis, 2003**] Nicolelis, M. A. 2003. Brain–machine interfaces to restore motor function and probe neural circuits. *Nature Reviews Neuroscience*, **4**(5), 417.

[**Niedermeyer & da Silva, 2005**] Niedermeyer, E., & da Silva, F. L. 2005. *Electroencephalography: basic principles, clinical applications, and related fields.* Lippincott Williams & Wilkins.

[**Nieuwenhuis et al., 2004**] Nieuwenhuis, S., Holroyd, C. B., Mol, N., & Coles, M. G. 2004. Reinforcement-related brain potentials from medial frontal cortex: origins and functional significance. *Neuroscience & Biobehavioral Reviews*, **28**(4), 441–448.

[**Nijholt et al., 2008**] Nijholt, A., Tan, D., Pfurtscheller, G., Brunner, C., Allison, B., Graimann, B., Popescu, F., Blankertz, B., et al. 2008. Brain-computer interfacing for intelligent systems. *IEEE intelligent systems*, 72–79.

[**Nunez, 2012**] Nunez, P. L. 2012. *Brain, mind, and the structure of reality.* Oxford University Press.

[**Nunez & Srinivasan, 2006**] Nunez, P. L., & Srinivasan, R. 2006. *Electric fields of the brain: the neurophysics of EEG.* Oxford University Press, USA.

[**O'Connell et al., 2012**] O'Connell, R. G., Dockree, P. M., & Kelly, S. P. 2012. A supramodal accumulation-to-bound signal that determines perceptual decisions in humans. *Nature neuroscience*, **15**(12), 1729–1735.

[**O'donnell et al., 1997**] O'donnell, B. F., Swearer, J. M., Smith, L. T., Hokama, H., & McCarley, R. W. 1997. A topographic study of ERPs elicited by visual feature discrimination. *Brain topography*, **10**(2), 133–143.

[**Ofner et al., 2017**] Ofner, P., Schwarz, A., Pereira, J., & Müller-Putz, G. R. 2017. Upper limb movements can be decoded from the time-domain of low-frequency EEG. *PloS one*, **12**(8), e0182578.

[**Ogawa et al., 1990**] Ogawa, S., Lee, T.-M., Kay, A. R., & Tank, D. W. 1990. Brain magnetic resonance imaging with contrast dependent on blood oxygenation. *Proceedings of the National Academy of Sciences*, **87**(24), 9868–9872.

[**Omedes et al., 2013a**] Omedes, J., Iturrate, I., & Montesano, L. 2013a. Detection of event-less error related potentials. *Towards a robot-enabled, Neuroscience-guided healthy society*, 28.

[**Omedes et al., 2013b**] Omedes, J., Iturrate, I. n., Montesano, L., & Minguez, J. 2013b. Using frequency-domain features for the generalization of EEG error-related potentials among different tasks. *In: Int. Conf. of the IEEE Engineering in Medicine and Biology Society (EMBC).* IEEE.

[Omedes et al., 2014a] Omedes, J., Iturrate, I., & Montesano, L. 2014a. Asynchronous detection of error potentials. *In: Proceedings of the 6th Brain-Computer Interface Conference 2014.*

[Omedes et al., 2014b] Omedes, J., Iturrate, I., & Montesano, L. 2014b. Brain connectivity in continuous error tasks. *Pages 3997–4000 of: Engineering in Medicine and Biology Society (EMBC), 2014 36th Annual International Conference of the IEEE.* IEEE.

[Omedes et al., 2015a] Omedes, J., Iturrate, I., Minguez, J., & Montesano, L. 2015a. Analysis and asynchronous detection of gradually unfolding errors during monitoring tasks. *Journal of neural engineering,* **12**(5), 056001.

[Omedes et al., 2015b] Omedes, J., Iturrate, I., Chavarriaga, R., & Montesano, L. 2015b. Asynchronous Decoding of Error Potentials During the Monitoring of a Reaching Task. *Pages 3116–3121 of: Systems, Man, and Cybernetics (SMC), 2015 IEEE International Conference on.* IEEE.

[Omedes et al., 2017] Omedes, J., Schwarz, A., Montesano, L., & Müller-Putz, G. 2017. Hierarchical decoding of grasping commands from EEG. *Pages 2085–2088 of: Engineering in Medicine and Biology Society (EMBC), 2017 39th Annual International Conference of the IEEE.* IEEE.

[Omedes et al., 2018] Omedes, J., Schwarz, A., Müller-Putz, G. R., & Montesano, L. 2018. Factors that affect error potentials during a grasping task: toward a hybrid natural movement decoding BCI. *Journal of neural engineering,* **15**(4).

[Pascual-Marqui, 2002] Pascual-Marqui, R. D. 2002. Standardized low resolution brain electromagnetic tomography (sLORETA): Technical details. *Methods Find Exp Clin Pharmacol,* 5–12.

[Pavone et al., 2016] Pavone, E. F., Tieri, G., Rizza, G., Tidoni, E., Grisoni, L., & Aglioti, S. M. 2016. Embodying others in immersive virtual reality: electro-cortical signatures of monitoring the errors in the actions of an avatar seen from a first-person perspective. *Journal of Neuroscience,* **36**(2), 268–279.

[Pearson et al., 2011] Pearson, J. M., Heilbronner, S. R., Barack, D. L., Hayden, B. Y., & Platt, M. L. 2011. Posterior cingulate cortex: adapting behavior to a changing world. *Trends in cognitive sciences,* **15**(4), 143–151.

[Pfurtscheller & Da Silva, 1999] Pfurtscheller, G., & Da Silva, F. L. 1999. Event-related EEG/MEG synchronization and desynchronization: basic principles. *Clinical neurophysiology,* **110**(11), 1842–1857.

[Pfurtscheller et al., 2000] Pfurtscheller, G., Guger, C., Müller, G., Krausz, G., & Neuper, C. 2000. Brain oscillations control hand orthosis in a tetraplegic. *Neuroscience letters*, **292**(3), 211–214.

[Pfurtscheller et al., 2003] Pfurtscheller, G., Müller, G. R., Pfurtscheller, J., Gerner, H. J., & Rupp, R. 2003. Thought–control of functional electrical stimulation to restore hand grasp in a patient with tetraplegia. *Neuroscience letters*, **351**(1), 33–36.

[Pfurtscheller et al., 2010] Pfurtscheller, G., Allison, B. Z., Bauernfeind, G., Brunner, C., Solis Escalante, T., Scherer, R., Zander, T. O., Mueller-Putz, G., Neuper, C., & Birbaumer, N. 2010. The hybrid BCI. *Frontiers in neuroscience*, **4**, 3.

[Pistohl et al., 2008] Pistohl, T., Ball, T., Schulze-Bonhage, A., Aertsen, A., & Mehring, C. 2008. Prediction of arm movement trajectories from ECoG-recordings in humans. *Journal of neuroscience methods*, **167**(1), 105–114.

[Pistohl et al., 2012] Pistohl, T., Schulze-Bonhage, A., Aertsen, A., Mehring, C., & Ball, T. 2012. Decoding natural grasp types from human ECoG. *Neuroimage*, **59**(1), 248–260.

[Pizzagalli et al., 2001] Pizzagalli, D., Pascual-Marqui, R. D., Nitschke, J. B., Oakes, T. R., Larson, C. L., Abercrombie, H. C., Schaefer, S. M., Koger, J. V., Benca, R. M., & Davidson, R. J. 2001. Anterior cingulate activity as a predictor of degree of treatment response in major depression: evidence from brain electrical tomography analysis. *American Journal of Psychiatry*, **158**(3), 405–415.

[Ploran et al., 2007] Ploran, E. J., Nelson, S. M., Velanova, K., Donaldson, D. I., Petersen, S. E., & Wheeler, M. E. 2007. Evidence accumulation and the moment of recognition: dissociating perceptual recognition processes using fMRI. *The Journal of Neuroscience*, **27**(44), 11912–11924.

[Polich, 1997] Polich, J. 1997. EEG and ERP assessment of normal aging. *Electroencephalography and Clinical Neurophysiology/Evoked Potentials Section*, **104**(3), 244–256.

[Polich, 2007] Polich, J. 2007. Updating P300: an integrative theory of P3a and P3b. *Clinical neurophysiology*, **118**(10), 2128–2148.

[Proverbio & Riva, 2009] Proverbio, A. M., & Riva, F. 2009. RP and N400 ERP components reflect semantic violations in visual processing of human actions. *Neuroscience Letters*, **459**(3), 142–146.

[**Quandt & Hummel, 2014**] Quandt, F., & Hummel, F. C. 2014. The influence of functional electrical stimulation on hand motor recovery in stroke patients: a review. *Experimental & translational stroke medicine*, **6**(1), 9.

[**Rabbitt, 1966**] Rabbitt, P. 1966. Errors and error correction in choice-response tasks. *Journal of experimental psychology*, **71**(2), 264.

[**Ramón y Cajal, 1995**] Ramón y Cajal, S. 1995. *Histology of the nervous system of man and vertebrates*. Vol. 1. Oxford University Press, USA.

[**Ramos-Murguialday et al., 2012**] Ramos-Murguialday, A., Schürholz, M., Caggiano, V., Wildgruber, M., Caria, A., Hammer, E. M., Halder, S., & Birbaumer, N. 2012. Proprioceptive feedback and brain computer interface (BCI) based neuroprostheses. *PloS one*, **7**(10), e47048.

[**Ramos-Murguialday et al., 2013**] Ramos-Murguialday, A., Broetz, D., Rea, M., Läer, L., Yilmaz, Ö., Brasil, F. L., Liberati, G., Curado, M. R., Garcia-Cossio, E., Vyziotis, A., et al. 2013. Brain–machine interface in chronic stroke rehabilitation: a controlled study. *Annals of neurology*, **74**(1), 100–108.

[**Ray et al., 1999**] Ray, P. G., Meador, K., Smith, J., Wheless, J., Sittenfeld, M., & Clifton, G. 1999. Physiology of perception Cortical stimulation and recording in humans. *Neurology*, **52**(5), 1044–1044.

[**Reinkensmeyer, 2003**] Reinkensmeyer, D. 2003. How to retrain movement after neurologic injury: a computational rationale for incorporating robot (or therapist) assistance. *Pages 1479–1482 of: Engineering in Medicine and Biology Society, 2003. Proceedings of the 25th Annual International Conference of the IEEE*, vol. 2. IEEE.

[**Ren & Wu, 2014**] Ren, Y., & Wu, Y. 2014. Convolutional deep belief networks for feature extraction of EEG signal. *Pages 2850–2853 of: Neural Networks (IJCNN), 2014 International Joint Conference on*. IEEE.

[**Restuccia et al., 2009**] Restuccia, D., Zanini, S., Cazzagon, M., Del Piero, I., Martucci, L., & Della Marca, G. 2009. Somatosensory mismatch negativity in healthy children. *Developmental Medicine & Child Neurology*, **51**(12), 991–998.

[**Rice et al., 1993**] Rice, K. M., Blanchard, E. B., & Purcell, M. 1993. Biofeedback treatments of generalized anxiety disorder: preliminary results. *Biofeedback and self-regulation*, **18**(2), 93–105.

[**Rinne et al., 2006**] Rinne, T., Särkkä, A., Degerman, A., Schröger, E., & Alho, K. 2006. Two separate mechanisms underlie auditory change detection and involuntary control of attention. *Brain research*, **1077**(1), 135–143.

[**Rivet et al., 2009**] Rivet, B., Souloumiac, A., Attina, V., & Gibert, G. 2009. xDAWN algorithm to enhance evoked potentials: application to brain–computer interface. *IEEE Transactions on Biomedical Engineering*, **56**(8), 2035–2043.

[**Rockstroh, 1989**] Rockstroh, B. 1989. *Slow cortical potentials and behaviour.* Urban & Schwarzenberg.

[**Rohm et al., 2013**] Rohm, M., Schneiders, M., Müller, C., Kreilinger, A., Kaiser, V., Müller-Putz, G. R., & Rupp, R. 2013. Hybrid brain–computer interfaces and hybrid neuroprostheses for restoration of upper limb functions in individuals with high-level spinal cord injury. *Artificial intelligence in medicine*, **59**(2), 133–142.

[**Rolls, 2000**] Rolls, E. T. 2000. On the brain and emotion. *Behavioral and brain sciences*, **23**(2), 219–228.

[**Rosa et al., 2010**] Rosa, M. J., Daunizeau, J., & Friston, K. J. 2010. EEG-fMRI integration: a critical review of biophysical modeling and data analysis approaches. *Journal of Integrative Neuroscience*, **09**(04), 453–476.

[**Rupp et al., 2015**] Rupp, R., Rohm, M., Schneiders, M., Kreilinger, A., & Müller-Putz, G. R. 2015. Functional rehabilitation of the paralyzed upper extremity after spinal cord injury by noninvasive hybrid neuroprostheses. *Proceedings of the IEEE*, **103**(6), 954–968.

[**Schalk et al., 2000**] Schalk, G., Wolpaw, J. R., McFarland, D. J., & Pfurtscheller, G. 2000. EEG-based communication: presence of an error potential. *Clinical Neurophysiology*, **111**(12), 2138–2144.

[**Schalk et al., 2004**] Schalk, G., McFarland, D. J., Hinterberger, T., Birbaumer, N., & Wolpaw, J. R. 2004. BCI2000: a general-purpose brain-computer interface (BCI) system. *IEEE Transactions on biomedical engineering*, **51**(6), 1034–1043.

[**Scherer et al., 2007**] Scherer, R., Müller-Putz, G., & Pfurtscheller, G. 2007. Self-initiation of EEG-based brain–computer communication using the heart rate response. *Journal of neural engineering*, **4**(4), L23.

[**Schirrmeister et al., 2017**] Schirrmeister, R. T., Springenberg, J. T., Fiederer, L. D. J., Glasstetter, M., Eggensperger, K., Tangermann, M., Hutter, F., Burgard, W., &

Ball, T. 2017. Deep learning with convolutional neural networks for EEG decoding and visualization. *Human brain mapping*, **38**(11), 5391–5420.

[**Schlögl et al., 2007**] Schlögl, A., Keinrath, C., Zimmermann, D., Scherer, R., Leeb, R., & Pfurtscheller, G. 2007. A fully automated correction method of EOG artifacts in EEG recordings. *Clinical neurophysiology*, **118**(1), 98–104.

[**Schmidhuber, 2015**] Schmidhuber, J. 2015. Deep learning in neural networks: An overview. *Neural networks*, **61**, 85–117.

[**Schubert et al., 2006**] Schubert, R., Blankenburg, F., Lemm, S., Villringer, A., & Curio, G. 2006. Now you feel itnow you don't: ERP correlates of somatosensory awareness. *Psychophysiology*, **43**(1), 31–40.

[**Schwarz et al., 2017**] Schwarz, A., Ofner, P., Pereira, J., Sburlea, A. I., & Müller-Putz, G. R. 2017. Decoding natural reach-and-grasp actions from human EEG. *Journal of neural engineering*, **15**(1), 016005.

[**Sellers et al., 2006**] Sellers, E. W., Krusienski, D. J., McFarland, D. J., Vaughan, T. M., & Wolpaw, J. R. 2006. A P300 event-related potential brain-computer interface (BCI): The effects of matrix size and inter stimulus interval on performance. *Biol Psychol*, **73**(3), 242–52.

[**Sellers et al., 2010**] Sellers, E. W., Vaughan, T. M., & Wolpaw, J. R. 2010. A brain-computer interface for long-term independent home use. *Amyotrophic lateral sclerosis*, **11**(5), 449–455.

[**Shenhav et al., 2013**] Shenhav, A., Botvinick, M. M., & Cohen, J. D. 2013. The expected value of control: an integrative theory of anterior cingulate cortex function. *Neuron*, **79**(2), 217–240.

[**Sitnikova et al., 2008**] Sitnikova, T., Holcomb, P. J., Kiyonaga, K. A., & Kuperberg, G. R. 2008. Two neurocognitive mechanisms of semantic integration during the comprehension of visual real-world events. *Journal of cognitive neuroscience*, **20**(11), 2037–2057.

[**Smith et al., 2003**] Smith, G. V., Alon, G., Roys, S. R., & Gullapalli, R. P. 2003. Functional MRI determination of a dose-response relationship to lower extremity neuromuscular electrical stimulation in healthy subjects. *Experimental Brain Research*, **150**(1), 33–39.

[**Spackman et al., 2007**] Spackman, L., Boyd, S., & Towell, A. 2007. Effects of stimulus frequency and duration on somatosensory discrimination responses. *Experimental brain research*, **177**(1), 21.

[**Spiegel et al., 1999**] Spiegel, J., Tintera, J., Gawehn, J., Stoeter, P., & Treede, R.-D. 1999. Functional MRI of human primary somatosensory and motor cortex during median nerve stimulation. *Clinical Neurophysiology*, **110**(1), 47–52.

[**Spinelli et al., 2018**] Spinelli, G., Tieri, G., Pavone, E., & Aglioti, S. 2018. Wronger than wrong: graded mapping of the errors of an avatar in the performance monitoring system of the onlooker. *NeuroImage*, **167**, 1–10.

[**Spüler & Niethammer, 2015**] Spüler, M., & Niethammer, C. 2015. Error-related potentials during continuous feedback: using EEG to detect errors of different type and severity. *Frontiers in human neuroscience*, **9**, 155.

[**Spüler et al., 2012**] Spüler, M., Bensch, M., Kleih, S., Rosenstiel, W., Bogdan, M., & Kübler, A. 2012. Online use of error-related potentials in healthy users and people with severe motor impairment increases performance of a P300-BCI. *Clinical Neurophysiology*, **123**(7), 1328–1337.

[**Stein, 1966**] Stein, L. 1966. Habituation and stimulus novelty: A model based on classical conditioning. *Psychological Review*, **73**(4), 352.

[**Steinhauser & Yeung, 2010**] Steinhauser, M., & Yeung, N. 2010. Decision processes in human performance monitoring. *The Journal of neuroscience*, **30**(46), 15643–15653.

[**Stemmer et al., 2004**] Stemmer, B., Vihla, M., & Salmelin, R. 2004. Activation of the human sensorimotor cortex during error-related processing: a magnetoencephalography study. *Neuroscience letters*, **362**(1), 44–47.

[**Sterman, 2000**] Sterman, M. B. 2000. Basic concepts and clinical findings in the treatment of seizure disorders with EEG operant conditioning. *Clinical electroencephalography*, **31**(1), 45–55.

[**Sutton & Barto, 1998**] Sutton, R. S., & Barto, A. G. 1998. *Reinforcement learning: An introduction*. Vol. 1. MIT press Cambridge.

[**Tan & Nijholt, 2010**] Tan, D., & Nijholt, A. 2010. Brain-computer interfaces and human-computer interaction. *Pages 3–19 of: Brain-Computer Interfaces*. Springer.

[**Tarkka et al., 1996**] Tarkka, I. M., Micheloyannis, S., & Stokić, D. S. 1996. Generators for human P300 elicited by somatosensory stimuli using multiple dipole source analysis. *Neuroscience*, **75**(1), 275–287.

[**Taylor et al., 2007**] Taylor, S. F., Stern, E. R., & Gehring, W. J. 2007. Neural systems for error monitoring: recent findings and theoretical perspectives. *The Neuroscientist*, **13**(2), 160–172.

[**Tessadori et al., 2017**] Tessadori, J., Schiatti, L., Barresi, G., & Mattos, L. S. 2017. Does tactile feedback enhance single-trial detection of error-related eeg potentials? *Pages 1417–1422 of: Systems, Man, and Cybernetics (SMC), 2017 IEEE International Conference on.* IEEE.

[**Thomaz & Breazeal, 2006**] Thomaz, A. L., & Breazeal, C. 2006. Reinforcement learning with human teachers: evidence of feedback and guidance with implications for learning performance. *Pages 1000–1005 of: Proceedings of the 21st national conference on Artificial intelligence - Volume 1.* AAAI'06. AAAI Press.

[**Tomberg, 1999**] Tomberg, C. 1999. Cognitive N140 electrogenesis and concomitant 40 Hz synchronization in mid-dorsolateral prefrontal cortex (area 46) identified in non-averaged human brain potentials. *Neuroscience letters*, **266**(2), 141–144.

[**Tourville et al., 2008**] Tourville, J. A., Reilly, K. J., & Guenther, F. H. 2008. Neural mechanisms underlying auditory feedback control of speech. *Neuroimage*, **39**(3), 1429–1443.

[**Twomey et al., 2015**] Twomey, D. M., Murphy, P. R., Kelly, S. P., & O'connell, R. G. 2015. The classic P300 encodes a build-to-threshold decision variable. *European journal of neuroscience*, **42**(1), 1636–1643.

[**Tyler et al., 2002**] Tyler, W. J., Alonso, M., Bramham, C. R., & Pozzo-Miller, L. D. 2002. From acquisition to consolidation: on the role of brain-derived neurotrophic factor signaling in hippocampal-dependent learning. *Learning & memory*, **9**(5), 224–237.

[**Ullsperger et al., 2014a**] Ullsperger, M., Fischer, A. G., Nigbur, R., & Endrass, T. 2014a. Neural mechanisms and temporal dynamics of performance monitoring. *Trends in Cognitive Sciences*, **18**(5), 259–267.

[**Ullsperger et al., 2014b**] Ullsperger, M., Danielmeier, C., & Jocham, G. 2014b. Neurophysiology of performance monitoring and adaptive behavior. *Physiological reviews*, **94**(1), 35–79.

[**Van Petten & Luka, 2006**] Van Petten, C., & Luka, B. J. 2006. Neural localization of semantic context effects in electromagnetic and hemodynamic studies. *Brain and language*, **97**(3), 279–293.

[**Van Veen & Carter, 2002**] Van Veen, V., & Carter, C. S. 2002. The anterior cingulate as a conflict monitor: fMRI and ERP studies. *Physiology & behavior*, **77**(4-5), 477–482.

[**Vanderhasselt & De Raedt, 2009**] Vanderhasselt, M.-A., & De Raedt, R. 2009. Impairments in cognitive control persist during remission from depression and are related to the number of past episodes: an event related potentials study. *Biological Psychology*, **81**(3), 169–176.

[**Vidal, 1973**] Vidal, J. J. 1973. Toward direct brain-computer communication. *Annual review of Biophysics and Bioengineering*, **2**(1), 157–180.

[**Vidaurre et al., 2011a**] Vidaurre, C., Sannelli, C., Müller, K.-R., & Blankertz, B. 2011a. Co-adaptive calibration to improve BCI efficiency. *Journal of neural engineering*, **8**(2), 025009.

[**Vidaurre et al., 2011b**] Vidaurre, C., Kawanabe, M., von Bünau, P., Blankertz, B., & Müller, K.-R. 2011b. Toward unsupervised adaptation of LDA for brain-computer interfaces. *IEEE Transactions on Biomedical Engineering*, **58**(3), 587 –597.

[**Völker et al., 2018**] Völker, M., Hammer, J., Schirrmeister, R. T., Behncke, J., Fiederer, L. D., Schulze-Bonhage, A., Marusič, P., Burgard, W., & Ball, T. 2018. Intracranial Error Detection via Deep Learning. *arXiv preprint arXiv:1805.01667*.

[**Volz et al., 2005**] Volz, K. G., Schubotz, R. I., & Cramon, D. 2005. Variants of uncertainty in decision-making and their neural correlates. *Brain research bulletin*, **67**(5), 403–412.

[**Wander et al., 2013**] Wander, J. D., Olson, J. D., Ojemann, J. G., & Rao, R. P. 2013. Cortically-derived error-signals during BCI use. *In: Proceedings of the Fifth International BCI Meeting*.

[**Wei et al., 2005**] Wei, Y., Bajaj, P., Scheidt, R. A., & Patton, J. L. 2005. Visual error augmentation for enhancing motor learning and rehabilitative relearning. *Pages 505–510 of: 9th International Conference on Rehabilitation Robotics, ICORR*. Institute of Electrical and Electronics Engineers.

[**West & Alain, 2000**] West, R., & Alain, C. 2000. Effects of task context and fluctuations of attention on neural activity supporting performance of the Stroop task. *Brain research*, **873**(1), 102–111.

[Wolpaw & McFarland, 2004] Wolpaw, J. R., & McFarland, D. J. 2004. Control of a two-dimensional movement signal by a noninvasive brain-computer interface in humans. *Proceedings of the National Academy of Sciences of the United States of America*, **101**(51), 17849–17854.

[Wolpaw & Tennissen, 2001] Wolpaw, J. R., & Tennissen, A. M. 2001. Activity-dependent spinal cord plasticity in health and disease. *Annual review of neuroscience*, **24**(1), 807–843.

[Wolpaw et al., 2000] Wolpaw, J. R., Birbaumer, N., Heetderks, W. J., McFarland, D. J., Peckham, P. H., Schalk, G., Donchin, E., Quatrano, L. A., Robinson, C. J., Vaughan, T. M., et al. 2000. Brain-computer interface technology: a review of the first international meeting. *IEEE transactions on rehabilitation engineering*, **8**(2), 164–173.

[Wolpaw et al., 2002] Wolpaw, J. R., Birbaumer, N., McFarland, D. J., Pfurtscheller, G., & Vaughan, T. M. 2002. Brain–computer interfaces for communication and control. *Clinical neurophysiology*, **113**(6), 767–791.

[Wriessnegger et al., 2014] Wriessnegger, S. C., Steyrl, D., Koschutnig, K., & Müller-Putz, G. R. 2014. Short time sports exercise boosts motor imagery patterns: implications of mental practice in rehabilitation programs. *Frontiers in human neuroscience*, **8**, 469.

[Wright et al., 2001] Wright, C. I., Fischer, H., Whalen, P. J., McInerney, S. C., Shin, L. M., & Rauch, S. L. 2001. Differential prefrontal cortex and amygdala habituation to repeatedly presented emotional stimuli. *Neuroreport*, **12**(2), 379–383.

[Yeung et al., 2004] Yeung, N., Botvinick, M. M., & Cohen, J. D. 2004. The neural basis of error detection: conflict monitoring and the error-related negativity. *Psychological review*, **111**(4), 931.

[Zander & Kothe, 2011] Zander, T. O., & Kothe, C. 2011. Towards passive brain–computer interfaces: applying brain–computer interface technology to human–machine systems in general. *Journal of Neural Engineering*, **8**(2), 025005.

[Zhang et al., 2012] Zhang, H., Chavarriaga, R., Goel, M. K., Gheorghe, L., & del Millán, J. d. R. 2012. Improved recognition of error related potentials through the use of brain connectivity features. *Pages 6740–6743 of: Int. Conf. of the IEEE Engineering in Medicine and Biology Society (EMBC)*. IEEE.

[**Zhang et al., 2015a**] Zhang, H., Chavarriaga, R., & Millán, J. d. R. 2015a. Discriminant brain connectivity patterns of performance monitoring at average and single-trial levels. *NeuroImage*, **120**, 64–74.

[**Zhang et al., 2015b**] Zhang, H., Chavarriaga, R., Khaliliardali, Z., Gheorghe, L., Iturrate, I., & d R Millán, J. 2015b. EEG-based decoding of error-related brain activity in a real-world driving task. *Journal of neural engineering*, **12**(6), 066028.